NASA CR-73087

STUDY OF STRUCTURAL WEIGHT SENSITIVITIES FOR LARGE ROCKET SYSTEMS

FINAL REPORT

VOLUME 2 OF 2

DETAILED ANALYSIS AND RESULTS

7 JULY 1967

PREPARED FOR

NATIONAL AERONAUTICS AND SPACE ADMINISTRATION

OFFICE OF ADVANCED RESEARCH AND TECHNOLOGY

NASA CONTRACT NAS2-3811

APOLLO SUPPORT DEPARTMENT
MISSILE AND SPACE DIVISION
GENERAL ELECTRIC COMPANY

NASA CR-73087

STUDY OF STRUCTURAL WEIGHT SENSITIVITIES FOR LARGE ROCKET SYSTEMS

FINAL REPORT

VOLUME 2 OF 2

DETAILED ANALYSIS AND RESULTS

7 July 1967

Prepared for

National Aeronautics and Space Administration
Office of Advanced Research and Technology
NASA Contract NAS2-3811

Apollo Support Department
Missile and Space Division
General Electric Company
Daytona Beach, Florida

TABLE OF CONTENTS

TABLE OF CONTENTS (Cont.)

TABLE OF CONTENTS (Cont.)

TABLE OF CONTENTS (Cont.)

LIST OF ILLUSTRATIONS

LIST OF ILLUSTRATIONS (Cont.)

LIST OF ILLUSTRATIONS (Cont.)

LIST OF TABLES

LIST OF TABLES (Cont.)

LIST OF TABLES (Cont.)

NOMENCLATURE

Symbols are listed in the order of appearance in each section of the report.

SECTION 2

F	Total axial force
M	Bending moment
T	Axial force resulting from the thrust load
P	Local pressure (gauge) in the propellant tank
R	Local radius of the vehicle structure
N_x	Axial (or meridional) stress resultant
N_y	Hoop (or circumferential) stress resultant
β	Instantaneous acceleration in g's
γ	Specific weight of the propellant in the tanks
d	Distance of station "x" below the level of the propellant
N_o	Equivalent uniaxial stress resultant
W	Weight per square foot of surface area
t	Shell thickness
UFS	Ultimate factor of safety
$\sigma_{ultimate}$	Ultimate strength
A	Surface area
ρ	Material density
F_β	Fabrication factor

SECTION 3

T	Instantaneous total thrust
P	Local atmospheric pressure
T_{vac}	Total vacuum thrust
A	Total nozzle throat area
e	Nozzle expansion ratio

NOMENCLATURE (Cont.)

SECTION 5

ρ_s	Shell density
E_s	Young's modulus

SECTION 6

F_T	Total thrust
δ	Incremental thrust over segment (usually 180-degree) of motor
F_R	Total side thrust
F_L	Total axial thrust
b	Lateral displacement of F_L from roll axis
a	Distance from engine mount to center of gravity
M_s	Total steering moment
β	Equivalent gimbal angle
M_L	Applied moment at gimbal plane
M_R	Moment due to lateral thrust at gimbal plane
α	Angle of cant of individual engine module
F_{L_H}	Magnitude of axial forces through high pressure segments
F_{L_L}	Magnitude of axial forces through low pressure segments
F_{R_H}	Magnitude of side forces from high pressure segments
F_{R_L}	Magnitude of side forces from low pressure segments
n	Total number of engine modules
ℓ_c	Distance from center of gravity to center of pressure
ℓ_g	Distance from center of gravity to aft gimbal point
K	Ratio of front-end steering contribution to total steering moment
T	Thrust from main engines
P_w	Propellant weight
I_{sp}	Specific impulse

NOMENCLATURE (Cont.)

W_E	Weight of one engine module
W_S	Weight of thrust structure
W	Total weight of reaction control system
M_c	Control moment
N_c	Normal force of front end controls
C_{L_δ}	Slope of the lift force coefficient curve due to control deflection
δ_c	Control fin deflection measured with respect to relative wind
q	Free stream dynamic pressure
S_{FIN}	Area of two control fins
M	Moment
N	Normal or ring thrust load
Q	Transverse shear
R	Ring radius
E	Young's modulus
I	Areal moment of inertia
A_f	Flange area
A_w	Web area
h	Total ring depth back-to-back of the flanges
h_f	Distance between flange centroids
h_w	Web depth
t_w	Web thickness
A	Total ring cross sectional area
σ_f	Stress in flange
σ_w	Stress in web
F_{LY}	Yield stress of material
b	Panel width
b_s	Width of sheet between stiffeners
b_w	Height of stiffener web
K_s	Compressive buckling coefficient of sheet of width b_s

NOMENCLATURE (Cont.)

ℓ	Frame spacing
N_x	Membrane load per unit width
R	Shell radius
t	Thickness of flat unstiffened plate
$\bar{t}_p$	Equivalent flat plate thickness of a stiffened panel
$\bar{t}_s$	Thickness of sheet between stiffeners
$\bar{t}_F$	Equivalent frame thickness per unit length
$\bar{t}_T$	Equivalent total shell thickness per unit length
ϵ	Structural efficiency
η_L	Plasticity reduction factor for general instability
η_T	Tangent modulus to Young's modulus ratio
$\bar{\eta}$	$= \sqrt{\eta_L \eta_T}$
ζ	Radius of gyration
σ	Compressive stress
ν	Poisson's ratio
σ_{CR}	Buckling stress for local instability
σ_{COL}	Buckling stress for wide column instability
M_x	Applied moment
F	Axial thrust
δ_R	Radial static deflection
δ_T	Tangential static deflection
q	$= W/2\pi R$
W	Weight of engines module plus ring
R	Ring mean modulus
ω	Vibration frequency

SECTION 7

h_1	Gage thickness of cap
h_2	Gage thickness of barrel
N_1, N_2	Principal stress resultants

NOMENCLATURE (Cont)

μ_p	Plastic Poisson's ratio
N_o	Equivalent uniaxial stress resultant
W	Weight of cylindrical shell
N_x	Meridional stress
C	Buckling coefficient

SECTION 8

E_c	Compressive modulus of elasticity
E_{sec}	Compressive secant modulus
E_{tan}	Compressive tangent modulus
η	Tangent-secant modulus reduction factor
η_w	Tangent modulus reduction factor
η_i	Secant modulus reduction factor
ρ	Density of material
σ_{yield}	Yield stress
σ_{ult}	Ultimate stress
σ_o	Secant yield stress at 0.70E
$\sigma_{0.85}$	Secant yield stress at 0.85E
μ	Poisson's ratio

SECTION 1

INTRODUCTION

The structural weight of a launch vehicle has been shown to exert a significant effect on the attainable level of a system's cost-effectiveness. Its reduction leads to increased payload capacity or margin of safety for constant system weight. A body of structural weight sensitivity data, relating weight decrements to variations in design parameters and methods, is therefore very desireable, not only for current design ventures but also as a basis for formulating effective research programs in structural technology.

The general unavailability of such information has been answered by the results of the study documented in this report. Performed by the General Electric Company under Contract NAS2-3811, the study evaluated the relative sensitivities of structural weight to variations in design parameters and techniques in the following areas:

a. Design Criteria.
b. Unique Design Approaches.
c. Materials and Fabrication.
d. Analysis Techniques.

The parametric analyses were performed on each of the three baseline vehicle configurations illustrated in Figures 1-1, 1-2, and 1-3. These vehicles, in the million-pound payload class, were selected from a Post-Saturn Vehicle study performed by the Martin Company (References 1 and 2) and represent a span of vehicle technology extending from the near to the distant future. Their structural designs are based on sound state-of-the-art design practice and criteria similar to those employed in the Saturn V vehicle. Thus, they serve as a sound point of departure for the parametric analyses. In each analysis, the parameters of interest were varied about their nominal values for each base vehicle and the effects on their structural weight noted.

In addition to these three configurations, five others were derived from the 201 Vehicle shown in Figure 1-2. While thrust, payload and propellant loading were held fixed, the fineness ratio, payload density and tank positions were varied. Figure 1-4 shows the basic 201 Vehicle and the four modified versions reflecting the fineness ratio (Vehicles 202 and 203) and payload density (Vehicles 204 and 205) variations. The fifth 201 derivative (Vehicle 202RT) is not shown here but is identical to the 202 Vehicle

VEHICLE DATA

Gross Weight at Liftoff	20,139,000 lbs (9,135,050 Kg)
First Stage Thrust	
At Liftoff	25,200,000 lbs (112,089,600 N)
Nominal (Vacuum)	28,337,000 lbs (126,042,976 N)
Vehicle Reference Diameter	65.5 ft. (19.96 m)
Aerodynamic Reference Area	3,369.55 sq. ft. (313.03 sq. m)
Vehicle Length	415.4 ft. (126.61 m)
First Stage Effective Nozzle Exit Area	215,909 sq. in. (139.26 sq. m)
First Stage Propellant Weight Flow Rate	95,093 lb/sec (43.134 Kg/sec)
Propellant Mixture Ratio	
First Stage N-1 (LOX/RP-1)	2.25
Second Stage N-11 (LOX/LH_2)	5.0
Number of Engines	14 F-1/3 M-1
Nominal Vehicle Structural Weight	
Second Stage Structure	304,134 lbs (137,955 Kg)
First Stage Structure	452,171 lbs (205,105 Kg)
Total Vehicle Structure	756,305 lbs (343,060 Kg)
Nominal Payload	811,000 lbs (367,870 Kg)

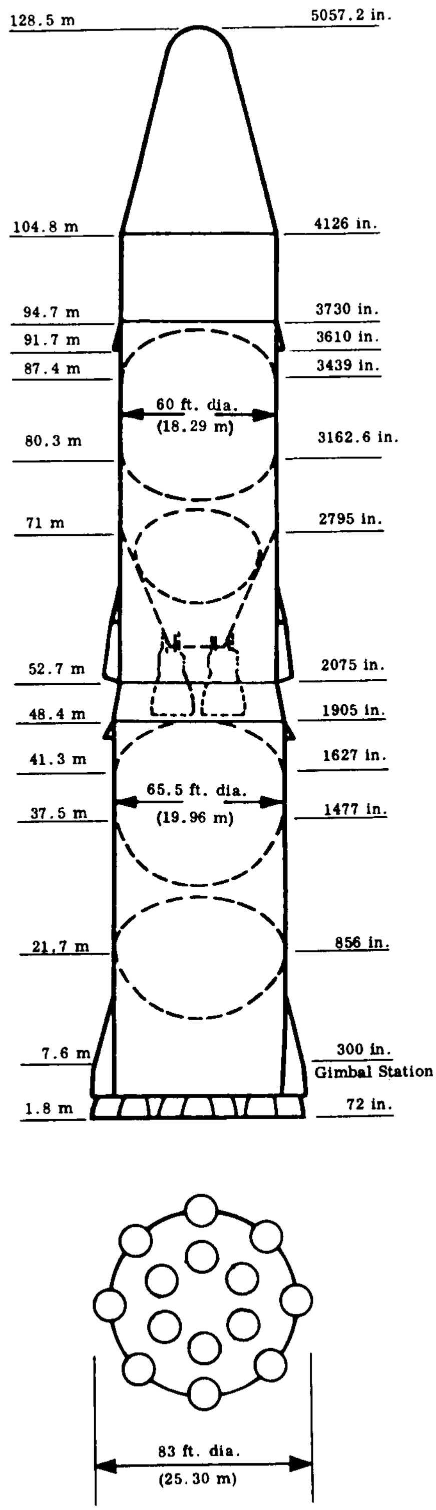

Figure 1-1. Vehicle 101 Configuration

VEHICLE DATA

Gross Weight at Liftoff	14,400,000 lbs (6,531,840 Kg)
Thrust	
At Liftoff	18,000,000 lbs (80,064,000 N)
Nominal (Vacuum)	21,851,000 lbs (97,193,248 N)
Vehicle Reference Diameter	70 ft. (21.34 m)
Aerodynamic Reference Area	3,848.45 sq. ft. (357.52 sq. m)
Vehicle Length	422.5 ft. (128.78 m)
Effective Nozzle Exit Area	262,044 sq. in. (169.02 sq. m)
Propellant Weight Flow Rate	47,452 lb/sec (21,524 Kg/sec)
Propellant Mixture Ratio	
N-1 (LOX/LH_2)	6.5
N-11 (LOX/LH_2)	6.5
Number of Engines	18/2 High Pressure
Nominal Vehicle Structural Weight	
Second Stage Structure	123,429 lbs (55,987 Kg)
First Stage Structure	567,393 lbs (257,369 Kg)
Total Vehicle Structure	690,822 lbs (313,356 Kg)
Nominal Payload	1,019,000 lbs (462,218 Kg)

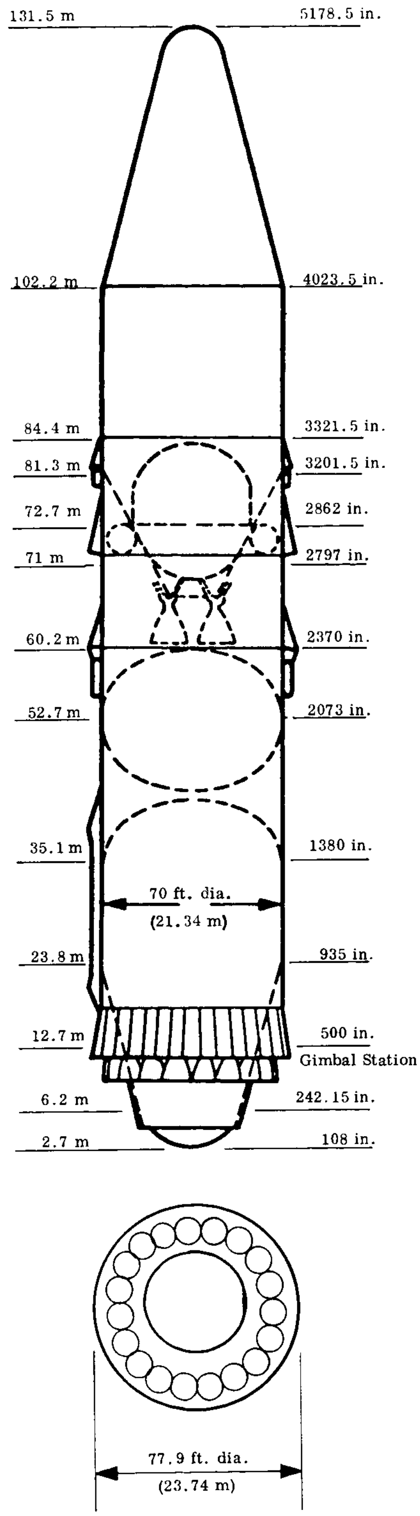

Figure 1-2. Vehicle 201 Configuration

VEHICLE DATA

Gross Weight at Liftoff	24,000,000 lbs (10,886,400 Kg)
Thrust	
At Liftoff	30,000,000 lbs (133,440,000 N)
Nominal (Vacuum)	35,570,000 lbs (158,215,360 N)
Vehicle Reference Diameter	80.0 ft. (24.38 m)
Aerodynamic Reference Area	5,026.548 sq. ft. (466.966 sq. m)
Vehicle Length	402.1 ft. (122.57 m)
Effective Nozzle Exit Area	379,008 sq. in. (244.46 sq. m)
Propellant Weight Flow Rate	79,576 lb/sec (36,096 Kg/sec)
Propellant Mixture Ratio	(LOX/LH_2) 7.0
Number of Engine Modules	24 High Pressure
Nominal Vehicle Structural Weight	641,320 lbs (290,903 Kg)
Nominal Payload	1,358,000 lbs (615,989 Kg)

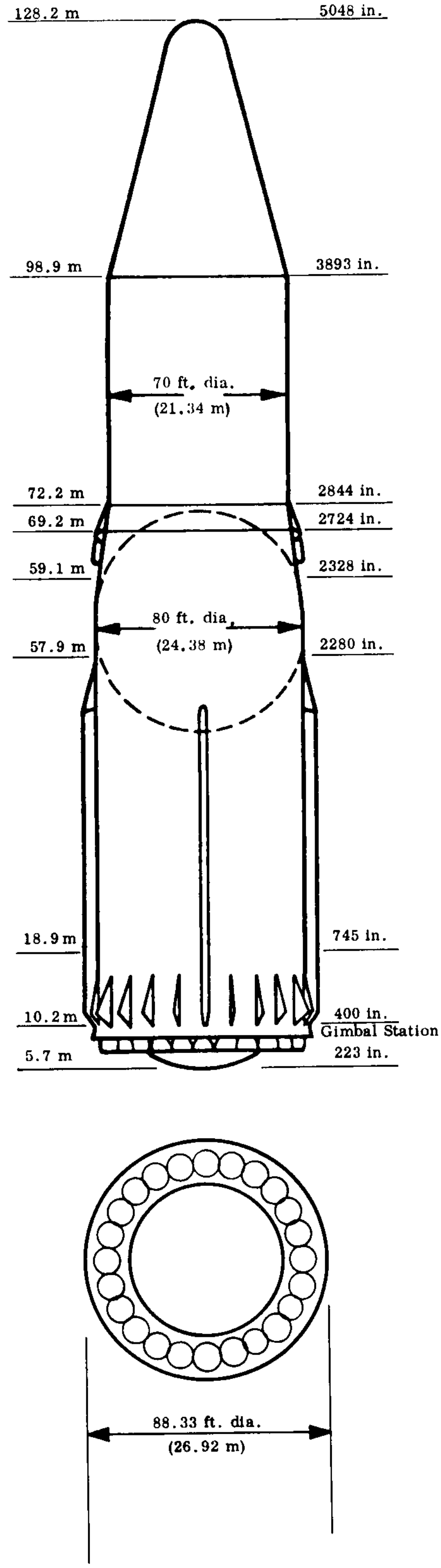

Figure 1-3. Vehicle 301 Configuration

201 CONFIGURATION
Diameter - 70' -840"
Length - 422.5' -5070.5"
L/D - 6.04
Payload Density - 2.5 Lb/Ft^3

202 CONFIGURATION
Diameter - 55' - 660"
Length - 531.0' - 6372.2"
L/D - 9.65
Payload Density - 2.5 Lb/Ft^3

203 CONFIGURATION
Diameter - 80' - 960"
Length - 377.5' - 4529.6"
L/D - 4.72
Payload Density - 2.5 Lb/Ft^3

204 CONFIGURATION
Diameter - 70' - 840"
Length - 387.7' - 4652.4"
L/D - 5.54
Payload Density - 4.0 Lb/Ft^3

205 CONFIGURATION
Diameter - 70' - 840"
Length - 364.0' - 4368.6"
L/D - 5.2
Payload Density - 6.2 LB/Ft^3

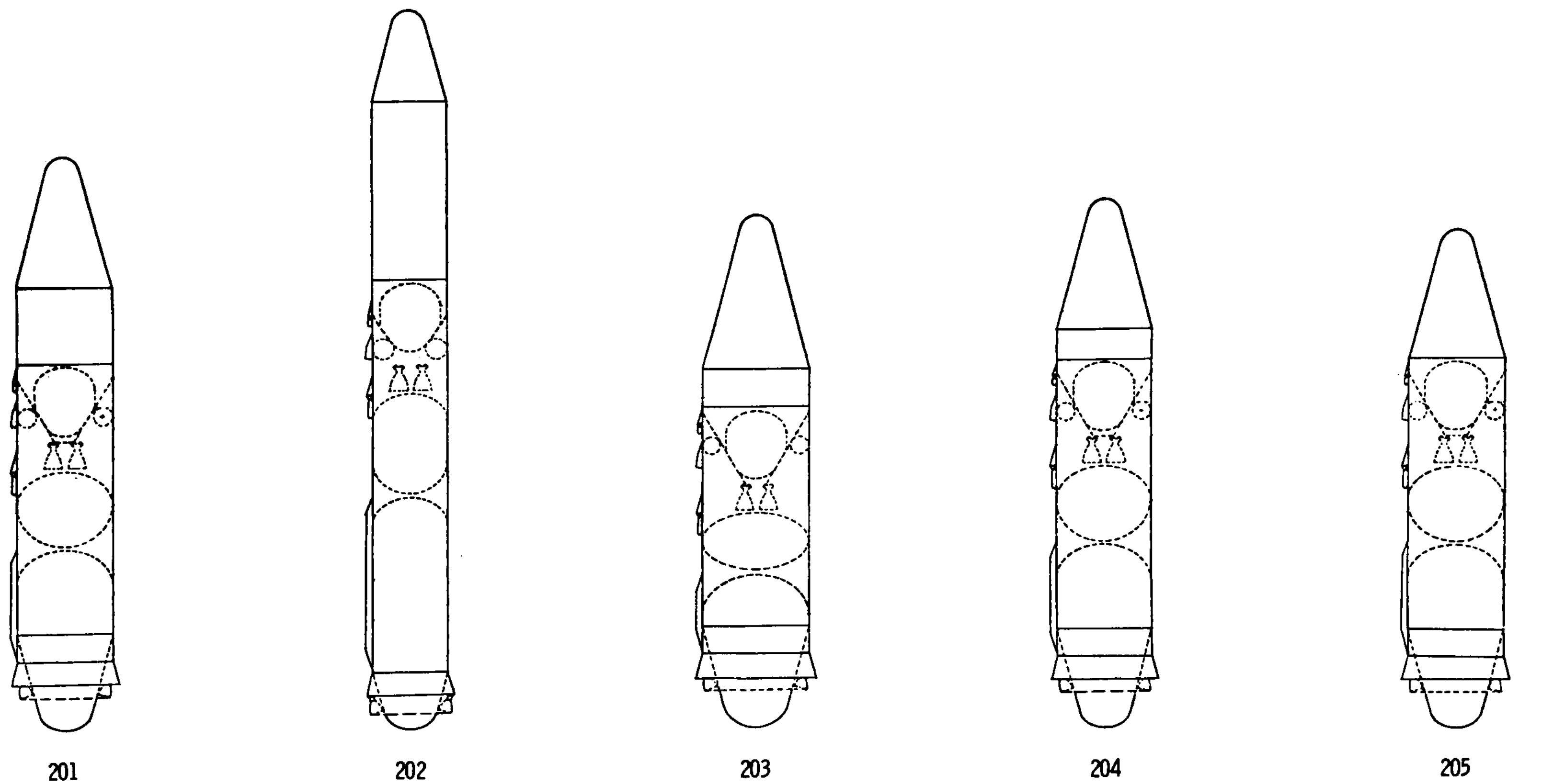

Figure 1-4. Variations of 201 Configuration

except that the first-stage propellant tank positions are reversed. This was done as a part of the investigation of front-end steering—to evaluate the effect of mass distribution.

These parametric analyses were performed with the aid of specialized computational modules developed by the General Electric Company in earlier efforts. These modules, described in Appendices A and B, were integrated into a novel approach to parametric analysis of structures to enable the efficient evaluation of a very large number of individual and combined parameter variations. This procedure, which is discussed in detail in Section 2, reduced the data handling task to manageable proportions.

The remaining study topics, not involving parametric analyses, consisted of special studies which evaluated the effects of varying design approaches and analysis techniques. These were conducted primarily as analytical efforts, using small, specialized computer programs where necessary.

Structural weight sensitivities were determined by calculating the aggregate structural weight of each vehicle when designed to meet the specified design criteria and configuration. In a typical vehicle, the various sections were calculated by several different methods, some employing the above computation modules and some by special hand calculations. Table 1-1 illustrates the method of analysis (analytical and numerical) for a typical vehicle used in this study.

Since the objectives of the study included development of data suitable for planning structural research efforts, the parameter and technology variations were not limited to current state of the art. These currently practical limitations were relaxed so that the most profitable areas for future advancement might be identified.

Volume 1 of this report presents a summary discussion of the study approach and its principal results and conclusions. This volume presents the technical details of the study. Section 2 describes the parametric analysis procedure in detail while the remaining sections discuss, in depth, the parametric analysis and special studies.

Table 1-1

Methods of Analysis for a Typical Vehicle

Vehicle 201

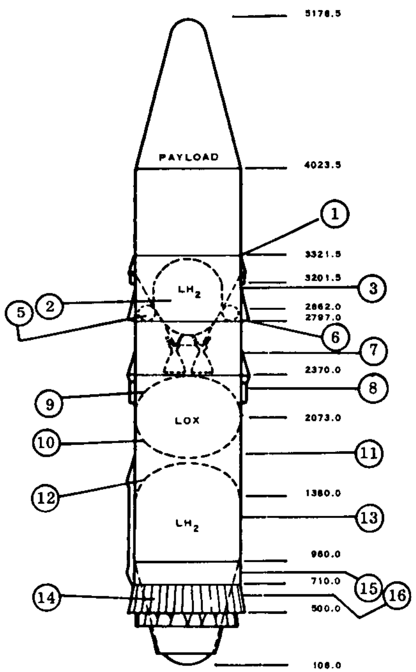

*The payload is all forward of station 3321.5 and was not analyzed in this study.

Components*	Location	Analytic Procedure
(1) Instrument Unit (IU) and Forward Skirt	Stations 3201.5 to 3321.5	This is unpressurized section and was analyzed by automated methods of Reference 19 and Appendix A.
(2) LH_2 Tank and Thrust Structure (Stage II)	Stations 2634 to 3285.5	These components are analyzed by special methods considering combined pressure, inertia, and thrust loads. Refer to paragraph 6.9.
(3) Intertank	Stations 2862 to 3201.5	This is an unpressurized section and was analyzed by the automated methods of Reference 19 and Appendix A.
(4) Baffles and Insulation (Stage II)	NA	These items were not analyzed numerically for this study but were estimated from data given in References 1 through 4.
(5) LOX Tank (Stage II)	Station 2862	Analyzed by membrane analysis for hydrostatic and ullage pressures. See paragraph 6.9.
(6) Aft Skirt (Stage II)	Stations 2797 to 2862	This is an unpressurized section and is analyzed by the automated methods of Reference 19 and Appendix A.
(7) Interstage	Stations 2370 to 2797	This is an unpressurized section and is analyzed by the automated methods of Reference 19 and Appendix A.
(8) Forward Skirt (Stage I)	Stations 2073 to 2370	This is an unpressurized section and is analyzed by the automated methods of Reference 19 and Appendix A.
(9) LOX Tank Top Head (Stage I)	Stations 2073 to 2307	This is an elliptical upper dome head of a bulkhead tank and is analyzed by the automated methods of Reference 19 and Appendix A.
(10) LOX Tank Bottom Head (Stage I)	Stations 1713 to 2073	This is an elliptical lower dome of a bulkhead tank and is analyzed by the automated methods of Reference 19 and Appendix A.
(11) Intertank	Stations 1380 to 2073	This is an unpressurized section and is analyzed by the automated methods of Reference 19 and Appendix A.
(12) LH_2 Tank Top Head (Stage I)	Stations 1380 to 1587	This is an elliptical upper dome head of a bulkhead tank and is analyzed by the automated methods of Reference 19 and Appendix A.
(13) LH_2 Tank Cylinder (Stage I)	Stations 960 to 1380	This is a pressure relieved compression cylinder and is analyzed by the methods of Reference 19 and Appendix A.
(14) LH_2 Tank Bottom Head (Stage I)	Stations 108 to 960	This is a hung tank composed of a conical and spherical parts. It is analyzed similar to the components in (2).
(15) Thrust Takeout	Stations 710 to 960	This is an unpressurized section and is analyzed by the automated methods of Reference 19 and Appendix A.
(16) Thrust Structure	Stations 500 to 710	This is a special hand calculation. The solution is discussed in paragraph 6.8. A sample calculation for the 201 is included.
(17) Baffles and Insulation (Stage I)	NA	These items were not analyzed numerically for this study but were estimated from data given in References 1 through 5.

SECTION 2

ANALYSIS PROCEDURES AND BASIC EQUATIONS

2.1 GENERAL

Structural weight sensitivities were determined for a wide spectrum of variables. Literally tens of thousands of possible vehicles, featuring changes of one or several parameters, were analyzed using automated computation systems whenever possible. Special studies, involving either hand calculations or "one shot" computer programs written by the investigating engineer, supplemented these automated calculations. A series of continuing supporting studies simultaneously provided the basic data for the above parametric studies, as well as supplying a source of ready reference material.

The emphasis of this section will be the explanation of the automated analyses. The details of the special studies and the continuing supporting studies are dealt with in Sections 6 and 7 of this volume. Coverage of the automated analyses is presented in the following three paragraphs of this section. First, the basic equations used in the loads analysis will be presented. This will be followed by a detailed account of the organization and use of the basic tools for structural analysis which were developed during this study. The last paragraph will briefly summarize the overall procedure for evaluating structural weights for various vehicle designs.

2.2 BASIC EQUATIONS

The major structural elements of a launch vehicle were represented as thin shells of revolution. It was further assumed that all structural loads were axisymmetric.

The axial force transmitted along the vehicle axis was derived from three sources:

a. The axial thrust loads.

b. The bending moment.

c. The tank pressure.

The magnitudes of these three loads were considered to be dependent upon the location along the vehicle axis and the time of flight. The total equivalent axial force at a distance "x" along the vehicle axis for an arbitrary flight time "t," is expressed by Equation 2-1.

$$F(x, t) = -T(x, t) \pm \frac{2M(x, t)}{R(x)} + \pi R^2(x)\, P(x, t) \tag{2-1}$$

where:

F is the total axial force.

M is the bending moment.

T is the axial force resulting from the thrust load.

P is the local pressure (gauge) in the propellant tank.

R is the local radius of the vehicle structure.

In the above equation, the minus sign signifies compression and the plus sign signifies tension. The plus or minus sign on the bending moment term results from the non-axisymmetry of the bending load. Since there is no preferential direction for the bending moment to act, either the plus or minus sign was chosen to produce the most severe load. The thrust loads are compressive and the pressure loads are tensile. In performing a buckling analysis on a shell, the terms of Equation 2-1 were chosen such that the maximum compressive load was developed. Thus, the minus sign was used for the bending moment term which would add to the compressive thrust load. The pressure load, on the other hand, has a positive sign and tends to relieve the compressive loads. Design loads are obtained by increasing the limit loads by the factors of safety with the exception that pressure relieving loads are left unchanged. Hence, the first two terms of Equation 2-1 were multiplied by the factor of safety to obtain the design load, and the pressure term added directly to the design load without increase.

For convenience, the load defined by Equation 2-1 was divided by the local circumference of the shell to yield a stress resultant (or load intensity) N_x as shown by Equation 2-2.

$$N_x(x, t) = \frac{-T(x, t)}{2\pi R(x)} \pm \frac{M(x, t)}{\pi R^2(x)} + \frac{P(x, t) R(x)}{2} \qquad (2\text{-}2)$$

In a similar manner, the hoop loads due to the tank pressures were divided by the local circumference of the shell to obtain the stress resultant N_y given by Equation 2-3.

$$N_y = R(x) P(x, t) + \beta(t) \gamma d(x) R(x) \qquad (2\text{-}3)$$

where:

P is the local pressure (gauge) in the propellant tank.

R is the local radius of the vehicle structure.

β is the instantaneous acceleration in g's.

γ is the specific weight of the propellant in the tanks.

d is the distance of station "x" below the level of the propellant.

The relative directions of N_x and N_y are shown on typical shell elements in Figure 2-1.

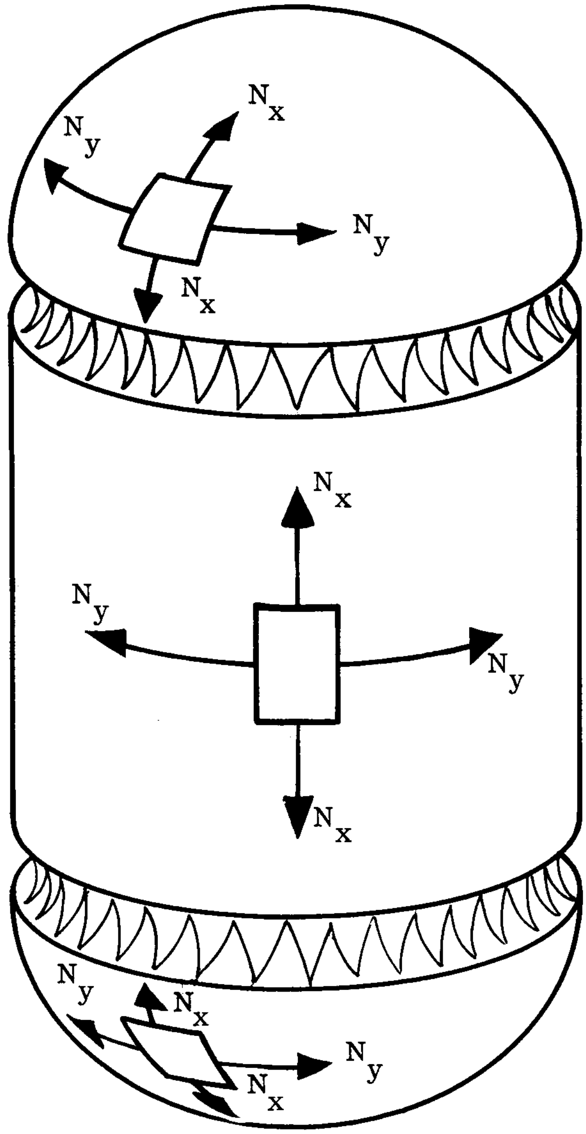

Figure 2-1. Representation of Stress Resultants on Typical Shells

All possible failure modes were considered in applying these loads to the analysis of the vehicle structure. In general, all failure modes were classified in two categories—stability failures and strength failures. The buckling modes of failure were considered to be sensitive only to the compressive axial loads, whereas, the strength modes of failure are dependent upon both the axial and hoop loads.

For isotropic materials, the Hencky-von Mises theory of failure was used to combine the biaxial components of load. The resulting equivalent stress resultant was used in the analysis of strength failures, based on the uniaxial strength properties of the structural materials evaluated. In terms of the biaxial stress resultants N_x and N_y, the equivalent uniaxial stress resultant N_o is expressed by Equation 2-4.

$$N_o = \left(N_x^2 - N_x N_y + N_y^2\right) \qquad (2\text{-}4)$$

where:

N_x is the axial (or meridional) stress resultant.

N_y is the hoop (or circumferential) stress resultant.

N_o is the equivalent uniaxial stress resultant.

Two other failure criteria (i.e., Hill's Criterion and the maximum principal stress criterion) were also applied during the study in order to evaluate the sensitivity of the structural weight to methods of combining the biaxial loads.

For anisotropic materials, such as filamentary compositities, the methods of combining N_y and N_x to predict strength failures were more complex. The variety of winding patterns, filament materials, and binder materials preclude generalizations about the interactions of stress components. For this reason, the relationship between loads and structural weight are treated differently than for isotropic materials as discussed in Section 5.

2.3 ANALYSIS PROCEDURES

2.3.1 THE CRITICAL LOADS ENVELOPE

The stress resultants N_x and N_o completely characterize (for isotropic materials) the loading of a structural element at any particular instant of time. Stability or buckling analyses are dependent on N_x and the strength analyses are dependent on N_o. The procedures for determining the critical values (i.e., the largest) of N_x and N_o were based on comparative selection from the loads at the five design points, as follows:

a. Prelaunch unpressurized.

b. Prelaunch pressurized.

c. Maximum $q\alpha$ product.

d. Maximum pressure on propellant tank bottom heads.

e. Maximum acceleration.

Each design point enumerated is shown in Figure 2-2. A stepwise procedure is included here to illustrate selection methods of $N_x(x, t)$.

Step 1—The N_x due to axial thrust loads, i.e.,

$$N_x(x, t) = \frac{-T(x, t)}{2\pi R(x)}$$

in Equation 2-2 was distributed along the vehicle as represented in Figure 2-2(a). For the prelaunch conditions, the load was the weight of the vehicle being carried through its own structure. The distribution of the inflight loads changed with time as the engine thrust increased with altitude and the propellants were expended.

Step 2—Adding the bending moments, i.e.,

$$N_x(x, t) = \frac{-T(x, t)}{2\pi R(x)} - \frac{M(x, t)}{\pi R^2(x)}$$

in Equation 2-2 the load distributions represented in Figure 2-2(b) were obtained. The prelaunch bending moments were greatest at the base of the vehicle and gradually attenuated to zero at the nose of the vehicle. Inflight bending moments, on the other hand, were greatest somewhere in the middle of the vehicle and attenuated toward both ends. The greatest inflight bending moments occurred at the maximum $q\alpha$ condition and were negligible at the time of maximum acceleration when the vehicles were outside the wind disturbances of the atmosphere.

Step 3—Adding the loads due to propellant tank pressures, i.e.,

$$N_x(x, t) = \frac{-T(x, t)}{2\pi R(x)} - \frac{M(x, t)}{\pi R^2(x)} + \frac{P(x, t) R(x)}{2}$$

modified the load distributions as shown in Figure 2-2(c). The pressures of the various propellant tanks vary throughout the vehicle's flight. This was used to advantage in decreasing the critical load of pressurized tank cylinders. There were limitations to be concerned with, however. By increasing the propellant tank pressure the critical values of N_x for the tank walls were decreased, but the critical loads on the heads of the tank were increased.

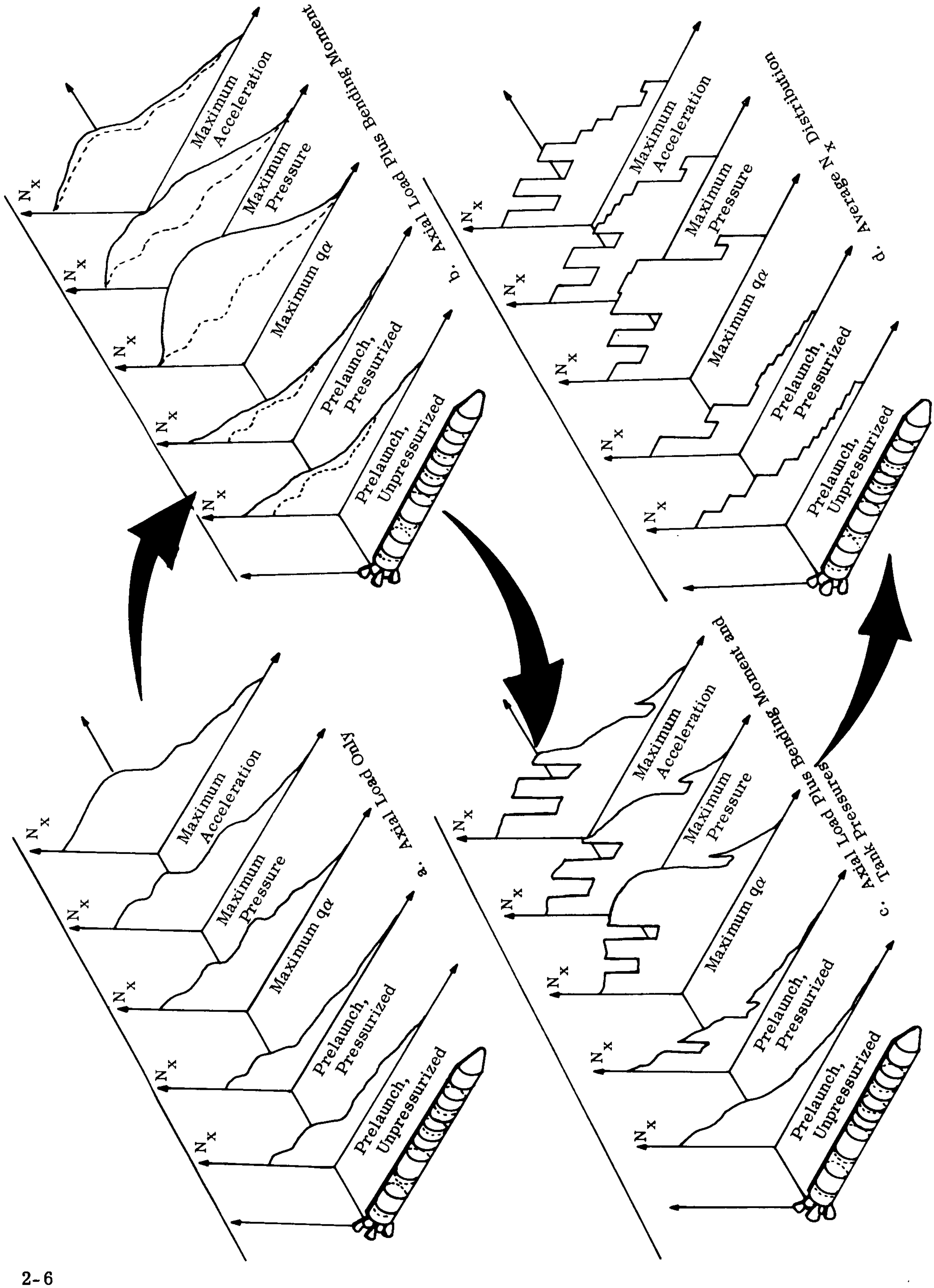

Figure 2-2. Construction of Loads Profile Envelope for a Typical Launch Vehicle

Step 4—The difficulties of representing the irregular load distributions of Figure 2-2(c) in a concise format were overcome by breaking the vehicle into several structural elements. The average value of N_x was then considered to be representative for each element. The vehicles were conveniently divided into 15 to 20 shells such as interstages, tank walls, tank heads, skirts, etc. Usually, the value of the stress resultant did not vary greatly along the separate structural elements, so the actual load distribution shown in Figure 2-2(c) is approximated as shown in Figure 2-2(d). The critical loads envelope was then developed by choosing the maximum value of N_x from the five design points for each of the structural elements of the vehicle.

A similar procedure was used to find the critical loads distribution for N_o. For unpressurized sections, there are no hoop loads so N_o is equal to N_x as can be seen in Equation 2-4. The critical loads envelope in the unpressurized cylinders, therefore, was completely described by the critical N_x envelope. The tank heads, on the other hand, carried no compressive loads so their loads envelopes were completely described by the critical N_o envelope. Only the pressurized tank cylinders required critical values of both N_x and N_o to describe the loading conditions.

In constructing the critical loads envelopes as represented in Figure 2-2 it was apparent that a total mission profile must be considered. For example, the prelaunch bending moment was significantly decreased by varying the prelaunch wind criteria. Major reductions in the vehicle loads at prelaunch resulted. However, reduction in the loads is not necessarily accompanied by a reduction in the structural weight, but is affected only by changes in the critical loads envelope. Since the prelaunch loads did not contribute to the critical load envelope, there was no advantage to decreasing the prelaunch wind loads from a structural weight point of view. Although the prelaunch loads were used as an example, the same arguments are valid when the loads at the other design points are considered. Before any valid conclusions could be drawn from the evaluation of changes in the loads at a particular design point, the impact on the critical loads profile was considered.

It was also observed that each of the structural elements can derive its critical load from different design points. For instance, an interstage might be designed by the loads occurring at the time of maximum $q\alpha$, and a tank wall of the same vehicle might be designed by the loads occurring at the time of maximum acceleration. For a particular structural element, it was also observed that the critical values of N_o and N_x are not necessarily derived from the same design point.

Although Figure 2-2 serves well to illustrate the method of constructing a critical loads envelope, it does not lend itself to a concise presentation of the numerical data associated with a particular configuration. Consider instead the tabular presentation of data as shown in Table 2-1. Each row of this table describes the load distribution for one of the five design points shown in Figure 2-2.

The columns of Table 2-1 are associated with the structural elements (or sections) of a typical vehicle which are numbered as indicated. The entries of numerical data in the rows of Table 2-1 are the average values of N_x and N_o for their respective sections of the vehicle structure as illustrated in Figure 2-2(d). The critical load distribution was constructed by choosing the largest numerical value in each column. As was explained earlier, the pressurized tank cylinders were identified with critical values of both N_x and N_o. Another simplification was employed by normalizing the entries in each column of Table 2-1 with respect to the nominal critical load of that section. This resulted in a presentation of the data as shown in Table 2-2.

The load distributions presented in Table 2-1 and Table 2-2 were based on one set of load parameters such as inflight winds, prelaunch winds, maximum boost accelerations, type of nozzle, and propellant tank pressures. When different values of these load parameters were considered, the load distributions for the five design points changed. The net effect was that Tables 2-1 and 2-2 gained additional rows of data for each design point. Considering the 201 Vehicle configuration as an example, the Loads Summary Chart shown in Table 2-3 is an expansion of the format of Table 2-2. The load distributions associated with several representative values of the load parameters of interest were summarized in this chart. Loads were normalized with respect to the critical load distribution associated with the nominal loading conditions.

The nominal load parameters listed below are considered to be representative of current design practices.

Prelaunch Winds	99.9 percent probability of occurrence, vehicle pressurized or unpressurized (vented).
Inflight Winds	95 percent probability of occurrence, vehicle pressurized.
Maximum Boost Acceleration	101 Vehicle—4.8 g's. All 200 Series Vehicles—5.55 g's. 301 Vehicle—2.5 g's.
Type of Nozzle	101 Vehicle—Gimbal Nozzle All Others—Plug Nozzle

Table 2-1

Example of Load Distributions at Design Points

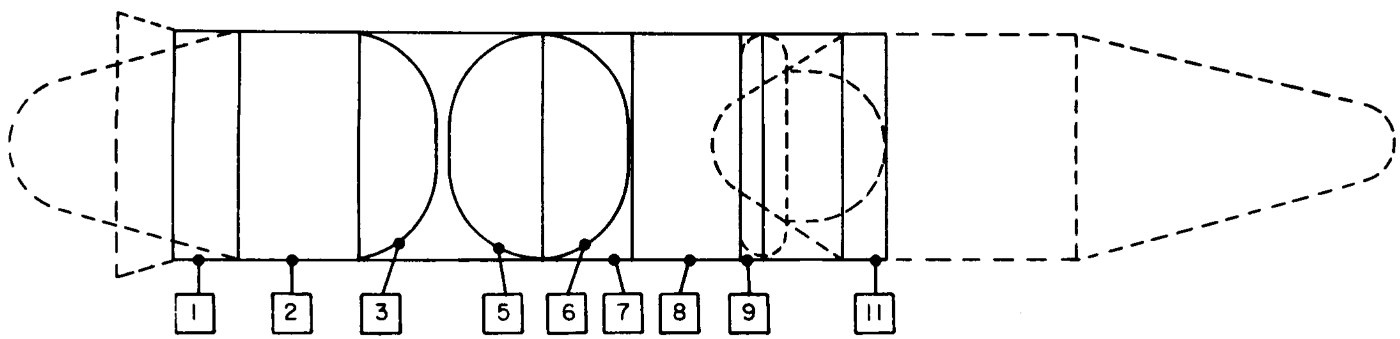

Loading Conditions \ Section Number	N_x Distribution, $\frac{\text{lbs.}}{\text{Inch}}$						N_o Distribution, $\frac{\text{lbs.}}{\text{Inch}}$			
	1	2	7	8	9	11	2	3	5	6
Prelaunch Unpressurized	-6647	-5837	-1906	-1557	-1426	-620	-6130	-41	-4721	-1415
Prelaunch Pressurized	-6647	-4591	-1906	-1557	-1426	-620	-7034	-1969	-5312	-1581
Maximum $q\alpha$	-10163	-6457	-6379	-5538	-5111	-3069	-13193	-5436	-8842	-3352
Maximum Pressure	-7927	-2344	-4519	-4194	-4029	-1467	-13710	-7657	-9386	-4308
Maximum Acceleration	-7958	-2189	-6617	-6279	-6041	-2197	-14356	-8137	-4402	-4308
Critical Loads Distribution	-10163	-6457	-6617	-6279	-6041	-3069	-14356	-8137	-9386	-4308

Table 2-2
Example of Normalized Load Distributions at Design Points

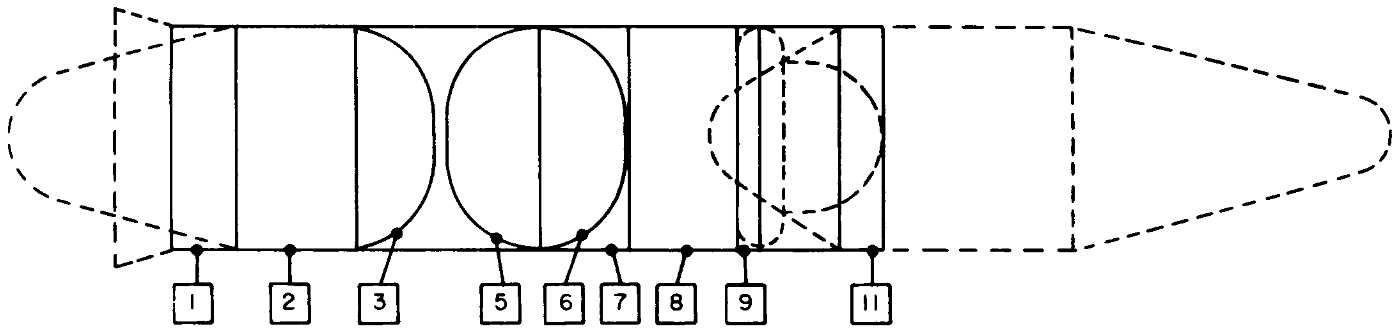

Loading Conditions \ Section Number	$\frac{N_x}{N_{x_{nominal}}}$ Distribution: 1	2	7	8	9	10	$\frac{N_o}{N_{o_{nominal}}}$ Distribution: 2	3	5	6
Prelaunch Unpressurized	.654	.904	.288	.248	.236	.202	.427	.005	.503	.347
Prelaunch Pressurized	.654	.711	.288	.248	.236	.202	.490	.242	.566	.367
Maximum $q\alpha$	1.000	1.000	.964	.882	.846	1.000	.919	.668	.942	.778
Maximum Pressure	.780	.363	.683	.668	.667	.478	.955	.941	1.000	1.000
Maximum Acceleration	.783	.339	1.000	1.000	1.000	.716	1.000	1.000	.469	1.000
Critical Loads Distribution	1.000	1.000	1.000	1.000	1.000	1.000	1.000	1.000	1.000	1.000

Table 2-3

Loads Summary Chart
201 Vehicle Configuration

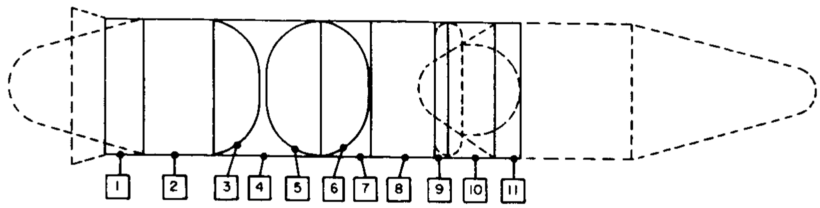

Loading Condition				Section											
				N_x/N_x Nominal								N_θ/N_θ Nominal			
				1	2	4	7	8	9	10	11	2	3	5	6
Prelaunch	99.9% Ground Winds		Unpressurized Tanks	.654	.904	.524	.288	.248	.236	.224	.202	.427	.005	.503	.347
			Pressurized Tanks	.654	.711	.524	.288	.248	.236	.224	.202	.490	.242	.566	.367
	95.0% Ground Winds		Unpressurized Tanks	.574	.797	.477	.233	.204	.199	.176	.155	.380	.005	.503	.347
			Pressurized Tanks	.574	.605	.477	.233	.204	.199	.176	.155	.450	.242	.566	.367
Maximum qα	95% Inflight Winds	Pressurized Tanks	Plug Nozzle	1.000	1.000	1.000	.964	.882	.846	1.000	1.000	.919	.668	.942	.778
			Front Steering	.767	.566	.680	.502	.504	.525	.616	.716	.781	.668	.942	.778
			Gimbal Nozzle	.801	.775	.934	.906	.843	.821	.970	.973	.841	.668	.942	.778
		Vented Tanks	Plug Nozzle	1.000	1.530	1.000	.964	.882	.846	1.000	1.000	.699	0.0	.710	.053
			Front Steering	.767	1.093	.680	.502	.504	.525	.616	.716	.505	0.0	.710	.053
			Gimbal Nozzle	.801	1.323	.934	.906	.843	.821	.970	.973	.586	0.0	.710	.053
	90% Inflight Winds	Pressurized Tanks	Plug Nozzle	.991	.985	.986	.942	.863	.829	.975	.975	.913	.668	.942	.778
			Front Steering	.767	.565	.679	.499	.500	.520	.606	.702	.781	.668	.942	.778
			Gimbal Nozzle	.800	.764	.923	.887	.826	.804	.946	.948	.839	.668	.942	.778
		Vented Tanks	Plug Nozzle	.991	1.513	.986	.942	.863	.829	.975	.975	.692	0.0	.710	.053
			Front Steering	.767	1.093	.679	.499	.500	.520	.606	.702	.505	0.0	.710	.053
			Gimbal Nozzle	.800	1.293	.923	.887	.826	.804	.946	.948	.591	0.0	.710	.053
Maximum Total Pressure	5.55 g's		Pressurized Tanks	.780	.363	.666	.683	.668	.667	.553	.478	.955	.941	1.000	1.000
			Vented Tanks	.780	1.121	.666	.683	.668	.667	.553	.478	.505	0.0	.771	0
Maximum Boost Acceleration	5.55 g's	Pressurized Tanks	Plug Nozzle	.783	.339	.653	1.000	1.000	1.000	.829	.716	1.000	1.000	.469	1.000
			Front Steering	.783	.339	.653	1.000	1.000	1.000	.829	.716	1.000	1.000	.469	1.000
			Gimbal Nozzle	.783	.339	.653	1.000	1.000	1.000	.829	.716	1.000	1.000	.469	1.000
		Vented Tanks	Plug Nozzle	.783	1.125	.653	1.000	1.000	1.000	.829	.716	.506	0.0	.076	0
			Front Steering	.783	1.125	.653	1.000	1.000	1.000	.829	.716	.506	0.0	.076	0
			Gimbal Nozzle	.783	1.125	.653	1.000	1.000	1.000	.829	.716	.506	0.0	.076	0
	2.0 g's	Pressurized Tanks	Plug Nozzle	.836	.652	.746	.564	.523	.514	.523	.503	.835	.702	.997	.814
			Front Steering	.778	.545	.668	.451	.430	.435	.428	.431	.804	.702	.997	.814
			Gimbal Nozzle	.785	.594	.729	.550	.513	.507	.515	.496	.818	.702	.997	.814
		Vented Tanks	Plug Nozzle	.836	1.206	.746	.564	.523	.514	.523	.503	.555	0.0	.771	.010
			Front Steering	.778	1.100	.668	.451	.430	.435	.428	.431	.507	0.0	.771	.010
			Gimbal Nozzle	.785	1.148	.729	.550	.513	.507	.515	.496	.528	0.	.771	.010

The specific pressure profiles for the propellant tanks, and the synthetic wind profiles are presented in detail in Section 3 of this volume.

The loads summary chart of Table 2-3 is a flexible tool which was developed to help obtain the critical load envelopes for a variety of loading conditions. This was done by selecting the appropriate rows from the loads summary chart, corresponding to the design points and load conditions of interest. These selected rows were then arranged in a format similar to the one presented in Table 2-2. Then, the critical loads envelope was obtained by selecting the largest number in each column.

2.3.2 USE OF WEIGHT/LOAD RELATIONSHIPS

Once the critical load envelopes were identified, the evaluation of the weight of the structure necessary to sustain these loads remained. Toward this end, Weight/Load matrices were developed. Typical examples of these matrices are shown in Figure 2-3. These matrices present the structural weights of various sections of the vehicle over a range of the normalized values of N_x and N_o. Each matrix presents the weight of a structural element for several types of wall construction and for a specific material. A collection of the Weight/Load matrices used in this study is presented in Appendix C for various materials and types of construction.

When the critical loads envelope was established, the structural weights of the vehicle sections could be obtained by interpolation. For example, under the conditions of nominal load, the normalized values of N_x and N_o were 1.0 and 1.0 respectively. From Figure 2-3, therefore, the weight of the 201 Vehicle first stage hydrogen tank cylinder (Section Number 2), constructed of aluminum honeycomb sandwich was 40,281 pounds. If the load parameters were such that the critical values of the normalized stress resultants N_x and N_o are 0.7 and 0.9 respectively, the weight of Section 2 made with aluminum honeycomb sandwich was 36,090 pounds. Interpolation between the normalized values of N_x and N_o yields the structural weight associated with any critical load considered.

2.3.3 WEIGHT/LOAD RELATIONSHIPS—COMPOSITES

The weight/load relationships for the filamentary composite materials were somewhat different due to the complexity of the failure modes. The structural weights of compressively loaded cylinders were obtained with the aid of curves, such as those presented in Figure 2-4. This figure is a plot of W/R versus N_x/R where W is the weight per square foot of surface area and R is the local radius of the shell in inches. Three types of construction are considered in this figure—monocoque and honeycomb sandwich

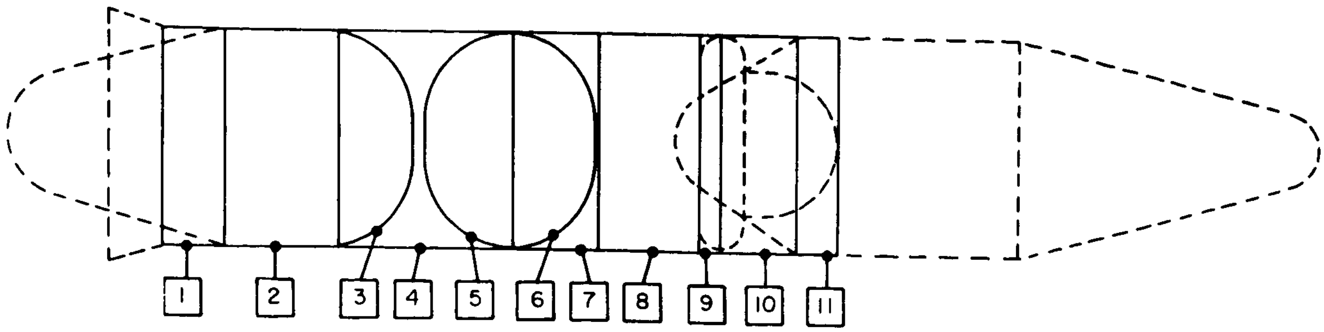

201 Vehicle Configuration
Section Number 1
Thrust Takeout (710" - 960")

Material: Aluminum, 2219-T87
N_x Nominal: -10,163 lb/in.
N_o Nominal: 10,163 lb/in.

$\frac{N_x}{N_x \text{ Nom}}$ ↓	$\frac{N_o}{N_o \text{ Nom}}$ →	.7	.8	.9	1.0	1.1
.7	HYC	17,842				
	ISS	39,517				
	MON	79,861				
	OFC	35,005				
	SFC	30,427				
.8	HYC		20,164			
	ISS		43,665			
	MON		84,074			
	OFC		37,421			
	SFC		32,553			
.9	HYC			22,462		
	ISS			48,896		
	MON			87,975		
	OFC			39,692		
	SFC			34,552		
1.0	HYC				24,754	
	ISS				53,698	
	MON				91,616	
	OFC				41,962	
	SFC				36,448	
1.1	HYC					27,038
	ISS					57,125
	MON					95,041
	OFC					43,881
	SFC					41,362

201 Vehicle Configuration
Section Number 2
LH_2 Tank Cylinder (960" - 1380")

Material: Aluminum, 2219 - T87
N_x Nominal: - 6,457 lbs/in.
N_o Nominal: 14,356 lbs/in.

$\frac{N_x}{N_x \text{ Nom}}$ ↓	$\frac{N_o}{N_o \text{ Nom}}$ →	.7	.8	.9	1.0	1.1
.7	HYC	28,520	32,290	36,090	39,911	43,747
	ISS	59,754	59,754	59,754	59,754	59,754
	MON	116,596	116,596	116,596	116,596	116,596
	OFC					
	SFC					
.8	HYC	28,690	32,440	36,226	40,035	43,860
	ISS	60,867	60,867	60,867	60,867	60,867
	MON	122,747	122,747	122,747	122,747	122,747
	OFC					
	SFC					
.9	HYC	28,869	32,591	36,360	40,157	43,974
	ISS	61,984	61,984	61,984	61,984	61,984
	MON	128,442	128,442	128,442	128,442	128,442
	OFC					
	SFC					
1.0	HYC	29,120	32,746	36,496	40,281	44,088
	ISS	63,411	63,411	63,411	63,411	63,411
	MON	133,759	133,759	133,759	133,759	133,759
	OFC					
	SFC					
1.1	HYC	29,841	32,932	36,634	40,404	44,201
	ISS	67,484	67,484	67,484	67,484	67,484
	MON	138,758	138,758	133,758	138,758	138,758
	OFC					
	SFC					

201 Vehicle Configuration
Section Number 3
LH_2 Tank Top Head

Material: Aluminum, 2219 - T87
N_x Nominal: ----
N_o Nominal: 8,137 lbs/in.

$\frac{N_x}{N_x \text{ Nom}}$ ↓	$\frac{N_o}{N_o \text{ Nom}}$ →	.7	.8	.9	1.0	1.1
.7	HYC					
	ISS					
	MON					
	OFC					
	SFC					
.8	HYC					
	ISS					
	MON					
	OFC					
	SFC					
.9	HYC					
	ISS					
	MON					
	OFC					
	SFC					
1.0	HYC	13,394	15,291	17,188	19,085	20,982
	ISS					
	MON	11,154	12,748	14,341	15,935	17,528
	OFC					
	SFC					
1.1	HYC					
	ISS					
	MON					
	OFC					
	SFC					

201 Vehicle Configuration
Section Number 4
Intertank (1380" - 2073")

Material: Aluminum, 2219 - T87
N_x Nominal: -10,334 lbs/in.
N_o Nominal: 10,334 lbs/in.

$\frac{N_x}{N_x \text{ Nom}}$ ↓	$\frac{N_o}{N_o \text{ Nom}}$ →	.7	.8	.9	1.0	1.1
.7	HYC	53,173				
	ISS	115,361				
	MON	235,813				
	OFC	126,048				
	SFC	90,154				
.8	HYC		60,097			
	ISS		127,605			
	MON		248,253			
	OFC		134,751			
	SFC		96,316			
.9	HYC			66,958		
	ISS			145,892		
	MON			259,770		
	OFC			142,925		
	SFC			102,235		
1.0	HYC				73,784	
	ISS				156,026	
	MON				270,524	
	OFC				150,657	
	SFC				107,841	
1.1	HYC					80,633
	ISS					165,879
	MON					280,635
	OFC					158,010
	SFC					122,378

201 Vehicle Configuration
Section Number 5
LOX Tank Bottom Head

Material: Aluminum, 2219 - T87
N_x Nominal: ----
N_o Nominal: 9,386 lbs/in.

$\frac{N_x}{N_x \text{ Nom}}$ ↓	$\frac{N_o}{N_o \text{ Nom}}$ →	.7	.8	.9	1.0	1.1
.7	HYC					
	ISS					
	MON					
	OFC					
	SFC					
.8	HYC					
	ISS					
	MON					
	OFC					
	SFC					
.9	HYC					
	ISS					
	MON					
	OFC					
	SFC					
1.0	HYC	16,227	18,527	20,827	23,127	25,427
	ISS					
	MON	13,523	15,455	17,387	19,318	21,250
	OFC					
	SFC					
1.1	HYC					
	ISS					
	MON					
	OFC					
	SFC					

201 Vehicle Configuration
Section Number 6
LOX Tank Top Head

Material: Aluminum, 2219 - T87
N_x Nominal: ----
N_o Nominal: 4,308 lbs/in.

$\frac{N_x}{N_x \text{ Nom}}$ ↓	$\frac{N_o}{N_o \text{ Nom}}$ →	.7	.8	.9	1.0	1.1
.7	HYC					
	ISS					
	MON					
	OFC					
	SFC					
.8	HYC					
	ISS					
	MON					
	OFC					
	SFC					
.9	HYC					
	ISS					
	MON					
	OFC					
	SFC					
1.0	HYC	7,403	8,445	9,486	10,527	11,568
	ISS					
	MON	6,122	6,997	7,871	8,746	9,620
	OFC					
	SFC					
1.1	HYC					
	ISS					
	MON					
	OFC					
	SFC					

Figure 2-3. Typical Weight/Load Matrices

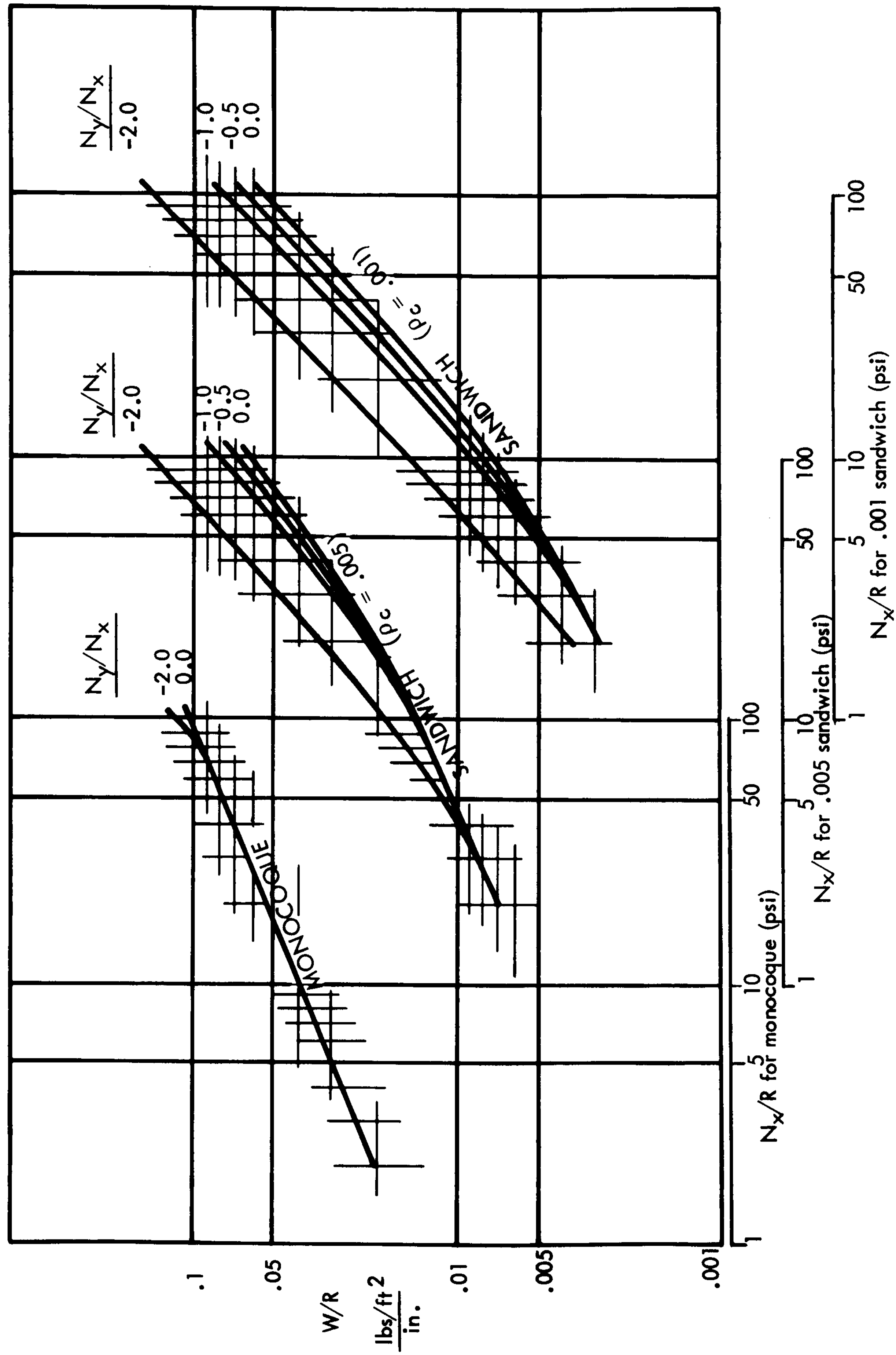

Figure 2-4. Typical Weight/Load Relationships for Composite Materials

with two different core densities. It is important to notice that abscissae for the three different materials are shifted one cycle relative to one another to avoid the confusion of overlapping curves. There is a family of curves for each type of construction for various values of N_y/N_x. For unpressurized cylinders N_y is zero but pressurized tank cylinders can have relatively large values of N_y. The application of these curves is demonstrated by the following example.

Consider a cylindrical shell 1000 inches long with a 400-inch radius. The critical values of N_x and N_y for this shell are taken to be -4000 lbs/inch and 8000 lbs/inch respectively. Therefore

$$\frac{N_x}{R} = \frac{-4000}{400} = -10 \text{ lbs/inch}^2$$

and

$$\frac{N_y}{N_x} = \frac{8000}{-4000} = -2.0$$

From Figure 2-3 for a honeycomb sandwich construction with a core density of 0.001 lbs/inch^3, it is found that

$$\frac{W}{R} = \frac{0.015 \text{ lbs/ft}^2}{\text{inch}}$$

or

$$W = (0.015)(400 \text{ inches}) = 6.0 \text{ lbs/ft}^2$$

The surface area of the shell is

$$\begin{aligned} A &= 2\pi R \ell \\ &= 2\pi (400)(1000) \times \frac{1}{144} \\ &= 17{,}453 \text{ ft}^2 \end{aligned}$$

The total weight of the shell is therefore

$$\text{Total Weight} = W A = (6.0)(17{,}453) = 104{,}720 \text{ lbs}$$

Curves similar to those presented in Figure 2-4 are included in paragraph 5.2 of this report for other materials and other winding patterns.

The weights of the propellant tank of composite materials were calculated by an equally simple netting analysis. The netting analysis assumed that the filaments sustained the entire tensile load. The shell thickness required for a given loading condition was found from the equation

$$t = \frac{(N_x + N_y)UFS}{\sigma_{ultimate}}$$

where:

t is the shell thickness.

N_x and N_y are the average stress resultants.

UFS is the ultimate factor of safety.

$\sigma_{ultimate}$ is the ultimate strength of the filaments.

The filaments were assumed to be aligned in the meridional or circumferential directions proportional to the magnitudes of N_x and N_y. Once the thickness of the shell was calculated, the structural weight was determined by the equation

$$\text{Weight} = A\, t\, \rho\, F_B$$

where:

A is the surface area of the head.

t is the thickness of the head.

ρ is the density of the material.

F_B is the fabrication factor to account for noncalculable weights such as weld lands, doublers, etc. Fabrication factors for the various types of construction considered are presented in Appendix A.

As an example, consider a hemispherical head with a radius of 400 inches. The surface area is

$$A = 2\pi R^2 = (2)(\pi)(400)^2 = 1{,}005{,}309 \text{ in.}^2$$

All of the filaments evaluated in this study were assumed to have an ultimate strength of 200,000 psi. If the load on this example head is

$$N_x = N_y = 4000 \text{ lbs/in.}$$

and the ultimate factor of safety is 1.4, then the required thickness of the head is

$$t = \frac{(4000 + 4000)1.4}{200{,}000} = 0.056 \text{ inches}$$

The density of the materials used in this study were

Glass/Epoxy	0.07898 lbs/inch^3
Boron/Epoxy	0.0731 lbs/inch^3
Carbon/Aluminum	0.0804 lbs/inch^3

These densities are based on a 30 percent binder volume using the constituent properties listed in Section 5.

For a Boron/Epoxy material, the total weight of the example head is

$$\text{Weight} = A\, t\, \rho\, F_B = (1{,}005{,}309)\,(0.056)\,(0.0731)\,(1.05)$$
$$= 4321 \text{ lbs}$$

The fabrication factor of 1.05 was used for all monocoque heads.

2.4 SUMMARY OF OVERALL ANALYSIS PROCEDURE

The overall flow of logic used to obtain the numerical results of this study is summarized in the following five steps which are illustrated in Figure 2-5.

1. The basic configuration of the vehicle is selected. That is, the aerodynamic shape, mass characteristics, reference trajectory, wind loads, tank pressures, nozzle configurations, etc., are specified.
2. The load distributions calculated for each of the design points are tabulated in the Loads Summary Charts. For a specific set of loading conditions the appropriate rows are selected.
3. The critical loads envelope is determined by selecting the largest load in each column where the columns are associated with the structural elements of the launch vehicle.
4. The calculated weights for the structural elements are tabulated in either the Weight/Load Matrices (for isotropic materials) or the plots of N_x/R versus W/R (for composite materials). For specified materials and types of construction the structural weights corresponding to the critical loads envelope are evaluated by interpolation in the appropriate matrices.
5. The weights of the various structural elements are tabulated and summed to obtain total vehicle weights.

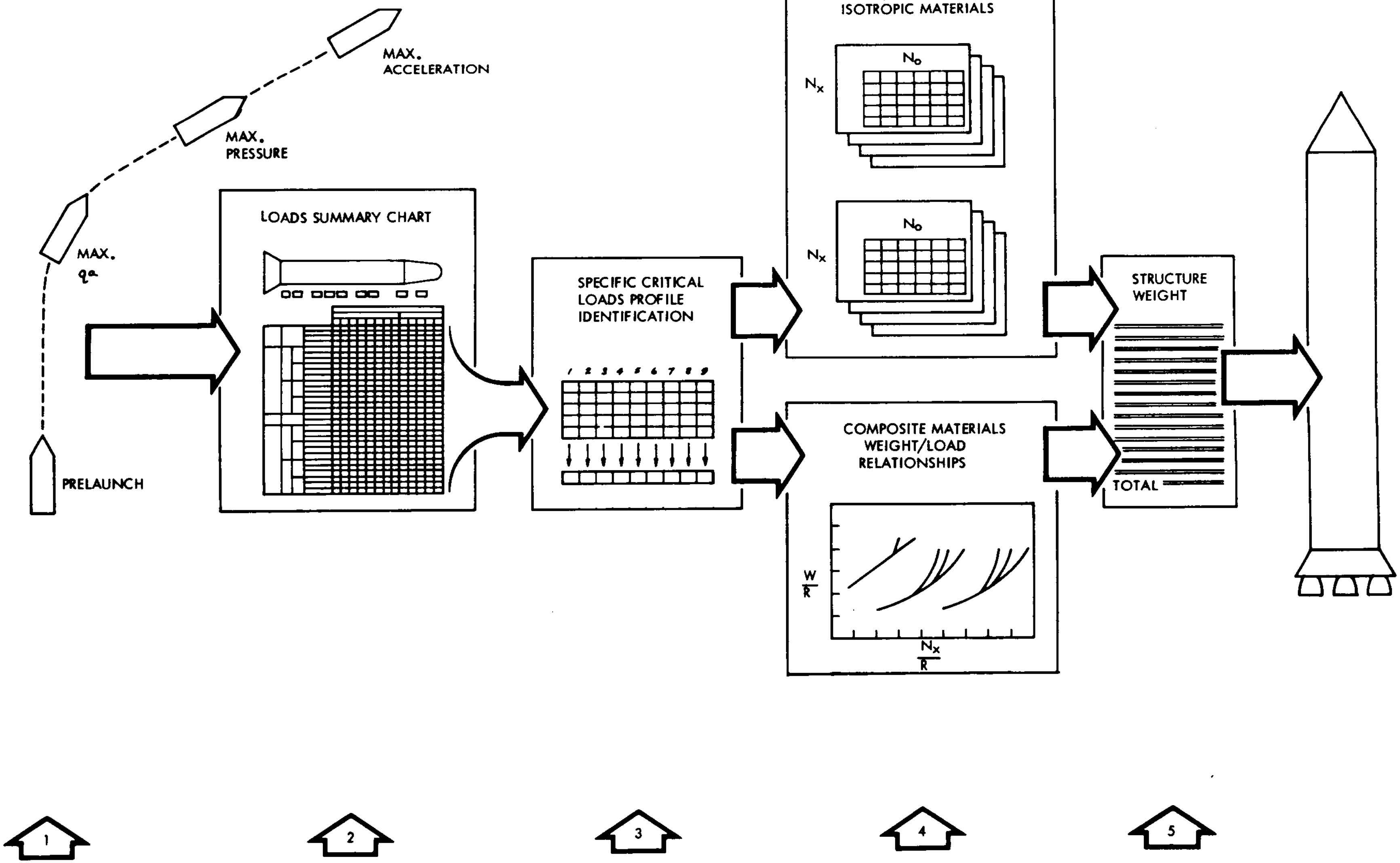

Figure 2-5. Procedure for Calculating Vehicle Structural Weight for Specified Loads and Configuration

SECTION 3

GENERAL LOADS ANALYSIS

3.1 GENERAL

The loads analyses for the representative vehicles were completed in three parts as outlined in the description of the SSPD computer program in Appendix A. In the first part of the analysis, the rigid-body response of the vehicle to inflight winds was calculated. The second part of the analysis analyzed the vehicle as a nonuniform beam and calculated the axial force distributions and bending moment distributions at specific design points. In the third and final part of the loads analysis, the representative vehicles were described as a collection of thin shells of revolution. All of the loads on the vehicle, including the pressure loads in the propellant tanks, were resolved into orthogonal stress resultants in the plane of the shells. Once the stress resultants were obtained for various conditions of load, they were normalized by the nominal stress resultants and were recorded in the Loads Summary Charts as described in Section 2 of this volume.

This section presents the input parameters which were used in each of the three parts of the analysis. Some of the intermediate results of the loads analysis are also presented. The Loads Summary Charts are presented at the end of this section for the representative vehicles involved in the load interactions evaluations. References 1 and 2 were used extensively as a source of input data to describe the representative vehicles. Input data were checked by independent analyses, however, and the data of References 1 and 2 were modified to correct for some inconsistencies. These changes pertain to the $CP/_D$, C_{Z_α}, and C_D plots for the 101, 201, and 301 Vehicles in Figures 3-1 and 3-2.

Load profiles were developed for various combinations of the load parameters of Table 3-1 over the range shown. The load condition which corresponds to the simultaneous reduction of these parameters to the lowest values shown in Table 3-1 is called the lower bound load.

Table 3-1

Design Criteria Parameter Variations

Parameter	Nominal Value Of Parameter	Lowest Value Of Parameter
Prelaunch Winds	99.9% Probability of Occurrence	95% Probability of Occurrence
Inflight Winds	95% Probability of Occurrence	90% Probability of Occurrence
Maximum Boost Acceleration	101 Vehicle - 4.8 g's 200 Series - 5.55 g's 301 Vehicle - 2.5 g's	2.0 g's
Tank Pressures	See Figures 3-13 & 3-14	Vented

3.2 RIGID BODY ANALYSIS

The mass characteristics and the aerodynamic characteristics for the rigid body configurations of the representative vehicles are presented in Figures 3-1 and 3-2. The weight of the representative vehicles at any flight time was determined from the initial weight and the weight flow rate data presented in Section 1, Volume 2. It should be observed that the initial weight and weight flow rate of the 201 vehicle configuration was used for all 200 series vehicles.

The aerodynamic shapes of the rigid bodies were completely specified by the plots of overall normal and axial force coefficients and the center of pressure locations versus Mach number presented in Figures 3-1 and 3-2. The Mach number at any specific flight time was found by integrating the equations of motion in the rigid body trajectory program, as explained in Appendix A. There were some basic vehicle similarities. These can be observed when the shapes of the curves in Figures 3-1 and 3-2 are compared between the various vehicle configurations. However, the relative magnitudes of the various curves varied significantly between the vehicle configurations, and gave rise to differences in the critical loads envelopes between the various vehicles.

The thrust model for all vehicle configurations is conveniently expressed by Equation 3-1.

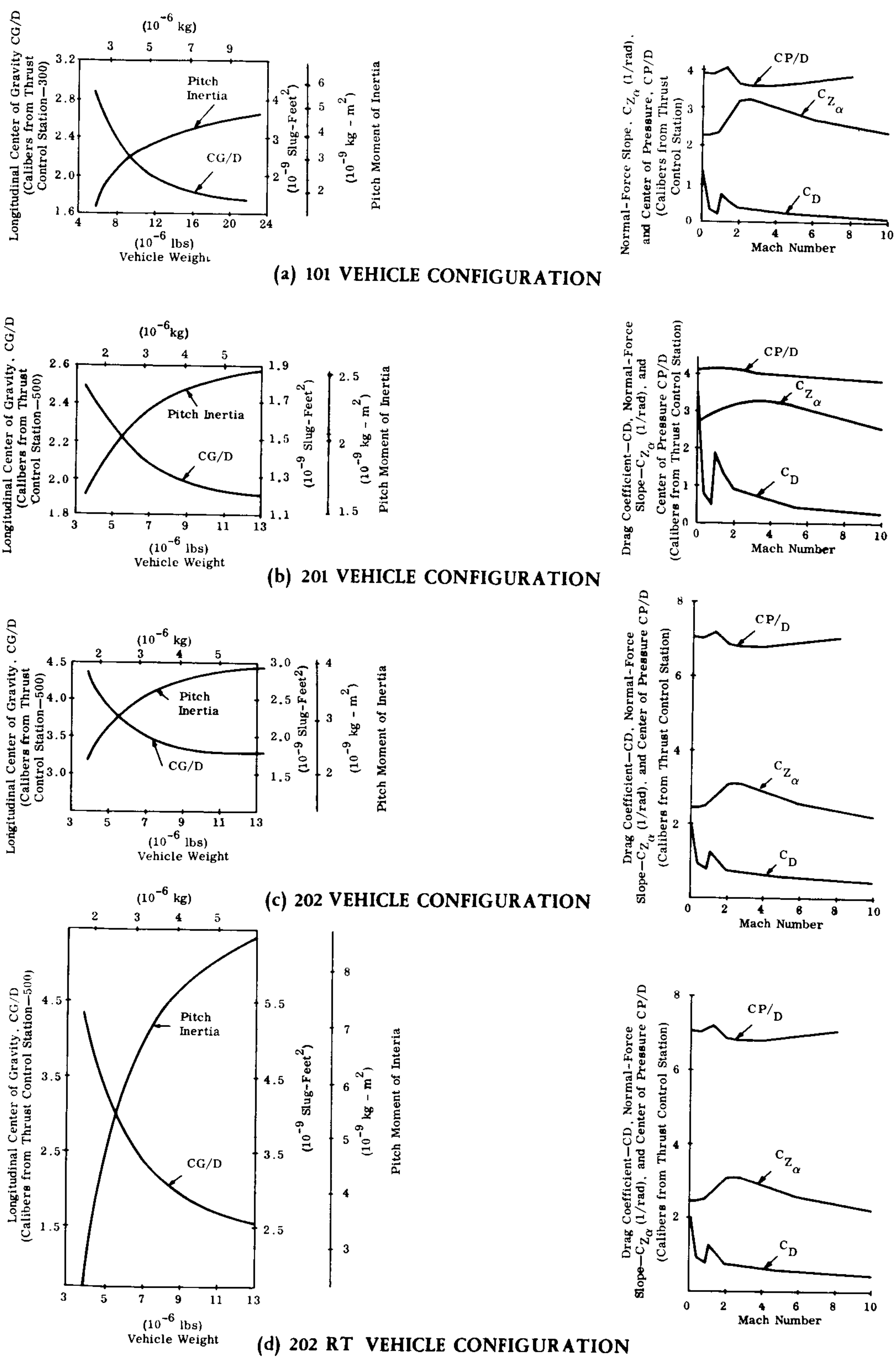

Figure 3-1. Rigid Body Mass Characteristics and Overall Aerodynamic Coefficients For the Representative Vehicle Configurations (Vehicles 101, 201, 201RT)

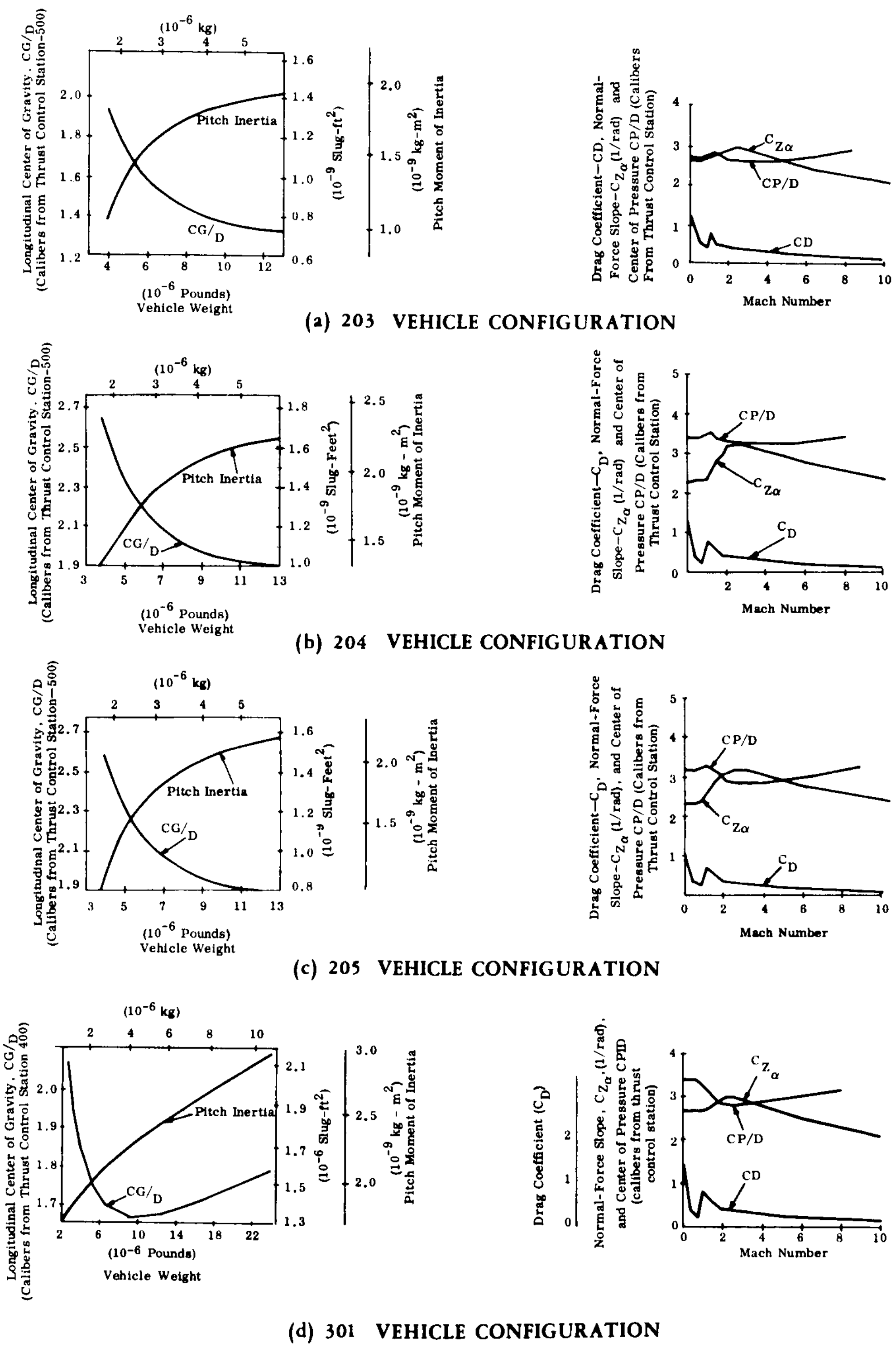

Figure 3-2. Rigid Body Mass Characteristics and Overall Aerodynamic Coefficients For the Representative Vehicle Configurations (Vehicles 203, 204, 205, 301)

$$T = T_{vac} - PAe \tag{3-1}$$

where:

T	is the instantaneous total thrust
P	is the local atmospheric pressure
T_{vac}	is the total vacuum thrust
A	is the total nozzle throat area
e	is the nozzle expansion ratio

The atmospheric pressure was derived from the 1959 ARDC model atmosphere and the values of A and e were chosen such that the above relation was satisfied at launch. The total vacuum thrust of the engines is specified in Section 1, Volume 2.

The reference trajectory for a specified vehicle configuration was described by a pitch-rate profile. Figure 3-3 gives the pitch-rate profiles and control system gains which were used for the representative vehicles. The pitch-rate profiles were chosen to conform to the reference trajectories given for the 101, 201, and 301 Vehicle configurations in References 1 and 2. The gains of the rate-displacement control system were chosen to produce similar response characteristics for the representative vehicles.

The inflight winds were represented by the synthetic wind profiles illustrated in Figure 3-4(b). These profiles were constructed by the method described in Reference 5. A 9 meter-per-second gust has been embedded in each of the idealized wind-speed envelopes. These idealized envelopes were identified by the percent of total time during the strongest wind month for which the envelope is not exceeded. The wind build-up portion of the synthetic profile was taken from the 99 percent probability of occurrence vertical wind change spectrum of Reference 5. The synthetic wind profile was constructed such that the winds build up to the maximum velocity of the idealized envelope at the time of maximum $q\alpha$ product. The square gust was also embedded at that altitude. Previous studies of Saturn V/Apollo configurations (Reference 13) showed that the rigid-body response is insensitive to changes in the wind build-up profile. For this reason, wind shear was not considered as a variable in the rigid-body analysis.

A 99 percent probability of occurrence of vertical wind-speed change was assumed for all three synthetic wind profiles used in this study.

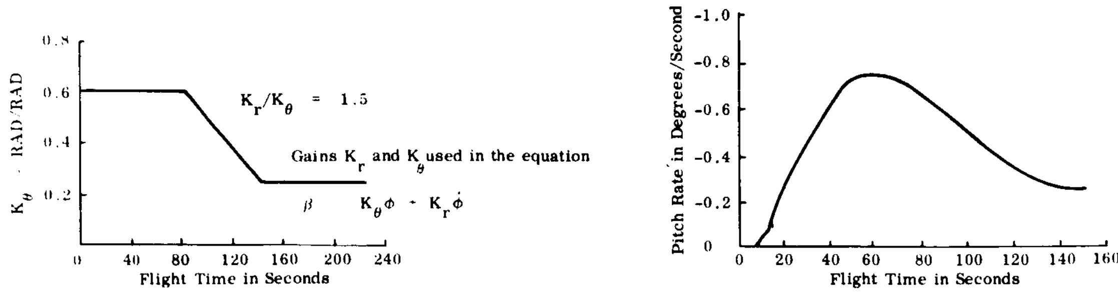

(a) 101 VEHICLE CONFIGURATION

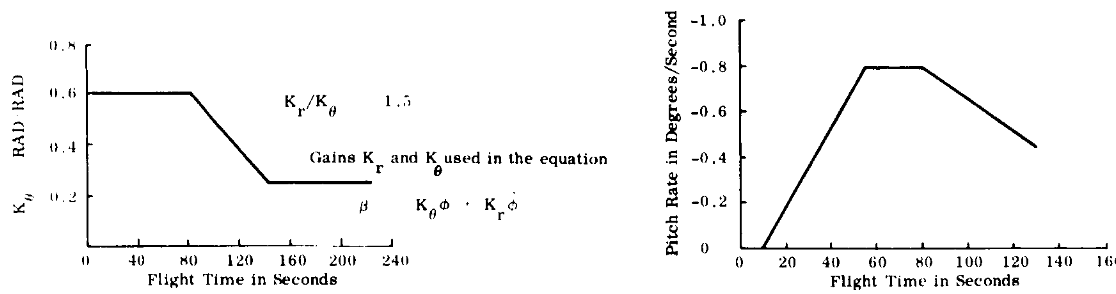

(b) 201 VEHICLE CONFIGURATION

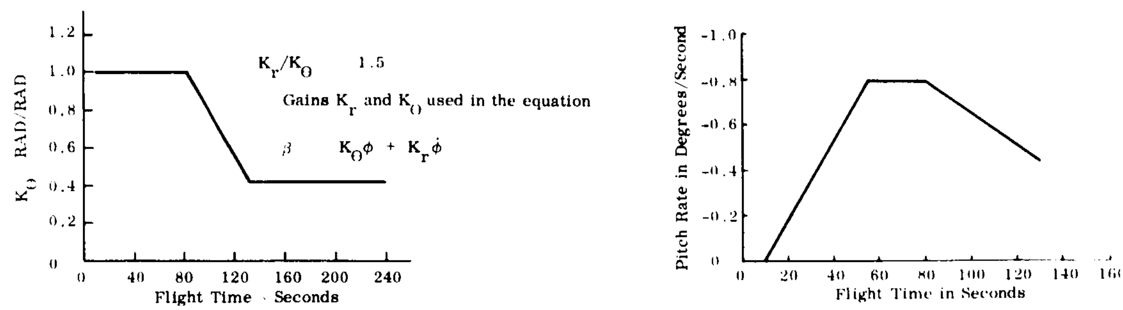

(c) 202 VEHICLE CONFIGURATION

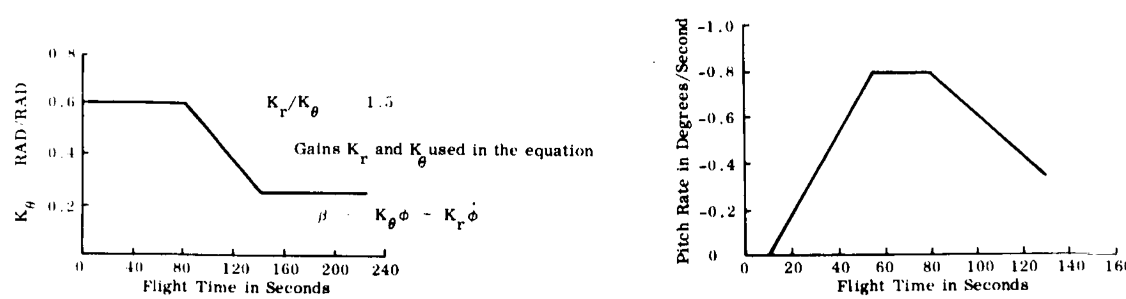

(d) 301 VEHICLE CONFIGURATION

Figure 3-3. Reference Trajectories and Control Gains For Representative Vehicles

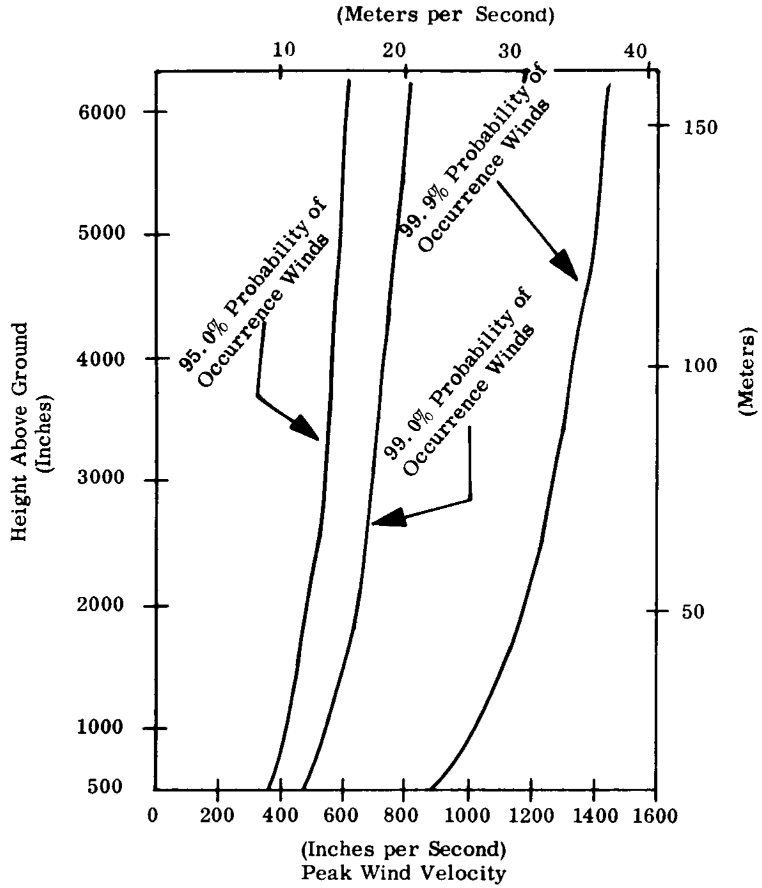

(a) PRELAUNCH WINDS

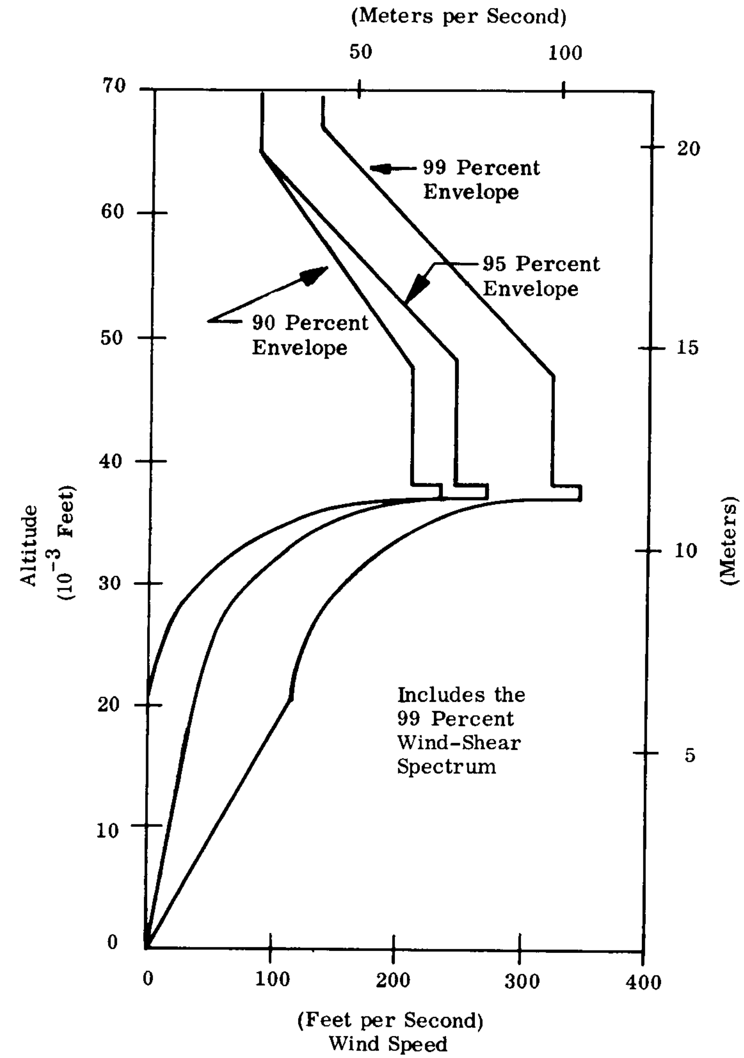

(b) INFLIGHT WINDS

Figure 3-4. Wind Profiles For Prelaunch and Inflight Winds

Results of the rigid-body analyses are summarized in Tables 3-2 and 3-3 for the representative vehicles exposed to the nominal, inflight loading conditions. The bending moments at the time of maximum boost acceleration were negligible so only the thrust loads were of concern for that design point.

3.3 CALCULATION OF BENDING MOMENT AND AXIAL FORCE DISTRIBUTIONS

The axial force distributions and the bending moment distributions were calculated in the second part of the loads analysis. The vehicle was analyzed as a nonuniform beam in quasi-static equilibrium at each of the design points. It was necessary for this part of the analysis to describe the distribution of the mass and aerodynamic coefficients along the vehicle axis. Figures 3-5 and 3-6 present the results of the calculations that were performed during this study to obtain the required distributions. The inert weight distributions were taken from References 1 and 2, and are represented by the shaded areas on the mass distribution plots. Propellant weights were calculated using an initial ullage volume of 8 percent in all propellant tanks. The propellant densities were as follows:

RP-1 - 50.5 lbs./ft.^{3}

LOX - 71.0 lbs./ft.^{3}

LH_2 - 4.4 lbs./ft.^{3}

Mass distributions represented in Figures 3-5 and 3-6 correspond to the conditions at launch. The distributions at all the other flight times of interest were determined using the appropriate values of propellant burn rate and mixture ratio presented in Section 1, Volume 2 for the representative vehicles. Expended propellants were subtracted from the tops of the appropriate propellant tanks to obtain the mass distribution at the flight time of interest.

The normal and axial aerodynamic coefficient distributions were calculated using the methods of References 7, 8, and 9. These coefficients were used to calculate the lateral and drag forces on the vehicle during inflight conditions. The plots shown in Figures 3-5 and 3-6 are presented for two specific Mach numbers which span the region for inflight conditions. The aerodynamic coefficient distributions for the Mach number of a specific design point was obtained by linear interpolation.

Table 3-2

Rigid Body Response to Nominal Loading Conditions at the Time of Maximum $q\alpha$ Product

	Vehicle Configuration						
	101	201	202	203	204	205	301
Dynamic Pressure, q (lbs/ft^2)	848.2	744.2	757.951	748.44	755.421	768.716	753.6
Angle of Attack, α (degrees)	-10.303	-10.886	-9.534	-10.469	-9.525	-9.118	-9.522
Mach Number, M	1.665	1.557	1.570	1.564	1.568	1.585	1.568
Time, t (seconds)	74.3	78.1	78.6	77.7	78.2	78.0	78.3
Engine Gimbal Angle, β (degrees)	3.682	4.138	2.681	4.206	2.903	2.403	2.153
Center of Gravity, CG (feet)	124.6	135.7	181.313	108.996	134.835	134.822	138.7
Thrust, T (pounds)	27,681,375	21,052,875	21,051,751	21,055,305	21,052,214	21,055,558	34,417,636

Table 3-3

Rigid Body Response to Nominal Loading Conditions at the Time of Maximum Boost Acceleration

	Vehicle Configuration		
	101	All 200 Series	301
Maximum Acceleration (g's)	4.8	5.55	2.5
Time, t (seconds)	148.8	220.8	125.6
Thrust, T (pounds)	28,400,000	21,851,000	35,570,000

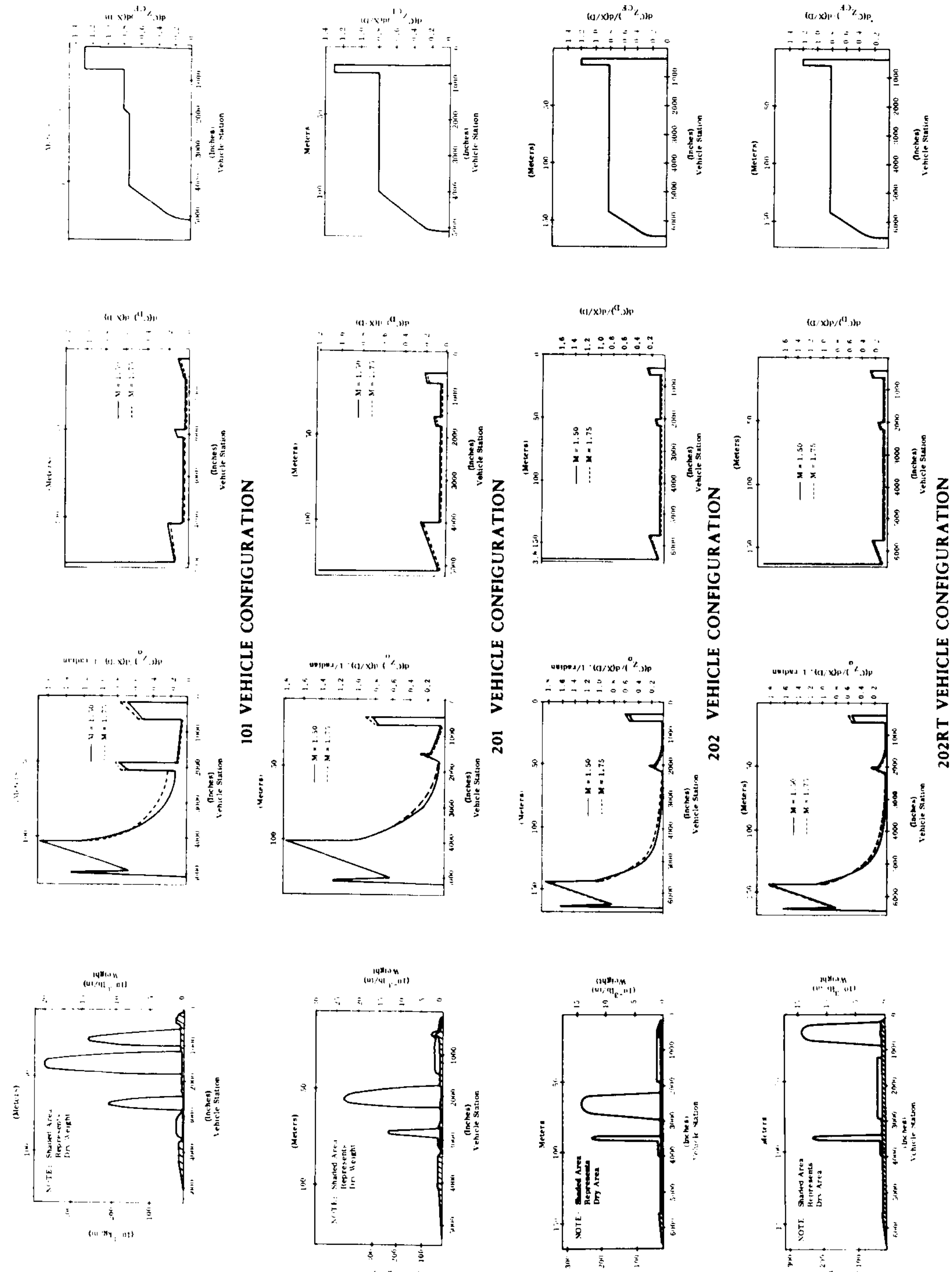

Figure 3-5. Distributions of Mass and Aerodynamic Coefficients Along Axis of Representative Vehicle (Vehicles 101, 201, 202, 202RT)

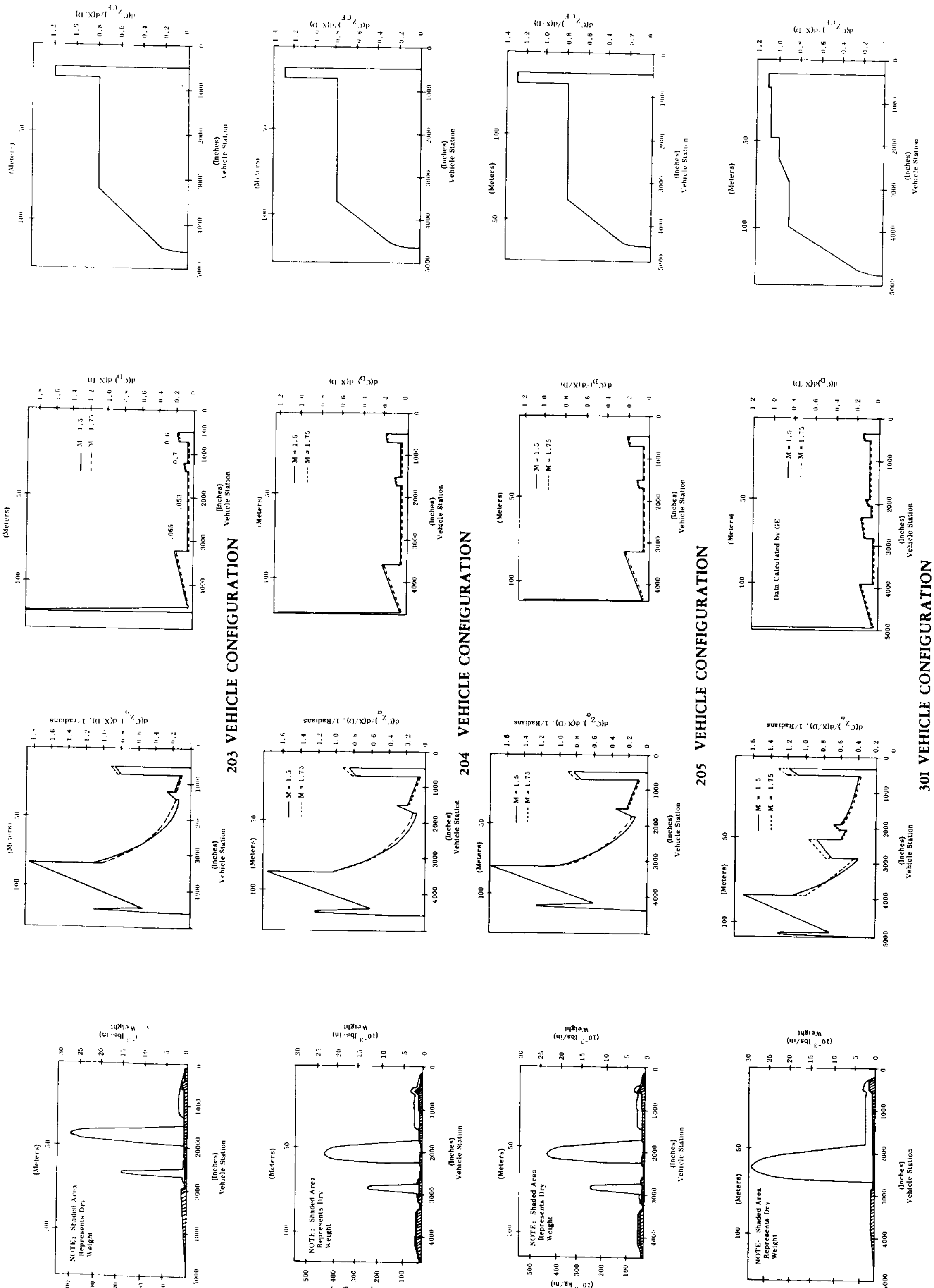

Figure 3-6. Distributions of Mass and Aerodynamic Coefficients Along Axis of Representative Vehicle (Vehicles 203, 204, 205, 301)

The cross-flow coefficient distributions shown in Figures 3-5 and 3-6 were used to calculate the lateral prelaunch wind loads on the launch vehicle. These distributions were calculated using the method described in Reference 11.

Figures 3-5 and 3-6 show that the distribution of mass and aerodynamic coefficients are strongly dependent on the vehicle's external shape. It is also observed that the propellant weight completely dominates the vehicle's mass characteristics. The dominance of the propellant weight justifies the assumption that changes in vehicle structural weight had no significant effect on the loads envelope. Even if the inert weights were reduced to half their original value, it can be seen from Figures 3-5 and 3-6 that the mass distribution (and therefore the moment of inertia) would be changed very little.

Prelaunch wind profiles for three different probabilities of occurrence are shown in Figure 3-4(a). These data were taken from Reference 13. In each case, the profiles are the envelopes which are not exceeded a specified percentage of the total time during the windiest month. A factor of 1.4 was included to account for wind gusts. For each of the representative vehicles, the 99.9 percent envelope was the nominal prelaunch wind. Other envelopes were considered as variations from the nominal to evaluate the effect of prelaunch winds on vehicle loads.

Figures 3-7, 3-8, 3-9, 3-10, and 3-11 are typical results of the bending moment and axial force analysis for the 101, 201, 202, 203, and 301 Vehicle configurations respectively. Since tank pressures were not considered until the next step of the analysis, the loads at the time of maximum pressure were not available here. Also, there was no distinction between pressurized and unpressurized conditions at prelaunch. Since the shear distribution at the time of maximum $q\alpha$ product dominates over those of other design points, the shear distributions are not shown for prelaunch and maximum boost acceleration.

Figure 3-12 compares the bending moment distribution at the time of maximum $q\alpha$ product for three nozzle designs. The 201 Vehicle is used as an example where the bending moment distribution for gimbaled bell nozzles, throttled plug nozzles, and front-end steering designs are compared. The large reduction in bending moment when front steering methods were used indicates that this might be a fruitful area for potential structural weight savings. However, these results are misleading, as is seen when the total loads envelope is considered. The load envelope was explained earlier in Section 2 of this volume.

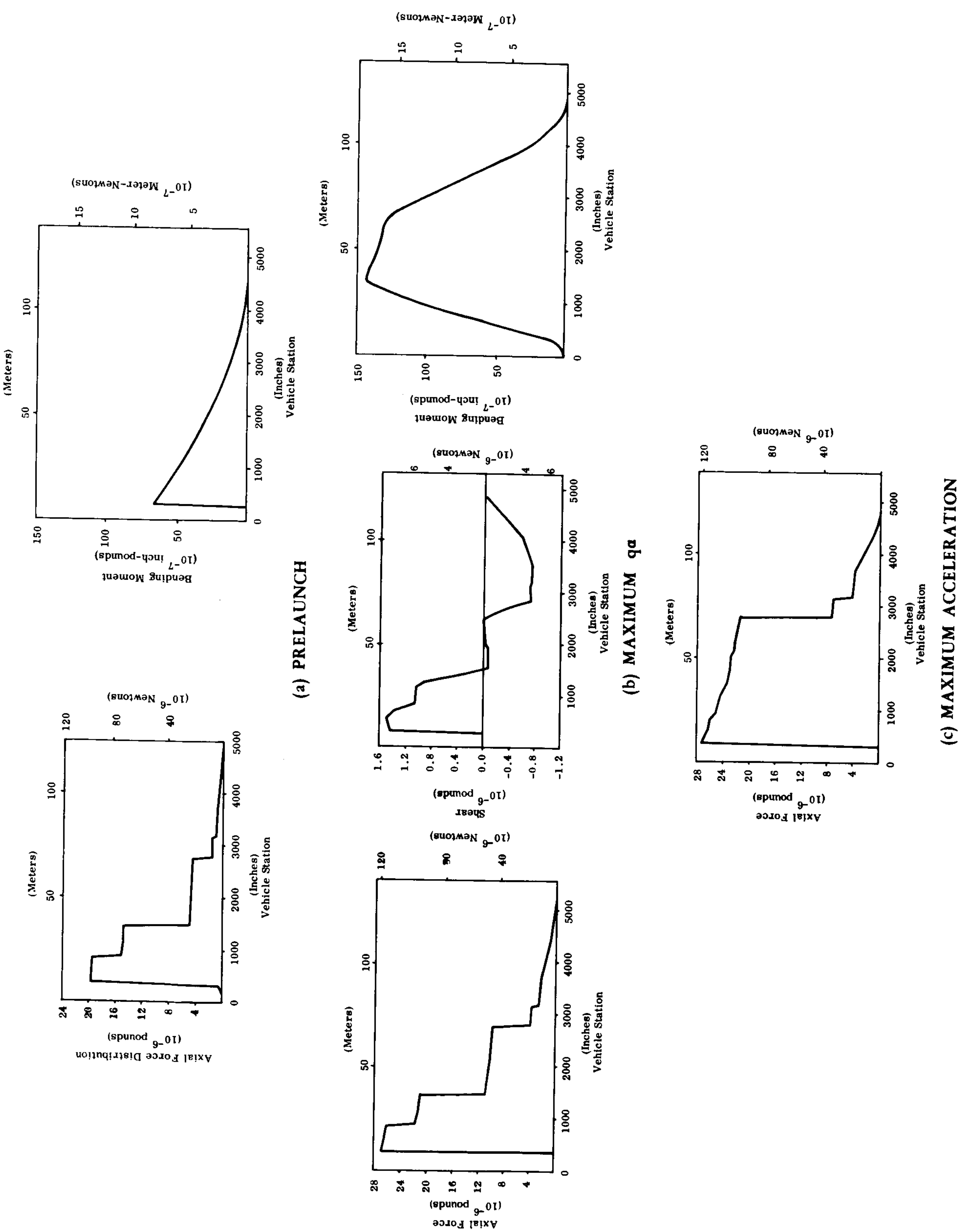

Figure 3-7. Nominal Load Distributions For the 101 Vehicle Configuration

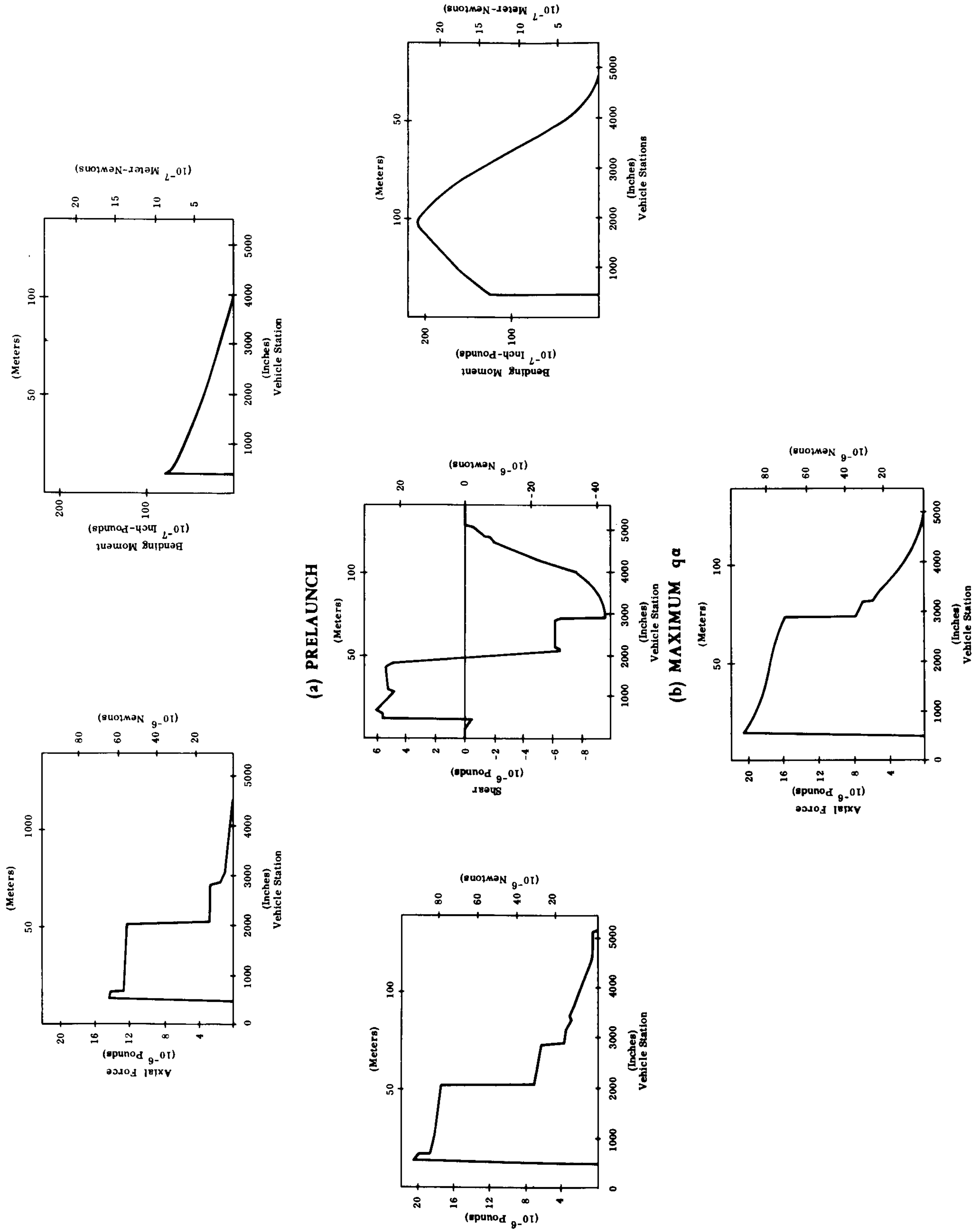

Figure 3-8. Nominal Load Distributions For the 201 Vehicle Configuration

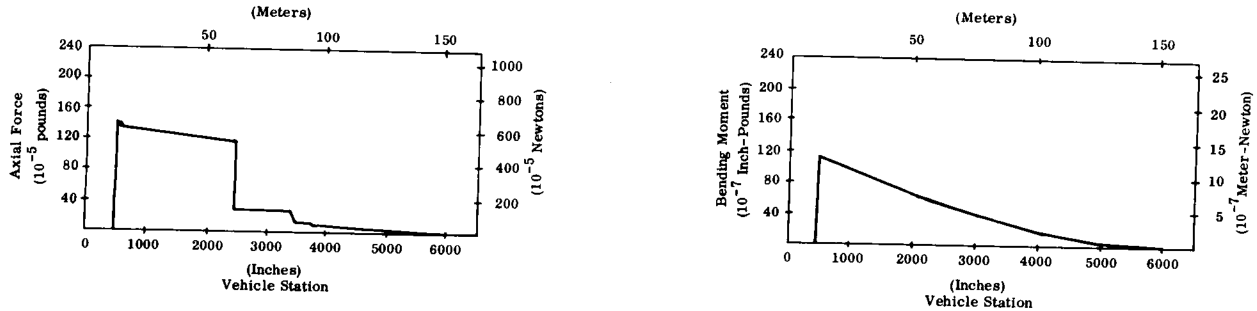

(a) PRELAUNCH

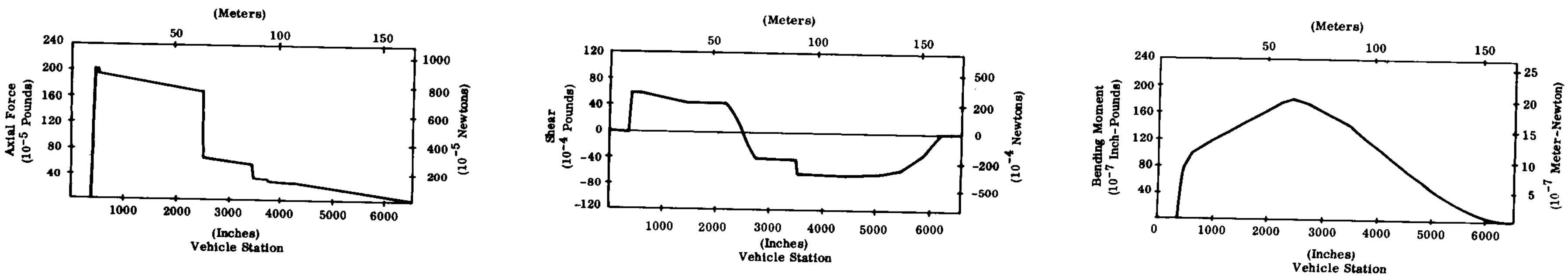

(b) MAXIMUM $q\alpha$

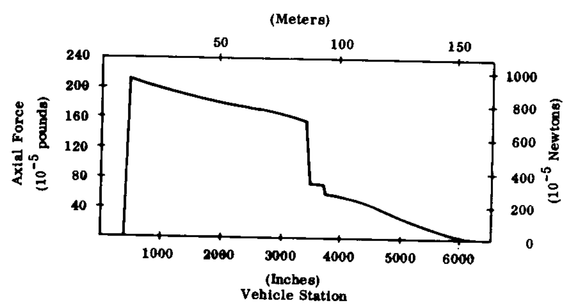

(c) MAXIMUM ACCELERATION

Figure 3-9. Nominal Load Distributions For the 202 Vehicle Configuration

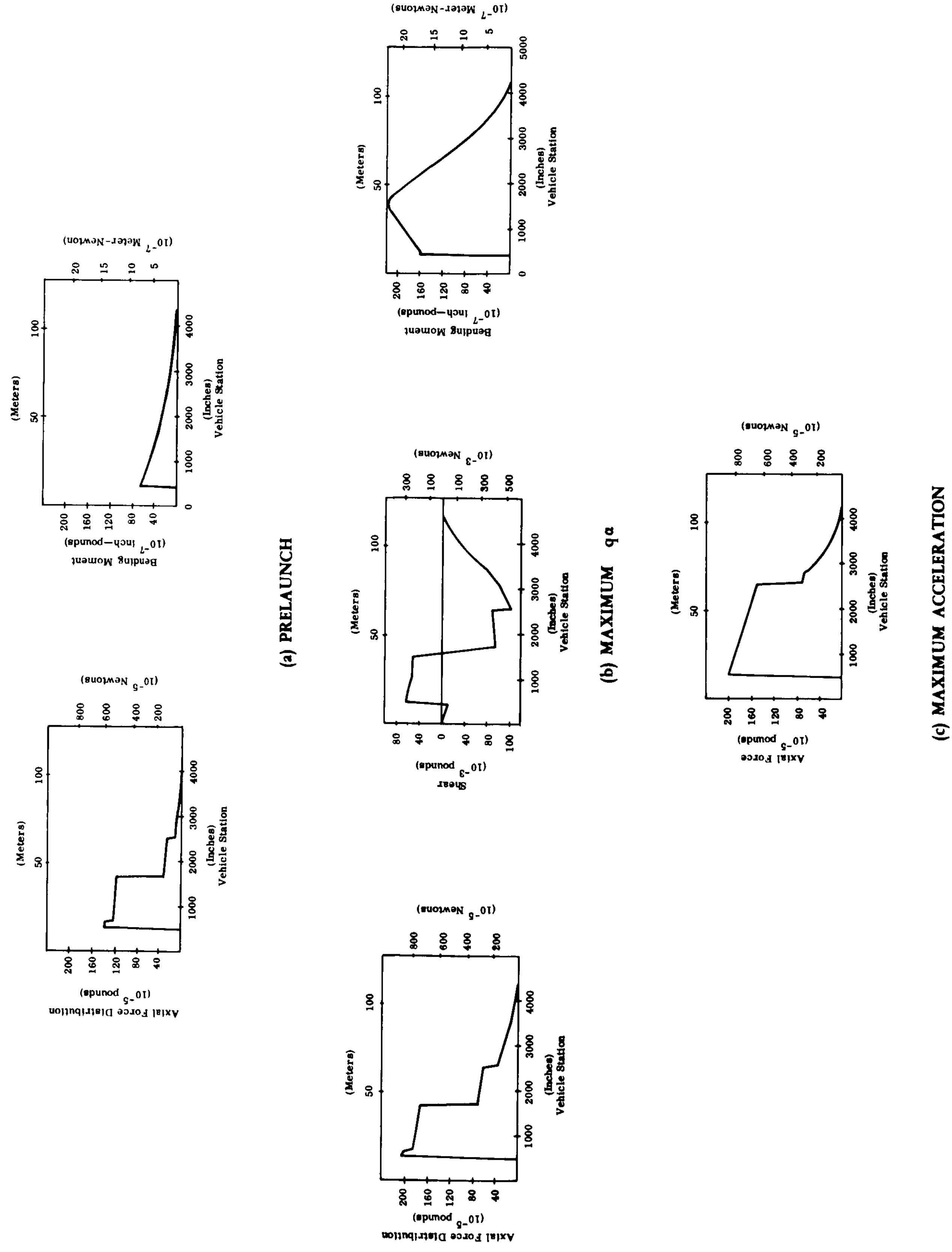

Figure 3-10. Nominal Load Distributions For the 203 Vehicle Configuration

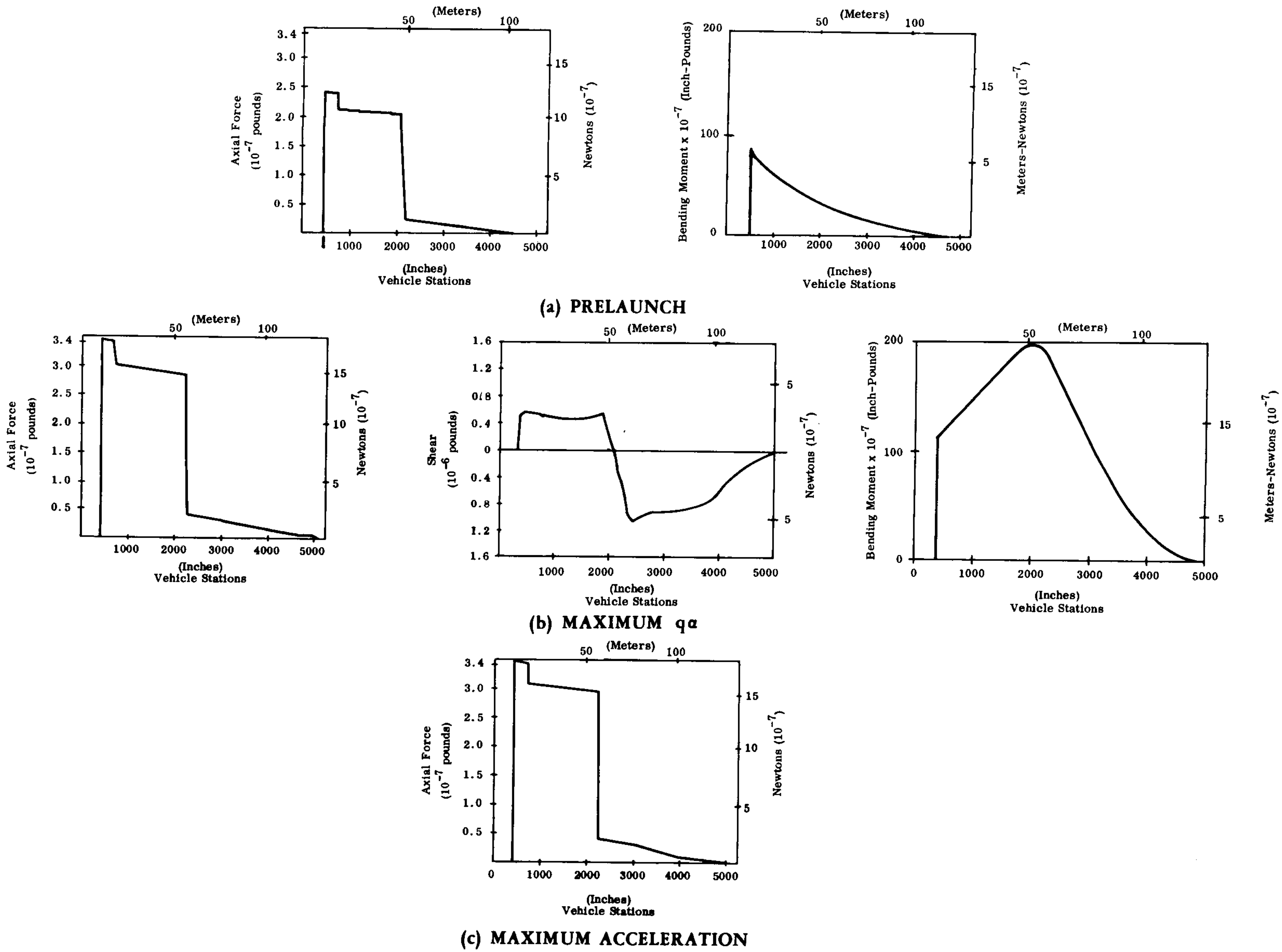

Figure 3-11. Nominal Load Distributions For the 301 Vehicle Configuration

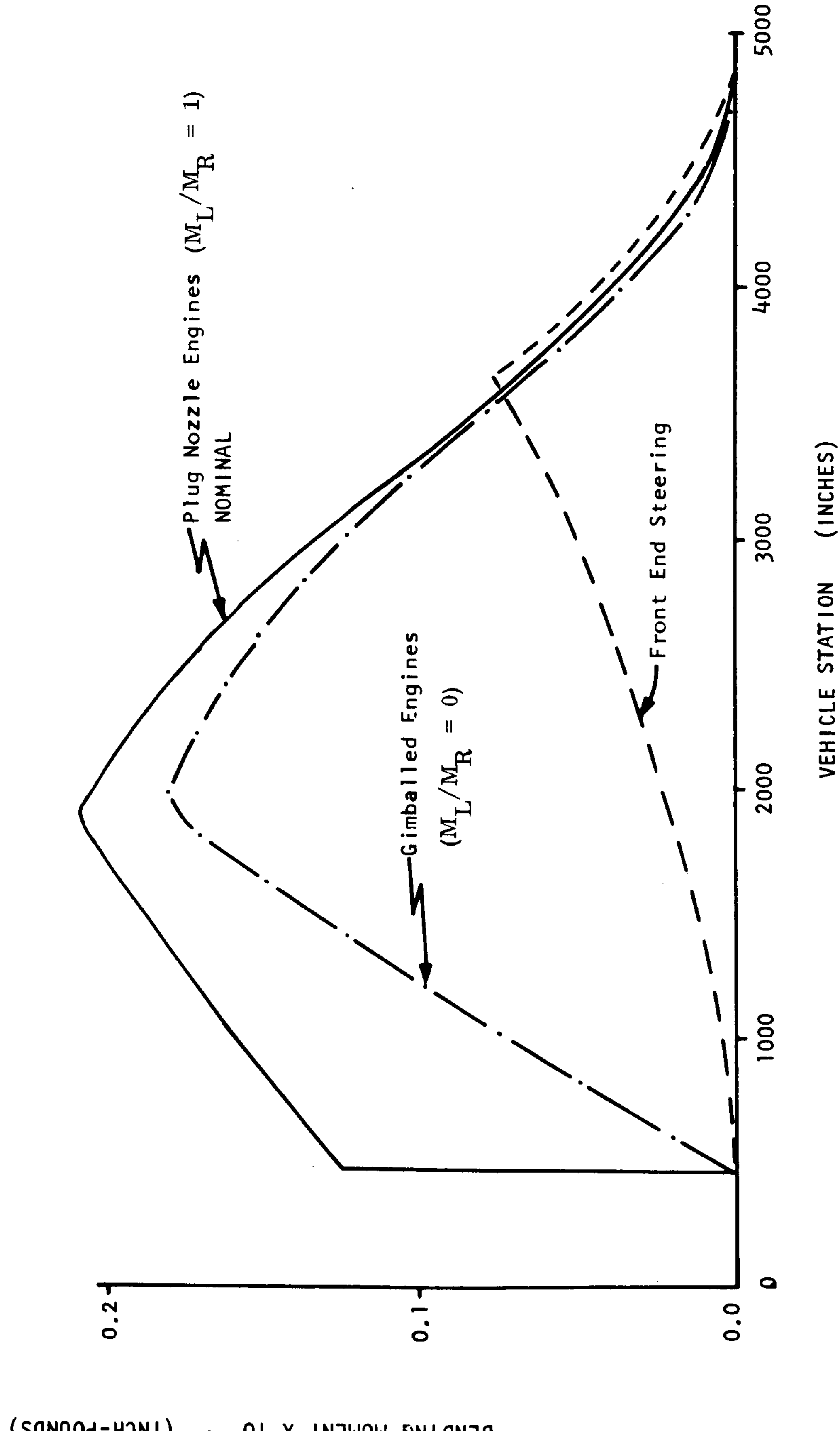

Figure 3-12. Bending Moment Distribution For the 201 Configuration, 78.1 Seconds, Maximum $q\alpha$ Product Condition

Even though the load distribution at the maximum $q\alpha$ condition was significantly reduced, by front-end steering, the loads at the other design points then governed. Structural weight savings are therefore relatively small. Weight which is added by the front steering system must also be considered. The added weight of the steering system, in some cases, more than offset savings that were available through reducing the bending moment, as noted in Section 6.

For a gimbaled bell nozzle design, the control moment was supplied by a lateral component of the thrust vector passing through the gimbal point. The bending moment was zero at the gimbal station and reached a peak near station 2,000 before going to zero at the forward end of the vehicle.

The plug nozzle, with differential throttling for thrust vector control, induced steering moment by increasing the thrust of the engines on one side of the vehicle and by decreasing the thrust of the engines on the opposite side. The resulting moment was considered as the sum of two components. One component, M_L, was an applied couple at the gimbal point and the other, M_R, was due to a lateral force applied at the gimbal point, as discussed in Section 6. The relative contribution of these two components for the representative vehicle configurations is summarized in Table 3-4.

Table 3-4

Ratio of M_L to M_R for Representative Vehicle Configuration

Vehicle Configuration	M_L/M_R For Plug Nozzle Using Differential Throttling	M_L/M_R For Gimbal Engine
101	1.0	0
201	1.0	0
202	0.65	0
202RT	Front-End Steering Only	Front-End Steering
203	1.6	0
204	1.0	0
205	1.0	0
301	1.0	0

3.4 CALCULATION OF STRESS RESULTANTS AND LOAD SUMMARY CHARTS

The final step in the loads analysis was to include the propellant tank pressure loads. The vehicles were assumed to be composed of a collection of conical, cylindrical, spherical, and elliptical thin shells of revolution in this part of the analysis. Vehicle loads were resolved into orthogonal stress resultants, N_x and N_y, in the plane of the shells using the SWOP computational module explained in Appendix A. Stress resultant distributions were calculated at design point for a variety of loading conditions and design criteria. The loads data were then normalized and summarized in the Loads Summary Charts for the vehicle configurations involved in the interaction analysis.

The propellant tank pressure profiles are shown in Figures 3-13 and 3-14 for the representative vehicle configuration. These data were taken from References 2 and 3 for the 101, 201, and 301 configurations. The pressure profiles for the other 200 series vehicles were assumed to be based on those of the 201 configuration through an inverse ratio of the tank diameters. Figures 3-13 and 3-14 are plots of the absolute ullage pressure. The gauge pressures were obtained by subtracting the local atmospheric pressure. Atmospheric pressure was expressed as a function of flight time for specific vehicle configurations as shown in Figure 3-15. These relationships were calculated as a part of the rigid-body trajectory analysis using an ARDC model atmosphere.

The description and use of the Loads Summary Charts is documented in detail in Section 2. These charts were used to summarize the loads analyses completed during this study. They proved to be a very flexible tool for evaluating the effects of vehicle design parameters on the critical design loads. Summary charts are presented in Tables 3-5, 3-6, 3-7, 3-8, and 3-9 for the 101, 201, 202, 203, and 301 Vehicle configurations respectively.

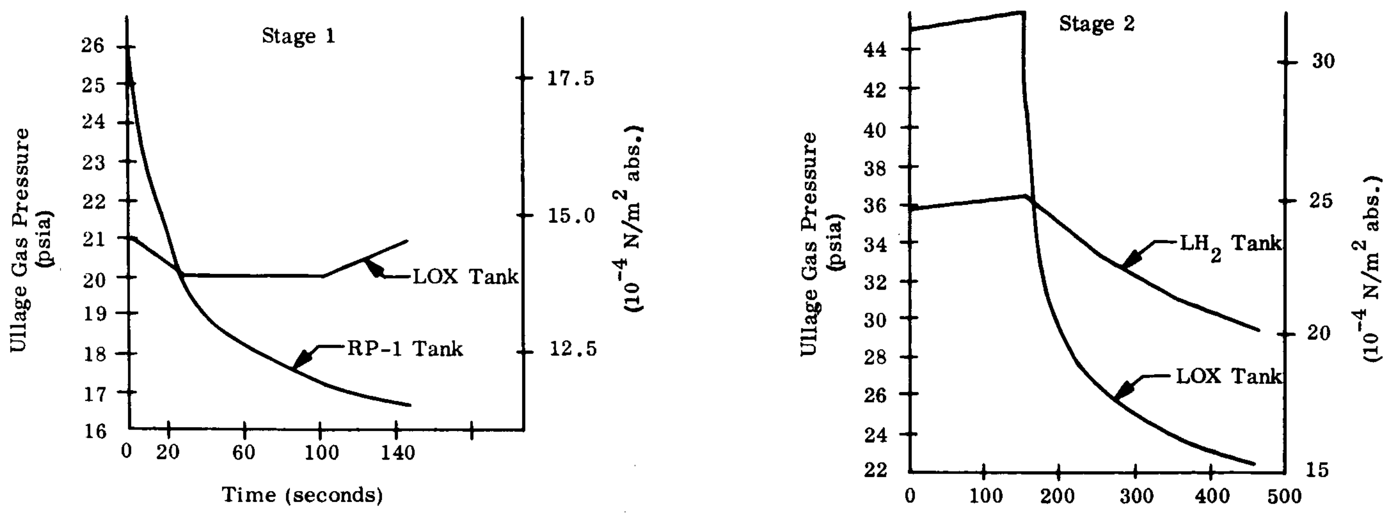

101 VEHICLE CONFIGURATION

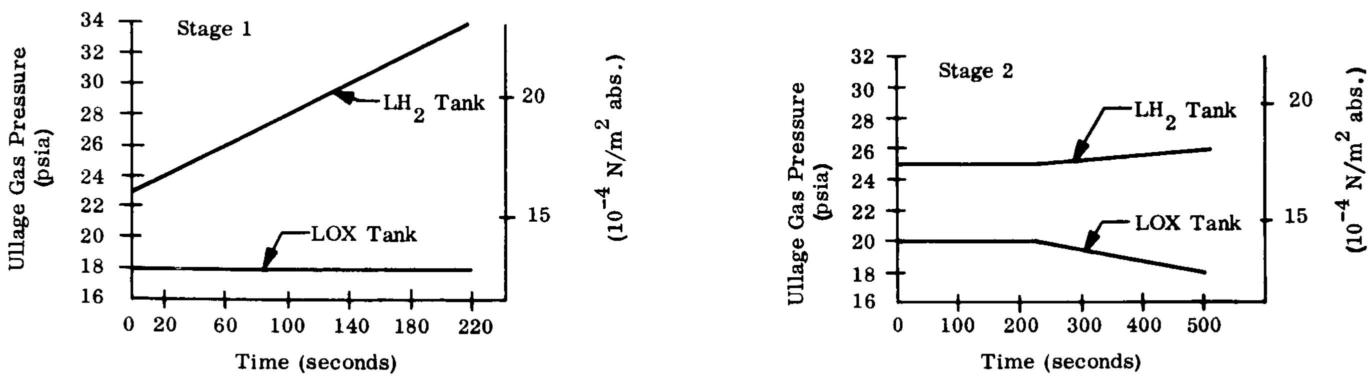

201, 204, & 205 VEHICLE CONFIGURATIONS

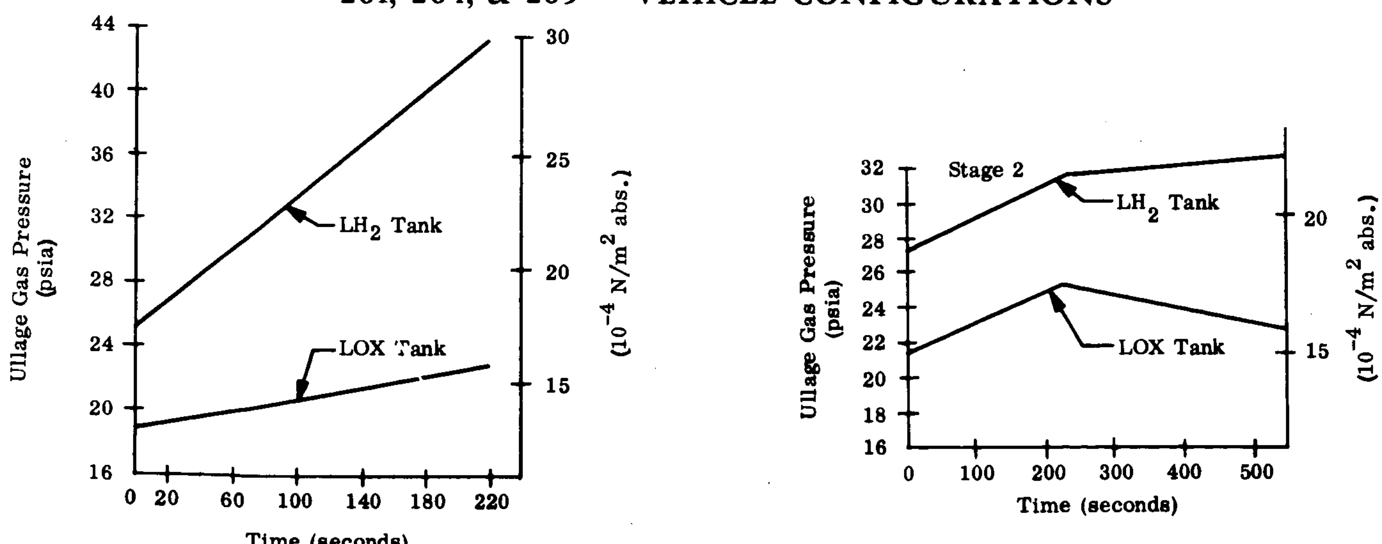

202 & 202RT VEHICLE CONFIGURATIONS

Figure 3-13. Propellant Tank Pressure Profiles For Representative Vehicle Configurations (Vehicles 101, 201, 204, 205, 202 and 202RT)

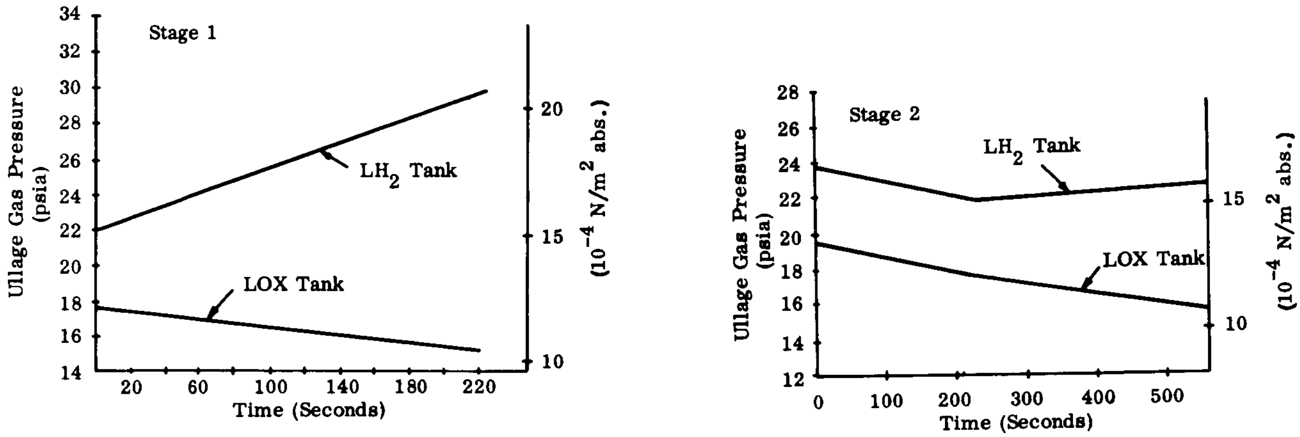

203 VEHICLE CONFIGURATION

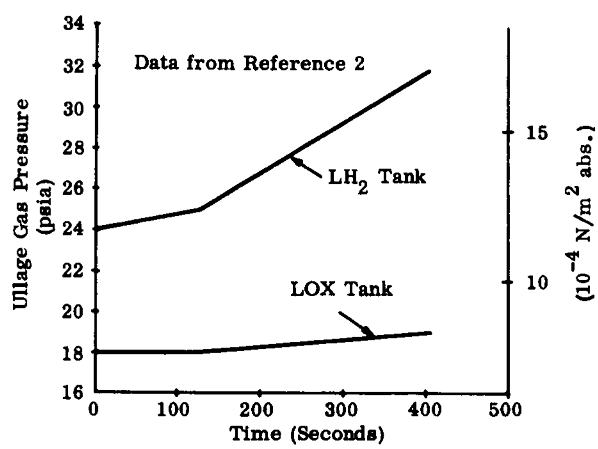

301 VEHICLE CONFIGURATION

Figure 3-14. Propellant Tank Pressure Profiles For Representative Vehicle Configurations (Vehicles 203 and 301)

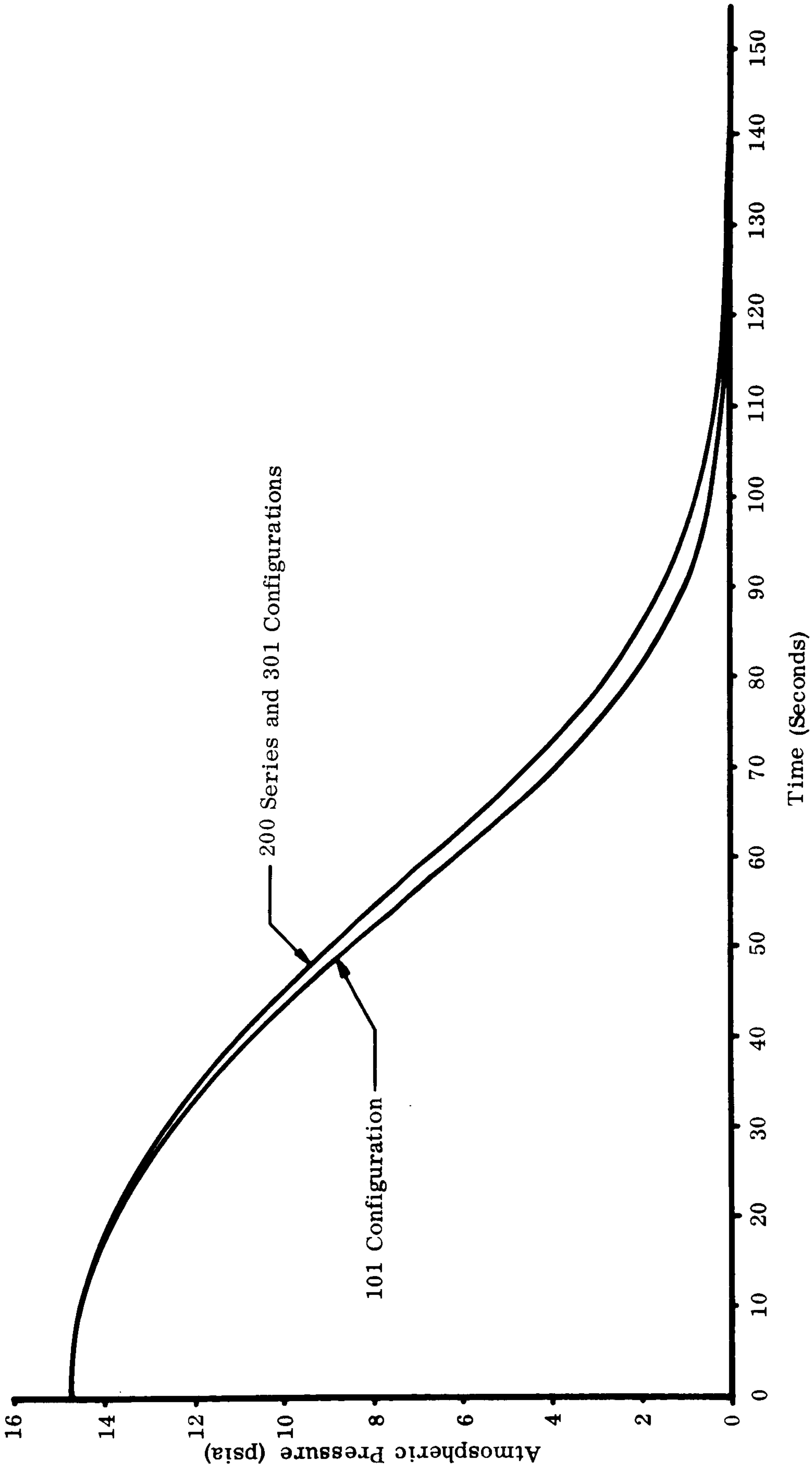

Figure 3-15. Atmospheric Pressure Profiles

Table 3-5
Loads Summary Chart
101 Vehicle Configuration

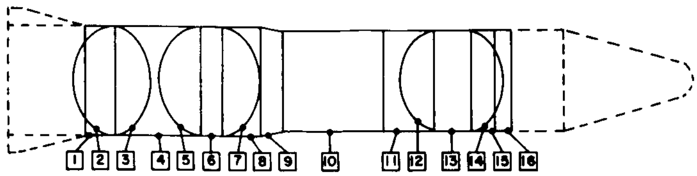

Loading Condition				Section: N_x/N_x Nominal										N_o/N_o Nominal							
				1	4	6	8	9	10	11	13	15	16	2	3	5	6	7	12	13	14
Prelaunch	99.9% Ground Winds		Unpressurized Tanks	.771	.623	.437	.291	.284	.271	.231	1.000	.205	.213	.418	.157	.541	.535	.220	.040	.067	.006
Prelaunch	99.9% Ground Winds		Pressurized Tanks	.771	.623	.300	.291	.284	.271	.231	0.0	.205	.213	.821	.670	.680	.651	.355	.510	.535	.581
Prelaunch	95% Ground Winds		Unpressurized Tanks	.702	.566	.356	.241	.238	.233	.181	.763	.161	.173	.418	.157	.541	.500	.220	.040	.055	.006
Prelaunch	95% Ground Winds		Pressurized Tanks	.702	.566	.218	.241	.238	.233	.181	0.0	.161	.173	.821	.670	.680	.629	.355	.510	.533	.581
Maximum qα	95% Inflight Winds (2.0 g's)	Pressurized Tanks	Plug Nozzle	1.177	1.117	.992	.890	.892	.869	1.047	0.0	1.035	1.030	.918	.786	.953	.906	.722	.778	.850	.861
Maximum qα	95% Inflight Winds (2.0 g's)	Pressurized Tanks	Front Steering	.904	.791	.436	.537	.560	.602	.825	0.0	1.130	1.112	.918	.786	.953	.672	.722	.788	.850	.861
Maximum qα	95% Inflight Winds (2.0 g's)	Pressurized Tanks	Gimbal Nozzle	1.000	1.000	.842	.800	.818	.819	1.000	0.0	1.000	1.000	.918	.786	.953	.834	.722	.778	.847	.861
Maximum qα	95% Inflight Winds (2.0 g's)	Vented Tanks	Plug Nozzle	1.177	1.177	1.321	.890	.892	.869	1.047	5.069	1.035	1.030	.571	0.0	.678	.762	0.0	.081	.294	.013
Maximum qα	95% Inflight Winds (2.0 g's)	Vented Tanks	Front Steering	.904	.791	.770	.537	.560	.602	.825	5.135	1.130	1.112	.571	0.0	.678	.460	0.0	.081	.296	.013
Maximum qα	95% Inflight Winds (2.0 g's)	Vented Tanks	Gimbal Nozzle	1.000	1.000	1.170	.800	.818	.819	1.000	4.871	1.000	1.000	.571	0.0	.678	.677	0.0	.081	.284	.013
Maximum qα	90% Inflight Winds (2.0 g's)	Pressurized Tanks	Plug Nozzle	1.164	1.100	.962	.871	.872	.851	1.018	0.0	1.007	1.005	.918	.786	.953	.839	.723	.778	.849	.862
Maximum qα	90% Inflight Winds (2.0 g's)	Pressurized Tanks	Front Steering	.904	.790	.433	.535	.557	.597	.807	0.0	1.100	1.085	.918	.786	.953	.666	.723	.778	.848	.862
Maximum qα	90% Inflight Winds (2.0 g's)	Pressurized Tanks	Gimbal Nozzle	.996	.990	.821	.787	.804	.806	.976	0.0	.976	.977	.918	.786	.953	.829	.723	.778	.845	.862
Maximum qα	90% Inflight Winds (2.0 g's)	Vented Tanks	Plug Nozzle	1.164	1.100	1.291	.871	.872	.851	1.018	4.926	1.007	1.005	.571	0.0	.678	.746	0.0	.081	.287	.013
Maximum qα	90% Inflight Winds (2.0 g's)	Vented Tanks	Front Steering	.904	.790	.761	.535	.557	.597	.807	5.000	1.100	1.085	.571	0.0	.678	.457	0.0	.081	.289	.013
Maximum qα	90% Inflight Winds (2.0 g's)	Vented Tanks	Gimbal Nozzle	.996	.990	1.150	.787	.804	.806	.976	4.746	.976	.977	.571	0.0	.678	.669	0.0	.081	.278	.013
Maximum Total Pressure	4.8 g's		Pressurized Tanks	.909	.808	.481	.626	.626	.626	.467	0.0	.429	.471	1.000	1.000	1.000	.758	.944	.916	.939	.989
Maximum Total Pressure	4.8 g's		Vented Tanks	.909	.608	.911	.626	.626	.626	.467	1.978	.429	.471	.606	0.0	.668	.499	0.0	.118	.148	.021
Maximum Boost Acceleration	4.8 g's	Pressurized Tanks	Plug Nozzle	.884	.672	1.000	1.000	1.000	1.000	.717	0.0	.642	.710	.758	.991	.608	1.000	1.000	1.000	1.000	1.000
Maximum Boost Acceleration	4.8 g's	Pressurized Tanks	Front Steering	.884	.872	1.000	1.000	1.000	1.000	.717	0.0	.642	.710	.758	.991	.608	1.000	1.000	1.000	1.000	1.000
Maximum Boost Acceleration	4.8 g's	Pressurized Tanks	Gimbal Nozzle	.884	.872	1.000	1.000	1.000	1.000	.717	0.0	.642	.710	.758	.991	.605	1.000	1.000	1.000	1.000	1.000
Maximum Boost Acceleration	4.8 g's	Vented Tanks	Plug Nozzle	.884	.872	1.455	1.000	1.000	1.000	.717	2.969	.642	.710	.277	0.0	.152	.797	0.0	.192	.229	.034
Maximum Boost Acceleration	4.8 g's	Vented Tanks	Front Steering	.884	.872	1.455	1.000	1.000	1.000	.717	2.969	.642	.710	.277	0.0	.152	.797	0.0	.192	.229	.034
Maximum Boost Acceleration	4.8 g's	Vented Tanks	Gimbal Nozzle	.884	.872	1.455	1.000	1.000	1.000	.717	2.969	.642	.710	.277	0.0	.152	.797	0.0	.192	.229	.034

Table 3-6
Loads Summary Chart
201 Vehicle Configuration

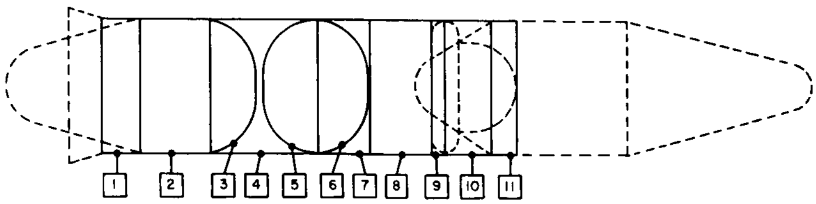

Loading Condition				Section: N_x/N_x Nominal 1	2	4	7	8	9	10	11	N_o/N_o Nominal 2	3	5	6
Prelaunch	99.9% Ground Winds		Unpressurized Tanks	.654	.904	.524	.288	.248	.236	.224	.202	.427	.005	.503	.347
Prelaunch	99.9% Ground Winds		Pressurized Tanks	.654	.711	.524	.288	.248	.236	.224	.202	.490	.242	.566	.367
Prelaunch	95.0% Ground Winds		Unpressurized Tanks	.574	.797	.477	.233	.204	.199	.176	.155	.380	.005	.503	.347
Prelaunch	95.0% Ground Winds		Pressurized Tanks	.574	.605	.477	.233	.204	.199	.176	.155	.450	.242	.566	.367
Maximum qα	95% Inflight Winds	Pressurized Tanks	Plug Nozzle	1.000	1.000	1.000	.964	.882	.846	1.000	1.000	.919	.668	.942	.778
Maximum qα	95% Inflight Winds	Pressurized Tanks	Front Steering	.767	.566	.680	.502	.504	.525	.616	.716	.781	.668	.942	.778
Maximum qα	95% Inflight Winds	Pressurized Tanks	Gimbal Nozzle	.801	.775	.934	.906	.843	.821	.970	.973	.841	.668	.942	.778
Maximum qα	95% Inflight Winds	Vented Tanks	Plug Nozzle	1.000	1.530	1.000	.964	.882	.846	1.000	1.000	.699	0.0	.710	.053
Maximum qα	95% Inflight Winds	Vented Tanks	Front Steering	.767	1.093	.680	.502	.504	.525	.616	.716	.505	0.0	.710	.053
Maximum qα	95% Inflight Winds	Vented Tanks	Gimbal Nozzle	.801	1.323	.934	.906	.843	.821	.970	.973	.586	0.0	.710	.053
Maximum qα	90% Inflight Winds	Pressurized Tanks	Plug Nozzle	.991	.985	.986	.942	.863	.829	.975	.975	.913	.668	.942	.778
Maximum qα	90% Inflight Winds	Pressurized Tanks	Front Steering	.767	.565	.679	.499	.500	.520	.606	.702	.781	.668	.942	.778
Maximum qα	90% Inflight Winds	Pressurized Tanks	Gimbal Nozzle	.800	.764	.923	.887	.826	.804	.946	.948	.839	.668	.942	.778
Maximum qα	90% Inflight Winds	Vented Tanks	Plug Nozzle	.991	1.513	.986	.942	.863	.829	.975	.975	.692	0.0	.710	.053
Maximum qα	90% Inflight Winds	Vented Tanks	Front Steering	.767	1.093	.679	.499	.500	.520	.606	.702	.505	0.0	.710	.053
Maximum qα	90% Inflight Winds	Vented Tanks	Gimbal Nozzle	.800	1.293	.923	.887	.826	.804	.946	.948	.591	0.0	.710	.053
Maximum Total Pressure	5.55 g's		Pressurized Tanks	.780	.363	.666	.683	.668	.667	.553	.478	.955	.941	1.000	1.000
Maximum Total Pressure	5.55 g's		Vented Tanks	.780	1.121	.666	.683	.668	.667	.553	.478	.505	0.0	.771	0
Maximum Boost Acceleration	5.55 g's	Pressurized Tanks	Plug Nozzle	.783	.339	.653	1.000	1.000	1.000	.829	.716	1.000	1.000	.469	1.000
Maximum Boost Acceleration	5.55 g's	Pressurized Tanks	Front Steering	.783	.339	.653	1.000	1.000	1.000	.829	.716	1.000	1.000	.469	1.000
Maximum Boost Acceleration	5.55 g's	Pressurized Tanks	Gimbal Nozzle	.783	.339	.653	1.000	1.000	1.000	.829	.716	1.000	1.000	.469	1.000
Maximum Boost Acceleration	5.55 g's	Vented Tanks	Plug Nozzle	.783	1.125	.653	1.000	1.000	1.000	.829	.716	.506	0.0	.076	0
Maximum Boost Acceleration	5.55 g's	Vented Tanks	Front Steering	.783	1.125	.653	1.000	1.000	1.000	.829	.716	.506	0.0	.076	0
Maximum Boost Acceleration	5.55 g's	Vented Tanks	Gimbal Nozzle	.783	1.125	.653	1.000	1.000	1.000	.829	.716	.506	0.0	.076	0
Maximum Boost Acceleration	2.0 g's	Pressurized Tanks	Plug Nozzle	.836	.652	.746	.564	.523	.514	.523	.503	.835	.702	.997	.814
Maximum Boost Acceleration	2.0 g's	Pressurized Tanks	Front Steering	.778	.545	.668	.451	.430	.435	.428	.431	.804	.702	.997	.814
Maximum Boost Acceleration	2.0 g's	Pressurized Tanks	Gimbal Nozzle	.785	.594	.729	.550	.513	.507	.515	.496	.818	.702	.997	.811
Maximum Boost Acceleration	2.0 g's	Vented Tanks	Plug Nozzle	.836	1.206	.746	.564	.523	.514	.523	.503	.555	0.0	.771	.010
Maximum Boost Acceleration	2.0 g's	Vented Tanks	Front Steering	.778	1.100	.668	.451	.430	.435	.428	.431	.507	0.0	.771	.010
Maximum Boost Acceleration	2.0 g's	Vented Tanks	Gimbal Nozzle	.785	1.148	.729	.550	.513	.507	.515	.496	.528	0.	.771	.010

Table 3-7

Loads Summary Chart
202 Vehicle Configuration

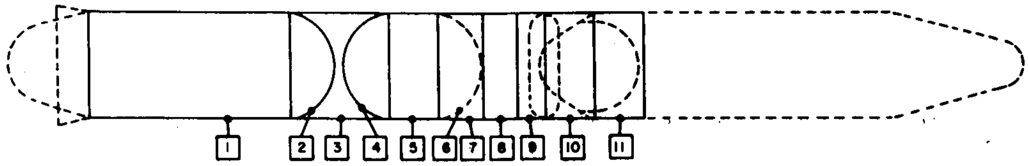

Loading Condition				Section												
				N_x/N_x Nominal								N_o/N_o Nominal				
				1	3	5	7	8	9	10	11	1	2	4	5	6
Prelaunch	99.9% Ground Wind		Unpressurized Tanks	.944	.570	.500	.333	.319	.308	.271	.240	.590	0.0	.531	.545	.125
			Pressurized Tanks	.811	.570	.428	.333	.319	.308	.271	.240	.633	.244	.601	.599	.218
	95% Ground Wind		Unpressurized Tanks	.761	.484	.363	.234	.229	.225	.183	.154	.481	0.0	.531	.482	.125
			Pressurized Tanks	.628	.484	.291	.234	.229	.225	.183	.154	.532	.244	.601	.545	.218
Maximum qα	95% Inflight Winds	Pressurized Tanks	Plug Nozzle	1.000	1.000	1.000	.994	.977	.967	1.000	1.000	1.000	.670	.970	1.000	.781
			Front Steering	.607	.651	.311	.454	.462	.471	.445	.457	.820	.670	.970	.725	.781
			Gimbal Nozzle	.816	.943	.925	.944	.935	.932	.967	.969	.908	.670	.970	.970	.781
		Vented Tanks	Plug Nozzle	1.364	1.000	1.307	.994	.997	.967	1.000	1.000	.832	0.0	.676	.844	0.0
			Front Steering	.971	.651	.618	.454	.462	.471	.445	.457	.601	0.0	.676	.476	0.0
			Gimbal Nozzle	1.180	.943	1.232	.944	.935	.932	.967	.969	.721	0.0	.676	.844	0.0
	90% Inflight Winds	Pressurized Tanks	Plug Nozzle	.961	.968	.937	.944	.929	.920	.945	.942	.981	.670	.970	.976	.781
			Front Steering	.605	.648	.302	.446	.453	.462	.432	.440	.820	.670	.970	.727	.781
			Gimbal Nozzle	.800	.921	.878	.905	.897	.893	.921	.920	.901	.670	.970	.950	.781
		Vented Tanks	Plug Nozzle	1.326	.968	1.245	.944	.929	.920	.945	.942	.809	0.0	.676	.810	0.0
			Front Steering	.970	.648	.609	.446	.453	.462	.432	.440	.600	0.0	.676	.475	0.0
			Gimbal Nozzle	1.165	.921	1.185	.905	.897	.893	.921	.920	.712	0.0	.676	.778	0.0
Maximum Total Pressure	5.55 g's		Pressurized Tanks	.488	.646	.458	.665	.665	.665	.493	.391	1.000	.941	1.000	.703	1.000
			Vented Tanks	1.000	.646	.852	.665	.665	.665	.493	.391	.604	0.0	.696	.468	0.0
Maximum Boost Acceleration	5.55 g's	Pressurized Tanks	Plug Nozzle	.460	.633	.814	1.000	1.000	1.000	.740	.588	.998	1.000	.470	.845	1.000
			Front Steering	.460	.633	.814	1.000	1.000	1.000	.740	.588	.998	1.000	.470	.845	1.000
			Gimbal Nozzle	.460	.633	.814	1.000	1.000	1.000	.740	.588	.998	1.000	.470	.845	1.000
		Vented Tanks	Plug Nozzle	1.004	.633	1.207	1.000	1.000	1.000	.740	.588	.604	0.0	.077	.663	0.0
			Front Steering	1.004	.633	1.207	1.000	1.000	1.000	.740	.588	.604	0.0	.077	.663	0.0
			Gimbal Nozzle	1.004	.633	1.207	1.000	1.000	1.000	.740	.588	.604	0.0	.077	.663	0.0
	2.0 g's	Pressurized Tanks	Plug Nozzle	.700	.745	.465	.578	.574	.572	.523	.490	.888	.709	1.000	.767	.822
			Front Steering	.650	.646	.265	.421	.423	.426	.359	.328	.841	.709	1.000	.700	.822
			Gimbal Nozzle	.592	.730	.446	.441	.563	.563	.515	.482	.864	.709	1.000	.825	.822
		Vented Tanks	Plug Nozzle	1.086	.745	.788	.578	.574	.577	.523	.490	.667	0.0	.696	.542	0.0
			Front Steering	.978	.646	.589	.421	.423	.426	.359	.328	.603	0.0	.696	.438	0.0
			Gimbal Nozzle	1.036	.730	.769	.441	.563	.563	.515	.482	.637	0.0	.696	.535	0.0

Table 3-8
Loads Summary Chart
203 Vehicle Configuration

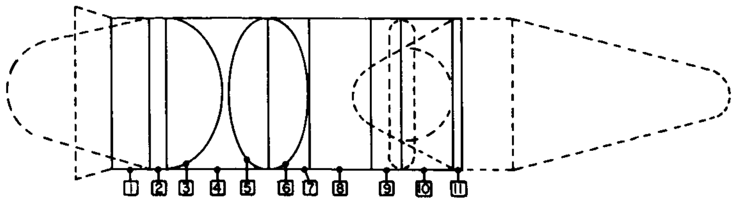

Loading Condition				Section											
				N_x/N_x Nominal								N_o/N_o Nominal			
				1	2	4	7	8	9	10	11	2	3	5	6
Prelaunch	99.9% Ground Winds		Unpressurized Tanks	.600	.919	.521	.246	.232	.220	.224	.218	.366	.010	.427	.530
			Pressurized Tanks	.600	.682	.521	.246	.232	.220	.224	.218	.441	.241	.485	.540
	95% Ground Winds		Unpressurized Tanks	.546	.837	.484	.203	.198	.194	.186	.180	.335	.010	.427	.530
			Pressurized Tanks	.546	.600	.484	.203	.198	.194	.186	.180	.415	.241	.485	.540
Maximum $q\alpha$	95% Inflight Winds	Pressurized Tanks	Plug Nozzle	1.000	1.000	1.000	.899	.836	.776	1.000	1.000	.876	.666	.823	.830
			Front Steering	.748	.523	.691	.456	.491	.523	.702	.825	.759	.666	.823	.830
			Gimbal Nozzle	.782	.711	.905	.816	.781	.743	.959	.964	.797	.666	.823	.830
		Vented Tanks	Plug Nozzle	1.000	1.647	1.000	.899	.836	.776	1.000	1.000	.630	0.0	.562	.267
			Front Steering	.748	1.170	.691	.456	.491	.523	.702	.825	.452	0.0	.562	.267
			Gimbal Nozzle	.782	1.358	.905	.816	.781	.743	.959	.964	.518	0.0	.562	.267
	90% Inflight Winds	Pressurized Tanks	Plug Nozzle	.992	.985	.990	.884	.823	.764	.982	.960	.873	.666	.823	.830
			Front Steering	.748	.523	.690	.454	.488	.519	.693	.812	.759	.666	.823	.830
			Gimbal Nozzle	.781	.705	.897	.803	.769	.733	.942	.947	.796	.666	.823	.830
		Vented Tanks	Plug Nozzle	.992	1.632	.990	.884	.823	.764	.982	.960	.625	0.0	.562	.267
			Front Steering	.748	1.170	.690	.454	.488	.519	.693	.812	.452	0.0	.562	.267
			Gimbal Nozzle	.781	1.352	.897	.803	.769	.733	.942	.947	.516	0.0	.562	.267
Maximum Total Pressure	5.55 g's		Pressurized Tanks	.755	.447	.689	.667	.667	.667	.609	.594	.952	.941	1.000	1.000
			Vented Tanks	.755	1.206	.689	.667	.667	.667	.609	.594	.455	0.0	.695	0.0
Maximum Boost Acceleration	5.55 g's	Pressurized Tanks	Plug Nozzle	.733	.389	.678	1.000	1.000	1.000	.912	.889	1.000	1.000	.820	1.000
			Front Steering	.733	.389	.678	1.000	1.000	1.000	.912	.889	1.000	1.000	.820	1.000
			Gimbal Nozzle	.733	.389	.678	1.000	1.000	1.000	.912	.889	1.000	1.000	.820	1.000
		Vented Tanks	Plug Nozzle	.733	1.212	.678	1.000	1.000	1.000	.912	.889	.458	0.0	.567	0.0
			Front Steering	.733	1.212	.678	1.000	1.000	1.000	.912	.889	.458	0.0	.567	0.0
			Gimbal Nozzle	.733	1.212	.678	1.000	1.000	1.000	.912	.889	.458	0.0	.567	0.0
	2.0 g's	Pressurized Tanks	Plug Nozzle	.764	.502	.692	.427	.426	.424	.443	.451	.791	.709	.868	.852
			Front Steering	.759	.493	.685	.417	.419	.419	.436	.447	.788	.709	.868	.852
			Gimbal Nozzle	.759	.496	.689	.425	.425	.423	.442	.450	.790	.709	.868	.852
		Vented Tanks	Plug Nozzle	.764	1.191	.692	.427	.426	.424	.443	.451	.458	0.0	.603	.244
			Front Steering	.759	1.181	.685	.417	.419	.419	.436	.447	.455	0.0	.603	.244
			Gimbal Nozzle	.759	1.184	.689	.425	.425	.423	.442	.450	.456	0.0	.603	.244

Table 3-9
Loads Summary Chart
301 Vehicle Configuration

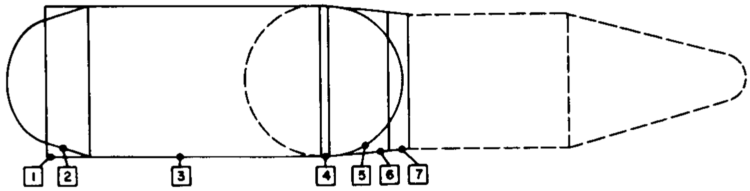

Loading Condition				Section N_x/N_x Nominal 1	3	4	6	7'	N_o/N_o Nominal 2	3	4	5
Prelaunch	99.9% Ground Winds		Unpressurized Tanks	.688	.850	.474	.220	.221	.145	.527	.675	.698
			Pressurized Tanks	.688	.669	170	.220	.221	.432	.608	.776	815
	95% Ground Winds		Unpressurized Tanks	.639	.803	.345	.163	.167	.145	.500	.663	.698
			Pressurized Tanks	.639	.622	.036	.163	.167	.432	.585	.769	.815
Maximum qα	95 % Inflight Winds	Pressurized Tanks	Plug Nozzle	1.000	1.000	1.000	1.000	1.000	.790	1.000	1.000	.858
			Front Steering	.871	.760	0.0	.603	.730	.790	.893	.918	.858
			Gimbal Nozzle	.901	.944	.952	.980	.982	.790	.969	.996	.858
		Vented Tanks	Plug Nozzle	1.000	1.370	2.145	1.000	1.000	.204	.822	.677	.227
			Front Steering	.871	1.130	1.085	.603	.730	.204	.687	.535	.227
			Gimbal Nozzle	.901	1.314	2.096	.980	.982	.204	.783	.670	.227
	90% Inflight Winds	Pressurized Tanks	Plug Nozzle	.993	.984	.913	.960	.962	.790	.994	1.000	.858
			Front Steering	.871	.757	0.0	.586	.706	.790	.892	.913	.858
			Gimbal Nozzle	.899	.930	.869	.943	.946	.790	.964	.996	.858
		Vented Tanks	Plug Nozzle	.993	1.354	2.059	.960	.962	.204	.813	.665	.227
			Front Steering	.871	1.127	1.058	.586	.706	.204	.686	.528	.227
			Gimbal Nozzle	.899	1.301	2.016	.943	.946	.204	.777	.659	.227
Maximum Boost Acceleration	2.0 g's	Pressurized Tanks	Plug Nozzle	.919	.797	0.0	.539	.548	.844	.946	.910	.880
			Front Steering	.884	.732	0.0	.432	.475	.844	.918	.891	.880
			Gimbal Nozzle	.891	.780	0.0	.534	.543	.844	.938	.909	.880
		Vented Tanks	Plug Nozzle	.919	1.196	1.146	.539	.548	.213	.724	.487	.164
			Front Steering	.884	1.130	.8567	.432	.475	.213	.687	.451	.164
			Gimbal Nozzle	.891	1.178	1.132	.534	.543	.213	.714	.485	.164
	2.5 g's	Pressurized Tanks	Plug Nozzle	.894	.661	0.0	.346	.363	1.000	.996	.764	1.000
			Front Steering	.894	.661	0.0	.346	.363	1.000	.996	.764	1.000
			Gimbal Nozzle	.894	.661	0.0	.346	.363	1.000	.996	.764	1.000
		Vented Tanks	Plug Nozzle	.894	1.133	.718	.346	.363	.234	.685	.179	0.0
			Front Steering	.894	1.133	.718	.346	.363	.234	.685	.179	0.0
			Gimbal Nozzle	.894	1.133	.718	.346	.363	.234	.685	.179	0.0
	6.0 g's	Pressurized Tanks	Plug Nozzle	.843	.506	.327	1.071	1.121	1.195	.988	.784	1.027
			Front Steering	.843	.506	.327	1.071	1.121	1.195	.988	.784	1.027
			Gimbal Nozzle	.843	.506	.327	1.071	1.121	1.195	.988	.784	1.022
		Vented Tanks	Plug Nozzle	.843	1.050	2.210	1.071	1.121	.382	.614	.371	0.0
			Front Steering	.843	1.050	2.210	1.071	1.121	.382	.614	.371	0.0
			Gimbal Nozzle	.843	1.050	2.210	1.071	1.121	.382	.614	.371	0.0

SECTION 4

OPTIMIZED STRUCTURAL WEIGHT ANALYSIS—ISOTROPIC MATERIALS

Tables 4-1, 4-2, 4-3, 4-4, and 4-5 summarize the results of the loads variation study for the 101, 201, 202, 203, and 301 Vehicles respectively. Except as noted, these tables present the structural weights for variations in loads where nominal material and types of construction have been used. The left side of each of these tables is concerned with single-parameter variations while the right side is concerned with multiple parameter variations. Table 4-3 includes the weight tabulation of the 202 RT configuration. The 202 RT configuration was considered to have front-end steering. It is observed that when its weight is compared with the 202 configuration with front steering, that reversing the first stage propellant tanks had only a small effect.

The last column of Table 4-2 shows the weight tabulation for a 201 configuration where the separate loads were taken to their lowest values and the structure was made of beryllium honeycomb sandwich. The weight savings available through these idealized conditions is 73 percent.

Table 4-6 shows the tabulated weights for the 201, 204, and 205 Vehicle configurations under nominal conditions. The only variable in this table is the payload density. The 201 Vehicle has a density of 2.5 lbs/ft^3 while the densities of the 204 and 205 Vehicles are 4.0 lbs/ft^3 and 6.2 lbs/ft^3 respectively.

Tables 4-7 through 4-15 are tabulations of structural weight for various combinations of materials and types of construction. The material properties of the aluminum, titanium, and beryllium considered in the analysis are presented in Tables 8-3, 8-6, and 8-10 respectively. These three metals were considered in combination with the five types of construction shown in Figure A-3. The loads were nominal for each of the five vehicle configurations considered. In the tabulations, monocoque heads were used for all construction types. When the corrugation constructions were examined, the pressurized cylinders were taken to be integrally stiffened skin.

Table 4-1

101 Vehicle—Structural Weights and Weight Savings

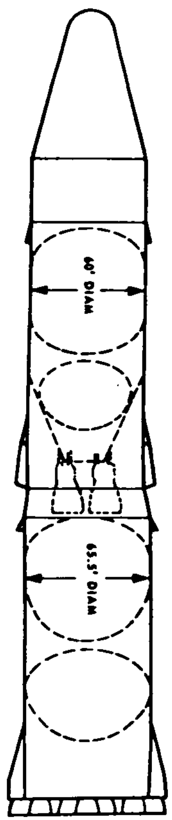

101 VEHICLE—STRUCTURAL WEIGHTS AND WEIGHT SAVINGS

Section \ Criteria and Configuration	Nominal Weight	Design Criteria: Reduction of Inflight Winds to 90 Percent	Design Criteria: Limitation of Maximum Acceleration to 2 g's	Design Criteria: Vented Tanks	Design Criteria: Factor of Safety 1.0, 1.1	Unique Design Configuration: Use of Plug Nozzle	Unique Design Configuration: Use of Front End Steering**	Eliminate Fabrication Factor	Combination of Design Criteria and Configuration Variables: Vented Tank 90% Winds Limited g Front End Steering**	Combination: Vented Tank 90% Winds Limited g Plug Nozzle	Combination: Vented Tank 90% Winds Limited g Gimballed Nozzle	Combination: Press. Tank 90% Winds Limited g Gimballed Nozzle
Instrument Unit	8,736	8,610	8,736	8,736	7,423	8,894	9,326	7,277	9,184	8,762	8,610	8,610
Forward Skirt	12,523	12,343	12,523	12,523	10,974	12,776	13,466	10,432	13,248	12,528	12,343	12,343
LH_2 Tank Top Head	10,557	10,557	9,090	1,321	9,597	10,557	10,557	10,050	1,321	1,321	1,321	9,090
LH_2 Tank Cylinder	24,613	24,613	24,613	24,870	24,393	24,613	24,613	20,503	25,269	25,035	24,475	12,835
LH_2 Tank Bottom Head	12,464	12,464	10,557	1,321	11,330	12,464	12,464	11,866	1,321	1,321	1,321	10,557
Intertank	35,527	34,910	35,527	35,527	30,747	36,668	31,547	29,594	31,209	35,964	34,910	34,910
Baffles and Insulation	*23,740	*23,740	*23,740	*23,740	*23,740	*23,740	*23,740	*23,740	*23,740	*23,740	*23,740	*23,740
LOX Tank and Thrust Structure	54,546	54,546	54,546	54,546	54,546	54,546	54,546	51,928	54,546	54,546	54,546	54,546
Aft Skirt	121,428	121,428	105,178	121,428	101,698	121,428	121,428	101,150	81,874	108,521	103,820	103,820
2nd Stage Total—lb	304,134	303,211	284,510	284,012	274,448	305,686	301,687	266,540	241,712	271,738	265,086	270,451
(2nd Stage Total—kg)	(137,955)	(137,537)	(129,054)	(128,828)	(124,490)	(138,659)	(136,845)	(120,903)	(109,641)	(123,260)	(120,243)	(122,677)
Interstage	33,583	33,583	28,347	33,583	27,413	33,583	33,583	27,975	20,821	29,858	27,956	27,956
Forward Skirt	52,357	52,357	43,159	52,357	42,508	52,357	52,357	43,613	31,087	46,407	42,555	42,555
LOX Tank Top Head	8,345	8,345	6,025	1,574	7,586	8,345	8,345	7,944	1,574	1,574	1,574	6,025
LOX Tank Cylinder	20,971	20,971	18,748	27,439	17,909	20,971	20,971	17,469	17,574	23,920	23,273	18,422
LOX Tank Bottom Head	14,614	14,614	13,927	9,909	13,284	14,614	14,614	13,913	9,909	9,909	9,909	13,927
Intertank	135,205	134,254	135,205	135,205	114,864	144,872	115,334	112,626	115,239	144,710	134,254	134,254
RP-1 Top Head	8,075	8,075	6,347	1,574	7,340	8,075	8,075	7,687	1,574	1,574	1,574	6,347
RP-1 Bottom Head	10,923	10,923	10,010	6,619	9,929	10,923	10,923	10,399	6,237	6,237	6,237	10,010
Thrust Takeout	47,291	47,167	47,291	47,291	40,591	52,054	44,471	39,393	44,321	51,704	47,167	47,167
Thrust Structure	81,537	81,537	81,537	81,537	81,537	81,537	79,757	81,537	79,757	81,537	81,537	81,537
Baffles and Insulation	*39,270	*39,270	*39,270	*39,270	*39,270	*39,270	*39,270	*39,270	*39,270	*39,270	*39,270	*39,270
1st Stage Total—lb	452,171	451,096	429,866	436,358	402,231	466,601	427,700	401,826	367,363	436,700	415,306	427,470
(1st Stage Total—kg)	(205,105)	(204,617)	(194,987)	(197,932)	(182,452)	(211,650)	(194,005)	(182,268)	(166,636)	(198,087)	(188,383)	(193,900)
Total Structure—lb	756,305	754,307	714,376	720,370	676,679	772,287	729,387	668,366	609,075	708,438	680,392	697,921
(Total Structure—kg)	(343,060)	(342,154)	(324,041)	(326,760)	(306,942)	(350,309)	(330,850)	(303,171)	(276,277)	(321,347)	(308,626)	(316,577)
Difference from Nominal	-	-1,998	-41,929	-35,935	-79,626	+15,982	-26,918	-87,939	-147,230	-47,867	-75,913	-58,384
Percent Weight Savings	-	0.26	5.54	4.75	10.53	-2.11	3.56	11.63	19.47	6.33	10.04	7.72

* Assumed values taken from References 1 and 2.
**Front End Steering results do not include weight of Front Steering Equipment which significantly reduces weight savings.
Note: In the interest of brevity, only total weights are expressed in kilograms.

Table 4-2

201 Vehicle—Structural Weights and Weight Savings

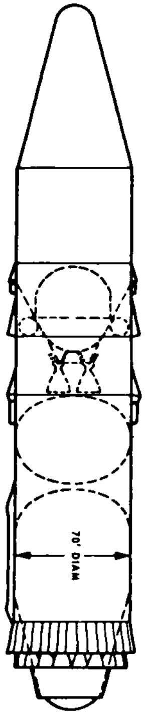

Criteria and Configuration / Section	201 VEHICLE—STRUCTURAL WEIGHTS AND WEIGHT SAVINGS												
		Design Criteria				Unique Design Configuration			Combination of Design Criteria and Configuration Variables				With Beryllium HYC
	Nominal Weight	Reduction of Inflight Winds to 90 Percent	Limitation of Maximum Acceleration to 2 g's	Vented Tanks	Factor of Safety 1.0, 1.1	Use of Gimballed Nozzle	Use of Front End Steering**	Eliminate Fabrication Factor	Vented Tank 90% Winds Limited g Front End Steering**	Vented Tank 90% Winds Limited g Plug Nozzle	Vented Tank 90% Winds Limited g Gimballed Nozzle	Press. Tank 90% Winds Limited g Gimballed Nozzle	Vented Tank 90% Winds Limited g Front End Steering**
IU and Forward Skirt	13,004	12,795	13,004	13,004	11,145	12,779	10,311	10,832	10,144	12,795	12,571	12,571	1,767
LH_2 Tank and Thrust Structure	39,323	39,323	39,323	39,323	39,323	39,323	39,323	37,435	39,323	39,323	39,323	39,323	18,511
Intertank	38,963	38,360	38,963	38,963	33,679	38,239	34,771	32,456	28,990	38,360	37,659	37,659	5,434
Baffles and Insulation	*12,900	*12,900	*12,900	*12,900	*12,900	*12,900	*12,900	*12,900	*12,900	*12,900	*12,900	*12,900	*12,900
LOX Tank	8,850	8,850	8,850	8,850	8,045	8,850	8,850	8,425	8,850	8,850	8,850	8,850	4,840
Aft Skirt	10,389	10,389	9,452	10,389	8,883	10,389	10,389	8,654	7,040	9,187	9,009	9,009	853
2nd Stage Total—lb	123,429	122,617	122,492	123,429	113,975	122,480	116,544	110,702	107,247	121,415	120,312	120,312	44,305
(2nd Stage Total—kg)	(55,987)	(55,619)	(55,562)	(55,987)	(51,699)	(55,557)	(52,864)	(50,214)	(48,647)	(55,074)	(54,574)	(54,574)	(20,097)
Interstage	65,266	65,266	58,940	65,266	55,684	65,266	65,266	54,366	43,300	59,091	57,437	57,437	8,558
Forward Skirt	46,882	46,882	45,825	46,882	39,898	46,882	46,882	39,053	28,901	45,179	43,490	43,490	6,509
LOX Tank Top Head	8,746	8,746	7,119	3,033	7,950	8,746	8,746	8,326	3,033	3,033	3,033	7,119	2,295
LOX Tank Bottom Head	19,318	19,318	19,260	14,894	17,561	19,318	19,318	18,391	14,894	14,894	14,894	19,260	11,715
Intertank	156,026	154,607	156,026	156,026	125,890	149,338	112,912	129,970	112,790	154,607	148,223	148,223	26,576
LH. Tank Top Head	15,935	15,935	11,186	1,800	14,484	15,935	15,935	15,170	1,800	1,800	1,800	11,186	1,258
LH Tank Cylinder	63,411	63,197	63,411	84,684	60,711	62,041	62,041	52,821	67,484	84,004	75,204	60,466	14,316
LH_2 Tank Bottom Head	35,330	35,330	32,808	5,682	29,815	35,330	35,330	33,634	5,682	5,682	5,682	32,808	3,740
Thrust Takeout	53,698	53,266	53,698	53,698	52,463	43,717	43,020	44,730	42,842	53,266	43,665	43,665	9,995
Thrust Structure	82,741	82,741	82,741	82,741	82,741	82,741	80,110	82,741	80,110	82,741	82,741	82,741	35,383
Baffles and Insulation	*20,040	*20,040	*20,040	*20,040	*20,040	*20,040	*20,040	*20,040	*20,040	*20,040	*20,040	*20,040	*20,040
1st Stage Total—lb	567,393	565,328	551,054	534,746	507,237	549,354	509,600	499,242	420,876	524,337	496,209	526,435	140,685
(1st Stage Total—kg)	(257,369)	(256,433)	(249,958)	(242,561)	(230,083)	(249,187)	(231,155)	(226,456)	(190,909)	(237,839)	(225,080)	(238,791)	(63,815)
Total Structure—lb	690,822	687,945	673,546	658,175	621,212	671,834	626,144	609,944	528,123	645,752	616,521	646,747	184,990
(Total Structure—kg)	(313,356)	(312,052)	(305,520)	(298,548)	(281,782)	(304,744)	(284,019)	(276,670)	(239,556)	(292,913)	(279,654)	(293,365)	(83,912)
Difference from Nominal	-	-2,877	-17,276	-32,647	-69,610	-18,988	-64,678	-80,878	-162,699	-45,070	-74,301	-44,075	-505,832
Percent Weight Savings	-	0.41	2.50	4.72	10.07	2.74	9.36	11.70	23.56	6.52	10.75	6.38	73.22

* Assumed values taken from References 1 and 2.
**Front End Steering results do not include weight of Front Steering Equipment which significantly reduces weight savings.
Note: In the interest of brevity, only total weights are expressed in kilograms.

Table 4-3

202 Vehicle—Structural Weights and Weight Savings

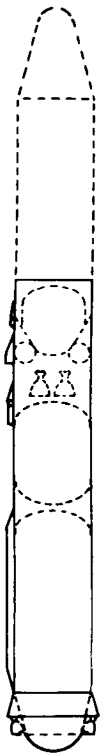

Criteria and Configuration / Section	202 VEHICLE—STRUCTURAL WEIGHTS AND WEIGHT SAVINGS												202 RT
		Design Criteria				Unique Design Configuration			Combination of Design Criteria and Configuration Variables				
	Nominal Weight	Reduction of Inflight Winds to 90 Percent	Limitation of Maximum Acceleration to 2 g's	Vented Tanks	Factor of Safety 1.0, 1.1	Use of Gimballed Nozzle	Use of Front End Steering**	Eliminate Fabrication Factor	Vented Tank 90% Winds Limited g Front End Steering**	Vented Tank 90% Winds Limited g Plug Nozzle	Vented Tank 90% Winds Limited g Gimballed Nozzle	Press. Tank 90% Winds Limited g Gimballed Nozzle	Combination of Reversed Propellant Tanks and Front End Steering
IU and Forward Skirt	25,561	25,030	25.561	25.561	22,263	25,300	16,120	21,292	10,000	25.030	24.703	24,703	17.848
LH_2 Tank and Thrust Structures	32,628	32,628	32,628	32,628	32,628	32,628	32,628	31,062	32.628	32.628	32,628	32,628	32.628
Intertank	36,971	35,780	36.971	36,971	33,251	36,240	32,330	30,797	23.500	35.780	35.345	35,345	34.268
Baffles and Insulation	*12,900	*12,900	*12,900	*12,900	*12,900	*12,900	*12,900	*12,900	*12.900	*12.900	*12.900	*12.900	*12.900
LOX Tanks	6,961	6,961	6,961	6,961	6,328	6,961	6,961	6,627	6.961	6.961	6.961	6.961	6.961
Aft Skirt	25,863	25,863	25.110	25.863	21.025	25,863	25,863	21,544	11.500	24.046	23.436	23.436	24.660
2nd Stage Total—lb	140.884	139.162	140.131	140.884	128.395	139,892	126,802	124,222	97,489	137,345	135.973	135.973	129.265
(2nd Stage Total—kg)	(63,905)	(63,124)	(63,563)	(63,905)	(58,240)	(63,455)	(57,517)	(56,347)	(44,221)	(62,300)	(61,677)	(61,677)	(58,635)
Interstage	24,126	24,126	23,980	24.126	20,676	24,126	24,126	20,097	12,500	22,964	22,452	22,452	24.233
Forward Skirt	31,677	31,677	31,555	31,667	25,824	31,677	31,667	26,387	19,640	30,537	29.744	29.744	31.715
LOX Tank Top Head	5,398	5,398	4,437	1,110	4,907	5,398	5,398	5,139	1,110	1,110	1.110	4,437	5.398
LOX Tank Cylinder	40,449	38,577	40,449	50,310	35,418	38,220	36,054	33,694	30,335	48,485	46,319	37,113	29,084
LOX Tank Bottom Head	11,590	11,590	11,590	8,067	10,535	11,590	11,590	11,034	8,067	8,067	8.067	11,590	28,472
Intertank	99,728	97,639	99,728	99,728	92,197	96,007	77,200	83,073	77.000	97.639	94.571	94.571	79.194
LH_2 Tank Top Head	9,838	9,838	6,976	1,110	9,740	9,838	9,838	9,366	1,110	1,110	1,110	6,976	9.838
LH_2 Tank Cylinder	181,402	176,448	181,402	228,820	154,336	174,289	174,289	151,108	178,607	223,880	202.850	156,181	164,013
LH_2 Tank Bottom Head	17,530	17,530	16,945	1,863	16,158	17,530	17,530	16,689	1,863	1,863	1.863	16,945	9.838
Thrust Takeout	-	-	-	-	-	-	-	-	-	-	-	-	-
Thrust Structure	93,297	93,297	93,297	93,297	93,297	93,297	92,184	93,297	92,184	93,297	93,297	93,297	92.184
Baffles and Insulation	*20,040	*20,040	*20,040	*20,040	*20,040	*20,040	*20,040	*20,040	*20,040	*20,040	*20,040	*20,040	*20,040
1st Stage Total—lb	535,075	526,160	530,399	560,138	483,128	522,012	499,916	469,924	442,456	548,992	521,423	493,346	494,009
(1st Stage Total—kg)	(242,710)	(238,666)	(240,589)	(254,079)	(219,147)	(236,785)	(226,762)	(213,158)	(200,698)	(249,023)	(236,517)	(223,782)	(224,082)
Total Structure—lb	675,959	665,322	670,530	701,022	611,523	661,904	626,718	594,146	539,945	686,337	657,396	629,319	623,274
(Total Structure—kg)	(306,615)	(301,790)	(304,152)	(317,984)	(277,387)	(300,240)	(284,279)	(269,505)	(244,919)	(311,322)	(298,194)	(285,459)	(282,717)
Differences from Nominal	-	-10,637	-5,429	+25,063	-64,436	-14,055	-49,241	-81,813	-136,014	+10,378	-18,563	-46,640	-52,685
Percent Weight Savings	-	1.57	0.80	-3.71	9.53	2.07	7.28	12.10	20.12	-1.54	2.75	6.90	7.79

* Assumed values taken from References 1 and 2.
**Front End Steering results do not include Front Steering Equipment which significantly reduces weight savings.
Note: In the interest of brevity, only total weights are expressed in kilograms.

Table 4-4

203 Vehicle—Structural Weights and Weight Savings

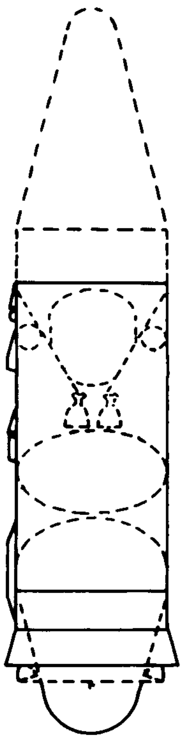

Section \ Criteria and Configuration	Nominal Weight	Design Criteria: Reduction of Inflight Winds to 90 Percent	Design Criteria: Limitation of Maximum Acceleration to 2 g's	Design Criteria: Vented Tanks	Design Criteria: Factor of Safety 1.0, 1.1	Unique Design Configuration: Use Gimballed Nozzle	Unique Design Configuration: Use of Front End Steering**	Eliminate Fabrication Factor	Combination of Design Criteria and Configuration Variables: Vented Tank 90% Winds Limited g Front End Steering**	Combination: Vented Tank 90% Winds Limited g Plug Nozzle	Combination: Vented Tank 90% Winds Limited g Gimballed Nozzle	Combination: Press. Tank 90% Winds Limited g Gimballed Nozzle
IU and Forward Skirt	3,030	2,952	3,030	3,030	2,648	2,959	2,817	2,524	2,6[illegible]7	2,952	2,926	2,926
LH_2 Tank and Thrust Structure	46,232	46,232	46,232	46,232	46,232	46,232	46,232	44,013	46,232	46,232	46,232	46,232
Intertank	37,658	37,099	37,658	37,658	32,473	36,384	34,923	31,369	29,523	37,099	35,855	35,855
Baffles and Insulation	*12,900	*12,900	*12,900	*12,900	*12,900	*12,900	*12,900	*12,900	*12,900	*12,900	*12,900	*12,900
LOX Tank	9,755	9,755	9,755	9,755	8,867	9,755	9,755	9,287	9,755	9,755	9,755	9,755
Aft Skirt	14,164	14,164	12,110	14,164	12,186	14,164	14,164	11,799	9,680	11,971	11,669	11,669
2nd Stage Total—lb	123,739	123,102	121,685	123,739	115,306	122,394	120,791	111,892	110,707	120,909	119,337	119,337
(2nd Stage Total—kg)	(56,128)	(55,839)	(55,196)	(56,128)	(52,303)	(55,518)	(54,791)	(50,754)	(50,217)	(54,844)	(54,131)	(54,131)
Interstage	91,099	91,099	81,270	91,099	78,246	91,099	91,099	75,885	60,550	80,492	77,189	77,189
Forward Skirt	44,531	44,531	41,789	44,531	38,779	44,531	44,531	37,079	29,500	41,376	39,230	39,230
LOX Tank Top Head	11,195	11,195	9,538	5,932	11,083	11,195	11,195	10,658	5,932	5,932	5,932	11,195
LOX Tank Bottom Head	47,755	47,755	41,451	33,190	47,278	47,755	47,755	45,463	28,797	28,796	28,796	47,755
Intertank	151,807	150,586	151,807	151,807	127,135	152,418	116,624	126,455	116,513	150,586	139,268	139,268
LH_2 Tank Top Head	20,814	20,814	14,757	2,348	20,606	20,814	20,814	19,815	2,348	2,348	2,348	20,818
LH_2 Tank Cylinder	17,170	17,007	17,170	18,038	16,693	16,902	16,902	14,303	17,311	18,015	17,578	16,929
LH_2 Tank Bottom Head	49,685	49,685	41,800	9,960	45,653	49,685	49,685	47,300	4,761	4,761	4,761	49,685
Thrust Takeout	60,423	60,046	60,423	60,423	50,492	50,314	49,289	50,332	49,289	60,046	50,269	50,269
Thrust Structure	100,585	100,585	100,585	100,585	100,585	100,585	98,372	100,585	98,372	100,585	100,585	100,585
Baffles and Insulation	*20,040	*20,040	*20,040	*20,040	*20,040	*20,040	*20,040	*20,040	*20,040	*20,040	*20,040	*20,040
1st Stage Total—lb	615,104	613,343	580,630	537,953	556,590	605,338	566,306	547,915	433,413	512,977	485,996	572,963
(1st Stage Total—kg)	(279,011)	(278,212)	(263,374)	(244,015)	(252,469)	(274,581)	(256,876)	(248,534)	(196,596)	(232,686)	(220,448)	(259,896)
Total Structure—lb	738,843	736,445	702,315	661,692	671,896	727,732	687,097	659,807	544,120	633,886	605,333	692,300
(Total Structure—kg)	(335,139)	(334,051)	(318,570)	(300,143)	(304,772)	(330,099)	(311,667)	(299,288)	(246,813)	(287,530)	(274,579)	(314,027)
Difference from Nominal	-	-2,398	-36,528	-77,151	-66,947	-11,111	-51,746	-79,036	-194,723	-104,957	-133,510	-46,543
Percent Weight Savings	-	0.32	4.94	10.44	9.06	1.50	7.00	10.70	26.36	14.21	18.07	6.30

* Assumed values taken from References 1 and 2.

**Front End Steering results do not include weight of Front Steering Equipment which significantly reduces weight savings.

Note: In the interest of brevity, only total weights are expressed in kilograms.

Table 4-5

301 Vehicle—Structural Weights and Weight Savings

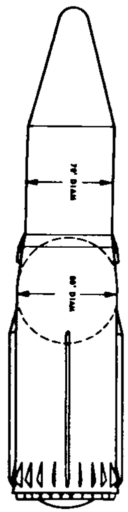

301 VEHICLE—STRUCTURAL WEIGHTS AND WEIGHT SAVINGS

Section \ Criteria and Configuration	Nominal Weight	Design Criteria					Unique Design Configuration		Eliminate Fabrication Factor	Combination of Design Criteria and Configuration Variables		
		Reduction of Inflight Winds to 90 Percent	Limitation of Maximum Acceleration to 2 g's	Limitation of Maximum Acceleration to 8 g's	Vented Tanks	Factor of Safety 1.0, 1.1	Use of Gimballed Nozzle	Use of Front End Steering**		Press. Tank 90% Winds Limited g Front End Steering**	Press. Tank 90% Winds Limited g Plug Nozzle	Press. Tank 90% Winds Limited g Gimballed Nozzle
Instrument Unit	13,647	13,045	13,647	14,161	13,647	12,376	13,995	12,504	11,368	12,402	13,486	13,418
Forward Skirt	52,748	49,430	52,748	54,970	52,748	46,246	48,949	40,514	43,939	39,982	51,455	50,905
LOX Tank Top Head	14,489	14,489	12,750	14,880	10,113	13,170	14,489	14,489	13,794	12,750	10,113	10,113
LOX Tank Cylinder	5,189	4,849	5,189	5,189	9,664	4,356	5,001	3,139	4,387	4,387	4,849	4,680
Common Bulkhead	63,425	63,425	59,390	83,240	65,625	60,396	63,425	63,425	61,820	59,390	59,390	59,390
LH_2 Tank Cylinder	316,615	313,022	316,615	316,615	406,513	279,167	304,041	274,538	263,740	274,004	313,022	300,897
LH_2 Tank Bottom Head	22,287	22,287	18,811	26,634	5,214	20,259	22,287	22,287	21,217	18,811	18,811	18,811
Thrust Takeout	78,745	78,439	78,745	78,745	78,745	69,388	74,416	74,110	65,595	73,672	78,439	74,328
Thrust Structure	56,175	56,175	56,175	56,175	56,175	56,175	56,175	54,939	56,175	54,939	56,175	56,175
Insulation	*18,000	*18,000	*18,000	*18,000	*18,000	*18,000	*18,000	*18,000	*18,000	*18,000	*18,000	*18,000
Total Structure—lb	641,320	633,161	632,070	668,609	716,444	579,533	620,778	577,945	560,035	568,337	623,740	606,717
(Total Structure—kg)	(290,903)	(287,202)	(286,707)	(303,281)	(324,979)	(262,876)	(281,585)	(262,156)	(254,032)	(257,798)	(282,928)	(275,207)
Difference from Nominal	-	-8,159	-9,250	27,289	75,124	-61,787	-20,542	-63,375	-81,285	-72,983	-17,580	-34,603
Percent Weight Savings	-	1.27	1.44	-4.26	-11.71	9.63	3.2	9.88	12.67	11.38	2.74	5.40

* Assumed values taken from References 1 and 2.
**Front End Steering results do not include weight of Front Steering Equipment which significantly reduces weight savings.
Note: In the interest of brevity, only total weights are expressed in kilograms.

Table 4-6

Summary of Vehicle Weights for Variations in Payload Density

Vehicle →	201	204	205
Payload Density lbs/ft^3 →	2.5	4.0	6.2
IU and Forward Skirt	13,004	10,248	10,246
LH_2 Tank and Thrust Structure	39,323	39,323	39,323
Intertank	33,963	34,556	34,552
Baffles and Insulation	*12,900	*12,900	*12,900
LOX Tank	8,850	8,850	8,850
Aft Skirt	10,389	10,389	10,389
2nd Stage Total	123,429	116,266	116,260
Interstage	65,266	65,268	65,266
Forward Skirt	46,882	46,358	46,357
LOX Tank Top Head	8,746	8,746	8,746
LOX Tank Bottom Head	19,318	19,318	19,318
Intertank	156,026	144,064	138,139
LH_2 Tank Top Head	15,935	15,935	15,935
LH_2 Tank Cylinder	63,411	62,169	62,169
LH_2 Tank Bottom Head	35,330	35,330	35,330
Thrust Takeout	53,698	51,183	50,260
Thrust Structure	82,741	82,741	82,741
Baffles and Insulation	*20,040	*20,040	*20,040
1st Stage Total	567,393	551,152	544,301
Total	690,822	667,418	660,561
Difference from 201		-23,040	-30,261
Percent Weight Saving		3.38	4.38

Table 4-7

101 Vehicle Configuration
Variation of Vehicle Structural Weight with Changes in Materials And Types of Construction Exposed to Nominal Loading Conditions

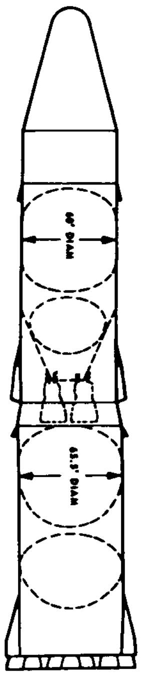

Section	Weight Variation With Change of Wall Construction For Material Same as Nominal						Weight Variation With Change of Material For Wall Construction Same as Nominal				Weight Variation With Change of Wall Construction For Beryllium				
		Wall Construction							Material		Wall Construction				
	Material as Used in Nominal	Monocoque Weight, Lb	Honeycomb Weight, Lb	OFC Weight, Lb	SFC Weight, Lb	ISS Weight, Lb	Wall Construction as Used in Nominal	Nominal (Aluminum) Weight, Lb	Titanium Weight, Lb	Beryllium Weight, Lb	Monocoque Weight, Lb	Honeycomb Weight, Lb	OFC Weight, Lb	SFC Weight, Lb	ISS Weight, Lb
Instrument Unit	Al	20867	2934	13959	6722	8736	ISS	8736	10444	2515	8114	1614	22999	2212	2515
Forward Skirt	Al	31197	4668	10164	10191	12523	ISS	12523	15651	3715	12130	2562	11271	3365	3715
LH_2 Tank Top Head	Al	10557	10557	10557	10557	10557	MONO	10557	6784	6685	6685	6685	6685	6685	6685
LH_2 Tank Cylinder	Al	28797	18972	24613	24613	24613	ISS	24613	15319	15259	11462	12533	15259	15259	15259
LH_2 Tank Bottom Head	Al	12464	12464	12464	12464	12464	MONO	12464	7921	8229	8229	8229	8229	8229	8229
Intertank	Al	81023	15432	31205	27955	35527	ISS	35527	43917	10793	31504	8249	36638	9282	10793
Baffles and Insulation		*23740	*23740	*23740	*23740	*23740		*23740	*23740	*23740	*23740	*23740	*23740	*23740	*23740
LOX Tank and Thrust Str.	Al	54546	54546	54546	54546	54546		54546	47740	26093	25093	26093	26093	26093	26093
Aft Skirt	Al	213332	60963	100673	92673	121428	ISS	121428	138051	32058	82950	30480	127608	26683	32058
Second Stage Total in lbs		476523	204296	281921	263461	304134		304134	309567	129087	210937	120185	278522	121548	129087
(Second Stage Total in kg)		(216151)	(92669)	(127879)	(119506)	(137955)		(137955)	(140420)	(58554)	(95681)	(54516)	(126338)	(55134)	(58554)
Interstage	Al	57684	15708	20487	22978	33583	ISS	33583	37246	8754	22429	7877	23169	7156	8754
Forward Skirt	Al	93473	24925	41101	37010	52357	ISS	52357	58504	14196	36345	12504	51468	11519	14196
LOX Tank Top Head	Al	8345	8345	8345	8345	8345	MONO	8345	5468	5043	5043	5043	5043	5043	5043
LOX Tank Cylinder	Al	43062	11267	20971	20971	20971	ISS	20971	25950	8937	17067	6995	8937	8937	8937
LOX Tank Bottom Head	Al	14614	14614	14614	14614	14614	MONO	14614	9311	9549	9549	9549	9549	9549	9549
Intertank	Al	226333	67584	142142	99653	135205	ISS	135205	157011	35629	88005	33798	208548	28519	35629
RP1 Top Head	Al	8075	8075	8075	8075	8075	MONO	8075	6151	4442	4442	4442	4442	4442	4442
RP1 Bottom Head	Al	10923	10923	10923	10923	10923	MONO	10923	8321	6009	6009	6009	6009	6009	6009
Thrust Takeout	Al	77042	24311	41192	34946	47291	ISS	47291	55241	12322	30759	12169	55401	10067	12322
Thrust Structure	Al	81537	81537	81537	81537	81537		81537	81537	49773	49773	49773	49773	49773	49773
Baffles and Insulation		*39270	*39270	*39270	*39270	*39270		*39270	*39270	*39270	*39270	*39270	*39270	*39270	*39270
First Stage Total in lbs		660358	306559	428657	378322	452171		452171	484019	193924	308691	187429	461829	180284	193924
(First Stage Total in kg)		(299538)	(139055)	(194439)	(171607)	(205105)		(205105)	(219551)	(87964)	(140022)	(85018)	(209486)	(81777)	(87964)
Vehicle Total in lbs		1136881	510855	710578	641783	756305		756305	793586	323011	519628	307614	740351	301832	323011
(Vehicle Total in kg)		(515689)	(231724)	(322318)	(291113)	(343060)		(343060)	(359971)	(146518)	(235703)	(139534)	(335824)	(136911)	(146518)
Difference From Nominal		380576	-245450	-45727	-114522	-		-	+37281	-433294	-236677	-448691	-15954	-454473	-433294
Percent Weight Saving		-50.32	32.45	6.05	15.14	-		-	-4.93	57.29	31.29	59.33	2.11	60.09	57.29

* Fixed Weights Taken From References 1 and 2.

NOTE: For clarity, only stage and vehicle total weights are expressed in kilograms within brackets.

Table 4-8

101 Vehicle Configuration
Variation of Vehicle Structural Weight with Changes in Materials And Types of Construction Exposed to Nominal Loading Conditions

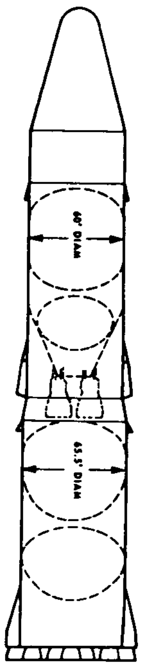

Weight Variation with Change of Wall Construction for Titanium

Section	Wall Construction: Monocoque Weight, lb	Honeycomb Weight, lb	OFC Weight, lb	SFC Weight, lb	ISS Weight, lb
Instrument Unit	28236	2640	17457	8629	10444
Forward Skirt	42213	4098	12865	13150	15651
LH_2 Tank Top Head	6784	6784	6784	6784	6784
LH_2 Tank Cylinder	38859	12276	15319	15319	15319
LH_2 Tank Bottom Head	7921	7921	7921	7921	7921
Intertank	109634	12525	39442	36125	43917
Baffles and Insulation	*23740	*23740	*23740	*23740	*23740
LOX Tank and Thrust Structure	47740	47740	47740	47740	47740
Aft Skirt	288665	45693	126652	111196	138051
Second Stage Total in lbs	593792	163417	297920	270604	309567
(Second Stage Total in kg)	(269344)	(74126)	(135137)	(122746)	(140420)
Interstage	78053	11861	25919	29512	37246
Forward Skirt	126481	18874	51859	48004	58504
LOX Tank Top Head	5468	5468	5468	5468	5468
LOX Tank Cylinder	58197	8821	25959	25959	25959
LOX Tank Bottom Head	9311	9311	9311	9311	9311
Intertank	306257	50389	178481	118310	157011
RP1 Top Head	6151	6151	6151	6151	6151
RP1 Bottom Head	8321	8321	8321	8321	8321
Thrust Takeout	107041	18042	51859	41592	55241
Thrust Structure	81537	81537	81537	81537	81537
Baffles and Insulation	*39270	*39270	*39270	*39270	*39270
First Stage Total in lbs	826087	258045	484135	413435	484019
(First Stage Total in kg)	(374713)	(117049)	(219604)	(187534)	(219551)
Vehicle Total in lbs	1419879	421462	782055	684039	793586
(Vehicle Total in kg)	(644057)	(191175)	(354741)	(310280)	(359971)
Difference from Nominal	+663574	-334843	+25750	-72266	+37281
Percent Weight Saving	-87.74	44.27	-3.40	9.56	-4.93

Weight Variation Using Lightest Material for Each Wall Construction

Section	Nominal Mt'l	Nominal Weight	Monocoque Mt'l	Monocoque Weight	Honeycomb Mt'l	Honeycomb Weight	Open-Face Corrugation Mt'l	Open-Face Corrugation Weight	Single-Face Corrugation Mt'l	Single-Face Corrugation Weight	Int. Str. and Ring Mt'l	Int. Str. and Ring Weight
Instrument Unit	Al	8736	Be	8144	Be	1614	Al	13959	Be	2212	Be	2515
Forward Skirt	Al	12523	Be	12130	Be	2562	Al	10164	Be	3365	Be	3715
LH_2 Tank Top Head	Al	10557	Be	6685	Be	6685	Be	6685	Be	6685	Be	6685
LH_2 Tank Cylinder	Al	24613	Be	11482	Ti	12276	Be	15259	Be	15259	Be	15259
LH_2 Tank Bottom Head	Al	12464	Ti	7921	Ti	7921	Ti	7921	Ti	7921	Ti	7921
Intertank	Al	35527	Be	31504	Be	8249	Al	31205	Be	9282	Be	10793
Baffles and Insulation		*23740		*23740		*23740		*23740		*23740		*23740
LOX Tank and Thrust Structure	Al	54546	Be	26093	Be	26093	Be	26093	Be	26093	Be	26093
Aft Skirt	Al	121428	Be	82950	Be	30480	Al	100673	Be	26683	Be	32058
Second Stage Total in lbs		304134		210649		119620		235699		121240		128779
(Second Stage Total in kg)		(137955)		(95550)		(54260)		(106913)		(54994)		(58414)
Interstage	Al	33583	Be	22429	Be	7877	Al	20487	Be	7156	Be	8754
Forward Skirt	Al	52357	Be	36345	Be	12504	Al	41101	Be	11519	Be	14196
LOX Tank Top Head	Al	8345	Be	5043	Be	5043	Be	5043	Be	5043	Be	5043
LOX Tank Cylinder	Al	20971	Be	17067	Be	6995	Be	8937	Be	8937	Be	8937
LOX Tank Bottom Head	Al	14614	Ti	9311	Ti	9311	Ti	9311	Ti	9311	Ti	9311
Intertank	Al	135205	Be	88005	Be	33798	Al	142142	Be	28519	Be	35629
RP1 Top Head	Al	8075	Be	4442	Be	4442	Be	4442	Be	4442	Be	4442
RP1 Bottom Head	Al	10923	Be	6009	Be	6009	Be	6009	Be	6009	Be	6009
Thrust Takeout	Al	47291	Be	30759	Be	12169	Al	41192	Be	10067	Be	12322
Thrust Structure	Al	81537	Be	49773	Be	49773	Be	49773	Be	49773	Be	49773
Baffles and Insulation		*39270		*39270		*39270		*39270		*39270		*39270
First Stage Total in lbs		452171		308453		187191		367707		180046		193686
(First Stage Total in kg)		(205105)		(139914)		(84910)		(166792)		(81669)		(87856)
Vehicle Total in lbs		756305		519102		306811		603406		301286		322465
(Vehicle Total in kg)		(343060)		(235464)		(139170)		(273705)		(136663)		(146270)
Difference from Nominal		-		-237203		-449494		-152899		-455019		-433840
Percent Weight Saving		-		31.36		59.43		20.22		60.16		57.36

Weight Variation Using Lightest Wall Construction for Each Material

Section	Nominal Wall Cons.	Nominal Weight	Aluminum Wall Cons.	Aluminum Weight	Titanium Wall Cons.	Titanium Weight	Beryllium Wall Cons.	Beryllium Weight	Lightest Metal Lt. Wall Cons. Wall Cons.	Lightest Metal Lt. Wall Cons. Weight
Instrument Unit	ISS	8736	Hyc	2934	Hyc	2640	Hyc	1614	Hyc	1614
Forward Skirt	ISS	12523	Hyc	4668	Hyc	4098	Hyc	2562	Hyc	2562
LH_2 Tank Top Head	Mono	10557	Mono	10557	Mono	6784	Mono	6685	Mono	6685
LH_2 Tank Cylinder	ISS	24613	Hyc	18972	Hyc	12276	Mono	11482	Mono	11482
LH_2 Tank Bottom Head	Mono	12464	Mono	12464	Mono	7921	Mono	8229	Mono	7921
Intertank	ISS	35527	Hyc	15432	Hyc	12525	Hyc	8249	Hyc	8249
Baffles and Insulation		*23740		*23740		*23740		*23740		*23740
LOX Tank and Thrust Structure		54546		54546		47740		26093		26093
Aft Skirt	ISS	121428	Hyc	60983	Hyc	45693	SFC	26683	SFC	26683
Second Stage Total in lbs		304134		204296		163417		115337		115029
(Second Stage Total in kg)		(137955)		(92669)		(74126)		(53317)		(52177)
Interstage	ISS	33583	Hyc	15708	Hyc	11861	SFC	7156	SFC	7156
Forward Skirt	ISS	52357	Hyc	24925	Hyc	18874	SFC	11519	SFC	11519
LOX Tank Top Head	Mono	8345	Mono	8345	Mono	5468	Mono	5043	Mono	5043
LOX Tank Cylinder	ISS	20971	Hyc	11267	Hyc	8821	Hyc	6995	Hyc	6995
LOX Tank Bottom Head	Mono	14614	Mono	14614	Mono	9311	Mono	9549	Mono	9311
Intertank	ISS	135205	Hyc	67584	Hyc	50389	SFC	28519	SFC	28519
RP1 Top Head	Mono	8075	Mono	8075	Mono	6151	Mono	4442	Mono	4442
RP1 Bottom Head	Mono	10923	Mono	10923	Mono	8321	Mono	6009	Mono	6009
Thrust Takeout	ISS	47291	Hyc	24311	Hyc	18042	SFC	10067	SFC	10067
Thrust Structure		81537		81537		81537		49773		49773
Baffles and Insulation		*39270		*39270		*39270		*39270		*39270
First Stage Total in lbs		452171		306559		258045		178342		178104
(First Stage Total in kg)		(205105)		(139055)		(117049)		(80896)		(80788)
Vehicle Total in lbs		756305		510855		421462		293679		293133
(Vehicle Total in kg)		(343060)		(231724)		(191175)		(133213)		(132965)
Difference from Nominal		-		-245450		-334843		-462626		-463172
Percent Weight Saving				32.45		44.27		61.17		61.24

* Fixed Weights Taken From References 1 and 2.

NOTE: For clarity, only stage and vehicle total weights are expressed in kilograms within brackets.

Table 4-9

201 Vehicle Configuration
Variation of Vehicle Structural Weight with Changes in Materials And Types of Construction Exposed to Nominal Loading Conditions

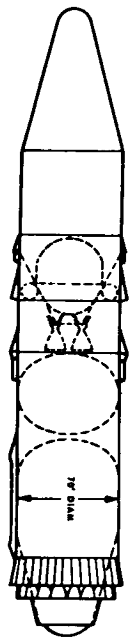

Section	Weight Variation With Change of Wall Construction For Material Same as Nominal						Weight Variation With Change of Material For Wall Construction Same as Nominal				Weight Variation With Change of Wall Construction For Beryllium				
		Wall Construction							Material		Wall Construction				
	Material as Used in Nominal	Monocoque Weight, Lb	Honeycomb Weight, Lb	OFC Weight, Lb	SFC Weight, Lb	ISS Weight, Lb	Wall Construction as Used in Nominal	Nominal (Aluminum) Weight, Lb	Titanium Weight, Lb	Beryllium Weight, Lb	Monocoque Weight, Lb	Honeycomb Weight, Lb	OFC Weight, Lb	SFC Weight, Lb	ISS Weight, Lb
Inst Unit and Forward Skirt	Al	29343	4292	30698	9481	13004	ISS	13004	15445	3313	11409	2354	55049	3144	3313
LH_2 Tank and Thrust Str.		39323	39323	39323	39323	39323		39323	39742	18511	18511	18511	18511	18511	18511
Intertank	Al	90458	14795	53507	30135	38963	ISS	38963	48047	10630	35173	8123	82480	9948	10630
Baffles and Insulation		*12900	*12900	*12900	*12900	*12900		*12900	*12900	*12900	*12900	*12900	*12900	*12900	*12900
LOX Tank		8850	8850	8850	9950	8850		8850	6523	4840	4840	4840	4840	4840	4840
Aft Skirt	Al	20630	2941	3131	7733	10389	ISS	10389	10965	2931	8021	1626	1037	2409	2931
Second Stage Total in lbs		201504	83101	148409	108425	123429		123429	132622	53125	90854	48354	174817	51752	53125
(Second Stage Total in kg)		(91402)	(37695)	(67318)	(49182)	(55987)		(55987)	(60157)	(24098)	(41211)	(21933)	(79297)	(23475)	(24098)
Interstage	Al	137480	28746	91149	51700	65266	ISS	65266	80982	19063	53455	14956	142644	16068	19063
Forward Skirt	Al	97515	20950	41181	36879	46882	ISS	46882	56323	13706	37917	10863	51622	11483	13706
LOX Tank Top Head	Al	8746	8746	8746	9746	8746	MONO	8746	5731	5284	5284	5284	5284	5284	5284
LOX Tank Bottom Head	Al	19318	19318	19318	19318	19318	MONO	19318	12309	12623	12623	12623	12623	12623	12623
Intertank	Al	270524	73764	150657	107841	156026	ISS	156026	173408	40825	105188	36965	210703	33565	40825
LH_2 Tank Top Head	Al	15935	15935	15935	15935	15935	MONO	15935	10268	9982	9982	9982	9982	9982	9982
LH_2 Tank Cylinder	Al	133759	40281	63411	63411	63411	ISS	63411	78635	34337	53249	25161	34337	34337	34337
LH_2 Bottom Head	Al	35330	35330	35330	35330	35330	MONO	35330	22514	23258	23258	23258	23258	23258	23258
Thrust Take Out	Al	91616	24754	41962	36448	53698		53698	59444	13953	35623	12404	55529	11317	13953
Thrust Structure		82741	82741	82741	82741	82741		82741	90601	36105	36105	36105	36105	36105	36105
Baffles and Insulation		*20040	*20040	*20040	*20040	*20040		*20040	*20040	*20040	*20040	*20040	*20040	*20040	*20040
First Stage Total in lbs		913004	370625	570470	478389	567393		567393	610255	229176	392724	207641	602127	214062	229176
(First Stage Total in kg)		(414139)	(168116)	(258765)	(216997)	(257369)		(257369)	(276812)	(103954)	(178140)	(94186)	(273125)	(97099)	(103954)
Vehicle Total in lbs		1114508	453726	718879	586814	690822		690822	742877	282301	483578	255995	776944	265814	282301
(Vehicle Total in kg)		(505541)	(205811)	(326083)	(266179)	(313356)		(313356)	(336969)	(128052)	(219351)	(116119)	(352422)	(120574)	(128052)
Difference from Nominal		+423686	-237096	+28057	-104008				+52055	-408521	-207244	-434827	+86122	-425008	-408521
Percent Weight Saving		-61.33	34.32	-4.06	15.06				-7.54	59.14	30.00	62.94	-12.47	61.52	59.14

* Fixed Weights Taken From References 1 and 2

NOTE: For clarity, only stage and vehicle total weights are expressed in kilograms within brackets

Table 4-10

201 Vehicle Configuration
Variation of Vehicle Structural Weight with Changes in Materials And Types of Construction Exposed to Nominal Loading Conditions

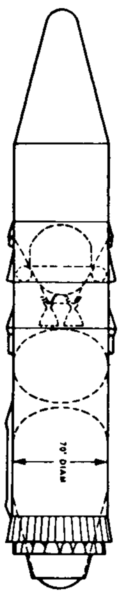

Section	Weight Variation with Change of Wall Construction for Titanium				
	Monocoque Weight, lb.	Honeycomb Weight, lb.	OFC Weight, lb.	SFC Weight, lb.	ISS Weight, lb.
Inst Unit and Forward Skirt	39704	3800	40132	12895	15445
LH_2 Tank and Thrust Str	38742	38742	38742	38742	38742
Intertank	122401	12563	67074	38793	48047
Baffles and Insulation	*12900	*12900	*12900	*12900	*12900
LOX Tank	6523	6523	6523	6523	6523
Aft Skirt	27914	2244	4031	9283	10965
Second Stage Total in lbs	248184	76772	169402	119136	132622
(Second Stage Total in kg)	(112576)	(34824)	(76841)	(54040)	(60157)
Interstage	186023	22804	114200	62593	80982
Forward Skirt	131950	16521	51957	44470	56323
LOX Tank Top Head	5731	5731	5731	5731	5731
LOX Tank Bottom Head	12309	12309	12309	12309	12309
Intertank	366051	55682	189465	138693	173408
LH_2 Tank Top Head	10268	10268	10268	10268	10268
LH_2 Tank Cylinder	180936	30189	78635	78635	78635
LH_2 Bottom Head	22514	22514	22514	22514	22514
Thrust Takeout	129367	18715	52700	46810	59444
Thrust Structure	90601	90601	90601	90601	90601
Baffles and Insulation	*20040	*20040	*20040	*20040	*20040
First Stage Total in lbs	1155790	305374	648420	532664	610255
(First Stage Total in kg)	(5242[illegible]6)	(138518)	(294305)	(241616)	(276812)
Vehicle Total in lbs	1403974	382146	817822	651800	742877
(Vehicle Total in kg)	(636842)	(173342)	(371146)	(295656)	(336969)
Difference from Nominal	+713152	-308676	+127000	-39022	+52055
Percent Weight Saving	-103.23	44.68	-18.38	-5.65	-7.54

Section	Weight Variation Using Lightest Material for Each Wall Construction											
	Nominal		Monoceque		Honeycomb		Open-Face Corrugation		Single Face Corrugation		Integ Str and Ring	
	Mt'l		Mt'l		Mt'l		Mt'l		Mt'l		Mt'l	
Inst Unit and Forward Skirt	Al	13004	Be	11409	Be	2354	Al	30698	Be	3144	Be	3313
LH_2 Tank and Thrust Str	Al	39323	Be	18511	Be	18511	Be	18511	Be	18511	Be	18511
Intertank	Al	38963	Be	35173	Be	8123	Al	53507	Be	9948	Be	10630
Baffles and Insulation	-	*12900	-	*12900	-	*12900	-	*12900	-	*12900	-	*12900
LOX Tank	Al	8850	Be	4840	Be	4840	Be	4840	Be	4840	Be	4840
Aft Skirt	Al	10389	Be	8021	Be	1626	Be	1037	Be	2409	Be	2931
Second Stage Total in lbs		123429		90854		48354		121493		51752		53125
(Second Stage Total in kg)		(55987)		(41211)		(21933)		(55109)		(23474)		(24098)
Interstage	Al	65266	Be	53455	Be	14956	Al	91149	Be	16068	Be	19063
Forward Skirt	Al	46882	Be	37917	Be	10863	Al	41181	Be	11483	Be	13706
LOX Tank Top Head	Al	8746	Be	5284	Be	5284	Be	5284	Be	5284	Be	5284
LOX Tank Bottom Head	Al	19318	Ti	12309	Ti	12309	Ti	12309	Ti	12309	Ti	12309
Intertank	Al	156026	Be	105188	Be	36965	Al	150657	Be	33565	Be	40825
LH_2 Tank Top Head	Al	15935	Be	9982	Be	9982	Be	9982	Be	9982	Be	9982
LH_2 Tank Cylinder	Al	63411	Be	53249	Be	25161	Be	34337	Be	34337	Be	34337
LH_2 Bottom Head	Al	35330	Ti	22514	Ti	22514	Ti	22514	Ti	22514	Ti	22514
Thrust Takeout	Al	53698	Be	35623	Be	12404	Al	41962	Be	11317	Be	13953
Thrust Structure	Al	82741	Be	36105	Be	36105	Be	36105	Be	36105	Be	36105
Baffles and Insulation		*20040		*20040		*20040		*20040		*20040		*20040
First Stage Total in lbs		567393		391666		206583		465520		213004		228118
(First Stage Total in kg)		(257369)		(177660)		(93706)		(211160)		(96635)		(103474)
Vehicle Total in lbs		690822		482520		254937		587013		264756		281243
(Vehicle Total in kg)		(313356)		(218871)		(115639)		(266269)		(120109)		(127572)
Difference from Nominal				-208302		-435885		-103809		-426066		-409579
Percent Weight Saving				30.15		63.10		15.03		61.68		59.29

Section	Weight Variation Using Lightest Wall Construction For Each Material									
	Nominal		Aluminum		Titanium		Beryllium		Lightest Metal Lightest Wall Cons.	
	Wall Cons		Wall Cons		Wall Cons		Wall Cons		Wall Cons	
Inst Unit and Forward Skirt	ISS	13004	Hyc	4292	Hyc	3800	Hyc	2354	Hyc	2354
LH_2 Tank and Thrust Str	-	39323	-	39323	-	38742	-	18511		18511
Intertank	ISS	38963	Hyc	14795	Hyc	12563	Hyc	8123	Hyc	8123
Baffles and Insulation	-	*12900	-	*12900	-	*12900	-	*12900		*12900
LOX Tank	-	8850	-	8850	-	6523	-	4840	-	4840
Aft Skirt	ISS	10389	Hyc	2941	Hyc	2244	OFC	1037	OFC	1037
Second Stage Total in lbs		123429		83101		76772		47765		47765
(Second Stage Total in kg)		(55987)		(37649)		(34824)		(21933)		(21933)
Interstage	ISS	65266	Hyc	28746	Hyc	22804	Hyc	14956	Hyc	14956
Forward Skirt	ISS	46882	Hyc	20950	Hyc	16521	Hyc	10863	Hyc	10863
LOX Tank Top Head	Mono	8746	Mono	8746	Mono	5731	Mono	5284	Mono	5284
LOX Tank Bottom Head	Mono	19318	Mono	19318	Mono	12309	Mono	12623	Mono	12309
Intertank	ISS	156026	Hyc	73784	Hyc	55682	SFC	33565	SFC	33565
LH_2 Tank Top Head	Mono	15935	Mono	15935	Mono	10268	Mono	9982	Mono	9982
LH_2 Tank Cylinder	ISS	63411	Hyc	40281	Hyc	30189	Hyc	25161	Hyc	25161
LH_2 Bottom Head	Mono	35330	Mono	35330	Hyc	22514	Mono	23258	Mono	22514
Thrust Takeout	ISS	53698	Hyc	24754	Hyc	18715	SFC	11317	SFC	11317
Thrust Structure	-	82741	-	82741	-	90601		36105	-	36105
Baffles and Insulation	-	*20040		*20040		*20040		*20040	-	*20040
First Stage Total in lbs		567393		370625		305374		203154		202096
(First Stage Total in kg)		(257369)		(168116)		(138518)		(93365)		(92[illegible])
Vehicle Total in lbs		690822		453726		382146		250919		249861
(Vehicle Total in kg)		(313356)		(205765)		(173342)		(115298)		(114818)
Difference from Nominal				-237096		-308676		-439903		-440961
Percent Weight Saving				34.32		44.68		63.68		63.83

* Fixed Weights Taken From References 1 and 2.

NOTE: For clarity, only stage and vehicle total weights are expressed in kilograms within brackets.

Table 4-11

202 Vehicle Configuration
Variation of Vehicle Structural Weight with Changes in Materials And Types of Construction Exposed to Nominal Loading Conditions

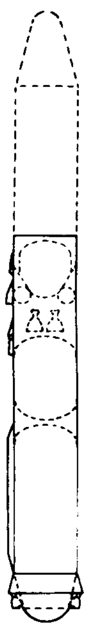

Section	Weight Variation With Change of Wall Construction For Material Same as Nominal					Weight Variation With Change of Material For Wall Construction Same as Nominal			Weight Variation With Change of Wall Construction For Beryllium			
	Material as Used in Nominal	Wall Construction				Wall Construction as Used in Nominal	Nominal Aluminum Weight, Lb	Beryllium Weight, Lb	Monocoque Weight, Lb	Honeycomb Weight, Lb	SFC Weight, Lb	ISS Weight, Lb
		Monocoque Weight, Lb	Honeycomb Weight, Lb	SFC Weight, Lb	ISS Weight, Lb							
IU and Forward Skirt	Al	54484	11279	20503	25561	ISS	25561	7521	21185	5890	6368	7521
LH_2 Tank and Thrust Str.	Al	32628	32628	32628	32628		32628	14437	14437	14437	14437	14437
Intertank	Al	77554	17920	29926	36971	ISS	36971	10993	30155	9241	9268	10993
Baffles and Insulation		*12900	*12900	*12900	*12900		*12900	*12900	*12900	*12900	*12900	*12900
LOX Tank	Al	6961	6961	6961	6961		6961	3781	3781	3781	3781	3781
Aft Skirt	Al	46548	12308	16436	25863	ISS	25863	7065	18099	6179	5743	7065
Second Stage Total in lbs		231075	93996	121354	140884		140884	56697	100557	52428	52497	56697
(Second Stage Total in kg)		(104816)	(42637)	(55046)	(63905)		(63905)	(25718)	(45613)	(23781)	(23813)	(25718)
Interstage	Al	45010	12093	17903	24126	ISS	24126	6932	17501	6063	5566	6932
Forward Skirt	Al	56045	15231	22288	31677	ISS	31677	8576	21792	7630	6951	8576
LOX Tank Top Head	Al	5398	5398	5398	5398	Mono	5398	3262	3262	3262	3262	3262
LOX Tank Cylinder	Al	80510	24270	39061	40449	ISS	40449	20493	31998	15528	23641	20493
LOX Tank Bottom Head	Al	11590	11590	11590	11590	Mono	11590	7573	7573	7573	7573	7573
Intertank	Al	162127	58937	90996	99728	ISS	99728	30159	63040	29590	24577	30159
LH_2 Tank Top Head	Al	9838	9838	9838	9838	Mono	9838	6163	6163	6163	6163	6163
LH_2 Tank Cylinder	Al	325438	107262	176111	181402	ISS	181402	96071	129525	68246	110430	96071
LH_2 Tank Bottom Head	Al	17530	17530	17530	17530	Mono	17530	11564	11564	11564	11564	11564
Thrust Takeout									-	-	-	-
Thrust Structure	Al	93297	93297	93297	93297	ISS	93297	39591	39591	39591	39591	39591
Baffles and Insulation		*20040	*20040	*20040	*20040		*20040	*20040	*20040	*20040	*20040	*20040
First Stage Total in lbs		826823	375486	504052	535075		535075	250424	352049	215250	259358	250424
(First Stage Total in kg)		(375047)	(170320)	(228638)	(242710)		(242710)	(113592)	(159689)	(97637)	(117645)	(113592)
Vehicle Total in lbs		1057898	469482	625406	675959		675959	307121	452606	267678	311855	307121
(Vehicle Total in kg)		(479863)	(212957)	(283684)	(306615)		(306615)	(139310)	(205302)	(121418)	(141458)	(139310)
Difference From Nominal		381939	-206477	50553	-			-368838	-223353	-406281	-364104	-368838
Percent Weight Saving		-56.50	30.55	7.48	-			54.57	33.04	60.40	53.86	54.57

*Fixed Weights Taken From References 1 and 2.

NOTE: For clarity, only stage and vehicle total weights are expressed in kilograms within brackets.

Table 4-12

202 Vehicle Configuration

Variation of Vehicle Structural Weight with Changes in Materials And Types of Construction Exposed to Nominal Loading Conditions

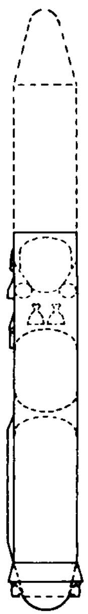

Section	Weight Variation Using Lightest Material for Each Wall Construction										Weight Variation Using Lightest Wall Construction for Each Material							
	Nominal		Monocoque		Honeycomb		Single Face Corrugation		Inter. Str. and Ring		Nominal		Aluminum		Beryllium		Lightest Metal Lightest Wall Cons.	
	Mt'l		Mt'l		Mt'l		Mt'l		Mt'l		Wall Cons.	Weight	Wall Cons.	Weight	Wall Cons.	Weight	Wall Cons.	Weight
IU and Forward Skirt	Al	25561	Be	21185	Be	5890	Be	6368	Be	7521	ISS	25561	Hyc	11279	Hyc	5890	Hyc	5890
LH_2 Tank and Thrust Str.	Al	32628	Be	14437	Be	14437	Be	14437	Be	14437		32628		32628		14437		14437
Intertank	Al	36971	Be	30155	Be	9241	Be	9268	Be	10993	ISS	36971	Hyc	17920	Hyc	9241	Hyc	9241
Baffles and Insulation		*12900		*12900		*12900		*12900		*12900		*12900		*12900		*12900		*12900
LOX Tank	Al	6961	Be	3781	Be	3781	Be	3781	Be	3781		6961		6961		3781		3781
Aft Skirt	Al	25863	Be	18099	Be	6179	Be	5743	Be	7065	ISS	25863	Hyc	12308	SFC	5743	SFC	5743
Second Stage Total in lbs		140884		100557		52428		52497		56697		140884		93996		51992		51992
(Second Stage Total in kg)		(63905)		(45613)		(23781)		(23813)		(25718)		(63905)		(42637)		(23584)		(23584)
Interstage	Al	24126	Be	17501	Be	6063	Be	5566	Be	6932	ISS	24126	Hyc	12093	SFC	5566	SFC	5566
Forward Skirt	Al	31677	Be	21792	Be	7630	Be	6951	Be	8576	ISS	31677	Hyc	15231	SFC	6951	SFC	6951
LOX Tank Top Head	Al	5398	Be	3262	Be	3262	Be	3262	Be	3262	Mono	5398	Mono	5398	Mono	3262	Mono	3262
LOX Tank Cylinder	Al	40449	Be	31998	Be	15528	Be	23641	Be	20493	ISS	40449	Hyc	24270	Hyc	15528	Hyc	15528
LOX Tank Bottom Head	Al	11590	Be	7573	Be	7573	Be	7573	Be	7573	Mono	11590	Mono	11590	Mono	7573	Mono	7573
Intertank	Al	99728	Be	63040	Be	29590	Be	24577	Be	30159	ISS	99728	Hyc	58937	SFC	24577	SFC	24577
LH_2 Tank Top Head	Al	9838	Be	6163	Be	6163	Be	6163	Be	6163	Mono	9838	Mono	9838	Mono	6163	Mono	6163
LH_2 Tank Cylinder	Al	181402	Be	129525	Be	68246	Be	110430	Be	96071	ISS	181402	Hyc	107262	Hyc	68246	Hyc	68246
LH_2 Tank Bottom Head	Al	17530	Be	11564	Be	11564	Be	11564	Be	11564	Mono	17530	Mono	17530	Mono	11564	Mono	11564
Thrust Takeout																		
Thrust Structure	Al	93297	Be	39591	Be	39591	Be	39591	Be	39591	ISS	93297	ISS	93297	ISS	39591	ISS	39591
Baffles and Insulation		*20040		*20040		*20040		*20040		*20040		*20040		*20040		*20040		*20040
First Stage Total in lbs		535075		352049		215250		259358		250424		535075		375486		209061		209061
(First Stage Total in kg)		(242710)		(159689)		(97637)		(117645)		(113592)		(242710)		(170320)		(94830)		(94830)
Vehicle Total in lbs		675959		452606		267678		311855		307121		675959		469482		261053		261053
(Vehicle Total in kg)		(306615)		(205302)		(121418)		(141458)		(139310)		(306615)		(212957)		(118414)		(118414)
Difference From Nominal				-223353		-408281		-364104		-368838				-206477		-414906		-414906
Percent Weight Saving				33.04		60.40		53.86		54.57				30.55		61.38		61.38

*Fixed Weights Taken From References 1 and 2.

NOTE: For clarity, only stage and vehicle total weights are expressed in kilograms within brackets.

Table 4-13

203 Vehicle Configuration
Variation of Vehicle Structural Weight with Changes in Materials And Types of Construction Exposed to Nominal Loading Conditions

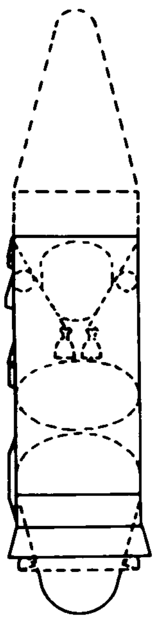

Section	Weight Variation With Change of Wall Construction For Material Same as Nominal					Weight Variation With Change of Material For Wall Construction Same as Nominal			Weight Variation With Change of Wall Construction For Berryllium			
	Material as Used in Nominal	Wall Construction				Wall Construction as Used in Nominal	Nominal (Aluminum) Weight, Lb	Material	Wall Construction			
		Monocoque Weight, Lb	Honeycomb Weight, Lb	SFC Weight, Lb	ISS Weight, Lb			Beryllium Weight, Lb	Monocque Weight, Lb	Honeycomb Weight, Lb	SFC Weight, Lb	ISS Weight, Lb
IU and Forward Skirt	Al	7284	537	2222	3030	ISS	3030	787	2832	299	740	787
LH_2 Tank and Thrust Str.	Al	46232	46232	46232	46232		46232	20675	20675	20675	20675	20675
Intertank	Al	92141	12188	29254	37658	ISS	37658	9963	35827	6811	9623	9963
Baffles and Insulation		*12900	*12900	*12900	*12900		*12900	*12900	*12900	*12900	*12900	*12900
LOX Tank	Al	9755	9755	9755	9755		9755	5281	5281	5281	5281	5281
Aft Skirt	Al	30638	3632	10295	14164	ISS	14164	3759	11913	2009	3432	3759
Second Stage Total in lbs		198950	85244	110658	123739		123739	53365	89428	47975	52651	53365
Second Stage Total in kg		(90244)	(38667)	(50194)	(56128)		(56128)	(24206)	(40565)	(21761)	(23882)	(24206)
Interstage	Al	197607	35402	66785	91099	ISS	91099	24754	76836	19158	22136	24754
Forward Skirt	Al	96497	17844	32799	44531	ISS	44531	12604	37521	9554	10900	12604
LOX Tank Top Head	Al	11195	11195	11195	11195	MONO	11195	6885	6885	6885	6885	6885
LOX Tank Bottom Head	Al	47755	47755	47755	47755	MONO	47755	31205	31205	31205	31205	31205
Intertank	Al	285711	66655	110261	151807	ISS	151807	41097	111093	33969	34153	41097
LH_2 Tank Top Head	Al	20814	20814	20814	20814	MONO	20814	13039	13039	13039	13039	13039
LH_2 Tank Cylinder	Al	35084	10420	19587	17170	ISS	17170	8807	14333	6525	12249	8807
LH_2 Tank Bottom Head	Al	49685	49685	49685	49685	MONO	49685	32880	32880	32880	32880	32880
Thrust Takeout	Al	115072	27206	44457	60423	ISS	60423	16395	44744	13836	13844	16395
Thrust Structure	Al	100585	100585	100585	100585		100585	38982	38982	38982	38932	38982
Baffles and Insulation		*20040	*20040	*20040	*20040		*20040	*20040	*20040	*20040	*20040	*20040
First Stage Total in lbs		980945	407603	523963	615104		615104	246688	427558	226073	236313	246688
(First Stage Total in kg)		(444957)	(184889)	(237670)	(279011)		(279011)	(111898)	(193940)	(102547)	(107192)	(111898)
Vehicle Total in lbs		1179895	492847	634621	738843		738843	300053	516986	274048	288964	300053
(Vehicle Total in kg)		(535201)	(223556)	(287864)	(335139)		(335139)	(136104)	(234505)	(124308)	(131074)	(136104)
Difference from Nominal		441052	-245926	-104222	-		-	-438790	-221857	-464795	-449879	-438790
Percent Weight Saving		-59.69	33.29	14.11	-		-	59.39	30.03	62.91	60.89	59.39

* Fixed Weights Taken From References 1 and 2.

NOTE: For clarity, only stage and vehicle total weights are expressed in kilograms within brackets.

Table 4-14

203 Vehicle Configuration
Variation of Vehicle Structural Weight with Changes in Materials And Types of Construction Exposed to Nominal Loading Conditions

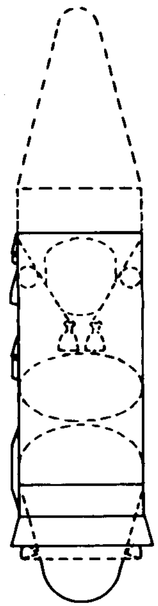

Section	Weight Variation Using Lightest Material For Each Wall Construction										Weight Variation Using Lightest Wall Construction For Each Material							
	Nominal		Monocoque		Honeycomb		Single Face Corrugation		Integ. Str. and Ring		Nominal		Aluminum		Beryllium		Lightest Metal Light. Wall Cons	
	Mt'l	Weight	Mt'l	Weight	Mt'l	Weight	Mt'l	Weight	Mt'l	Weight	Wall Cons	Weight	Wall Cons.	Weight	Wall Cons.	Weight	Wall Cons.	Weight
IU and Forward Skirt	Al	3030	Be	2832	Be	299	Be	740	Be	787	ISS	3030	Hyc	537	Hyc	299	Hyc	299
LH_2 Tank and Thrust Str.	Al	46232	Be	20675	Be	20675	Be	20675	Be	20675	-	46232	-	46232	-	20675	-	20675
Intertank	Al	37658	Be	35827	Be	6811	Be	9623	Be	9963	ISS	37658	Hyc	12188	Hyc	6811	Hyc	6811
Baffles and Insulation	-	*12900	-	*12900	-	*12900)	-	*12900	-	*12900	-	*12900	-	*12900	-	*12900	-	*12900
LOX Tank	Al	9755	Be	5281	Be	5281	Be	5281	Be	5281	-	9755	-	9755	-	5281	-	5281
Aft Skirt	Al	14164	Be	11913	Be	2009	Be	3432	Be	3759	ISS	14164	Hyc	3632	Hyc	2009	Hyc	2009
Second Stage Total in lbs		123739		89428		47975		52651		53365		123739		85244		47975		47975
(Second Stage Total in kg)		(56128)		(40565)		(21761)		(23882)		(24206)		(56128)		(38667)		(21761)		(21761)
Interstage	Al	91099	Be	76836	Be	19158	Be	22136	Be	24754	ISS	91099	Hyc	35402	Hyc	19158	Hyc	19158
Forward Skirt	Al	44531	Be	37521	Be	9554	Be	10900	Be	12604	ISS	44531	Hyc	17844	Hyc	9554	Hyc	9554
LOX Tank Top Head	Al	11195	Be	6885	Be	6885	Be	6885	Be	6885	Mon	11195	Mon	11195	Mon	6885	Mon	6885
LOX Tank Bottom Head	Al	47755	Be	31205	Be	31205	Be	31205	Be	31205	Mon	47755	Mon	47755	Mon	31205	Mon	31205
Intertank	Al	151807	Be	111093	Be	33969	Be	34153	Be	41097	ISS	151807	Hyc	66655	Hyc	33969	Hyc	33969
LH_2 Tank Top Head	Al	20814	Be	13039	Be	13039	Be	13039	Be	13039	Mon	20814	Mon	20814	Mon	13039	Mon	13039
LH_2 Tank Cylinder	Al	17170	Be	14333	Be	6525	Be	12249	Be	8807	ISS	17170	Hyc	10420	Hyc	6525	Hyc	6525
LH_2 Tank Bottom Head	Al	49685	Be	32880	Be	32880	Be	32880	Be	32880	Mon	49685	Mon	49685	Mon	32880	Mon	32880
Thrust Takeout	Al	60423	Be	44744	Be	13836	Be	13844	Be	16395	ISS	60423	Hyc	27208	Hyc	13836	Hyc	13836
Thrust Structure	Al	100585	Be	38982	Be	38982	Be	38982	Be	38982		100585		100585		38982		38982
Baffles and Insulation		*20040		*20040		*20040		*20040		*20040		*20040		*20040		*20040		*20040
First Stage Total in lbs		615104		427558		226073		236313		246688		615104		407603		226073		226073
(First Stage Total in kg)		(279001)		(193940)		(102547)		(107192)		(111898)		(279011)		(184889)		(102547)		(102547)
Vehicle Total in lbs		738843		516986		274048		288964		300053		738843		492847		274048		274048
(Vehicle Total in kg)		(335139)		(234505)		(124308)		(131074)		(136104)		(335139)		(223556)		(124308)		(124308)
Difference From Nominal				-221857		-464795		-449872		-438790				-245996		-464795		-464795
Percent Weight Saving				30.03		62.91		60.89		59.39				33.29		62.91		62.91

* Fixed Weights Taken From References 1 and 2.

NOTE: For clarity, only stage and vehicle total weights are expressed in kilograms within brackets.

Table 4-15

301 Vehicle Configuration
Variation of Vehicle Structural Weight with Changes in Materials And Types of Construction Exposed to Nominal Loading Conditions

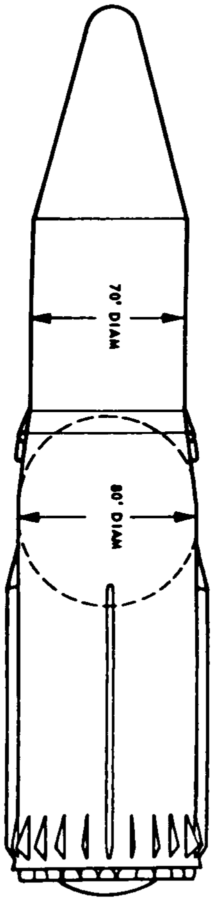

Weight Variation With Change of Wall Construction For Material Same as Nominal

Section	Material as Used in Nominal	Monocoque Weight, Lb	Honeycomb Weight, Lb	OFC Weight, Lb	SFC Weight, Lb	ISS Weight, Lb
Instrument Unit	Al	33252	5258	35512	10959	13647
Forward Skirt	Al	126522	19355	56012	41586	52748
LOX Tank Top Head	Al	14489	14489	14489	14489	14489
LOX Tank Cylinder	Al	11713	3821	5189	5189	5189
Common Bulkhead	Al	63425	63425	63425	63425	63425
LH_2 Tank Cylinder	Al	671404	175098	316615	316615	316615
LH_2 Tank Bottom Head	Al	22287	22287	22287	22287	22287
Thrust Takeout	Al	142122	40701	130752	62011	78745
Thrust Structure	Al	56175	56175	56175	56175	56175
Insulation		*18000	*18000	*18000	*18000	*18000
Vehicle Total in lbs		1159389	418609	718456	610736	641320
(Vehicle Total in kg)		(525899)	(189881)	(325882)	(277030)	(290903)
Difference from Nominal		+518069	-222711	+77136	-30584	
Percent Weight Savings		-80.78	34.73	-12.03	4.77	

Weight Variation With Change of Material for Wall Construction Same as Nominal

Section	Wall Construction as Used in Nominal	Nominal: Nominal (Aluminum) Weight, Lb.	Material: Titanium Weight, Lb.	Material: Beryllium Weight, Lb.
Instrument Unit	ISS	13647	18875	3898
Forward Skirt	ISS	52748	64595	14049
LOX Tank Top Head	MONO	14489	9403	9003
LOX Tank Cylinder	ISS	5189	4810	3429
Common Bulkhead	Hyc	63425	51310	52110
LH_2 Tank Cylinder	ISS	316615	393132	139139
LH_2 Tank Bottom Head	MONO	22287	14163	14714
Thrust Takeout	ISS	78745	98624	22871
Thrust Structure		56175	56175	30430
Insulation		*18000	*18000	*18000
Vehicle Total in lbs		641320	729087	307643
(Vehicle Total in kg)		(290903)	(330714)	(137969)
Difference from Nominal			87767	-333677
Percent Weight Savings			-13.69	52.03

Weight Variation With Change of Wall Construction For Beryllium

Section	Wall Construction: Monocoque Weight, Lb	Honeycomb Weight, Lb	OPC Weight, Lb	SFC Weight, Lb	ISS Weight, Lb
Instrument Unit	12930	2815	63909	3631	3898
Forward Skirt	49196	10570	77895	13718	14049
LOX Tank Top Head	9003	9003	9003	9003	9003
LOX Tank Cylinder	4667	2501	3429	3429	3429
Common Bulkhead	52110	52110	52110	52110	52110
LH_2 Tank Cylinder	267335	113558	139139	139139	139139
LH_2 Tank Bottom Head	14714	14714	14714	14714	14714
Thrust Takeout	55262	20647	220631	17779	22871
Thrust Structure	30430	30430	30430	30430	30430
Insulation	*18000	*18000	*18000	*18000	*18000
Vehicle Total in lbs	513647	274348	629260	301953	307643
(Vehicle Total in kg)	(232990)	(124444)	(285432)	(136966)	(137989)
Difference from Nominal	-127673	-366972	-12060	-339367	-333677
Percent Weight Savings	19.91	57.22	1.88	52.92	52.03

Weight Variation With Change of Wall Construction for Titanium

Section	Wall Construction: Monocoque Weight, lb	Honeycomb Weight, lb	OFC Weight, lb	SFC Weight, lb	ISS Weight, lb
Instrument Unit	44995	4519	44265	14212	18875
Forward Skirt	171200	16830	70452	53533	64595
LOX Tank Top Head	9403	9403	9403	9403	9403
LOX Tank Cylinder	15823	2458	4810	4810	4810
Common Bulkhead	51310	51310	51310	51310	51310
LH_2 Tank Cylinder	907929	139515	393132	393132	393132
LH_2 Tank Bottom Head	14163	14163	14163	14163	14163
Thrust Takeout	192308	30391	163366	73604	98624
Thrust Structure	56175	56175	56175	56175	56175
Insulation	*18000	*18000	*18000	*18000	*18000
Vehicle Total in lbs	1481306	342764	825076	688342	729087
(Vehicle Total in kg)	(671920)	(156545)	(373188)	(311165)	(330714)
Difference from Nominal	+839986	-298556	+183756	+47022	+87767
Percent Weight Savings	-130.98	46.55	-28.65	-7.33	-13.69

Weight Variation Using Lightest Material for Each Wall Construction

Section	Nominal Mt'l.	Nominal Weight	Monocoque Mt'l.	Monocoque Weight	Honeycomb Mt'l.	Honeycomb Weight	Open-Face Corrugation Mt'l.	Open-Face Corrugation Weight	Single-Face Corrugation Mt'l.	Single-Face Corrugation Weight	Int. Str. and Ring Mt'l.	Int. Str. and Ring Weight
Instrument Unit	Al	13647	Be	12930	Be	2815	Al	35512	Be	3631	Be	3898
Forward Skirt	Al	52748	Be	49196	Be	10570	Al	56012	Be	13718	Be	14049
LOX Tank Top Head	Al	14489	Be	9003	Be	9003	Be	9003	Be	9003	Be	9003
LOX Tank Cylinder	Al	5189	Be	4667	Ti	2458	Be	3429	Be	3429	Be	3429
Common Bulkhead	Al	63425	Ti	51310	Ti	51310	Ti	51310	Ti	51310	Ti	51310
LH_2 Tank Cylinder	Al	316615	Be	267335	Be	113558	Be	139139	Be	139139	Be	139139
LH_2 Tank Bottom Head	Al	22287	Ti	14163	Ti	14163	Ti	14163	Ti	14163	Ti	14163
Thrust Takeout	Al	78745	Be	55262	Be	20647	Al	130752	Be	17779	Be	22871
Thrust Structure	Al	56175	Be	30430	Be	30430	Be	30430	Be	30430	Be	30430
Insulation		*18000		*18000		*18000		*18000		*18000		*18000
Vehicle Total in lbs		641320		512296		272954		487750		300602		306292
(Vehicle Total in kg)		(290903)		(232377)		(123812)		(221243)		(136353)		(138934)
Difference from Nominal				-129024		-368366		-153570		-340718		-335028
Percent Weight Savings				20.12		57.44		23.95		53.13		52.24

Weight Variation Using Lightest Wall Construction for Each Material

Section	Nominal Wall Cons.	Nominal Weight	Aluminum Wall Cons.	Aluminum Weight	Titanium Wall Cons.	Titanium Weight	Beryllium Wall Cons.	Beryllium Weight	Lightest Metal and Wall Cons. Wall Cons.	Lightest Metal and Wall Cons. Weight
Instrument Unit	ISS	13647	Hyc	5258	Hyc	4519	Hyc	2815	Hyc	2815
Forward Skirt	ISS	52748	Hyc	19355	Hyc	16830	Hyc	10570	Hyc	10570
LOX Tank Top Head	Mono	14489	Mono	14489	Mono	9403	Mono	9003	Mono	9003
LOX Tank Cylinder	ISS	5189	Hyc	3821	Hyc	2458	Hyc	2501	Hyc	2458
Common Bulkhead	Hyc	63425	Hyc	63425	Hyc	51310	Hyc	52110	Hyc	51310
LH_2 Tank Cylinder	ISS	316615	Hyc	175098	Hyc	139515	Hyc	113558	Hyc	113558
LH_2 Tank Bottom Head	Mono	22287	Mono	22287	Mono	14163	Mono	14714	Mono	14163
Thrust Takeout	ISS	78745	Hyc	40701	Hyc	30391	SFC	17779	SFC	17779
Thrust Structure		56175		56175		56175		30430		30430
Insulation		*18000		*18000		*18000		*18000		*18000
Vehicle Total in lbs		641320		418609		342764		271480		270086
(Vehicle Total in kg)		(290903)		(189861)		(155478)		(124444)		(123812)
Difference from Nominal				-222711		-298556		-369840		-371234
Percent Weight Savings				34.73		46.55		57.67		57.89

* Fixed Weights Taken From References 1 and 2.

NOTE: For clarity, only stage and vehicle total weights are expressed in kilograms within brackets.

SECTION 5

OPTIMIZED STRUCTURAL WEIGHT ANALYSIS—ANISOTROPIC

5.1 GENERAL CONSIDERATIONS

An area of substantial promise for the increase in launch vehicle payload capacity is the use of advanced materials in the primary structure. An evaluation of advanced structures should include a consideration of materials other than the metals which are in common use. Recent advancements in strength and stiffness of filamentary materials have enhanced the potential for filament-wound composite pressure vessels. Therefore, a quantitative assessment was performed to assess the weight savings available using filamentary composite materials as the vehicle's primary structure.

The analytical methods used have drawn extensively on the structural efficiency methods developed in Reference 25 and applied in Reference 26. The computations were automated in the LILAC and SPACE computational modules described in Appendix B. The minimum structural weight was evaluated as a function of the design load and the structural geometry. These latter factors were defined by the structural index. The structural design of the advanced configurations treated herein were governed by values of the structural index within the range covered by contemporary boost vehicles (see Reference 25). Thus, the general conclusions of the previous studies were applicable to the presently considered vehicles. These conclusions, with some modifications, are stated in paragraph 5.4. Selection of appropriate materials and structural configurations drew on the previous experience with smaller vehicles. Failure criteria for pressurized tanks involved significant departures from previous methods.

5.2 SELECTION OF MATERIALS AND TYPES OF CONSTRUCTION

The composites chosen for consideration in this study were: the high-modulus glass-fiber epoxy-binder composite which is representative of present day materials already used for similar applications; a boron-fiber epoxy-binder composite which represents the stiffest continuous fiber available in a matrix which is readily fabricated into composite form; and a carbon-filament aluminum-binder composite which represents an advanced material now available in laboratory form. These materials were chosen to represent the spectrum of properties, which are conceivably available for future use. Properties of the above constituents are presented in Table 5-1.

Table 5-1

Material Properties of Constituents

Material	Elastic Modulus (psi)	Poisson's Ratio	Density (lb/in^3)
Filaments			
Glass	16.0×10^6	0.20	0.0194
Boron	60.0×10^6	0.20	0.0830
Carbon	60.0×10^6	0.18	0.0720
Binders			
Epoxy	0.5×10^6	0.350	0.050
Aluminum	10.7×10^6	0.315	0.100

The properties of the composite materials depend not only on the constituent properties, but also upon the arrangement of the filaments and the relative proportions of binder and filaments. For the composite materials selected for this study, the binder was assumed to be 30 percent of the total volume.

Two different winding patterns were considered. The isotropic laminate was composed of three equal-thickness layers, where the orientation of the filaments to the vertical in the three layers were -60, 0, and 60 degrees respectively. The other winding pattern is orthotropic, where the laminate was composed of two layers which were not of equal thickness. The filaments were arranged at 0 and 90 degrees to the vertical respectively for the two layers. The amount of material in the 0-degree layer was varied from 5 percent to 15 percent in order to obtain the highest practical stiffness and strength.

Two principal types of wall construction were selected for the cylindrical and conical shell sections of the vehicles under consideration. As a reference point, monocoque composite shells were evaluated. These laminates were considered to have a unidirectional set of fibers in each of the layers. Directions of principal stiffness of the layers were varied symmetrically such that the directions of principal stiffnesses of the laminate were coincident with the meridional and circumferential directions. Further patterns were selected to minimize coupling effects.

The second structural configuration was the honeycomb-core sandwich shell for which core densities of 0.005 and 0.001 lbs/inch^3 were considered. These represent the general case of efficient stiffening. Here the core was assumed to have adequate stiffness to stabilize the face sheets so that the sandwich failed due to overall instability. The core was assumed to carry no load and the face sheets had the properties described for the monocoque shells.

Additionally, an evaluation of future potential should assess whiskers and other high-modulus filaments. A recent study (Reference 35) showed that properly designed discontinuous fiber composites were expected to have essentially the same properties as continuous fiber composites of the same constituents. For the present compressive application, the important properties were the elastic stiffnesses and the compressive strengths. These properties were governed primarily by fiber modulus, binder modulus and yield strength (References 24 and 36). Boron and carbon fibers were close in stiffness to other available high-modulus fibers and whiskers. The results for boron/epoxy and carbon/aluminum composites were therefore considered to be representative of a wide range of other composites having the same matrix material.

5.3 WEIGHT/LOAD RELATIONSHIPS

Parametric relationships were established between the stress resultants of the critical loads envelope and the structural weight. Figures 5-1, 5-2, and 5-3 are concerned with the composite materials: glass/epoxy, boron/epoxy, and carbon/aluminum, respectively, with an isotropic (-60-, 0-, 60-degree) winding pattern. Curves were plotted for monocoque construction as well as honeycomb sandwich construction with core densities of 0.001 lbs/inch^3 and 0.005 lbs/inch^3. Various ratios of N_y and N_x are presented in order to obtain the structural weights of pressurized cylinders where N_y is not zero.

These curves were explained in detail in Section 2 of this volume. For a cylinder of specified radius, R, and load N_X; the weight, W, for unit surface area of the shell, was obtained for various materials and types of construction. The total weight of the shell was determined by multiplying W by the surface area of the shell.

Figure 5-4 presents similar results for an orthotropic (0-, 90-degree) winding pattern. The curves of Figure 5-4 are calculated for zero-hoop loads (i.e., $N_y = 0$). Figure 5-4 is therefore restricted to the evaluation of structural weights for unpressurized cylinders. Other values of N_y/N_x were not treated since the difference between the

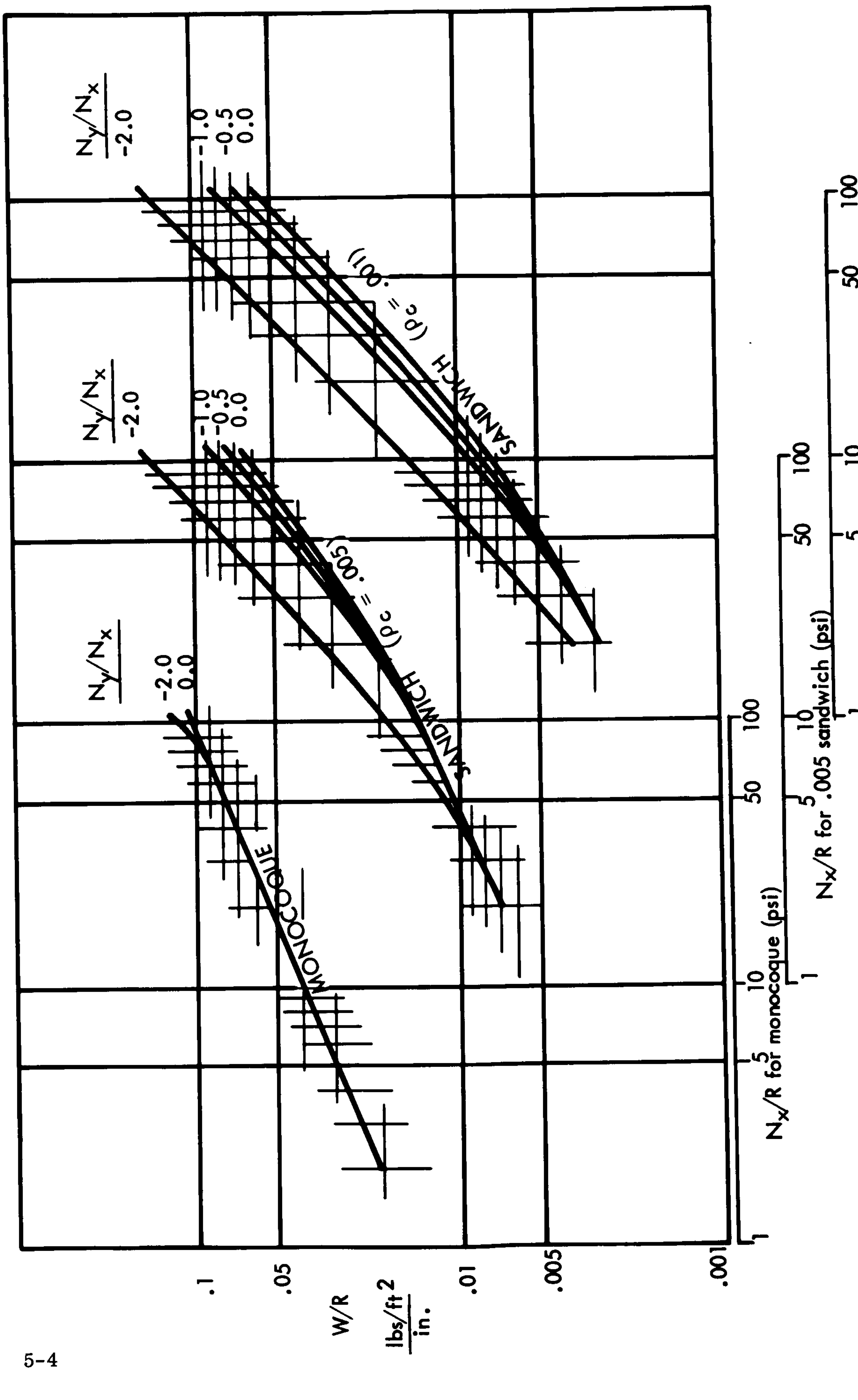

Figure 5-1. Weight/Load Relationship, Glass/Epoxy with Isotropic Winding

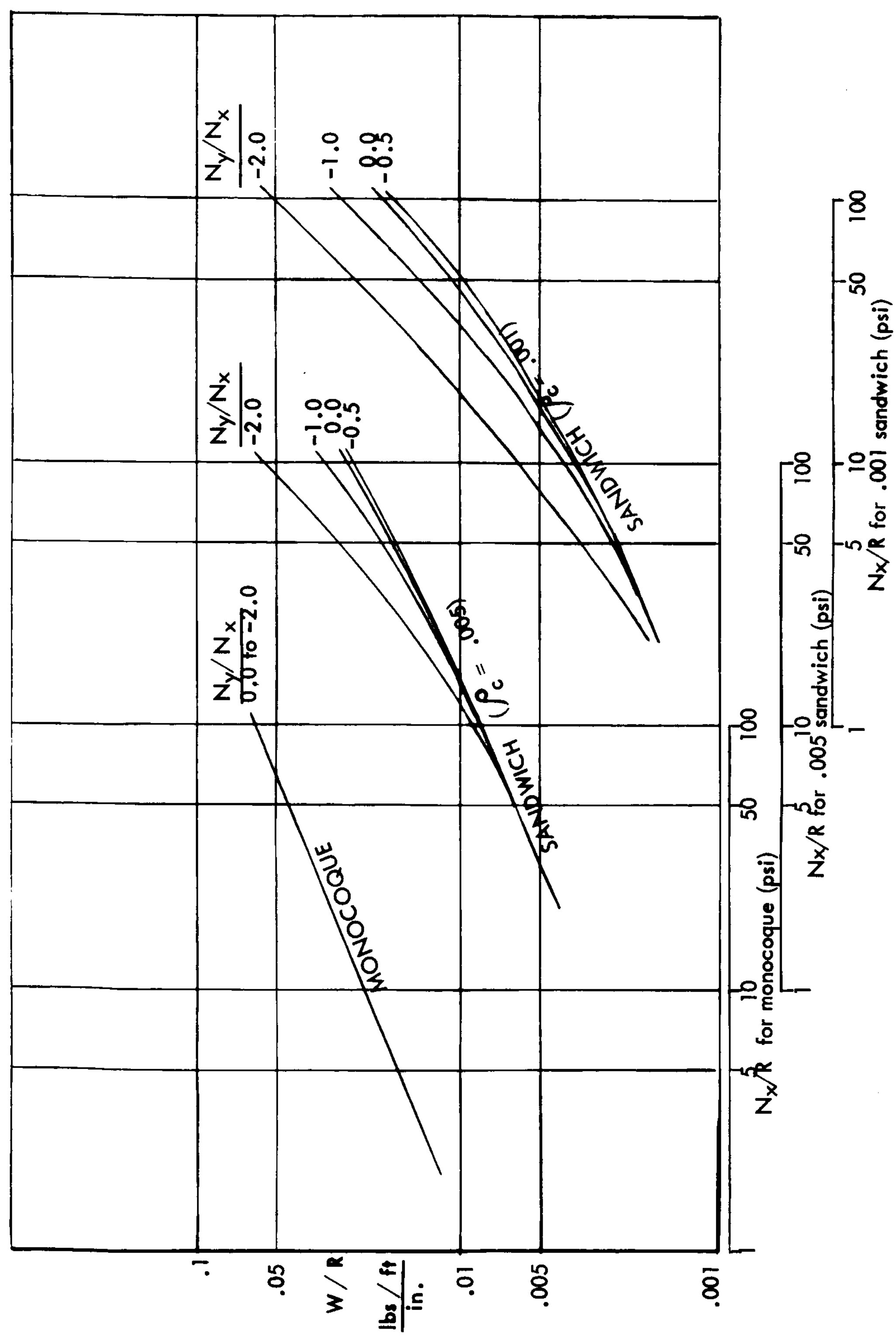

Figure 5-2. Weight/ Load Relationship, Boron/ Epoxy with Isotropic Winding

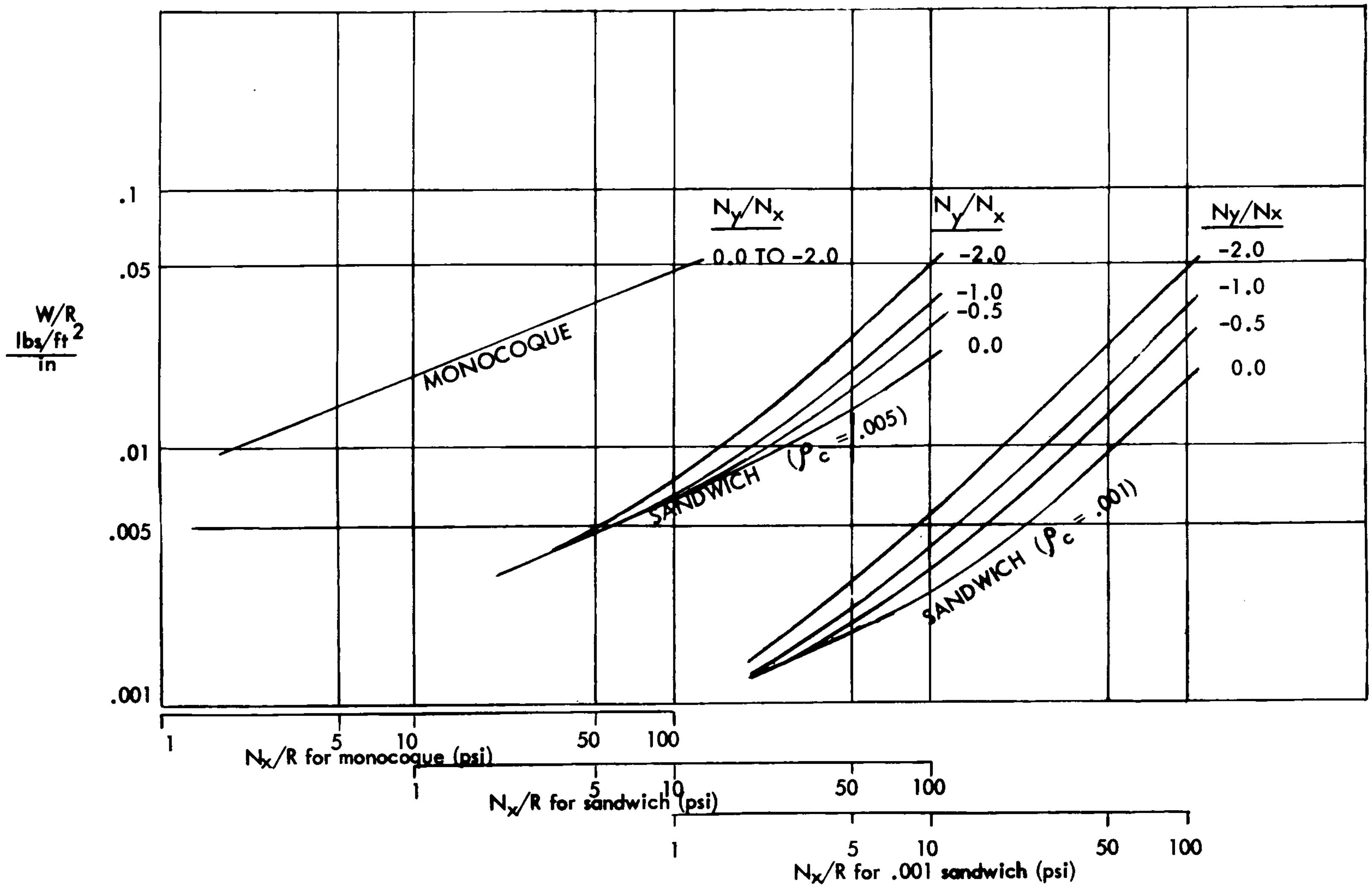

Figure 5-3. Weight/ Load Relationship, Carbon/ Aluminum with Isotropic Winding

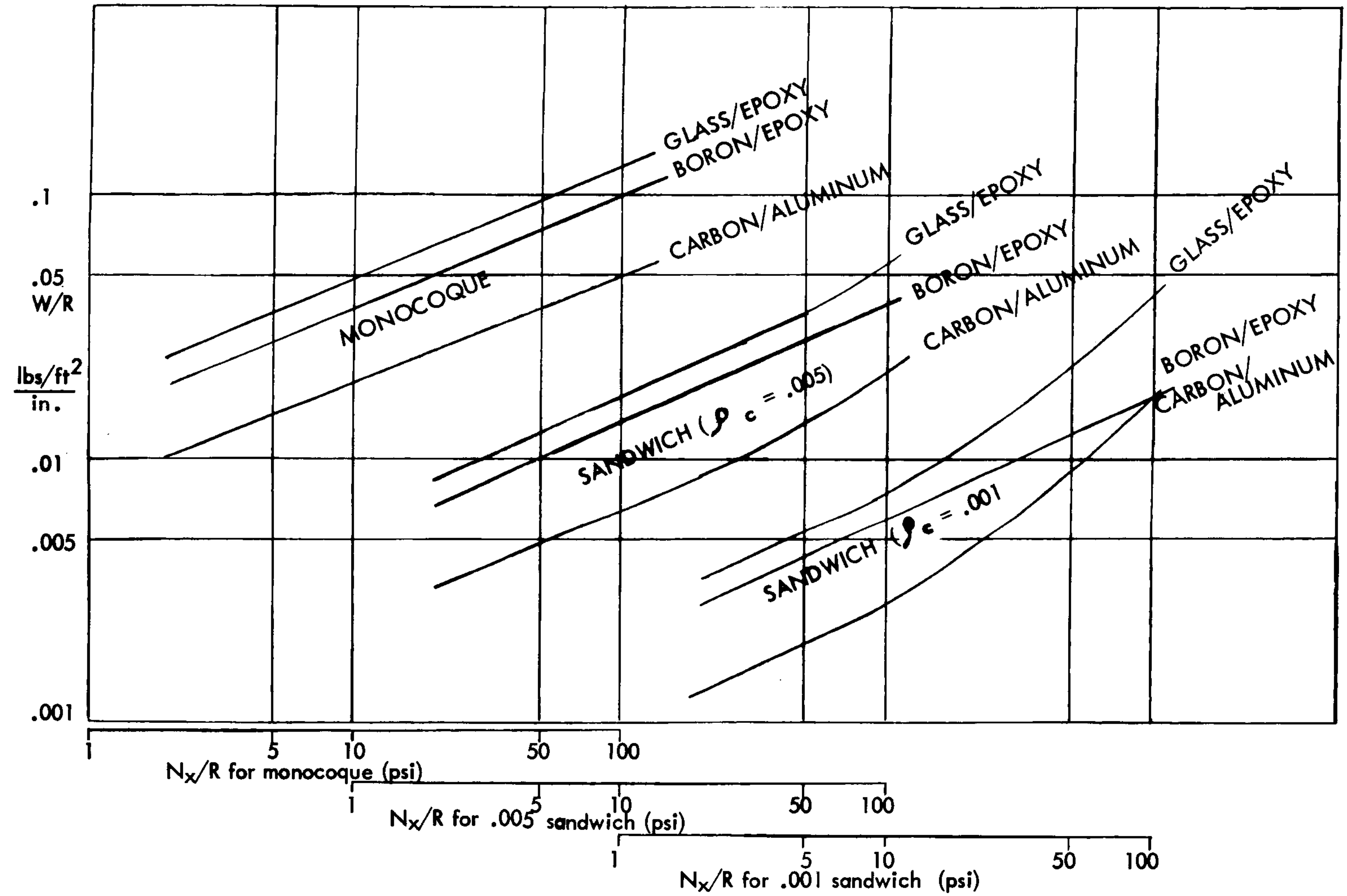

Figure 5-4. Weight/ Load Relationship, Orthotropic Windings

structural weights for an isotropic winding pattern and an orthotropic winding pattern was found to be small in unpressurized cylinders. The calculations to obtain weights for non-zero values of N_y/N_x of an orthotropic (0-, 90-degree) winding did not, therefore, seem justified.

5.4 EVALUATION OF STRUCTURAL WEIGHTS

Using the nominal loading conditions, structural weights were evaluated for the 101, 201, 202, 203, and 301 Vehicle configurations. Calculations were performed for various combinations of the composite materials and types of construction. The resulting weights are tabulated in Tables 5-2, 5-3, 5-4, and 5-5. In each of the tables, the weight of the hung tanks and thrust structures were those calculated for an aluminum structure and tabulated in Section 4. The fixed weights of baffles and insulation were held constant at the values taken from References 1 and 2. In the unpressurized cylinders, either the isotropic or orthotropic winding pattern was chosen depending upon which gave the lightest weight. The tabulated values of weight where an orthotropic laminate is lighter are enclosed with brackets. All other weights correspond to an isotropic laminate. In most instances the isotropic laminate yields the minimum weight design. Previous studies (Reference 26) indicated that this was to be expected at moderate structural index values, even for inelastic stability.

The propellant tank heads were designed as monocoques using a strength criterion and a netting analysis as explained in Section 2.

The following general observations were made from the results of this portion of the study.

a. Fibrous composites using high-modulus, high-strength filaments offer the potential of substantial reductions in boost vehicle structural weight.
b. Achievement of weight savings requires the use of efficient shell-stiffening configurations, such as low-core-density sandwiches, for interstage structures, and high-tensile-strength materials for tank structures. Additionally, it is of value to restate with some modifications certain of the conclusions of the earlier study (Reference 25) of contemporary boost vehicles, namely:
   (1) For the significant range of loading index over which optimum designs for compression shells fail by elastic instability, high-modulus filaments in an isotropic laminate were superior to metal shells. Relatively

small volume concentrations of such filaments produced materials of comparable efficiency to metals.

b. For sandwich construction, the elastic shell buckling efficiency was no longer proportional to the ratio of shell density, ρ_s, to the square root of Young's modulus, E_s, as for a monocoque shell, but was proportional to $(\rho_s/E_s)^{\frac{1}{2}}$ for the sandwich face material.

c. Poor layer in-plane shear strength and transverse extensional strength resulted in poor strength performance laminates. Configurations which were considerably heavier than optimum for buckling were frequently required to satisfy strength requirements. An effort to achieve improvements in matrix properties is necessary.

Table 5-2

101 Vehicle Weight Summary—Composite Materials
(101 Vehicle Nominal Weight = 756, 305 Lbs.)

Section	Glass/Epoxy			Boron/Epoxy			Carbon/Aluminum		
	Mon.	.005 Sand.	.001 Sand.	Mon.	.005 Sand.	.001 Sand.	Mon.	.005 Sand.	.001 Sand.
Instr. Unit	22554	7959	3640	13328	4718	1951	10822	3544	1455
Fwd. Skt.	33868	12008	5660	19984	7107	2945	16215	5333	2211
LH_2 Tank—Top Hd.	6327	6327	6327	5951	5951	5951	6417	6417	6417
LH_2 Tank Cyl.	36138	43940	43205	18651	15970	15185	15207	13467	12917
LH_2 Tank Bot. Hd.	7508	7508	7508	7045	7045	7045	7620	7620	7620
Intertank	89210	32171	[17315]	52357	18933	8011	42352	14159	[6485]
Baffles and Insul.	23740	23740	23740	23740	23740	23740	23740	23740	23740
LOX Tank and Thr. Str.	54546	54546	54546	54546	54546	54546	54546	54546	54546
Aft Skirt	241338	94461	56405	140361	52126	26251	112905	39172	[21993]
Second Stage Total in lbs. (Second Stage Total in kg.)	515229 (233708)	282660 (128215)	218346 (99042)	335963 (152393)	190136 (86246)	145625 (66056)	289824 (131464)	167998 (76204)	137384 (62317)
Interstage	61591	23992	[14271]	35836	13296	6643	28833	9984	[5557]
Forward Skirt	105207	40322	[23645]	61282	22658	11014	49343	16872	[9166]
LOX Tank—Top Hd.	5306	5306	5306	5026	5026	5026	5374	5374	5374
LOX Tank Cyl.	48746	21190	16612	28516	10613	6509	23023	8783	6491
LOX Tank—Bot. Hd.	11408	11408	11408	10692	10692	10692	11582	11582	11582
Intertank	256604	101955	[61548]	149098	55522	28631	119857	41852	[24081]
RP-1 Top Head.	3057	3057	3057	2828	2828	2828	3110	3110	3110
RP-1 Bottom Hd.	5614	5614	5614	5197	5197	5197	5716	5716	5716
Thrust Takeout	89954	36115	[21951]	52235	19486	10208	41974	14729	[8607]
Thrust Struct.	81537	81537	81537	81537	81537	81537	81537	81537	81537
Baffles and Insul.	39270	39270	39270	39270	39270	39270	39270	39270	39270
First Stage Total in lbs. (First Stage Total in kg.)	708294 (321282)	369766 (167726)	284219 (128922)	471517 (213880)	266125 (120714)	207555 (94147)	409619 (185803)	238809 (108324)	200491 (90943)
Vehicle Total in lbs. (Vehicle Total in kg.)	1223523 (554990)	652426 (295941)	502565 (227964)	807480 (366273)	456261 (206960)	353180 (160203)	699443 (317267)	406807 (184528)	337875 (153260)
Total Less Nominal	+467218	-103879	-253740	+51175	-300044	-403125	-56862	-349498	-418430
% Weight Saving	-61.8	+13.7	+33.5	-6.8	+39.7	+53.3	+7.5	+46.2	+55.3

Table 5-3

201 Vehicle Weight Summary—Composite Materials
(201 Vehicle Nominal Weight = 690, 822 Lbs.)

	Glass/Epoxy			Boron/Epoxy			Carbon/Aluminum		
	Mon.	.005 Sand.	.001 Sand.	Mon.	.005 Sand.	.001 Sand.	Mon.	.005 Sand.	.001 Sand.
Instr. Unit & Fwd. Skt.	31781	11248	5242	18763	6661	2759	15228	5001	2065
LH_2 Tank and Thr. Str.	39323	39323	39323	39323	39323	39323	39323	39323	39323
Intertank	98911	35294	17441	58248	20844	8663	47210	15622	6624
Baffles and Insul.	12900	12900	12900	12900	12900	12900	12900	12900	12900
LOX Tank	8850	8850	8850	8850	8850	8850	8850	8850	8850
Aft Skirt	22802	8264	[4539]	13360	4855	2122	10796	3628	[1714]
Second Stage Total in lbs.	214567	115879	88295	151444	93433	74617	134307	85324	71476
(Second Stage Total in kg.)	(97328)	(52563)	(40051)	(68695)	(42381)	(33846)	(60922)	(38703)	(32422)
Interstage	152415	55317	[30586]	89259	32486	14294	72111	24264	[11579]
Fwd. Skt.	108239	39798	[21944]	63352	23097	10251	51163	17245	[8331]
LOX Tank—Top Hd.	9300	9300	9300	8739	8739	8739	9436	9436	9436
LOX Tank—Bot. Hd.	12852	12852	12852	12044	12044	12044	13045	13045	13045
Intertank	304850	117593	[69371]	177483	65717	32303	142860	49305	[26944]
LH_2 Tank—Top Hd.	6512	6512	6512	6157	6157	6157	6596	6596	6596
LH_2 Tank Cylin.	151502	88354	78765	88698	38019	29236	71645	30020	23915
LH_2 Tank—Bot. Hd.	17848	17848	17848	16520	16520	16520	18169	18169	18169
Thrust Takeout	109199	42011	[24724]	63588	23531	11514	51190	17653	[9595]
Thrust Struct.	82741	82741	82741	82741	82741	82741	82741	82741	82741
Baffles and Insul.	20040	20040	20040	20040	20040	20040	20040	20040	20040
First Stage Total in lbs.	975498	92316	374683	628621	329091	243839	538996	288514	230391
(First Stage Total in kg.)	(442486	(223315)	(169956)	(285142)	(149276)	(110605)	(244489)	(130870)	(104505)
Vehicle Total in lbs.	1190065	608195	462978	780065	422524	318456	673303	373838	301867
(Vehicle Total in kg.)	(539814)	(275878)	(210007)	(353837)	(191657)	(144451)	(305411)	(169573)	(136927)
Total Less Nominal	+499243	-82627	-227844	+89243	-268298	-372366	-17519	-316984	-388955
% Weight Saving	-72.2	+12.0	+33.0	-12.9	+38.8	+53.9	+2.5	+45.9	+56.3

Table 5-4

202 and 203 Vehicles
Weight Summaries—Composite Materials

202 Vehicle Boron/Epoxy	.001 Sand.
I.U. and Fwd. Skt.	5630
LH_2 Tank & Thr. Str.	39323
Intertank	8432
Baffles and Insul.	12900
LOX Tank	8850
Aft Skirt	5459
Second Stage Total in lbs.	80594
(Second Stage Total in kg.)	(36557)
Interstage	5328
Fwd. Skirt	6683
LOX Tank—Top Hd.	5393
LOX Tank—Cyl.	11946
LOX Tank—Bot. Hd.	7202
Intertank	23598
LH_2 Tank—Top Hd.	3801
LH_2 Tank—Cyl.	66021
LH_2 Tank—Bot. Hd.	8182
Thrust Struct.	93270
Baffles and Insul.	20040
First Stage Total in lbs.	251464
(First Stage Total in kg.)	(114064)
Vehicle Total in lbs.	332058
(Vehicle Total in kg.)	(150621)
Total Less Nominal	-343901
% Weight Saving	+50.9

202 Vehicle Nominal
Weight = 675,959 Lbs.

203 Vehicle Boron/Epoxy	.001 Sand.
I.U. and Fwd. Skt.	667
LH_2 Tank & Thr. Str.	39323
Intertank	8585
Baffles and Insul.	12900
Lox Tank	8850
Aft Skirt	2968
Second Stage Total in lbs.	73293
(Second Stage Total in kg.)	(33246)
Interstage	19241
Fwd. Skt.	9457
LOX Tank—Top Hd.	9796
LOX Tank—Bot. Hd.	31495
Intertank	31202
LH_2 Tank—Top Hd.	8042
LH_2 Tank Cyl.	7769
LH_2 Tank—Bot. Hd.	22740
Thrust Takeout	12661
Thrust Struct.	100585
Baffles and Insul.	20040
First Stage Total in lbs.	273028
(First Stage Total in kg.)	(123846)
Vehicle Total in lbs.	346321
(Vehicle Total in kg.)	(157091)
Total Less Nominal	-392522
% Weight Saving	+53.1

203 Vehicle Nominal
Weight = 738,843 Lbs.

Table 5-5

301 Vehicle Weight Summary—Composite Materials
(301 Vehicle Nominal Weight = 641, 320 Lbs.)

	Glass/Epoxy			Boron/Epoxy			Carbon/Aluminum		
	Mon.	.005 Sand.	.001 Sand.	Mon.	.005 Sand.	.001 Sand.	Mon.	.005 Sand.	.001 Sand.
Instrument Unit	35445	12627	6161	20884	7461	3100	16931	5594	2356
Forward Skirt	124788	44186	20648	73663	26163	10837	59781	19640	8116
LOX Tank—Top Hd.	10561	10561	10561	10000	10000	10000	10697	10697	10697
LOX Tank Cyl.	12807	8074	7366	7609	3416	2768	6194	2731	2269
Common Bulkhead	32947	32947	32947	31659	31659	31659	33260	33260	33260
LH_2 Tank Cylinder	766295	314353	233719	447701	165951	96442	361163	137779	101517
LH_2 Tank—Bot. Hd.	16024	16024	16024	15057	15057	15057	16258	16258	16258
Thrust Takeout	160689	62862	[37521]	93460	34705	17463	75180	26078	[14628]
Thrust Structure	56175	56175	56175	56175	56175	56175	56175	56175	56175
Insulation	18000	18000	18000	18000	18000	18000	18000	18000	18000
Vehicle Total in lbs.	1233731	575809	439122	774208	368587	261501	653639	326212	263276
(Vehicle Total in kg.)	(559620)	(261187)	(199186)	(351181)	(167191)	(118617)	(296491)	(147970)	(119422)
Total Less Nominal	+592411	-65511	-202198	+132888	-272733	-379819	+12319	-315108	-3780444
% Weight Saving	-92.4	+10.2	+31.5	-20.7	+42.5	+59.2	-1.9	+49.1	+58.9

SECTION 6

ANALYSIS OF VEHICLE DESIGN APPROACHES

6.1 GENERAL CONSIDERATIONS

The majority of structural weight calculations were performed by computer programs, as outlined in the previous sections. Numerous additional calculations which were performed in the course of this study are documented in this and the following section to provide complete documentation of methods and techniques.

This section considers separately the effect on structural weight reduction due to the geometry of a launch vehicle family by means of the L/D (fineness ratio), reduction of maximum acceleration by throttling, methods of steering, and by variations in tank-pressure profiles. The effects of local loads due to strap-on solid rockets and strap-on propellant tanks are also analyzed. The analysis of each of the vehicle's upper stage thrust structure and hung-tank arrangement is detailed as are the results of the main stage thrust structure studies.

Additional restrictions and assumptions were made to carry out these calculations within a reasonable cost-time envelope, particularly as related to system weights and load and performance profiles on the 200 family of vehicles. The upper stage tank arrangements were not optimized for each vehicle, nor were system upper stage tank arrangements optimizations performed for non-structural elements associated with vehicle L/D changes. Trajectory profiles were assumed fixed for each class of vehicle. These assumptions are considered valid for a structure study of this nature since structural weight is insensitive to reasonable variations in trajectory. However it should be recognized that these results are valid only as applicable to structural weight since even small changes in the trajectory can have strong effects on the total vehicle performance.

6.2 FINENESS RATIO

Variation of the fineness or L/D ratio was studied by using a class of vehicles, namely the 201, 202, and 203, which retained all performance, payload, and thrust characteristics as closely as possible. Propellant weight and thrust were fixed and the length and diameter were varied to give a reasonable range of fineness ratio. Table 6-1 presents the results of the nominal and lower-bound load conditions. For the purpose of this study, the lower-bound load refers to the condition when wind loads, maximum boost accelerations and tank pressures were simultaneously reduced to the lowest values considered in this study as shown in Table 3-1. Table 6-2 presents the differences of the 201, 202, and 203 Vehicles for the nominal and lower-bound conditions. It is also interesting to compare the differences between the 202 with L/D ≅ 10 and 203 with L/D ≅ 5. For nominal flight conditions the 203 is 9.2 percent heavier than the 202, whereas, using the lower-bound conditions, it is only 0.79 percent heavier. It appears from this study that a change in fineness ratio from L/D ≅ 5 to L/D ≅ 10 changes the structural weight less than 8 percent for a similar family of vehicles. Figure 6-1 is a plot of the percent weight change compared to the 201 Vehicle. A curve through the three lower-bound points shows an optimum L/D of about 7 for this family of vehicles.

Table 6-1

Vehicle Nominal and Lower-Bound Structure Weights for 101, 201, and 301

Configuration Number	Nominal Weight, Lb.	Lower Bound Weight, Lb.	L/D
101	756,305	609,075	6.34
201	690,822	528,123	6.04
301	641,320	568,337	5.03

Table 6-2

Weight Comparisons Between 201, 202, and 203 Vehicles, Using 201 as Base

Configuration Number	Nominal Weight, Lb.	Percent Diff. From 201	Lower Bound, Lb.	Percent Diff. From 201	L/D
201	690,822	0	528,123	0	6.04
202	675,959	2.15	539,945	-2.24	9.65
203	738,843	-6.95	544,120	-3.03	4.72

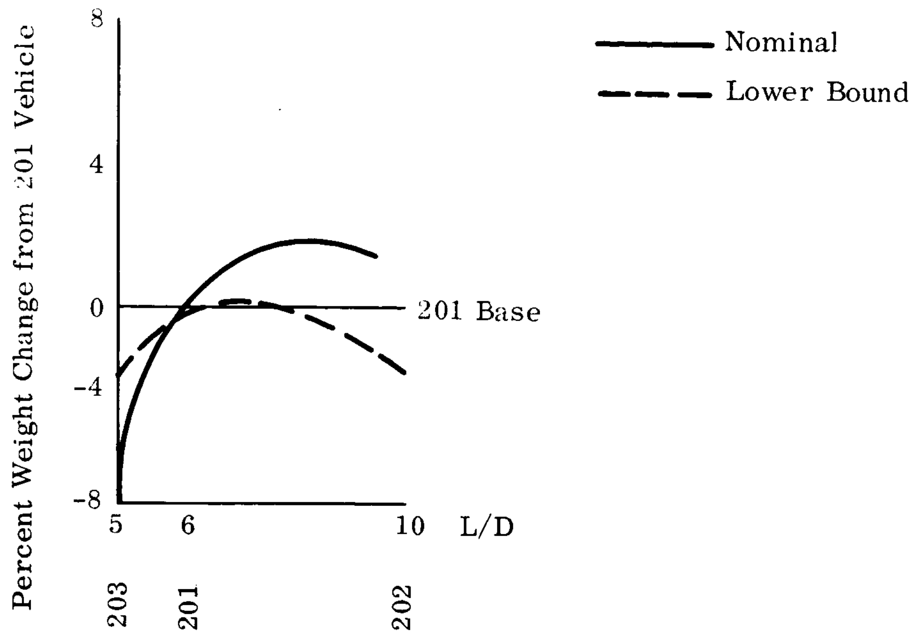

Figure 6-1. Weight Variations of 202 and 203 Vehicles From 201 for Nominal and Lower-Bound Conditions

Subsequent discussions point out some effects of L/D on the weight component parts for the 201, 202, and 203 family of vehicles. However, Figure 6-1 best summarizes the effects when one considers overall potential conditions. All-in-all, L/D has not been found to be a vital constraint for a wide range (5 to 10) of values.

6.3 PROPULSION TYPE, NOZZLE CONCEPTS

6.3.1 INTRODUCTION

The purpose of this area of study was to determine the effect or influence of the type of propulsion configuration. This was done by comparing the resulting weights of the chosen vehicles using gimbaled bell-nozzle engines and fixed plug-nozzle engines. The type of propulsion (rocket-nozzle configuration) has an influence in two ways:

a. Thrust structure and local supporting structure weight.
b. Vehicle structure weight penalty from distribution of loads during normal and thrust-vector control operation.

The vehicle control moment to counter aerodynamic disturbances during flight is generally produced by controlling the alignment of the main thrust vector. Gimbaled bell-nozzles produce the required control moment by applying, at the gimbal point, a lateral force that acts through a moment arm to the center of gravity. The control moment supplied by a plug nozzle using differential throttling is the sum of two components:

a. A lateral force applied to the vehicle times a moment arm.

b. An applied couple at the thrust structure resulting from the circumferential variation of the thrust intensity.

6.3.2 A SIMPLIFIED THEORY FOR THE ESTIMATION OF PLUG-NOZZLE THRUST-VECTOR CONTROL FORCES USING THRUST-MODULATION TECHNIQUES

6.3.2.1 Configuration

A plug nozzle with n number of engines with a total thrust of F_T is throttled by variation of chamber pressure, over 180-degree segments, to produce an incremental thrust (δ) at each segment. Dimensions are as noted in Figure 6-2.

The total resultant thrust vector, F_T, is shifted sideways through a displacement, b, and rotated so as to produce a side thrust, F_R, and maintain constant axial thrust, F_L.

6.3.2.2 Symbols

F_T = Total thrust, lb

δ = Incremental thrust over segment (usually 180-degree) of motor, lb/lb, $\frac{\Delta F}{F \text{ Nominal}}$

F_R = Total side thrust, lb

F_L = Total axial thrust (laterally displaced), lb

b = Lateral displacement of F_L from roll axis, ft

a = Distance from engine mount to CG, ft

M_S = Total steering moment, ft-lbs

β = Equivalent gimbal angle = $\sin^{-1}\left(\frac{M_S}{F_T a}\right)$, rad

α = Angle of cant of individual engine module

M_L = Applied moment at gimbal plane.

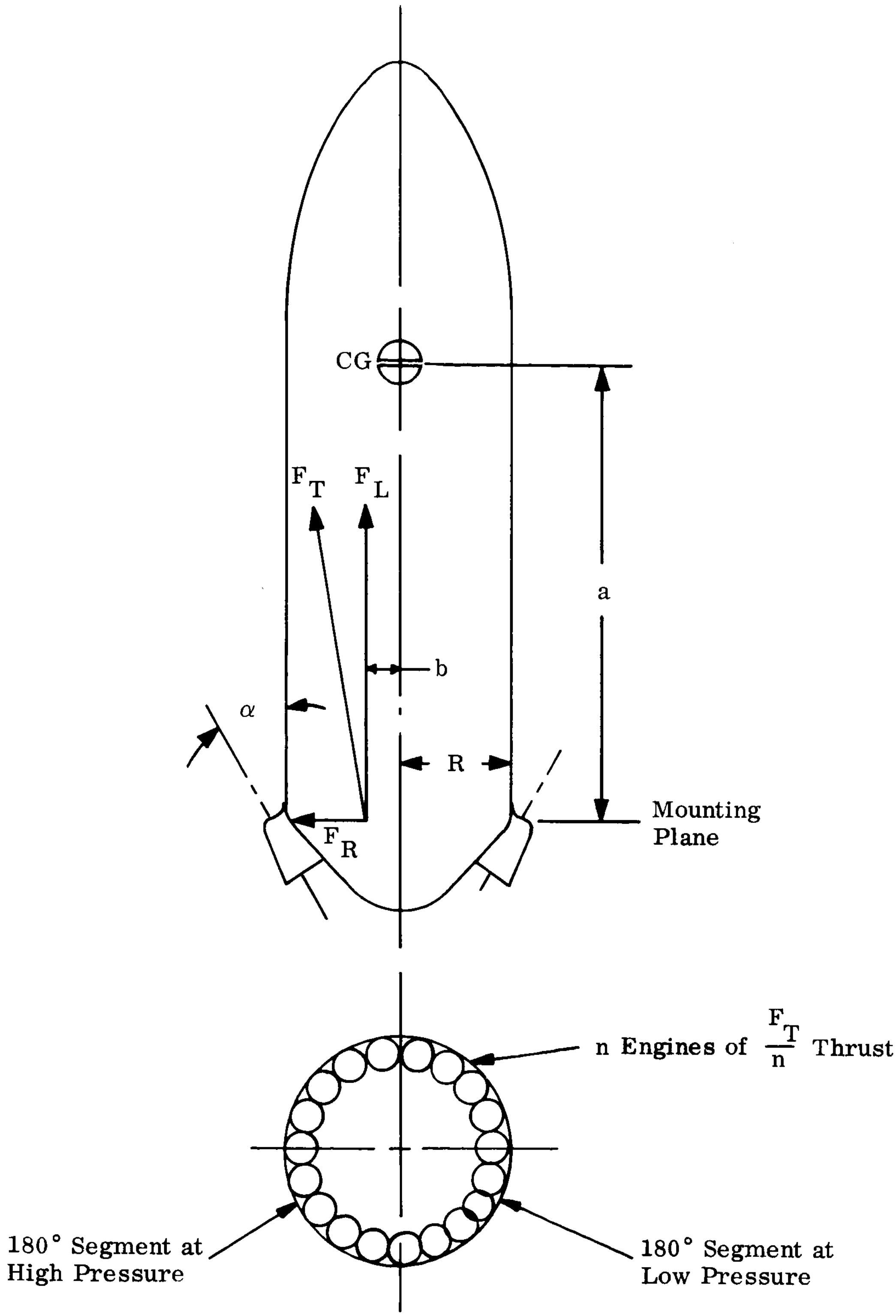

$$F_{L_H} = \frac{F_L}{2}(1 + \delta) \qquad F_{L_L} = \frac{F_L}{2}(1 - \delta)$$

Figure 6-2. Configuration

M_R	=	Moment due to lateral thrust at gimbal plane.
F_{L_H}, F_{L_L}	=	Magnitude of axial forces through high and low pressure segments, respectively, lb
F_{R_H}, F_{R_L}	=	Magnitude of side forces from high and low pressure segments, respectively, lb
n	=	Total number of engine modules

6.3.2.3 Steering Moment Distribution

The steering moment, M_S, is

$$M_S = F_L b + F_R a = M_L + M_R \tag{6-1}$$

For gimballed engines, no sideward displacement of the thrust vector is possible, and the steering moment becomes

$$M_S = F_R a \tag{6-2}$$

In practice, plug engines have a significant amount of "Wash-Around" of the exhaust, and both M_L and M_R exist.

6.3.2.4 Relationship of M_L and M_R

The relationship of M_L to M_R is important in establishing the load distribution in the vehicle near the engine. For convenience, the ratio M_L/M_R is introduced from Equation 6-1.

$$M_S = M_R\left(1 + \frac{M_L}{M_R}\right) = F_R a\left[1 + \left(\frac{F_L b}{F_R a}\right)\right] \tag{6-3}$$

6.3.2.5 Analysis Without the Central Plug

In solving for M_L consider the engine width as two 180-degree segments and the thrusts acting through the centroid of the respective areas,

$$F_T = F_{L_H} + F_{L_L} \tag{6-4}$$

$$M_L = F_{L_H} d_1 - F_{L_L} d_2 \tag{6-5}$$

For $d_1 = d_2$ = distance to centroid of the semi-circle = $2R/\pi$, then

$$M_L = F_T \cos \alpha b = \frac{2F_T R\delta}{\pi} \cos \alpha. \quad (6\text{-}6)$$

M_L is seen to be a direct, linear function of segment thrust increment, δ; engine module cant angle, α; and radius, R, of the vehicle, and

$$M_R = \frac{2F_T}{\pi} (\sin \alpha)\, \delta a. \quad (6\text{-}7)$$

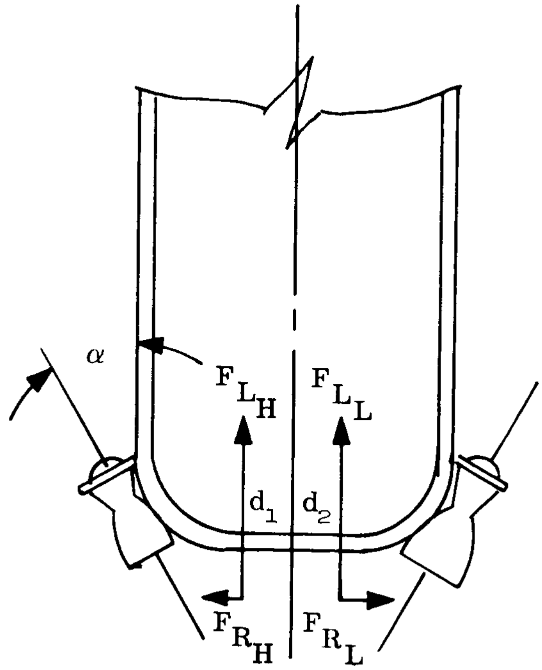

The ratio M_L/M_R is therefore,

$$\frac{M_L}{M_R} = \frac{\dfrac{2F_T R\delta}{\pi} \cos \alpha}{\dfrac{2F_T}{\pi} \sin \alpha\, \delta a} = \frac{R}{a} \cot \alpha \quad (6\text{-}8)$$

Thus, without the central plug M_L/M_R is a function of vehicle geometry and engine module cant angle, α.

Example: Vehicle 201

Assume the engines are not gimbaled and that thrust-vector control is achieved by throttling one segment and raising the thrust on the other.

For 201 Vehicle R = 35 - ft, a = 135.7 - ft and α = 13 degrees, and from Equation 6-8, $M_L/M_R = 1.11$.

From Equation 6-3

$$M_S = M_R \left[1 + \left(\frac{M_L}{M_R}\right)\right] = M_R \left[1 + 1.11\right] = 2.11\, M_R$$

$$M_R = \frac{2F_T}{\pi} (\sin \alpha)\, \delta a$$

Rearranging

$$\delta = \frac{\pi M_R}{2F_T (\sin \alpha) a} = \frac{\pi M_S}{4.22 F_T (\sin \alpha) a}$$

Assuming a required control moment of 216.5 million foot-pounds,

M_S = 216.5×10^6 foot-pounds

$\sin\alpha$ = $\sin 13°$ = 0.22495

a = 135.7 feet

F_T = local total thrust, lbs.

then

δ = 0.243

This is a reasonable upper limit with thrust decreased 24.3 percent in one 180-degree segment and raised 24.3 percent in other 180-degree segment. For this condition, the pump output pressures would be approximately 30 percent over design for nonmodulated TVC systems.

6.3.3 RESULTS

Assuming that the two components of the control moment (M_L and M_R) are of equal magnitude, a comparison of the resulting bending moment distribution was made with the bending moment distribution for a gimbaled bell-nozzle design, as shown in Figure 6-3.

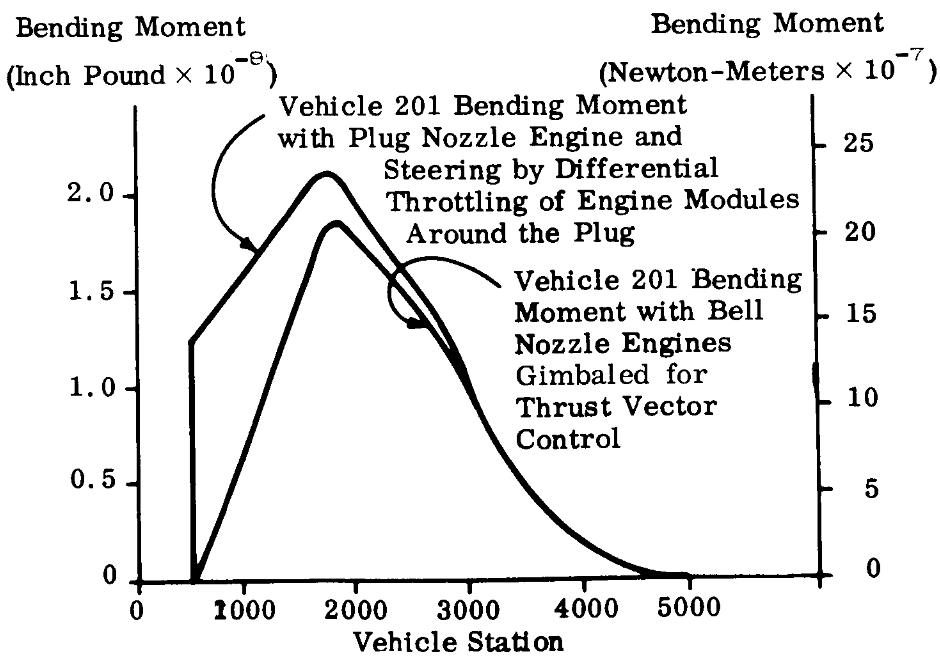

Figure 6-3. Bending Moment Due to Different Thrust Concepts

The weight changes for the given vehicles are summarized in Table 6-3 which has been extracted from the Weight/Load matrices. Data in Table 6-3 assumes the nominal thruster is the plug-nozzle engine and steering is by differential throttling of engine modules around the plug to obtain TVC. It is seen in all cases that gimbaling of engine shows a structural weight savings over the plug nozzle.

Table 6-3

Effect of Gimbaled Steering on Vehicle Structural Weight

Configuration Number	Structural Weight Diff. From Nominal, Lb.	Percent Structural Weight Savings	L/D
101	15982	2.11	6.34
201	18988	2.7	6.04
202	14055	2.07	9.65
203	11111	1.50	4.72
301	20542	3.20	5.03

Originally it was felt that while vehicle body weight would show an increase due to the larger bending moment the additional weight would be more than offset by weight reduction in the thrust structure. Subsequent investigations showed that this was not the case; differences were minor and substantially less than the weight changes in Table 6-3. One of the criteria in thrust structure design was that a minimum fundamental uncoupled 4 cps frequency was a necessary requirement for each component (frames, struts, and ties) making up the thrust structure. This made the weight differences minor (2000 to 2500 pounds) and hence they were assumed to be equal for this study. Subsequent investigation based on strength alone for the 201 showed the plug-nozzle thrust-structure weight could be reduced by 4800 pounds and the gimballed engine by 2470 pounds. Thus, large weight gains were not found in structural components between the engine types considered. It should be noted that relative system weights to provide guidance control and performance were not analyzed and are recognized to be potential weight adjustments to the above results. A detailed analysis of each vehicle main thrust structure is given in paragraph 6.8, and a detailed summary is given in paragraph 6.8.4.

The advanced technology of the toroidal combustor engine concept, such as the Aerospike engine, was considered in order to evaluate its impact on the results.

Data for the engines were estimated using the Martin Company work under Contract NAS8-5135, and data furnished by Rocketdyne, a division of North American Aviation, Inc. For the Aerospike engine with differential throttling for thrust-vector control, the influence on vehicle-structural weight and thrust-structure weight was the same as for the clustered plug-nozzle engine. With thrust-vector control by secondary injection, such as proposed by Rocketdyne, the bending moment curve would be between the two curves of Figure 6-3 and probably closer to the gimbaled engine curve. An overall evaluation of propulsion system weight would be required to evaluate the impact of advanced engines, such as the Aerospike, on total vehicle weight but this is beyond the scope of the current study.

6.4 INFLUENCE OF FRONT-END STEERING ON STRUCTURAL WEIGHT

6.4.1 RESULTS

The use of front-end steering can significantly decrease the bending moments applied to the vehicle structure as a result of inflight wind disturbances. This reduction in bending moment is accompanied by a significant decrease in the required structural weight. These reductions in structural weight are presented in Table 6-4 where front-end steering was considered not only as a single variable but also in combination with reductions in wind loads, tank pressures, and maximum boost acceleration. The reductions were as follows:

a. Prelaunch Winds—Nominal to 95 Percent Probability of Occurrence.
b. Inflight Winds—Nominal to 90 Percent Probability of Occurrence.
c. Maximum Boost Acceleration—Nominal to 2.0g's.
d. Tank Pressures—Nominal to Vented.

The weight reductions due to the lower bending moment must be offset against the weight of the front-end steering system required to provide vehicle stability. Both side-thrusting rocket engines and movable aerodynamic surfaces were evaluated for the front-end steering system. These systems were located in the vicinity of the center of pressure as illustrated in Figure 6-4.

The weight penalties for these front-end steering systems were calculated using both aluminum and beryllium materials, and are summarized in Table 6-5 for the 201, 202, and 202RT Configurations. For jet steering the total propellant weight for the side-thrusting jets is included in the tabulated weights. A summary of the propellant requirements is presented in Table 6-6 and the weight of the forward thrust structure

Table 6-4

Structural Weight Reductions for Front-End Steering

Vehicle Configuration	Front-End Steering Only		Front-End Steering Combined with Reduced Winds, Tank Pressures, and Boost Acceleration	
	Weight Change from Nominal, lbs	Percent Change	Weight Change from Nominal, lbs	Percent Change
101	-26,918	-4	-147,230	-19
201	-64,678	-9	-162,699	-24
202	-49,241	-7	-136,014	-20
202RT	-52,685	-8	—	—
203	-51,746	-7	-194,723	-26
301	-63,375	-10	-72,983	-11

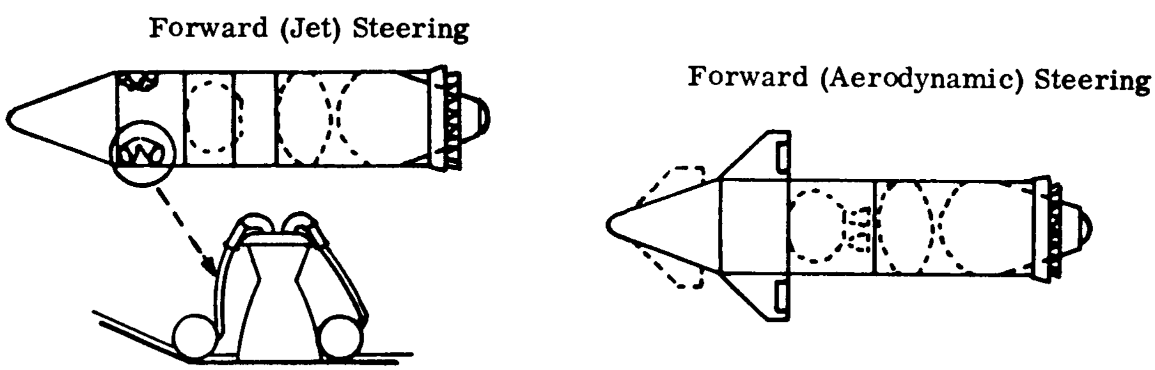

Figure 6-4. Front-End Steering Systems

Table 6-5

Weight Penalties for Front Steering Equipment

	Jet Steering		Aero Steering	
	Aluminum	Beryllium	Aluminum	Beryllium
201	412K (60 percent)	388K (56 percent)	223K (33 percent)	144K (21 percent)
202	249K (37 percent)	239K (35 percent)	132K (20 percent)	85K (13 percent)
202RT	210K (31 percent)	203K (30 percent)	112K (17 percent)	61K (9 percent)

and frames is summarized in Table 6-7. Note that the weights in both of these tables are included in Table 6-5 along with propellant tankage, pressurization system, engine modules, and attachment weights.

Table 6-6

Propellant Requirements

Configuration Number	Propellant Weight, Lb.
201	294,000
202	164,356
202RT	128,932

Table 6-7

Front-End Steering Weight—Forward Thrust Structure and Frames

Configuration Number	Jet Steering		Aerodynamic Steering	
	Al	Be	Al	Be
201	52,620	28,628	42,149	28,624
202	23,763	14,128	34,475	18,256
202RT	20,459	13,675	28,943	15,750

Comparing the structural weight reductions due to reduced bending with the front-end steering system weights suggest that no advantage is available when front-end steering is evaluated as a single variable. However, there may be some advantage to using front-end steering methods when other design loads are reduced. The reductions of structural weight for multiple variable changes reported in Table 6-4 tend to favor front-end steering since changes in load criteria would also affect structural weight when more conventional steering systems are used. Figure 6-5 shows the effect of three different steering designs where the loads criteria are simultaneously reduced to the values tabulated earlier. Results are shown for a plug-nozzle design (PN), a gimbaled bell-nozzle design (GBN), and a front-end steering design (FES), for the representative vehicle configurations. An evaluation of front-end steering can be made by comparing the margin between the gimbaled bell-nozzle and front-end steering in Figure 6-5 with the weight of the front steering systems tabulated in Table 6-5.

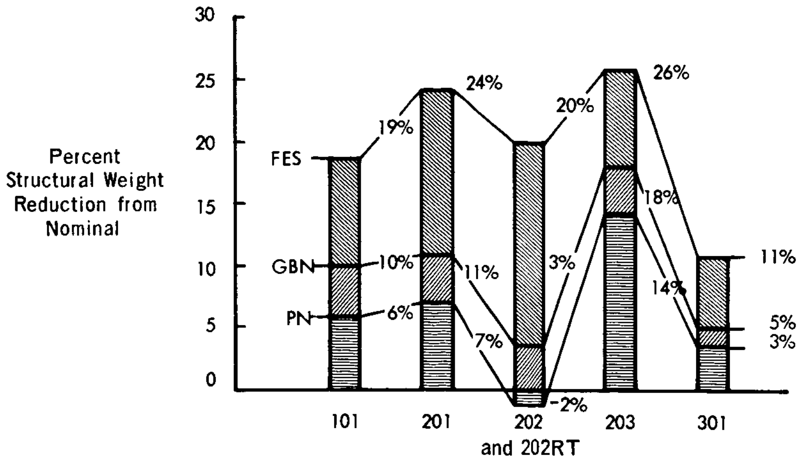

Figure 6-5. Effect of Three Steering Systems on Vehicle Weight

For instance, Figure 6-5 shows that the 201 Vehicle with front-end steering has a margin of 13 percent (24 percent minus 11 percent) of the nominal vehicle weight over a gimbaled bell-nozzle design. From Table 6-5 the smallest weight penalty to be expected for front-end steering equipment on the 201 Configuration is 21 percent of the nominal vehicle weight. This would indicate that the use of front-end steering would result in a net increase in structural weight for the 201 Vehicle.

Figure 6-5 shows the 202 and 202RT Configurations to have a margin of 17 percent of the nominal structural weight separating the front-end steering and gimbaled bell-nozzle designs. From Table 6-5, if aerodynamic steering is used and the additional structure (mounting structure, etc.) is fabricated of beryllium, the steering system weights for the 202 and 202RT Configurations are 13 percent and 9 percent respectively of the nominal structural weight. Therefore for the higher L/D vehicle configurations, it appears that front-end steering designs could provide additional structural weight reductions of 4 percent to 8 percent of the nominal vehicle structural weight. It is interesting to note that front-end steering can provide an advantage, but only for a vehicle designed for that purpose and with limits on maximum boost acceleration, design wind loads, and advantageous tank pressures.

The analysis of this study neglected the elastic body dynamics of the vehicle. This assumption would introduce an increasing amount of error for larger L/D designs. It was also assumed that the movable aerodynamic surfaces of the front-end steering system do not contribute to the aerodynamic disturbance loads. That is, if a vehicle flying a zero angle of attack experiences a sudden lateral gust of wind, the movable aerodynamic surfaces contribute to the instability of the vehicle until they can respond to the error signals. This effect on the vehicle aerodynamics was ignored during this study.

From Table 6-5 it is seen that reversing the first-stage propellant tanks has a significant effect on the weight of the front-end steering equipment. The effect on the critical loads profile is insignificant as can be seen from Figure 6-5.

The front-end steering method was judged only on the basis of changes in structural weight. It should be noted that the weight penalties of the front-end steering equipment are related to payload on a pound-for-pound basis. For two stage vehicles, this penalty could be reduced by staging the front steering equipment with the first stage structure.

6.4.2 SYSTEM REQUIREMENTS

6.4.2.1 Engines and Propellant Weight Calculations

Reaction control steering is obtained by firing rocket engines with the thrust vector normal to the vehicle centerline. The control force is determined by equating the reaction thrust control moment to the control moment given for aft thrust vector control. The forward control force is given by

$$N_c = KT \sin \beta \left(\frac{\ell_g}{\ell_c}\right) \tag{6-9}$$

where

ℓ_c and ℓ_g	=	distance from CG to CP and aft gimbal point respectively.
K	=	ratio of front-end steering contribution to total steering moment.
T	=	thrust, main engines.
β	=	gimbal angle of main thrusters.

The propellant required is calculated from the total impulse as given by

$$I_t = \int N_c dt, \text{ lb-sec} \tag{6-10}$$

The required propellant weight is

$$P_w = \frac{I_t}{I_{sp}}, \text{ lb} \tag{6-11}$$

where

I_{sp} = specific impulse-sec.

The total weight of the reaction control system is the sum

$$W = 4W_E + P_w + W_s \tag{6-12}$$

where

W_E = weight of one engine module

P_w = propellant weight

W_s = weight of thrust structure

W = total weight of reaction control system.

A representative calculation for the 201 Vehicle follows.

The steering force required is 1,551,204 pounds. The total impulse was calculated to be 129.6×10^6 lb-sec. Using an $I_{sp} = 440$ for LOX/LH_2 the total propellant weight is

$$129.6 \times 10^6/440 = 294{,}000 \text{ lbs.}$$

Assume engine modules weigh 15,000 pounds each. Based on upper stage weight calculations versus propellant weight the tankage plus pressurization system is estimated to weigh 5534 pounds. Total system weight excluding thrust structure is

$$4 \times 15{,}000 + 294{,}000 + 5534 = 359{,}534 \text{ pounds}$$

6.4.2.2 Aerodynamic System Requirements

The control moment required at maximum $q\alpha$ is determined from the Equation 6-13

$$M_c = T \sin\beta \, \ell_g \tag{6-13}$$

where

M_c = control moment

T = thrust of main engines

β = gimbal angle

ℓ_g = distance from gimbal plane to cg of vehicle

The normal force for front-end steering is given by

$$N_c = M_c/\ell_c \tag{6-14}$$

where

N_c = normal force of front-end controls

ℓ_c = distance to cg from cp, the center of pressure where N_c acts.

For small deflections, the lift-force coefficient is assumed to be linear with the control deflection, and can be calculated by

$$N_c = C_{L_\delta} \delta_c q S_{FIN} \tag{6-15}$$

where

C_{L_δ} = slope of the lift force coefficient curve due to control deflection, i.e., $\partial C_L/\partial\delta$

δ_c = control fin deflection measured with respect to the relative wind

q = free stream dynamic pressure

S_{FIN} = area of two control fins

Thus S_{FIN} can be computed by

$$S_{FIN} = \frac{T \sin\beta}{C_{L_\delta} \delta_c q} \frac{\ell_g}{\ell_c} \tag{6-16}$$

For the 201, 202, and 202RT Vehicles the following constants were taken from Reference 15.

$$C_{L_\delta} = 0.075$$

$$\delta_c = 10 \text{ degrees}.$$

Table 6-8 gives the results for each vehicle discussed using the trapazoidal plan form shown in Figure 6-9 in paragraph 6.4.3.3.

Table 6-8

Control Fin Size 201, 202, and 202RT Vehicle Configurations

Configuration Number	T	$\sin\beta$	ℓ_g, ft.	ℓ_c, ft.	q	S_{FIN}
201	21052875	.0722	135.7	132.4	744.2	2780
202	21051751	.0469	181.3	208.1	758	1520
202RT	21052390	.1000	94.7	295	743.7	1220

In order to determine the system weight the control surfaces were estimated from the calculations reported in Reference 15 to weigh 27.9 lb/ft and the actuator weight at 3820 pounds per surface. The weight penalties for four surfaces are calculated as

$$\Delta W = 55.8\, S_{FIN} + 4(3820).$$

For the 201 Vehicle the surface plus actuator weight is 170,404 pounds.

6.4.3 ANALYSIS OF LOCAL STRUCTURES

6.4.3.1 Main Thrust Structure

The main thrust cone weight can be reduced slightly due to the elimination of the applied moment resulting from rear-end steering. For example the 201 Vehicle thrust cone weight will be reduced by 2260 pounds.

6.4.3.2 Forward Thrust Structure

a. Load and Deformation Calculations

The front steering thrust structure is basically a ring or a pair of rings which transmit the side-thrust load to the main vehicle by means of shear flow. The engines are located such that their centerlines form right angles in a plane normal to the vehicle axis. Any thrust load is radially inward. The design load was assumed to occur when only one of the four equally spaced engines is firing at required thrust to turn the vehicle. This thrust is designated as N_c. For the design load assumed the maximum load point is at the engine that is firing. The elemental loads the ring is subjected to at that point are:

$$M = 0.24\, N_c R, \tag{6-17}$$

$$N = 0.24\, N_c, \tag{6-18}$$

$$Q = 0.5\, N_c, \tag{6-19}$$

where

M = moment,
N = normal or ring thrust load,
Q = transverse shear,
R = ring radius.

The maximum deflection of the ring is:

$$\Delta_r = .043 \frac{N_c R^3}{EI} \tag{6-20}$$

where:

E = Young's modulus of the material,

I = areal moment of inertia of the ring cross section.

Ring design criteria can be stress and/or deflection. For a weight study the ring depth and material can be used as variables.

b. Solid Ring Girder Section

For a solid section an approximation of the ring cross section is assumed to be I-shaped where:

A_f = flange area,

A_w = web area,

h = total ring depth back-to-back of the flanges,

h_f = distance between flange centroids,

h_w = web depth,

t_w = web thickness.

The web thickness was required to be $\geq \frac{h}{170}$ unless maximum shear stress dictated otherwise.

Using the preceding nomenclature one finds the total area by:

$$A = 2A_f + A_w, \tag{6-21}$$

The areal moment of inertia is approximated as:

$$I = 2A_f \left(\frac{h_f}{2}\right)^2 + \frac{1}{12} t_w h_w^3 \tag{6-22}$$

Equation 6-22 can be given a better form that leads to a good first order calculation of the ring section properties. Assume $h = h_f = h_w$ and Equation 6-22 becomes

$$I = \frac{h^2}{2} \left(A_f + \frac{A_w}{6}\right). \tag{6-23}$$

Since $h > h_f > h_w$ numerical results using Equation 6-23 are too high. In order to compensate for this fact the following equation was assumed to be more nearly correct

$$I = \frac{h^2}{2} \left(A_f + \frac{A_w}{8}\right), \tag{6-24}$$

The web is designed on the following basis

$$A_w \geq \frac{h^2}{170}, \tag{6-25}$$

or

$$A_w \geq \frac{Q}{.55F_{TY}} \qquad (6\text{-}26)$$

whichever is greater. A representative 201 calculation follows.

Given N_c = 1,551,204 lb is the required steering thrust load. Assume two rings are to be used,

$$P = \frac{1.4\ N_c}{2} = 1{,}085{,}842 \text{ pounds}$$

Assume $\frac{2R_{max}}{10} \geq h$

$$h_{max} = 420/5 = 84 \text{ inches}$$

For 7075-T6 with $E = 10.4 \times 10^6$, $F_{TY} = 64{,}000$, $F_{TU} = 77{,}000$ and $\gamma = 0.101$ lb/in^3 one finds

$$I = \frac{242{,}142}{\Delta}$$

Let $\Delta_{max} \geq 2$ in

$$I = 121{,}071 \text{ in}^4$$

$$A_w = \frac{h^2}{170} = 41.505 \text{ in}^2$$

$$\frac{Q}{.55F_{TY}} = \frac{.5 \times 1{,}085{,}842}{.55 \times 64{,}000} = 30.84 \text{ in}^2 < \frac{h^2}{170}$$

$$A_f = \frac{21}{h^2} - \frac{A_w}{8} = 29.129 \text{ in}^2$$

$$A = 2A_f + A_w = 99.763 \text{ in}^2$$

Since $2R/h = 9$, to compute stress use a 1.1 multiplying factor on M_c/I to account for curved beam stress on the inner fiber

$$\sigma_{max} = \frac{1.1\ Mh}{21} + \frac{N}{A} = 43087 < 77{,}000$$

Allow for a 10 percent increase in beam weight to account for web bracing and fastenings. The total structure weight is

$$2\,[1.1\,(2\pi\,RA\,\gamma)\,] \quad = \quad 52620 \text{ lbs.}$$

Adding the previous calculation for engines, propellant, etc. of 359,534 pounds, the total 201 System is 412,154 pounds.

c. Truss Type Ring Section

Where the vehicle is of large enough diameter a weight savings may be possible by using an articulated type of structure rather than a solid section. Figure 6-6 demonstrates the structural concept of a ring section where:

A_f = Flange area

A_w = Area of web member

σ_f = Stress in flange

σ_w = Stress in web

A flange at a section is sized by the equation

$$A_f = \frac{M}{\sigma_f h} \tag{6-27}$$

For M expressed as a function of N_c and R then:

$$A_f = C\left(\frac{N_c}{\sigma_{allow}}\right)\left(\frac{R}{h}\right) \tag{6-28}$$

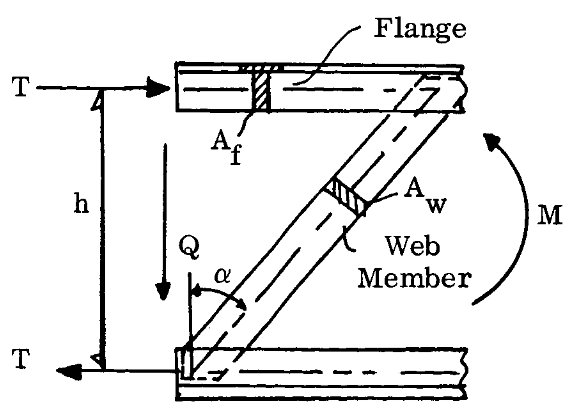

Figure 6-6. Structural Concept of a Ring Section

In Equation 6-28 $R = R_{outer} - \frac{h}{2} = R_{inner} + \frac{h}{2}$.

Web members are sized depending upon whether they are subjected to compression or tension. In this note the compression web member is denoted as a strut and the tension web member is called a diagonal. From Figure 6-6 the load in the member, S is calculated by the equation:

$$S = Q \sec \alpha \qquad (6\text{-}29)$$

For a diagonal:

$$A = S/\sigma_{allow} \qquad (6\text{-}30)$$

A strut is sized such the the Euler buckling load and yielding occur simultaneously, that is, Equations 6-31 and 6-32 are satisfied

$$I = \frac{SL_s^2}{2\pi^2 E} \qquad (6\text{-}31)$$

$$A = \frac{S}{F_{LY}} \qquad (6\text{-}32)$$

where

F_{LY} = yield stress of material.

An extensive study of the 201 Vehicle was performed based on the above analysis for Al, Ti, and Be alloys. The effects of R/h, and the steering ratio were considered. (Steering ratio, denoted by K, is the ratio of steering contribution of front jets to that of the total steering moment. If k = 1 all steering is by front jets.) The results for K = 1 are shown in Figure 6-7 for 7075-T6 and Be -.36 Al alloy.

6.4.3.3 Forward Frames for Aerodynamic Steering

The rings or frames of the main vehicle are assumed to be subjected to two applied tangential loads and moments in the plane of the ring and 180 degrees apart. See Figure 6-8. The analysis will be assumed to be in the linear elastic region, hence superposition of load conditions will be allowed. The two load conditions and the appropriate coefficients are given below for conditions at the point of load application.

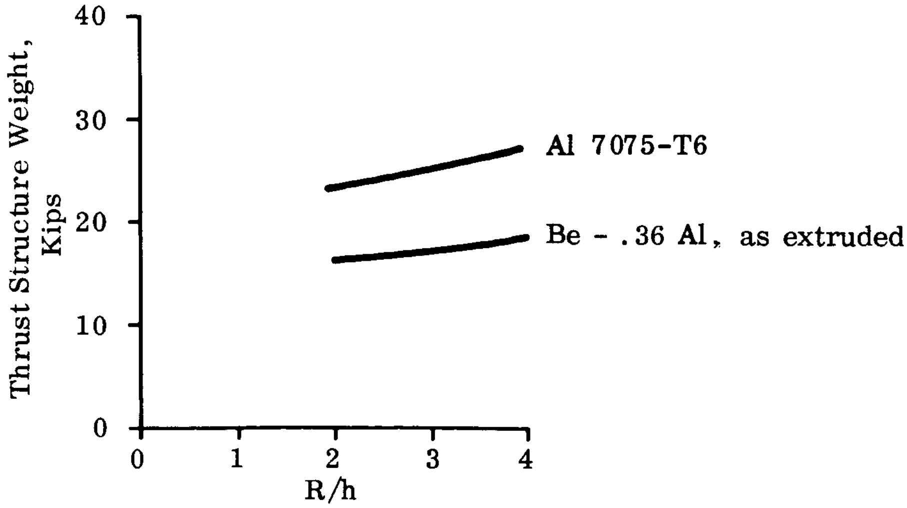

Figure 6-7. Ring-Depth Ratio Versus Thrust Structure Weight with a Steering Ratio, K = 1.

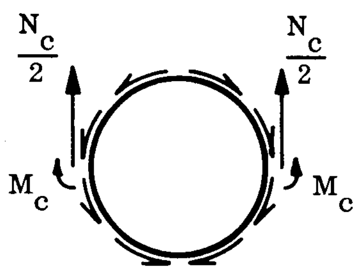

Figure 6-8. Tangential Loads Applied to Ring

At point 0

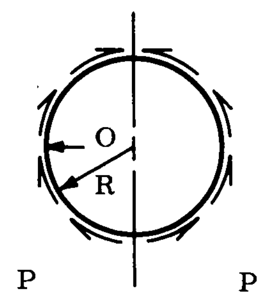

$\Delta_R^P = 0$, radial deflection,

$\theta^P = -.0115 \frac{PR^2}{EI}$, slope change,

$M^P = 0$, moment,

$Q^P = .16P$, shear,

$N^P = \pm .5P$, thrust.

At point 0

$\Delta_R^{M'} = 0$, radial deflection,

$\theta^{M'} = .16 \frac{R}{EI} M'$, slope change,

$M^{M'} = \pm\ .5M'$, moment,

$Q^{M'} = .63 \frac{M'}{R}$, shear,

$N^{M'} = 0$, thrust.

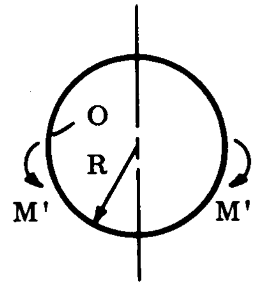

The airfoil surface is assumed to be a trapazoid in plan form with the loads distributed equally on the circular ring frames. Figure 6-9 demonstrates the assumed dimensions.

$$A = \frac{L}{2}(L + \frac{I}{6}) = \frac{7}{12} L^2 \qquad (6\text{-}33)$$

$$\bar{y} = \frac{8}{21} L \qquad (6\text{-}34)$$

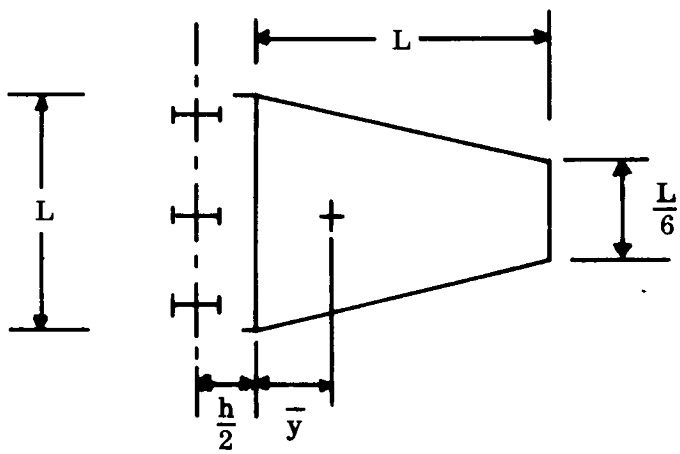

Figure 6-9. Assumed Dimensions of Airfoil

For a given lift load N_c, the load per ring is $P = N_c/6$ and $M' = P(\bar{y} + \frac{h}{2})$. For an assumed ring depth h the required I of the beam can be computed by using a deformation criterion. If the change in slope is required to be some value $\underline{\theta}$ then

$$I = \frac{RK}{E\underline{\theta}} [.16M' - .0115\ PR] \qquad (6\text{-}35)$$

where

K = steering ratio, defined at the end of paragraph 6.4.3.2.

I = areal moment of inertia of the ring cross section.

For a computed I from Equation 6-35 the section area can be computed by the equation

$$I = \frac{h^2}{2}\left(A_f + \frac{A_w}{8}\right),$$

that is, Equation 6-25 for the jet steering analysis. The stress can be calculated by the regular methods of mechanics of materials for a check on the limits of strength.

A representative calculation for the 201 Vehicle follows. Lift load required is 1,551,204 pounds. The surface area to provide this is 2780 ft^2 and the span L is 48.7 feet, $\bar{y} = \frac{8}{21}$, L = 18.552 feet. Using three frames, the load per frame is

$$M = 57{,}557{,}209 \text{ in-lb}$$

and

$$P = 258{,}540 \text{ lb}.$$

The total applied moment on the ring is

$$M' = M + P\frac{h}{2}$$

where h = ring depth. Assume the ring is 40 inches deep and

$$M' = 62{,}788{,}009 \text{ in-lb}.$$

As a design criterion require $\theta \leq 10$, and

$$I = 19545.61 \text{ in}^4$$

using 7075-T6 alloy with E = 10,400,000 psi. Require $A_w = h^2/170 = 9.41$ in^2

$$A_f = \frac{21}{Ah^2} - \frac{A_w}{8} = 23.26 \text{ in}^2,$$

$$A = 55.93 \text{ in}^2$$

Assume frame weight is increased by a factor of 25 percent to account for other loadings not considered, internal bracing, etc. The total weight is

$$1.25\,[\,3\,(2\pi A R \gamma)\,] \quad = \quad 52{,}686 \text{ lb}$$

This is essentially the same frame weight calculated for front-end steering with side thrusting jets.

The wings and actuators, controls, etc. weigh 170,404 pounds. The total system sums up to 223,090 pounds.

6.5 PROPELLANT TANK PRESSURE PROFILES

Propellant tank pressures are selected to:

a. Satisfy minimum NPSH requirements.
b. Prevent propellant boiling.
c. Minimize structural loads in the propellant tanks.

The best pressure profile for a given tank with a specified configuration and mission can be chosen only after an overall systems analysis is performed considering tradeoffs between the three requirements listed above. While an overall system analysis does not fall within the scope of this study, the results of the study performed by the Martin Company (NAS8-5135) provides an excellent base for structural weight sensitivity studies. The propellant tank pressures for each of the representative vehicles is presented in Section 3 of this volume. Structural weight sensitivities to changes in propellant tank pressures were evaluated by venting the propellant tanks to the atmosphere throughout the nominal mission. The resulting structural weights were compared to the nominal structural weights as shown in Table 6-9.

Table 6-9

Weight Differences for 101, 201, 202, 203, and 301 Vehicles due to Venting the Propellant Tanks

Configuration Number	Weight Change from Nominal, lb	Percent Change	Vehicle L/D
101	-35935	-4.75	6.34
201	-32647	-4.73	6.04
202	+25063	+3.71	9.65
203	-77151	-10.44	4.72
301	+75124	+11.71	5.03

It is clear that the effect of propellant tank pressures on structural weight is greatly influenced by the tank configuration. Venting the propellant tanks results in a 12 percent increase is structural weight for the 301 Vehicle while the 203 Vehicle structural weight is decreased 10 percent. These results are better understood by considering the effect of tank pressure on the structural components of the vehicles. Tank pressures reduce the large compressive loads in tank cylinders so decreases in pressure result in larger buckling loads and therefore increased structural weight in the tank wall. On the other hand, the loads on the tank heads are decreased as pressure is reduced. The effect of changes in tank pressure on total vehicle structural weight therefore depends upon how the total structural weight is divided between tank heads and tank cylinders. Tanks with long cylindrical tank sections such as the 202 and 301 Configurations show increases in weight as the pressure is reduced. Conversely, a vehicle such as the 203 which is primarily composed of heads, benefits from reduced pressure.

Throughout this study the pressure reduction was assumed to be achieveable in the limit by improved pumps with reduced NPSH requirements.

6.6 REDUCTION IN MAXIMUM ACCELERATION

The launch vehicles were studied to determine the effect of reducing maximum acceleration. The acceleration profiles are shown in Figure 6-10. It was assumed that the 202 and 203 Vehicles had the same profile as that shown for the 201.

The nominal 101 and 201 Configurations accelerate unthrottled to maximum accelerations of 4.8 and 5.55 g's respectively, while the nominal 301 Configuration is throttled at 2.5 g's. The effect of maximum boost acceleration on structural weight was evaluated by considering different boost acceleration profiles, shown in the sketches by broken lines. In every case it was assumed that the maximum boost acceleration of the second stage did not exceed the first stage maximum.

The results reported for comparison purposes are for the 2 g lower limit on maximum acceleration for all vehicles. A condensation of the results presented in Tables 4-1 through 4-5 is given in Table 6-10 for limiting maximum acceleration.

The effect of L/D or fineness ratio is once more apparent from Table 6-10 for the 200 family of vehicles. The lower L/D vehicle demonstrates the greatest weight savings. A plot of the percent weight savings versus fineness ratio for the 201, 202, and 203 Vehicles is given in Figure 6-11.

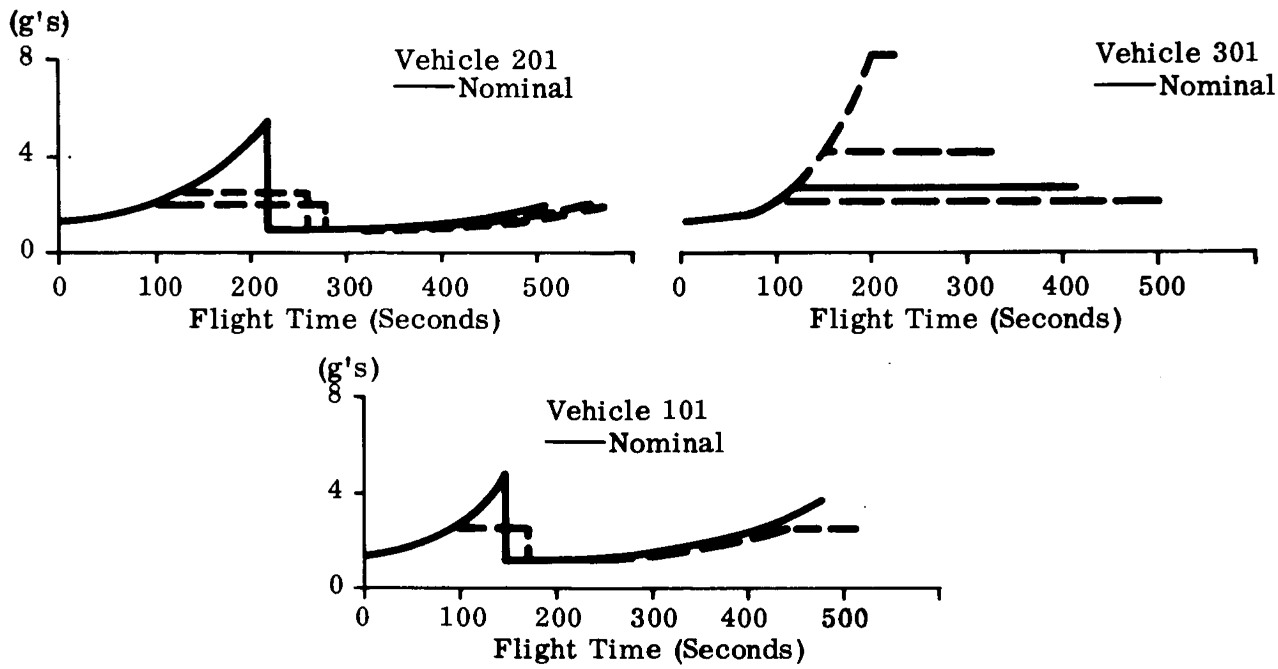

Figure 6-10. Acceleration Profiles

Table 6-10

Weight Differences from Nominal for Maximum Acceleration Throttled to 2 g's

Configuration Number	Weight Difference from Nominal, lb	Percent Weight Savings	L/D
101	41,929	5.54	6.34
201	17,276	2.5	6.04
202	5,429	0.8	9.65
203	36,528	4.94	4.72
301	9,250	1.44	5.03

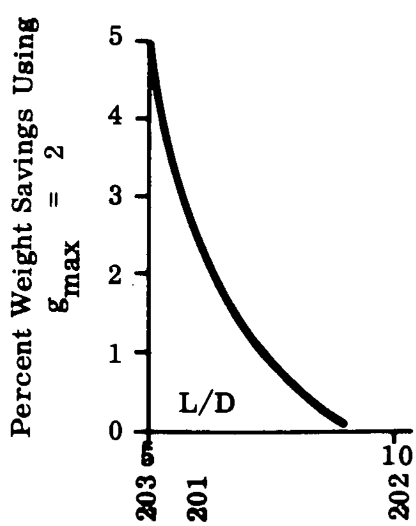

Figure 6-11. Percent Weight Savings versus L/D Ratio

6.7 STRAP-ON STRUCTURES

The 201 vehicle was considered as a core structure and the added weight required to attach solid rocket boosters and liquid propellant tanks was analyzed.

6.7.1 SOLID ROCKET MOTORS (SRM)

6.7.1.1 Weight of Core Vehicle Attachments

The effect of attaching the solid motors to the core was considered for two load conditions as follows:

a. All thrust delivered to aft of core vehicle.
b. Half of the solid rockets delivering thrust at the aft end of the core vehicle, and half at the forward attach points of SRM to core vehicle.

The methods of attaching used in this study are not at all to be construed as the optimum mechanical approach to the solution of the coupling problem. Due to the time limitations and relative importance of other phases of the study only one system of coupling the core and attach solids was considered for analysis. Future studies using other attaching methods may possibly demonstrate considerable weight reductions in the attach structure requirements.

In order to provide adequate liftoff thrust without firing the 201 thrusters in parallel, a minimum of eight 260-inch Solid Rocket Motors (SRM) are required. No cant of the solid thrust nozzles were assumed in the final analysis.

a. All Thrust Delivered at Aft End

The analysis assumed that the solid motors were attached to the core vehicle at two locations along the longitudinal axis. The aft attachment point was assumed to transfer all the thrust loads and the forward attachment point sustained only radial loads. It was further assumed that the weight of the solid motors was supported separately on the launch pad. Acoustic loads and buffet loads were assumed to be negligible. The calculated weights are those shown below.

Forward Kick Frame	19,822 lbs
Aft Thrust Structure	149,366 lbs
Total	169,188 lbs

The weight of the attachments includes all bearing seats and pins plus half the weight of all connecting struts between the core vehicle and strap-on solid motors.

(1) Forward Frame

The forward frame was designed as a ring girder with two connecting struts per attached solid rocket motor. The loads were assumed to act radially in the plane of the ring. The final radius-depth ratio was such that straight-beam theory was adequate for analysis.

The ring was sized on the basis of minimizing deflection such that the reaction load would not exceed 0.1 percent of the nominally calculated load (where deflection is not considered). Free ring inplane flexural vibration characteristics were considered for determining the number of rigid attachments of the ring to the core vehicle shell. Figure 6-12 shows a quarter circle representation of an axial view of the ring and attached solids. A cross-sectional view of the ring with bracing is also shown.

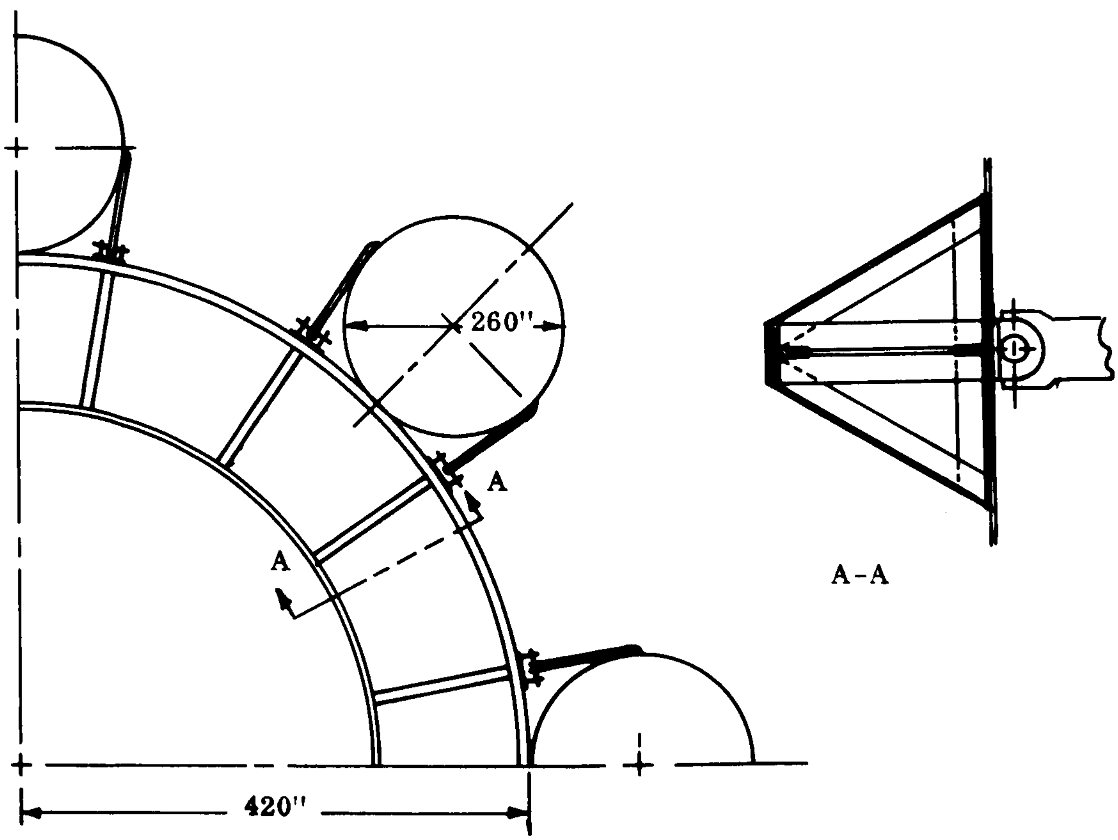

Figure 6-12. Axial View of Ring and Attached Solids

(2) Attachments

The forward struts were designed as Euler columns and for a minimum fundamental bending mode of 4 cps.

The pins and lugs were analyzed by methods presented in Reference 41 for bearing, shear, and tension failure. Ultimate strength methods using an idealized stress-strain curve were used for determining bending strength of pins and lugs. Figure 6-13 demonstrates the pin, strut, lug attachment.

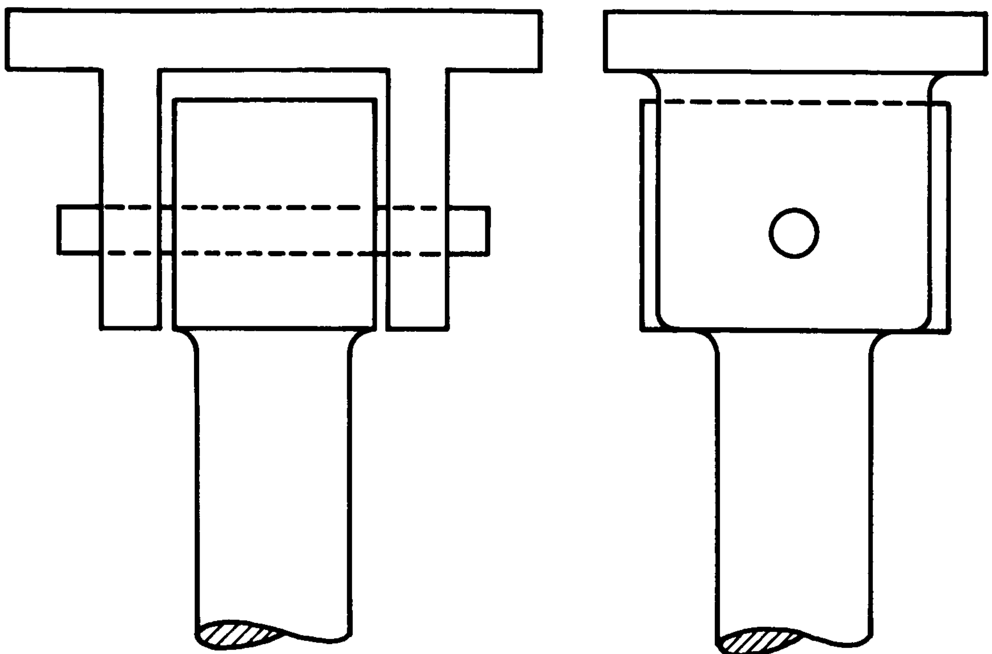

Not to Scale

Figure 6-13. Pin, Strut, Lug Attachment

The weight of the pins, struts, and lug attachments were assumed to be the same for both forward and aft attachment points. The total weight of connecting structure for eight solid rocket motors was calculated to be 9924 pounds.

(3) Aft Thrust Structure

The aft thrust structure was assumed to be a relatively heavy skin-enclosed structure composed of rings and longitudinal stringers. The thrust is assumed to be delivered by externally attached longerons which also act as beams on an elastic foundation being subjected to end-moment and shear induced by misalignment. Figure 6-14 is a representation of the thrust structure.

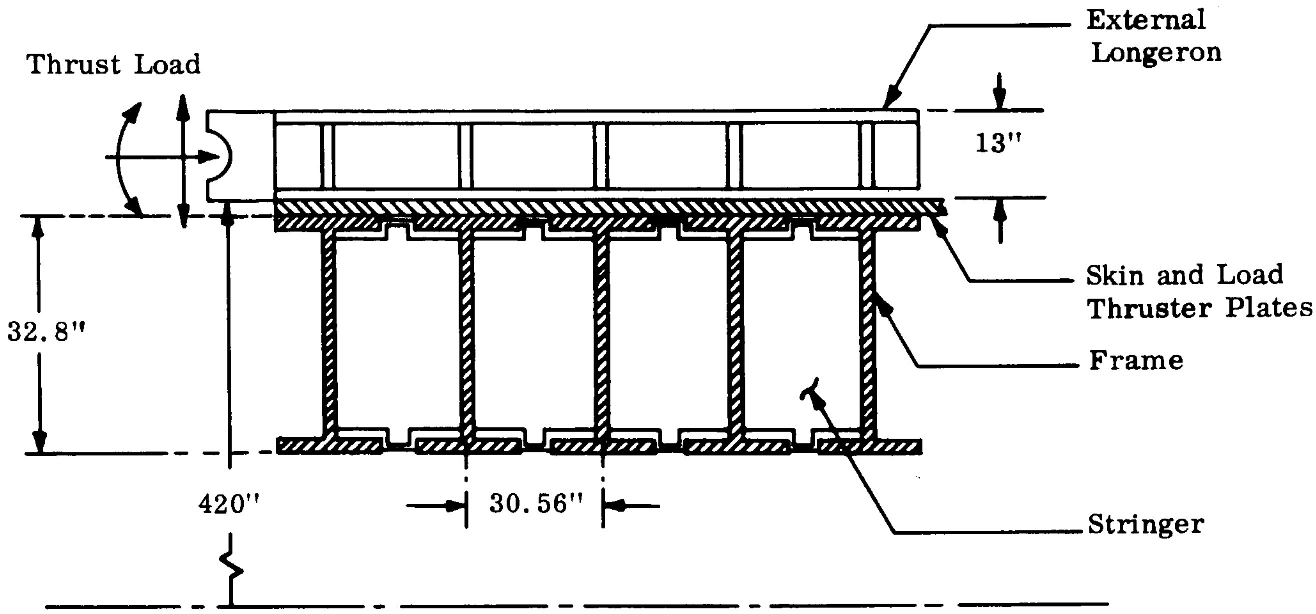

Figure 6-14. Aft Thrust Structure

The same attachments are assumed for the forward frame for taking the nominal radial load.

b. Thrust Equally Divided between Forward and Aft Attach Points

An investigation was performed to evaluate the increase in core structure weight due to the attach structure for eight 260-inch solid motors attached at two stations along the longitudinal axis. Four rockets were assumed to transfer the thrust load at the forward station and four were assumed to transfer the thrust load through the aft attachment points. The weights of the solids were assumed to be supported separately on the launch pad. Acoustic and buffet loads were ignored. The calculated weights are the same for both the forward and aft thrust structures. Each core attach structure was found to weigh 138,000 pounds for a total of 276,000 pounds. The weight calculations include all bearing seats, pins, and lugs, plus half the weight of all connecting struts and ties connecting the core vehicle to the solid motor.

(1) Thrust Structure

The forward and aft thrust structures were assumed to be similar. Each is made up of a relatively heavy skin enclosed structure of rings and longitudinal stringers. Thrust is transferred by externally attached longerons which transfer the loads by shear, but acts also as a beam on an elastic foundation subjected to an end moment and shear load. Figure 6-15 is a representation of the thrust structure.

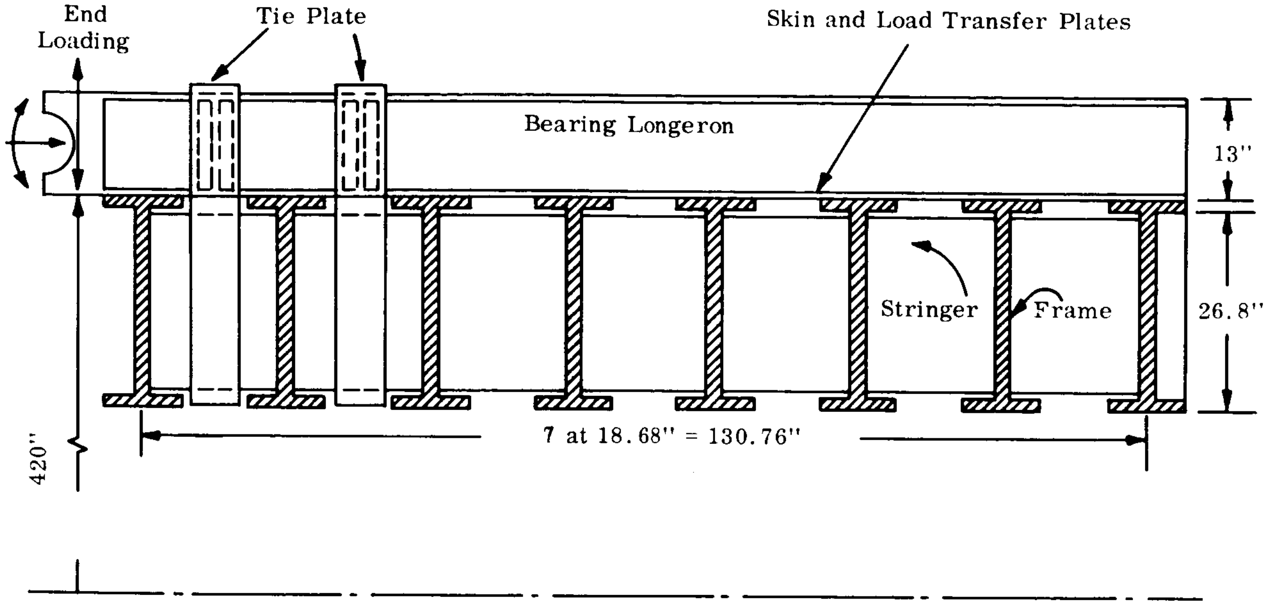

Figure 6-15. Thrust Structure

6.7.1.2 Attach Structure Solid Motors

The attach structure for the 260-inch solid motors was sized. The thrust transfer was assumed to occur by means of a ring on the solid motor subjected to a pair of out-of-plane loads. The ring was also designed to take the radial coupling loads between the solid motors and core vehicle. A second ring was designed to take only the radial vehicle coupling loads. The two rings are assumed interchangeable depending upon which end of the solid motor the thrust transfer is assumed to occur. The calculated weights including attachments are tabulated below:

Forward Ring	1,570 lb/260-inch solid
Aft Thrust Ring	68,356 lb/260-inch solid
Total	69,926 lb/260-inch solid

For eight solid rocket motors the total weight is therefore 559,408 pounds.

a. Thrust Structure

The thrust structure on the 260-inch solid used in transferring the solid boost to the core was designed as a non-prismatic ring subjected to out-of-plane loads. The minimum weight ring was designed to be made of maraging steel with F_{TY} = 280,000 psi. Figure 6-16 is a representation of the load transfer ring acting on the core vehicle.

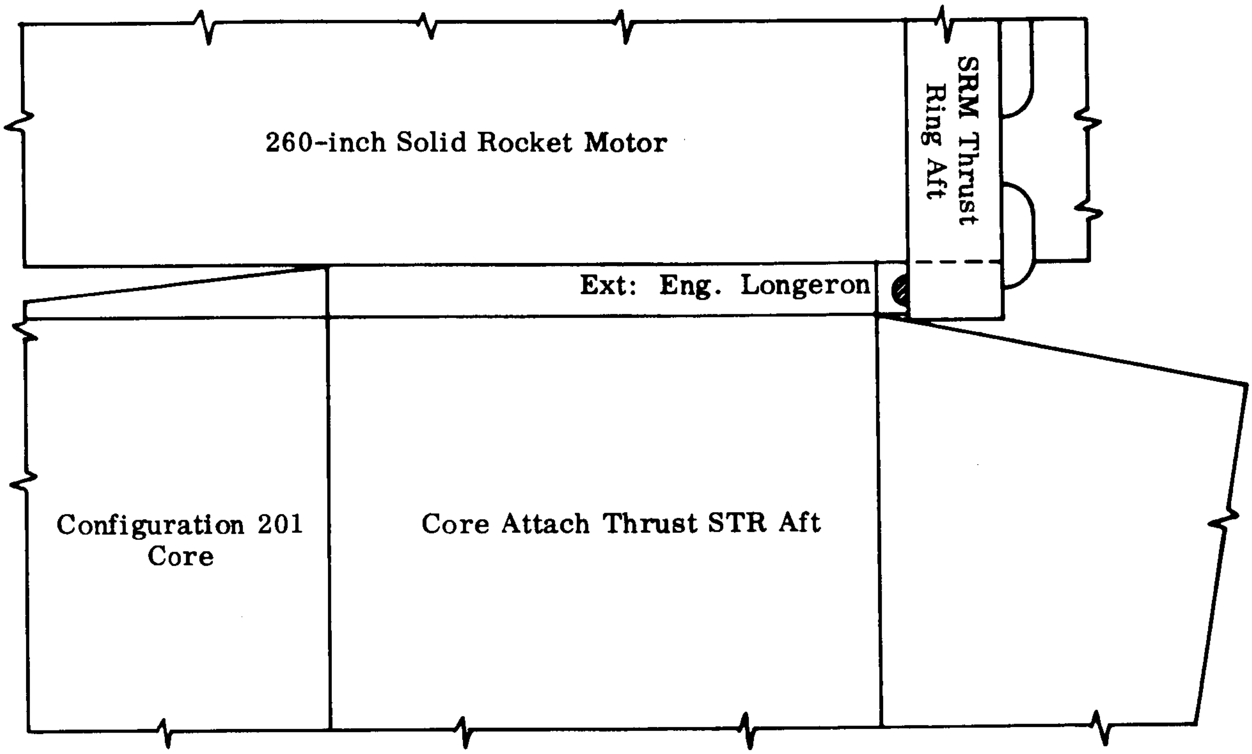

Figure 6-16. Load Transfer Ring Acting on Core Vehicle

b. Forward Ring

The forward ring is a small ring subjected to a pair of inplane loads. A representation of this method of attachment is shown in Figure 6-12.

6.7.1.3 Summary of Attachment Weight for Eight Solid Rocket Motors

The weights for each of the two methods of attachment are shown in Table 6-11.

Table 6-11
Summary of Attachment Weights

Load Delivery Points	Total of Core Plus 8 SRM Attachment Weights			
	Core	Attachments	SRM	Total
All aft	169,188	9,924	559,408	738,520
Half aft/half forward	265,932	9,924	559,408	835,264

These total weights increase the combined structural weight of the core vehicle and eight solid rocket motors by 36 percent and 40 percent, respectively. Therefore, it is evident that the magnitude of the weight penalties is high, particularly with respect to the increase to the solid motor structure weight. Expressed in terms of the ratio of structural weight to total liftoff weight for the 201 Core Vehicle without solid motors, this ratio is 690,822/14,400,000, or 0.048 for the nominal vehicle. Adding eight solid rocket motors, with an assumed gross weight of 3.5×10^6 pounds each, this ratio increases to 0.065, indicating a significant impact of these weight penalties on performance.

6.7.2 STRAP-ON LIQUID TANKS

In order to calculate the effect of strap-on liquid propellants on the 201 Vehicle it was assumed that four 260-inch solid rocket motors running in parallel with the core vehicle thrusters would be used. A thrust-to-weight ratio of 1.25 was required at liftoff in order to determine the amount of liquid propellants that could be attached by strap-on methods. It was found that 6,452,000 pounds of propellants plus tankage amounting to a total of 6,800,000 pounds could be carried. The weight of the additional tankage was calculated to be 348,000 pounds. The attach structure for the core vehicle was calculated to be 183,406 pounds as tabulated below.

Forward Frame	25,220 lbs
Aft Thrust Ring	158,186 lbs
Total	183,406 lbs

The attach structure for the four solid rocket motors and the connecting structure would be half of the values shown for a total of eight SRM. The attach structure and the connecting structure was not calculated for the additional tankage. Figure 6-17 represents the cross section view of the core plus tanks and attached solids.

A summary of the structure weights and attach weight penalties for the core vehicle plus four strap-on tanks plus four strap-on 260-inch solid motors is tabulated in Table 6-12.

Table 6-12

Summary of Structure Weights and Attach Weight Penalities

	4 Liquid Tanks	201 Core Vehicle	4 SRM	Total
Structure Weight, lb	348,000	690,822	688,000	1,726,822
Attach Structure and Penalties, lb	Not Calculated	183,406 84,594 268,000	279,904 4,962 284,666	552,666
		Total Structure, lb		2,279,488

The attach-structure weights increase the combined structural weights by 32 percent. The penalties of increased structural weight for attachment of the solid motors and liquid propellant tanks are sufficiently large to have a significant impact on performance. The ratio of structural weight to total liftoff weight is increased from 0.048 to 0.065.

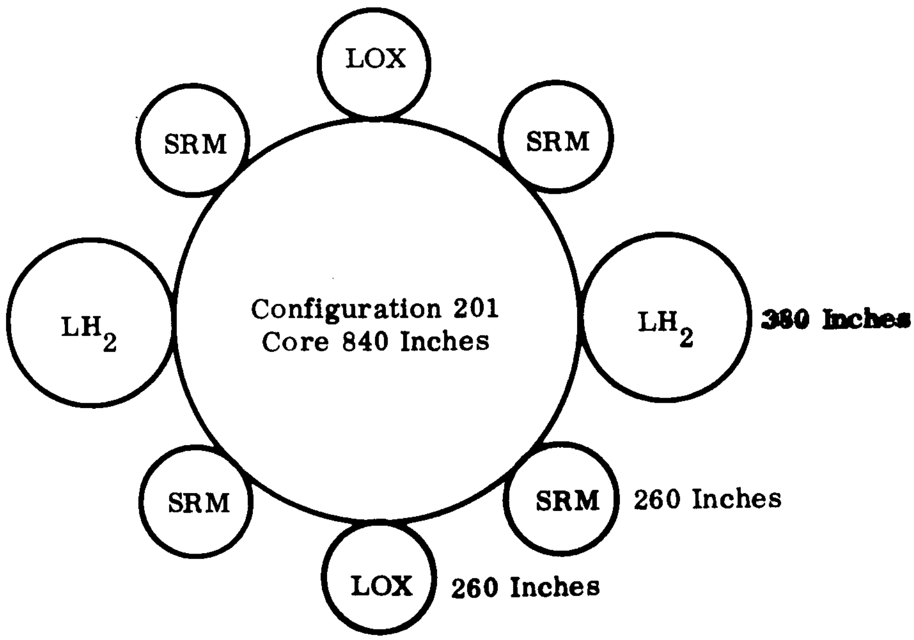

Figure 6-17. Cross-Section of Core with Tanks and Attached Solids

6.7.3 METHODS OF ANALYSIS

The type of problem is stated and then followed by the reference or references where a similar method is used, or formulas given, or table and/or curves of coefficients are available.

a. Ring Subjected to Static Loads

(1) In-Plane Loads. Reference 42, page 172 and page 178, Cases 2 and 25 respectively. Reference 41, Section B.6 dated 15 September 1961.

(2) Out-of-Plane Loads. Reference 41, Section B.6 dated 1 March 1965.

(3) Ring Girder Cross-Section Sizing. Reference 43, Chapter 6, "Plate Girders."

b. Beam on Elastic Foundation

Reference 44, Chapter IV, "Particular Cases of Loading on Finite Beams." Reference 45, Chapter 4, "Beam on Continuous Elastic Support."

c. Attachments

(1) Lugs and Shear Pins. Reference 41, Section B.2 dated 27 July 1961.

(2) Ultimate Strength Methods. Reference 45, Chapter 17, "Effect of Small Inelastic Strains in Axially Loaded Members and in Straight Beams," specifically Problem 311, page 536.

d. Vibrations

(1) Rings. Reference 46, Chapter 7, "Vibration of Systems Having Distributed Mass and Elasticity." Reference 47, page 479 and Reference 49.

(2) Struts. Reference 48, Chapter 4, "Vibration of Elastic Bodies," pages 300-302.

6.8 STAGE I THRUST STRUCTURE

Five basic vehicles were studied for thrust structure requirements at maximum load conditions inflight and on the stand. No holddown calculations were performed. The vehicles were designed using 7075-T6, aluminum alloy, Be-.36 Al alloy, and the 201 only was also designed using 6 Al-4V Ti alloy. The theory is given in paragraphs 6.8.2 and 6.8.3. The results are summarized in Tables 6-13 through 6-15. A sample calculation for the 201 vehicle is included.

6.8.1 SYMBOLS DEFINED

The following definitions for the symbols are in agreement with those given in Reference 30:

A	Area
b	Panel width
b_S	Width of sheet between stiffeners
b_W	Height of stiffener web
E	Young's modulus
I	Area moment of inertia
K_S	Compressive buckling coefficient of sheet of width b_s
ℓ	Frame spacing
N_x	Membrane load per unit width
R	Shell radius
t	Thickness of flat unstiffened plate
$\bar{t}_P$	Equivalent flat plate thickness of a stiffened panel
t_S	Thickness of sheet between stiffeners
$\bar{t}_F$	Equivalent frame thickness per unit length, A/ℓ
$\bar{t}_T$	Equivalent total shell thickness per unit length
ϵ	Structural efficiency
η_L	Plasticity reduction factor for general instability
η_T	Tangent modulus to Young's modulus ratio
$\bar{\eta}$	$\sqrt{\eta_L \eta_T}$
ρ	Radius of gyration
σ	Compressive stress
ν	Poisson's ratio

6.8.2 STRUCTURAL OPTIMIZATION

6.8.2.1 Axial Load

The buckling stress for local instability is given by Reference 31 and all equations are as given in Reference 30.

$$\sigma_{CR} = K_S \frac{\eta_L \pi^2 E}{12(1 - \nu^2)} \left(\frac{t}{b}\right)^2 \tag{6-36}$$

The buckling stress for wide column instability is given by

$$\sigma_{COL} = \frac{\eta_T \pi^2 E}{\left(\frac{\ell}{\rho}\right)^2} \tag{6-37}$$

also

$$N_x = \sigma \bar{t}_P \tag{6-38}$$

By setting σ_{CR} and σ_{COL} of Equations 6-36 and 6-37 to σ of Equation 6-38, Equations 6-39 and 6-40 are obtained.

$$\frac{N_x}{\eta_L E} = \frac{K_S \pi^2}{12(1 - \nu^2)} \left(\frac{t}{b}\right)^2 \bar{t}_P \tag{6-39}$$

$$\frac{N_x}{\eta_T E} = \frac{\pi^2}{\left(\frac{\ell}{\rho}\right)^2} \bar{t}_P \tag{6-40}$$

Equations 6-39 and 6-40 are combined to get the relationship

$$\frac{N_x^2}{\eta_T \eta_L E^2} = \frac{K_S \pi^4}{12(1 - \nu^2)} \left(\frac{t}{b}\right)^2 \left(\frac{\rho}{\ell}\right)^2 \bar{t}_P^2 \tag{6-41}$$

When the square root of Equation 6-41 is taken, Equation 6-42 is obtained.

$$\frac{N_x}{E\sqrt{\eta_T \eta_L}} = \pi^2 \left(\frac{t}{b}\right) \bar{t}_P \left(\frac{\rho}{\ell}\right) \sqrt{\frac{K_S}{12(1 - \nu^2)}} \tag{6-42}$$

Let $t_S = t$ and $b_S = b$. Then Equation 6-42 reduces to

$$\frac{N_x}{\bar{\eta}\, E\, \ell} = \epsilon \left(\frac{\bar{t}_P}{\ell}\right)^2 \tag{6-43}$$

$$\epsilon = \pi^2 \frac{\ell}{\bar{t}_P} \sqrt{\frac{K_S}{12(1 - \nu^2)}} \left(\frac{t_S}{b_S}\right) \tag{6-44}$$

By letting $K_S = 4$ (Reference 33) and $\nu = 0.3$, Equation 6-44 reduces to

$$\epsilon = 5.98 \left(\frac{\ell}{\bar{t}_P}\right)\left(\frac{t_S}{b_S}\right) \tag{6-45}$$

Equations 6-43 and 6-38 can be combined to obtain

$$\sigma = \sqrt{\frac{N_x\, \epsilon\, \bar{\eta}\, E}{\ell}} \tag{6-46}$$

Frame stiffness requirements can be determined from Reference 32 for

$$I = \frac{C_f\, 4M\, R^2}{E\, \ell} \tag{6-47}$$

where

$$C_f = \frac{1}{16000} \text{ (Reference 32)}$$

For a cylinder subjected to a membrane thrust load, N_x, per unit width, the moment, M, of Equation 6-46 becomes $\pi\, R^2\, N_x$. Thus, the relationship in Equation 6-48 is obtained.

$$I = \frac{4\pi\, R^4\, N_x}{16000\, E\, \ell} = \frac{N_x\, R^4}{1275\, E\, \ell} \tag{6-48}$$

Choosing a frame which has $I = 3A^2$ (Reference 30), the equivalent smeared frame thickness becomes

$$\bar{t}_F = \frac{A}{\ell} = \frac{R^2}{\ell} \sqrt{\frac{N_x}{3825\, E\, \ell}}$$

or

$$\bar{t}_F = \sqrt{\frac{N_x}{E}} \; \frac{R^2}{61.9 \, \ell^{3/2}} \tag{6-49}$$

From Equation 6-43

$$\bar{t}_P = \sqrt{\frac{N_x}{E}} \; \sqrt{\frac{\ell}{\bar{\eta} \, \epsilon}} \tag{6-50}$$

By combining Equations 6-49 and 6-50 the equivalent total shell thickness per unit length is obtained.

$$\bar{t}_T = \bar{t}_F + \bar{t}_P = \sqrt{\frac{N_x}{E}} \left(\frac{R^2}{61.9} \, \ell^{-3/2} + \frac{\ell^{1/2}}{\sqrt{\epsilon \, \bar{\eta}}} \right) \tag{6-51}$$

Assuming $\bar{\eta} = 1$, that is, the panel stress is in the elastic range, Equation 6-51 can be minimized and Equation 6-52 obtained.

$$\ell = 0.22 R \, \epsilon^{1/4} \tag{6-52}$$

Substituting Equation 6-52 into Equation 6-51, it is found that

$$\bar{t}_T = (0.157 + 0.47) \epsilon^{-3/8} \sqrt{\frac{N_x R}{E}} \tag{6-53}$$

or

$$\bar{t}_T = \frac{0.627}{\epsilon^{3/8}} \sqrt{\frac{N_x R}{E}} \tag{6-54}$$

From Equations 6-51 and 6-53 it can be seen that the stiffened panel weight is three times the frame weight under ideal circumstances.

Substitute Equation 6-52 into Equation 6-46 and obtain

$$\sigma = 2.13 \, \epsilon^{3/8} \sqrt{\frac{N_x}{R} E} \tag{6-55}$$

which for aluminum alloys reduces to

$$\sigma = 6850 \, \epsilon^{3/8} \sqrt{\frac{N_x}{R}} \tag{6-56}$$

From Equation 6-44, it can be seen, that for a given material, ϵ is a function of geometry. In Reference 30, a Z-stringer-sheet combination is shown that has a maximum $\epsilon = 0.89$, as opposed to 0.80 and 0.77 for two types of I-stringers.

Using data from plate and column buckling curves, the derived equations can be used to plot sets of design curves for optimum structure determination. (See Reference 30.) These curves are included in this report as Figures 6-18 through 6-25.

6.8.2.2 Moment Effects

The derivation of paragraph 6.8.2.1 can account for applied moment by the simple expedient

$$N_x = \frac{M_x}{\pi R^2} + \frac{F}{2\pi R} \tag{6-57}$$

where

M_x = applied moment.

F = axial thrust.

The form of the analysis of paragraph 6.8.2.1 was presented by W. R. Micks in 1950 (Reference 58) for stiffened cylinders subjected to pure bending in which moment was converted to axial membrane force by Equation 6-57 with $F = 0$. See also Reference 32. Chapters 4 and 15.

6.8.2.3 Design Curves for Optimum Z and I Integrally Stiffened Cylinders (Reference 30)

Figures 6-18 and 6-19 are plots of Equation 6-46 for the aluminum alloys 2219-T87 and 7075-T6 respectively.

Figure 6-20 is a plot of Equation 6-56 which represents the panel compressive stress for any minimum weight aluminum panel in the elastic range.

Figures 6-21 and 6-22 are plots made from plate and column buckling curves for 7075-T6 and 2219-T87 for determining the stress σ in the plastic range, $\bar{\eta} < 1$.

Figures 6-23 and 6-24 show the efficiency factor, ϵ, evaluated from Equation 6-44 for Z and two I-stringer sections.

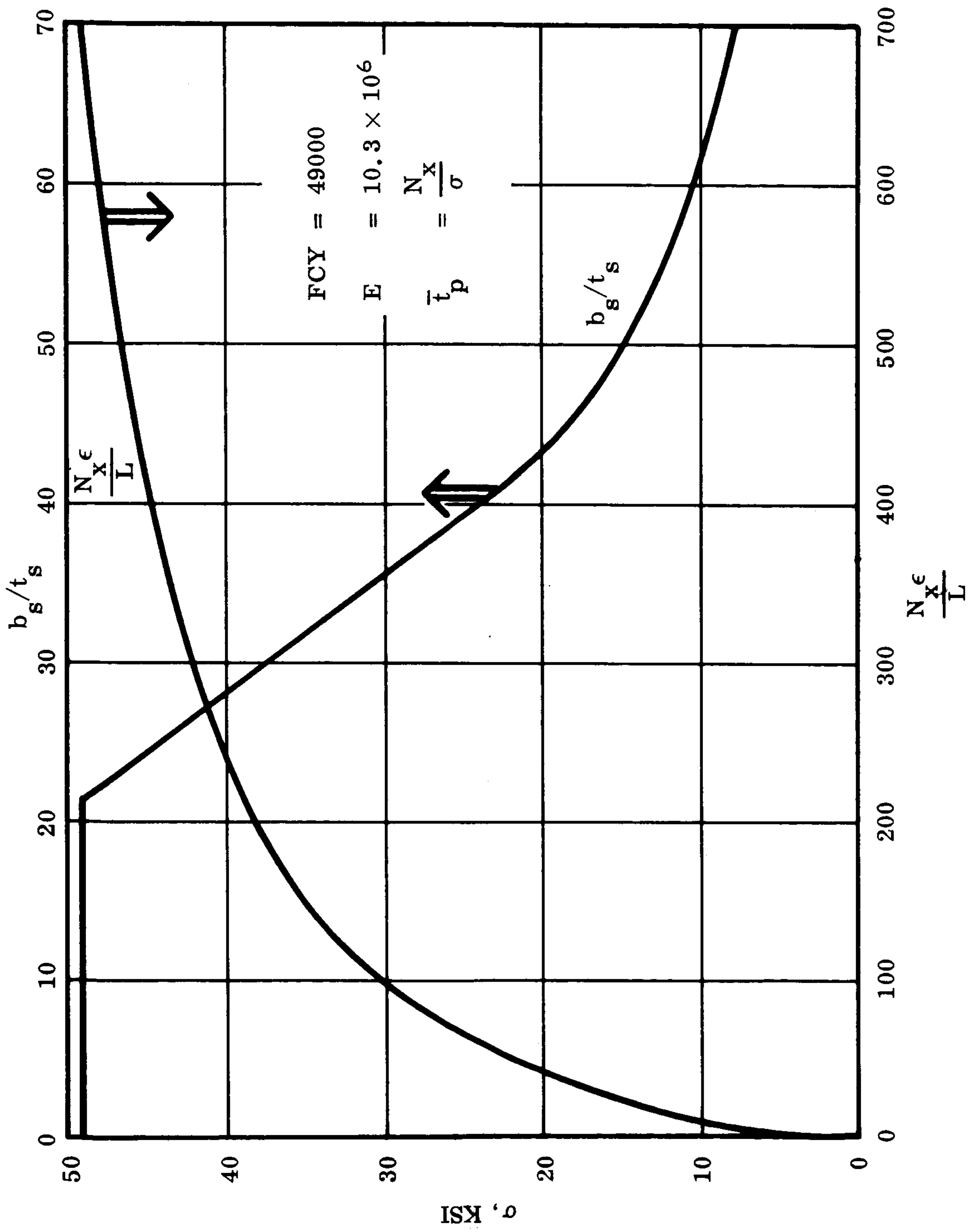

Figure 6-18. Plot of Equation 6-46 for 2219-T87 Aluminum Alloy

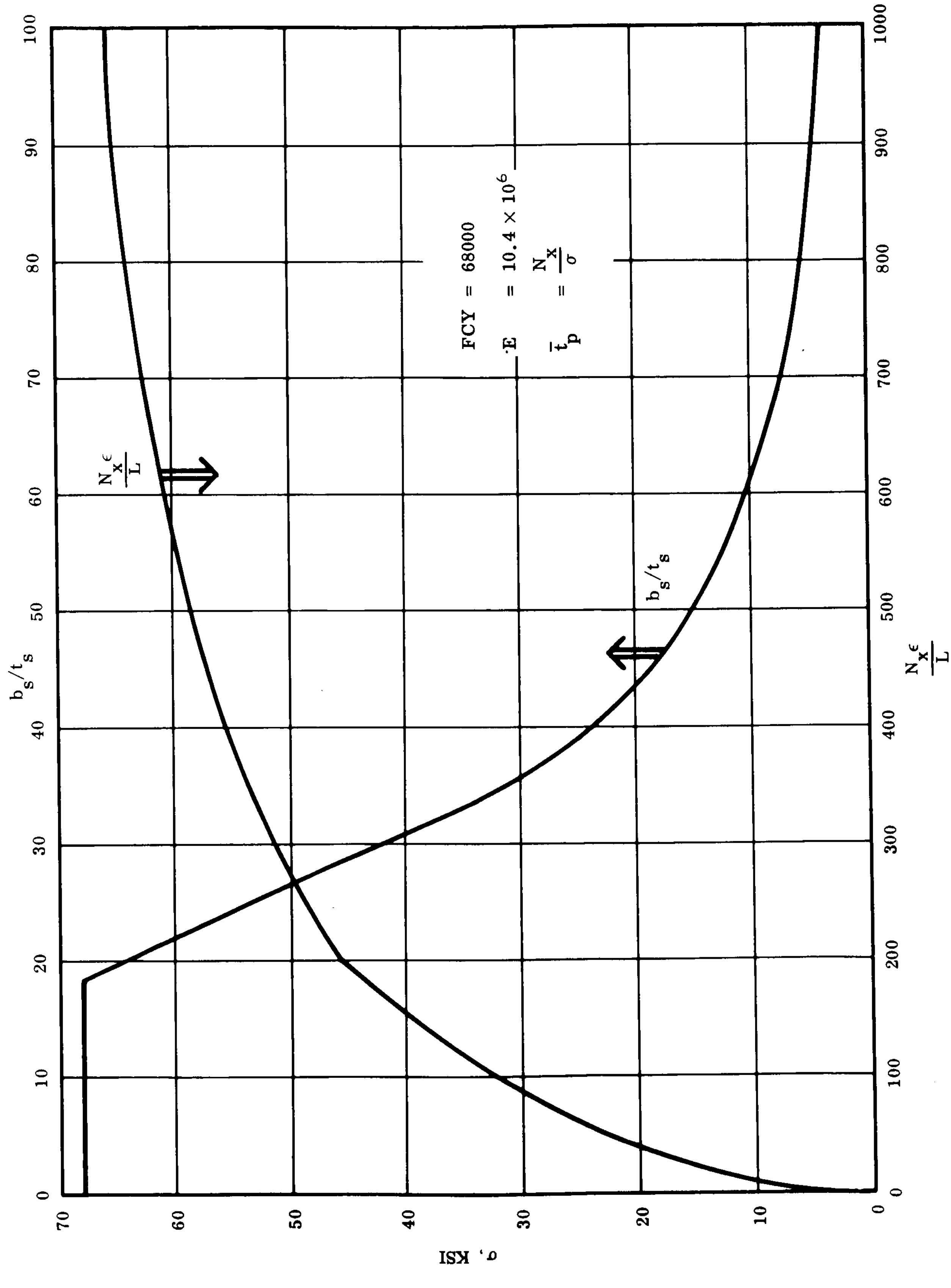

Figure 6-19. Plot of Equation 6-48 for 7075-T6 Aluminum Alloy

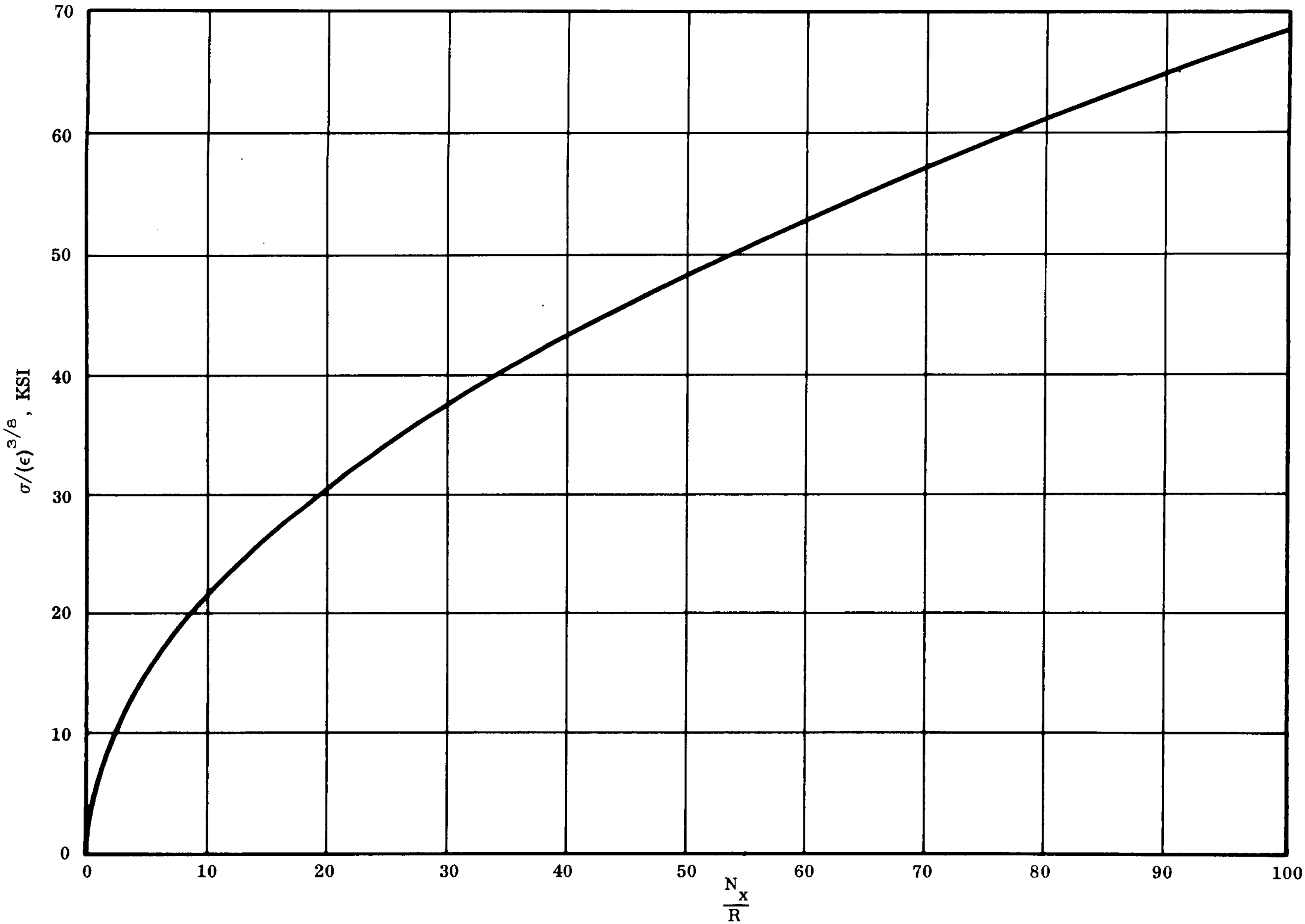

Figure 6-20. Optimum Minimum Weight Compression Panel

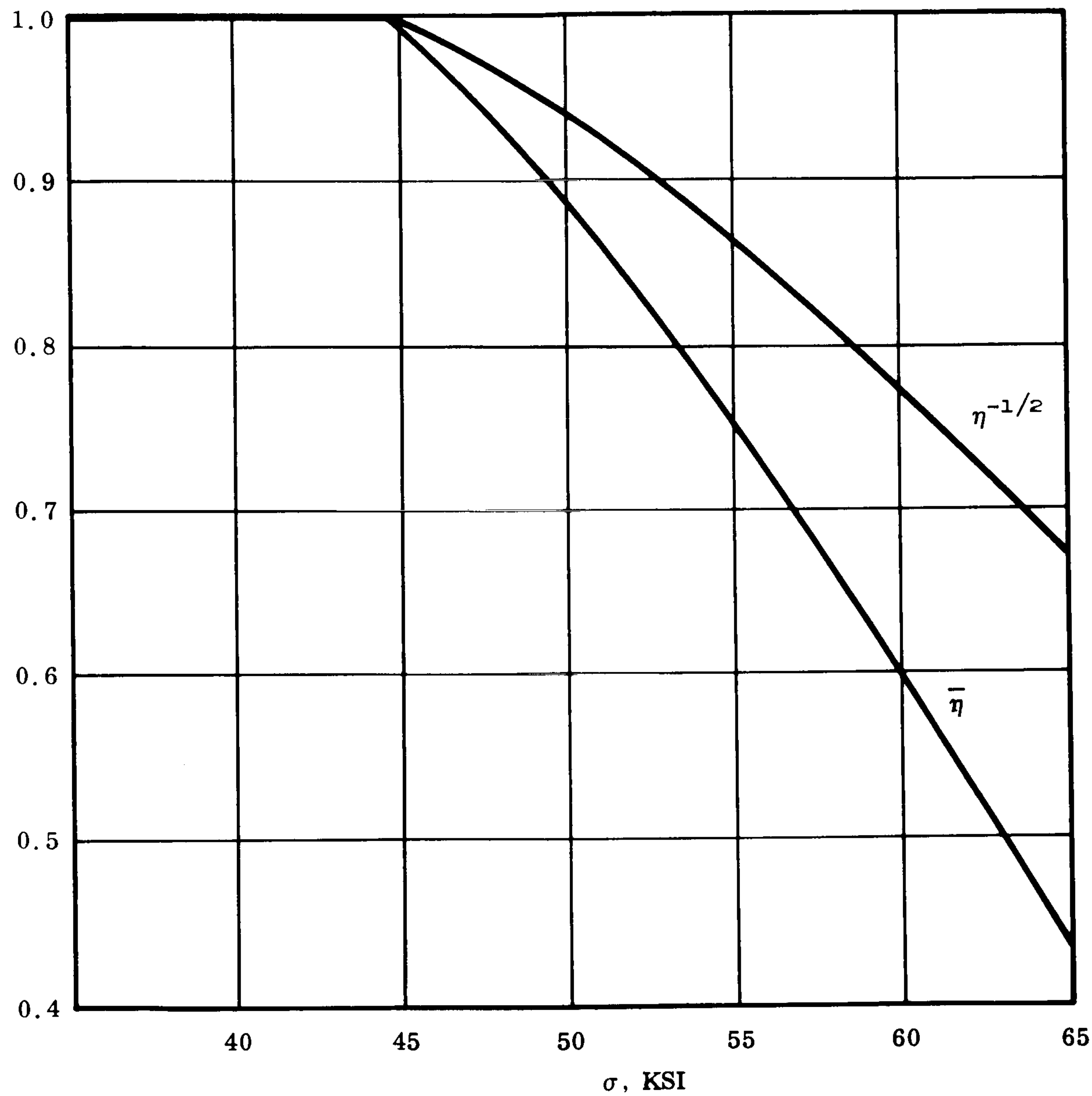

Figure 6-21. $\bar{\eta}$ versus σ for 7075-T6 Aluminum Alloy

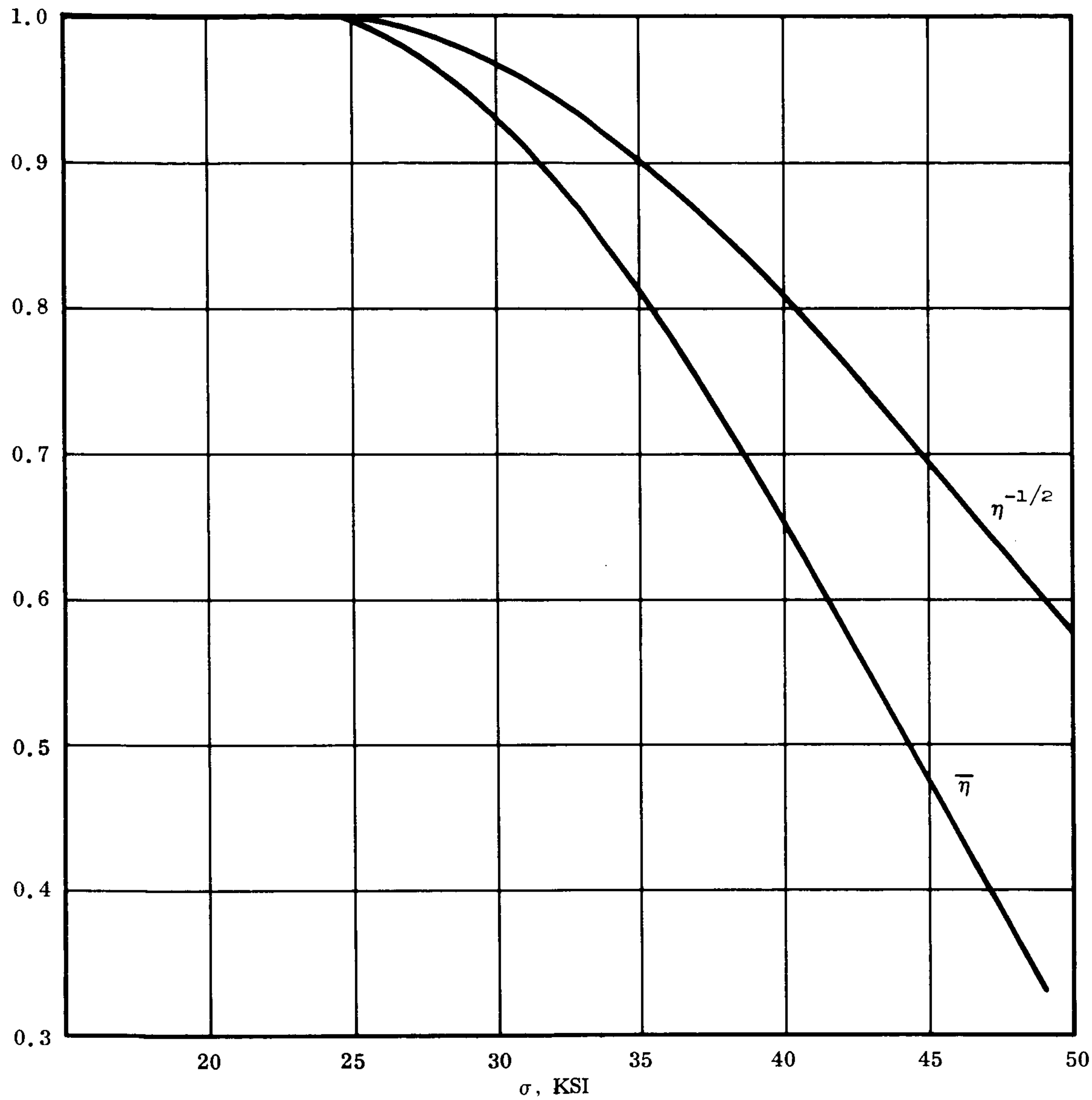

Figure 6-22. $\overline{\eta}$ versus σ for 2219-T87 Aluminum Alloy

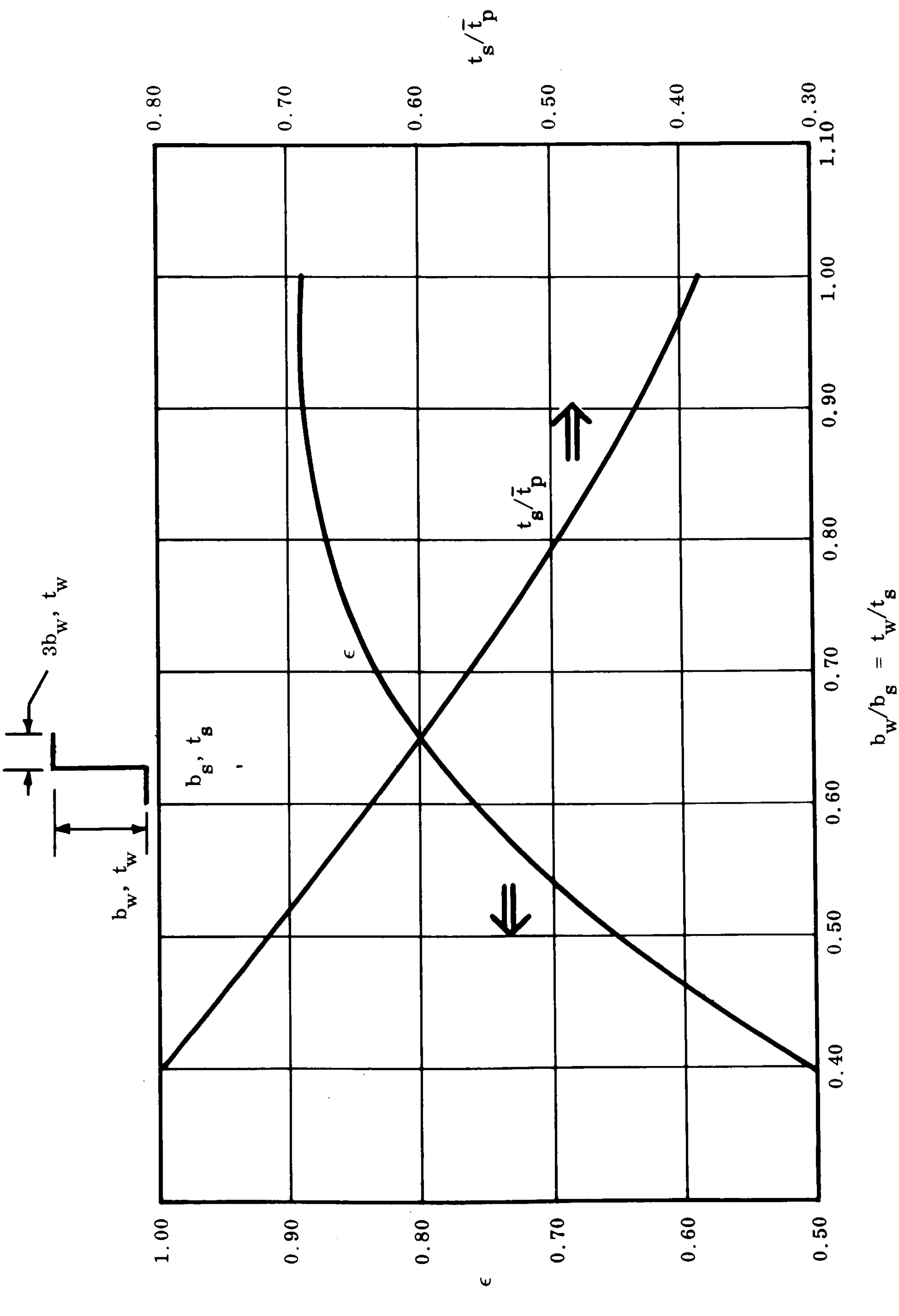

Figure 6-23. Efficiency Factor, ϵ, from Equation 6-44 for Z-Stringer

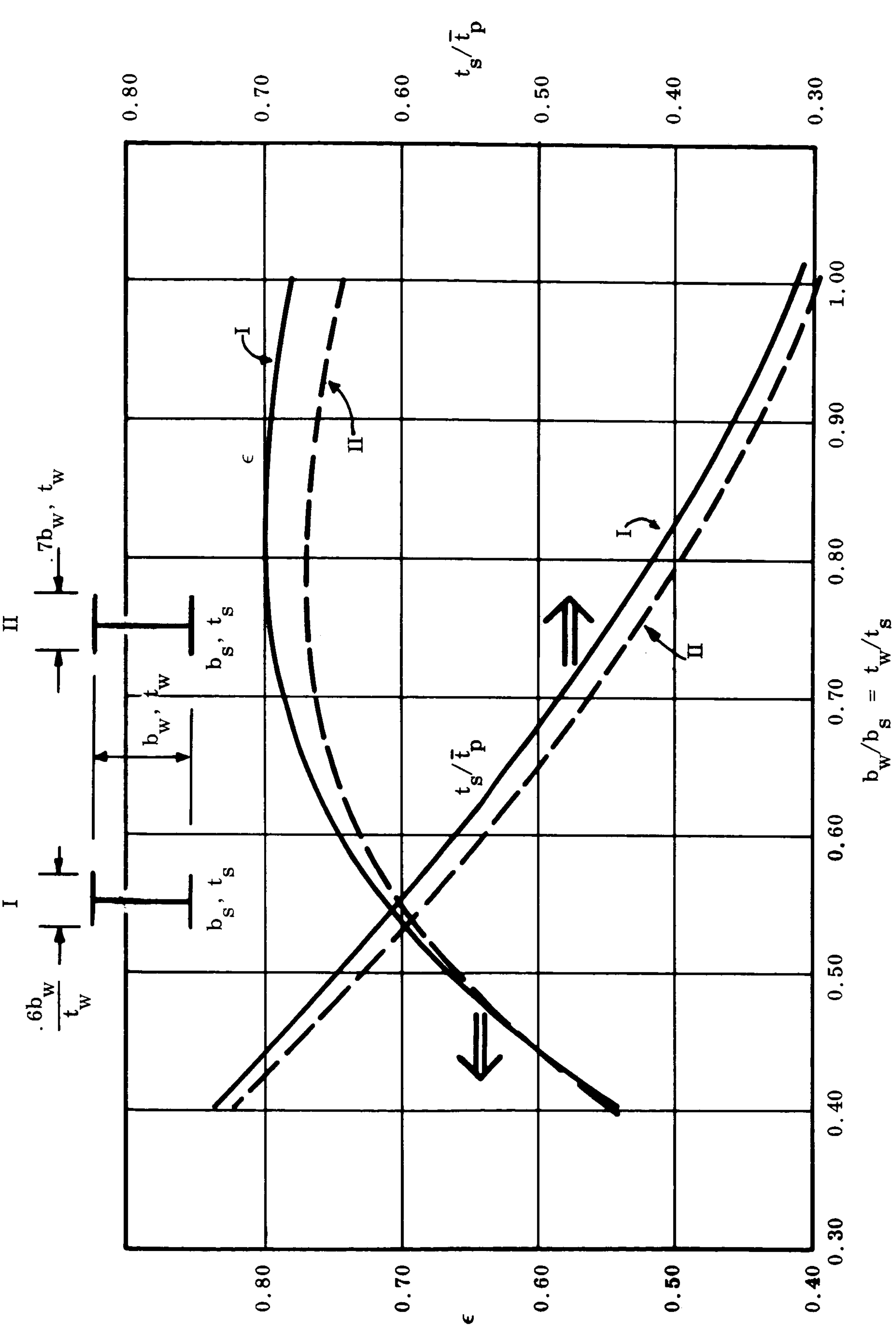

Figure 6-24. Efficiency Factor, ϵ, from Equation 6-44 for Two I-Stringers

Figure 6-25 is the cross-sectional properties of the frame used with $I = 3A^2$.

$h = 4.1\,A^{\frac{1}{2}}$

$t_w = 0.1025A^{\frac{1}{2}}$

$A_w = ht_w = .42A$

$A_f = bt_f = .29A$

$I = 3A^2$

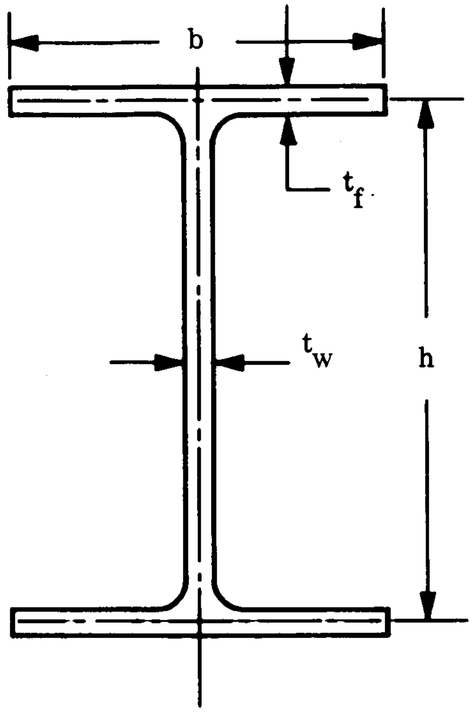

$t_w = \frac{h}{40}$

A = Total Area

Figure 6-25. Cross-Sectional Properties of Frame

6.8.3 RING ANALYSIS FOR VIBRATION

The engines deliver the load to the thrust cone by shear transfer through the bearing longerons. Due to engine misalignment, steering requirements, and vibration characteristics, the engines will also be attached to a ring in the plane normal to the vehicle axis. Reference 49 derives a relationship for inplane flexural bending modes for a uniform ring. Let

δ_R = radial static deflection

δ_T = tangential static deflection

$g = W/2\pi R$

W = weight of engines modules plus ring

R = ring mean radius

ω = vibration frequency (rad/sec)

From Flugge (Reference 47)

$$\delta_R = g \frac{R^4}{E\,I\,(n^2 - 1)^2} \cos(n\,\theta) \tag{6-58}$$

$$\delta_T = g \frac{R^4}{E\,I\,n^2 (n^2 - 1)^2} \sin(n\,\theta) \tag{6-59}$$

Reference 49 derives the expression

$$\omega^2 = \frac{g}{\delta_{Rmax} + \delta_{Tmax}} \tag{6-60}$$

For $n = 2$ and $\sin(n\,\theta) = \cos(n\,\theta) = 1$

$$\delta_{Rmax} = \frac{W\,R^3}{18\pi\,E\,I} \tag{6-61}$$

$$\delta_{Tmax} = \frac{W\,R^3}{72\pi\,E\,I}$$

$$\delta_{Rmax} + \delta_{Tmax} = \frac{5\,W\,R^3}{72\pi\,E\,I} \tag{6-62}$$

Substitute Equation 6-62 into Equation 6-60 and

$$\omega^2 = g \frac{72\pi\,E\,I}{5W\,R^3} \tag{6-63}$$

For design purposes require ω to satisfy some minimum value

$$\omega_o = 2\pi\,f_o \tag{6-64}$$

From Equation 6-63

$$I = \frac{20\pi}{72g} f_o^{\,2} \frac{R^3}{E} W \tag{6-65}$$

6.8.4 SUMMARY OF RESULTS

Table 6-13 summarizes the results of all the basic vehicles main-thrust structures using 7075-T6 aluminum alloy.

Table 6-14 itemizes each major component part of the thrust structure beside a sketch of the aft end of the particular vehicle.

Table 6-13

Summary of Thrust Structure Weight Using 7075-T6 Alloy

Configuration Number	Weight with Rear End Steering	Weight with Forward Steering
101	81538	-
201, 204, 205	82741	80110
202	93297	92187
203	100585	-
301	56175	-

Table 6-14

Thrust Structures Itemized

Configuration Number	Itemized Weight, lb	
101 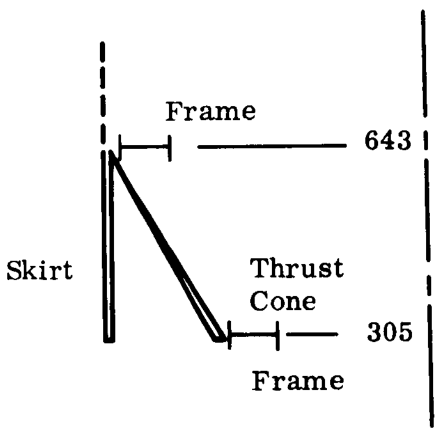	Frame 643	4452
	Frame 305	3163
	Thrust Cone	20080
	Skirt	53843
	Total	81538

Table 6-14

Thrust Structures Itemized (Cont.)

<table>
<tr><th>Configuration Number</th><th colspan="2">Itemized Weight, lb</th></tr>
<tr><td rowspan="6">201 (204, 205)
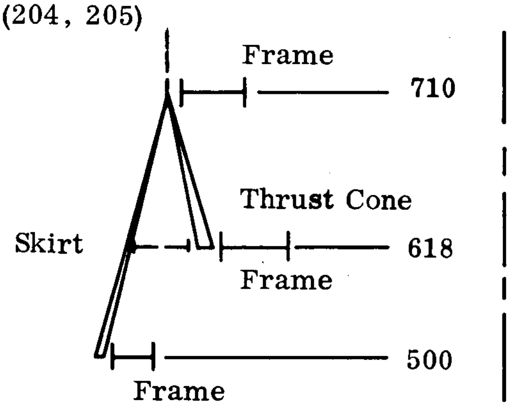
</td><td>Frame 710</td><td>12670</td></tr>
<tr><td>*Frame 618</td><td>15877</td></tr>
<tr><td>Frame 500</td><td>4594</td></tr>
<tr><td>Thrust Cone</td><td>14761</td></tr>
<tr><td>Skirt</td><td>34839</td></tr>
<tr><td>Total</td><td>82741</td></tr>
<tr><td rowspan="6">202
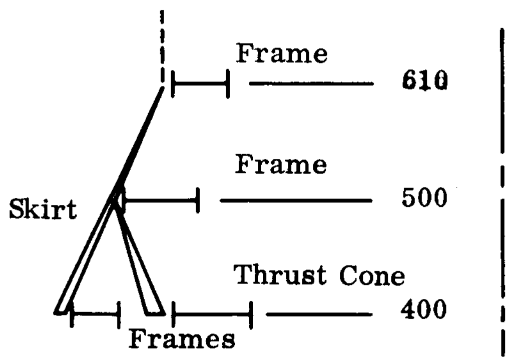
</td><td>Frames 400</td><td>21681</td></tr>
<tr><td>Frame 500</td><td>5637</td></tr>
<tr><td>Frame 610</td><td>19602</td></tr>
<tr><td>Thrust Cone</td><td>10470</td></tr>
<tr><td>Skirt</td><td>35907</td></tr>
<tr><td>Total</td><td>93297</td></tr>
<tr><td rowspan="6">203

See 201</td><td>Frame 710</td><td>16021</td></tr>
<tr><td>*Frame 618</td><td>24794</td></tr>
<tr><td>Frame 500</td><td>4500</td></tr>
<tr><td>Thrust Cone</td><td>17600</td></tr>
<tr><td>Skirt</td><td>37670</td></tr>
<tr><td>Total</td><td>100585</td></tr>
<tr><td rowspan="4">301
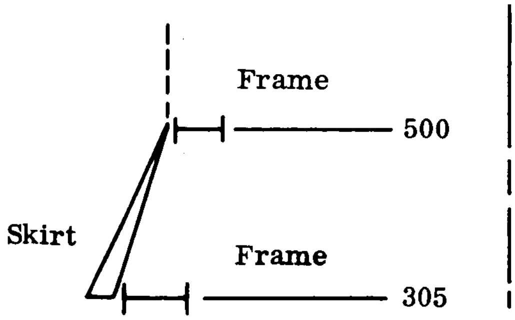
</td><td>Frame 350</td><td>11790</td></tr>
<tr><td>Frame 500</td><td>13269</td></tr>
<tr><td>Skirt</td><td>31116</td></tr>
<tr><td>Total</td><td>56175</td></tr>
</table>

*Includes shear connectors

Table 6-15 gives the results of the base vehicles designed for metals other than 7075-T6. Only the 201 was designed using titanium.

Table 6-15
Thrust Structures for Metals Other Than Aluminum

Configuration Number	Beryllium	Titanium
101	49773	-
201, 204, 205	36105	90601
202	39591	-
203	38982	-
301	51340	-

6.8.5 SAMPLE CALCULATION OF STAGE I THRUST STRUCTURE FOR 201 VEHICLE

The following sample calculation of the thrust structure of the 201 Vehicle illustrates the use of the equations and design curves of paragraphs 6.8.2 and 6.8.3. The specific elements of this thrust structure are calculated in the following sequence:

- Thrust Cone.
- Engine Frame.
- Outer Skirt.
- Aft Ring, Station 500.
- Kick Frame, Station 710.

A weight summary is included at the end of this example, showing the weights of the above elements, which add to a total of 82,741 pounds for the 201 thrust structure.

THRUST CONE

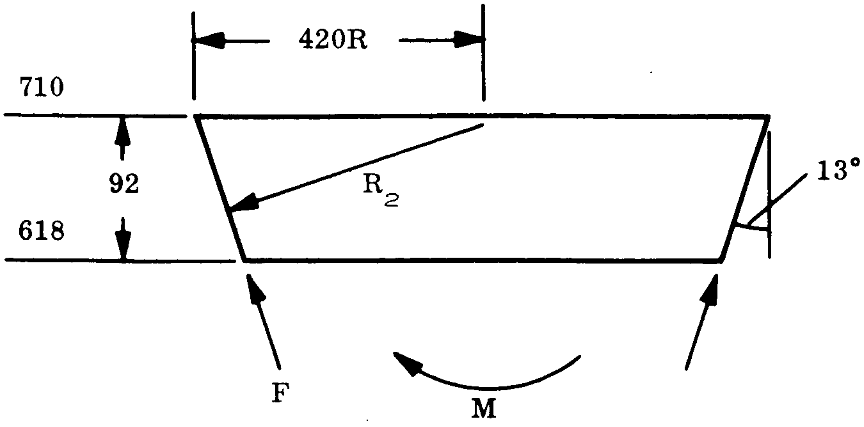

cos 13° = 0.9744

tan 13° = 0.2309

Figure a

Given

$$M = 143,000,000 \text{ in.-lb}$$

$$F = 21,052,875 \text{ lb}$$

Sta. 618:

$$R = 420 - 92 \tan 13° = 420 - 21.2$$

$$= 398.8 \cong 399 \text{ in.}$$

$$R_2 = \frac{399}{\cos 13°} = 410 \text{ in.}$$

$$N_x' = \frac{143000000}{\pi(410)^2} + \frac{21052875}{2\pi(399)} = 8668$$

For design use $N_x = 8700$ lb/in.

$$\frac{N_x}{R_2} = 21.2 \text{ lb/in}^2$$

Use an integral stiffened shell of the form shown in Figure b.

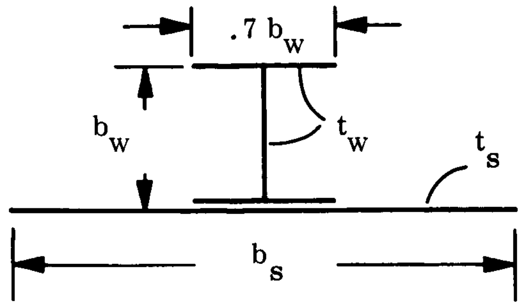

Figure b

From Figure 6-23 the maximum structural efficiency for the shell in Figure b is

$$\epsilon = 0.77$$

For $N_x/R_2 = 21.2$ one finds from Figure 6-19 that

$$\sigma = \epsilon^{3/8}(31500) = 28600$$

This falls into the elastic range for 7075-T6.

$$\therefore \ \bar{t}_P = \frac{N_x}{\sigma} = 0.304 \text{ in.}$$

and

$$\bar{t}_T = \frac{4}{3}\bar{t}_P = 0.405 \text{ in.}$$

Assume the average shell radius is 410 inches.

$$W = 2\pi \times 410 \times 0.405 \times 0.101 = 105.34 \text{ lb/in.}$$

$$\text{Total Shell Weight} = 92 \times 105.34 = 9690 \text{ lb}$$

Longeron Sizing

Use 1.5 on F_{TY} for bearing load

$$A_{total} = \frac{1.5 \times 21052875}{64000} = 493.4 \text{ in.}^2$$

Assume each longeron tapers to 3 in.^{2}

$$\text{Vol} = \left(\frac{493.4 + 3 \times 18}{2}\right)\frac{92}{\cos 13^\circ} = 25853.79 \text{ in.}^3$$

$$\text{Wgt} = (0.101)\text{Vol} = 2611 \text{ lb}$$

$$\text{Longerons + Shell} = 12301 \text{ lb}$$

Shell has been idealized as a cylinder. To account for off optimization, fabrication factors, etc., increase weight by 20 percent.

$$\text{Final W} = 1.2 \times 12301 = \underline{14761}\ \text{lb}$$

ENGINE FRAME

Assume ring is 60 inches deep and has an average R = 369 inches.

Use engine weights total* = 218330 lb.

Assume ring weighs 15000 lb.

$$W = 233,330 \text{ lb}$$

Use 7075-T6 with $E = 10,400,000 \text{ lb/in.}^2$, $g = 386$.

Require $f_o \geq 4$ cps*.

$$I = \frac{20\pi \times 16}{72 \times 386} \times \frac{369^3 \times 233330}{10400000} = 40800 \text{ in.}^4$$

For weight estimation assume the ring cross-section can be represented by an I-shape girder in Figure a.

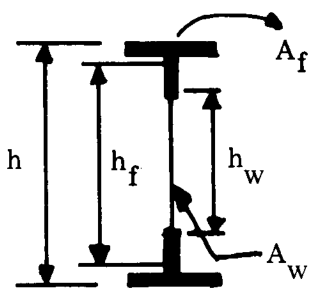

h = total depth

h_f = distance between flange centroids

h_w = depth of web plate

A_f = flange area

A_w = web area = $h_w t_w$

t_w = web thickness

Figure a

For girder sections as given in Figure a the areal moment of inertia may be calculated with sufficient accuracy by

$$I = A_f \frac{h_f^2}{2} + \frac{1}{12} t_w h_w^3$$

*PSTN-III-5 T10RE-3A

or

$$I = \frac{h_f^2}{2} A_f + \frac{h_w^2}{2} \frac{A_w}{6}$$

Assuming $h = h_f = h_w$, then

$$I = \frac{h^2}{2} \left(A_f + \frac{A_w}{6} \right)$$

Since $h > h_f > h_w$, the preceding equation is high. To compensate for this the equation is modified to

$$I = \frac{h^2}{2} \left(A_f + \frac{A_w}{8} \right)$$

To prevent web failure require

$$t_w \geq \frac{h}{170}$$

Hence

$$A_w \geq \frac{h^2}{170}$$

Where shear, Q, occurs

$$A_w \geq \frac{Q}{\tau_{all}} \geq \frac{h^2}{170}$$

Knowing h and A_w A_f is found

$$A_f = \frac{2I}{h^2} - \frac{A_w}{8}$$

Let

$$A_w = \frac{3600}{170} = 21.2 \text{ in.}^2$$

$$\therefore \; A_f = \frac{2 \times 40800}{3600} - \frac{21.2}{8} \cong 20 \text{ in.}^2$$

$$A = 2A_f + A_w = 40 + 21.2 = 61.2 \text{ in.}^2$$

$$W_{ring} = 2\pi R A \gamma = 6.28 \times 369 \times 61.2 \times 0.101$$

$$= 14180 \text{ lb}$$

Previous calculations show that the web must be stiffened. The added weight is about 5 percent of the total ring as computed above.

$$\therefore \text{ Final Weight} = 1.05 \times 14180 = \underline{14880} \text{ pounds}$$

ENGINE FRAME ATTACHMENT

Ring Shear Flow Attachments Calculations

The ring will be attached such that restraints will tie into supporting skirt.

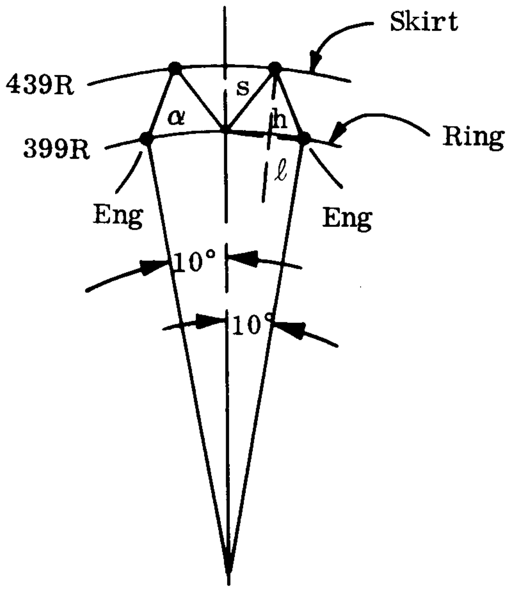

$$\ell = 399 \sin 5° = 34.8 \text{ in.}$$

$$h = 439 - 399 \cos 5° = 42 \text{ in.}$$

$$\alpha = \arctan \frac{h}{\ell} = 50° 20'$$

$$s = (h^2 + \ell^2)^{\frac{1}{2}} = 54.5 \text{ in.}$$

From vibration equation

$$\omega^2 = \frac{g}{\delta_{Rmax} + \delta_{Tmax}} = \frac{g}{1.25\delta_{Rmax}}$$

(refer to Equation 6-69). Therefore

$$\delta_{Rmax} = \frac{g}{1.25\omega^2} = \frac{386}{1.25 \times 64\pi^2} = 0.49 \text{ in.}$$

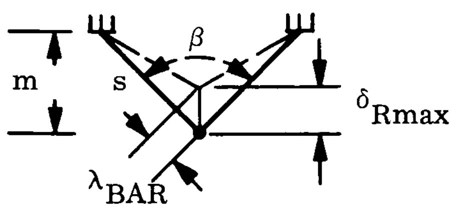

Referring to the figure to the left one sees that

$$\lambda_{BAR} = \delta_{Rmax} \cos \frac{\beta}{2}$$

$$\frac{\beta}{2} = \text{arc cos} \frac{m}{s}$$

$$m = 439 \cos 5° - 399 = 437.3 - 399 = 38.3$$

$$\cos\frac{\beta}{2} = \frac{m}{s} = \frac{38.3}{54.4} = 0.703$$

$$\therefore \lambda_{BAR} = 0.49 \times 0.703 = 0.344 \text{ in.}$$

$$\sigma = E\epsilon = E\frac{\lambda_{BAR}}{s} = 10.4 \times \frac{0.344}{54.5} \times 106 = 65701$$

For 7075-T6, $F_{CY} = 68000 > \sigma$

$$\frac{P_{CR}}{A} = \frac{\pi^2 E}{s^2}(\zeta)^2 = \sigma$$

$$\zeta = \frac{s}{\pi}\sqrt{\frac{\sigma}{E}} = \frac{54.4}{\pi}\sqrt{0.0063174}$$

$$\zeta = 17.36 \times 0.0795 = 1.38 \text{ in.}$$

For a round tube $\zeta \geq 1.387$ from <u>Aluminum Construction</u> Manual page 113

$\zeta = 1.5261 > 1.38$

OD = 4.5 in.

ID = 4.124 in.

A = 2.5403 in.^{2}

I = 5.9166 in.^{4}

Wgt = 0.254 lb/in.

Total Weight = $4 \times 18 \times 54.5 \times 0.254 \cong$ <u>997</u> pounds

OUTER SKIRT

Outer skirt support structure

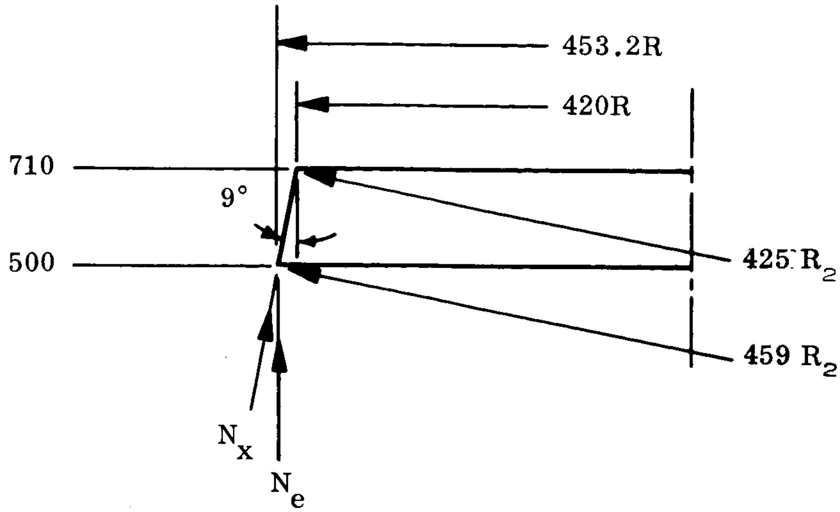

Assumptions: Vehicle weight at liftoff = 14,400,000 lb

Wind moment at 500 $= 75 \times 10^7$ in.-lb

For design condition use load at 710

$$N_x' = \left(\frac{14400000}{6.28 \times 420} + \frac{75 \times 10^7}{3.14 \times 420^2}\right) \sec 9°$$

$$= 6939 \text{ lb/in.}$$

Use a shutdown load factor = 2

$$N_x = 13878 \text{ lb/in.}$$

$$\frac{N_x}{R_2} = \frac{13878}{425} = 32.7 \text{ lb/in.}^2$$

Use a Z-stringer construction of the type used in Reference 30 and given in the following figure.

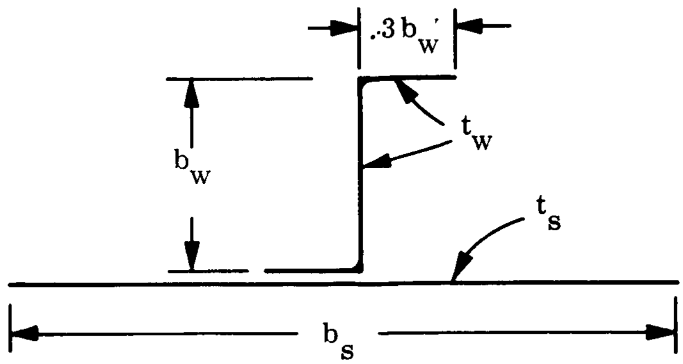

Z-Stringer

From Figure 6-22 the optimum structural efficiency for this configuration is

$$\epsilon = 0.89$$

From Figure 6-19

$$\sigma = \epsilon^{3/8}\, 39300 = 37610$$

This is still in the elastic region for 7075-T6

$$\bar{t}_P = \frac{N_x}{\sigma} = 0.369 \text{ in.}$$

$$\bar{t}_T = \frac{4}{3}\bar{t}_P = 0.492 \text{ in.}$$

For average shell R = 436.7 in.

Shell weighs approximately $2\pi R\, \bar{t}_T\, \gamma = 136.3$ lb in.

$$W = 210 \times 136.3 = \underline{28619} \text{ pounds}$$

Bearing longerons for support on stand = 3720.

Engine mount connectors estimated at 2500.

AFT RING

Aft ring on skirt

At station 500

$$N_x = 2 \sec 9° \left(\frac{14400000}{6.28 \times 453.2} + \frac{75 \times 10^7}{3.14 \times 453.2^2} \right)$$

$$= 12600 \text{ lb/in.}$$

Radial Load

$$N_R = N_x \sin 9° = 1970 \text{ lb/in.}$$

Hoop Load

$$P_\theta = N_R R = 1970 \times 453.2 = 892800 \text{ lb}$$

For 7075-T6 $F_{TU} = 77000$

$$A_f = \frac{1.4 \times 892800}{77000} = 16.23 \text{ in.}^2$$

For the kick frame used in Reference 30 with $I = 2A_f^2$ it is found that

$$h_f = 3.46 \sqrt{A_f} \cong 14 \text{ in.}$$

$$R_f = 453.2 - 7 = 446.2$$

$$W_{frame} = 6.28 \times 446.2 \times 16.23 \times 0.101 = \underline{4594} \text{ pounds}$$

Summary of skirt weight

Shell	28619	
Longerons	3720	
Connectors	2500	34829
Aft Frame	4594	
	39433 pounds	

KICK FRAME AT 710

$$N_R = N_x \sin 9° = 13878 \sin 9° = 2171 \text{ lb/in.}$$

Elastic stability of ring subjected to radial load

$$g_{CR} = \frac{(k^2 - 1)E\,I}{R^3}$$

For k = 2

$$g_{CR} = \frac{3EI}{R^3}$$

$$I = \frac{g_{CR}}{3E} R^3$$

Assume R = 410

$$I = 4796 \text{ in.}^4$$

Use kick frame such that $I = 2A_f^2$. Therefore

$$A_f = \sqrt{2398} = 48.97 \text{ in.}^2$$

$$h = 3.46 \sqrt{A_f} \cong 24.21 \text{ in.}$$

$$R = 408 \text{ in.}$$

$$\text{Wgt} = 6.28 \times 408 \times 48.97 \times 0.101 = \underline{12670} \text{ pounds}$$

Stress:

$$\sigma = \frac{2171 \times 408}{48.97} = \underline{18088} \text{ psi}$$

RESULTS

SUMMARY

Kick Frame Station 710	12670 pounds
Aft Skirt Frame Station 500	4594
Skirt Shell, Longerons, Etc.	34839
Thrust Cone	14761
Frame Station 618	14880
Shear Connection Station 618	997
Total	82741 pounds

6.9 SECOND STAGE THRUST STRUCTURE AND HUNG TANKS

Upper stage thrust structures and hung tanks were analyzed for aluminum, beryllium and titanium alloys. Maximum load conditions for the hung tanks was at N-1 burnout. The results are tabulated in Table 6-16. Table 6-17 itemizes the structural components making up the weights in Table 6-16.

Table 6-16

Weight of Second Stage Thrust Structure and Hung Tanks

Configuration Number	Material		
	Al Alloys	Be Alloy	Ti Alloy
101	54546	26093	47740
201, 204, 205	48173	23351	45265
202	39589	18218	37581
203	55987	25952	53063

Table 6-17

Upper Stage Components

Configuration Number	Components Analyzed
101	LOX tank, thrust cone, kick frame
201, 202, 203, 204, 205	LOX tank, LH_2 tank, thrust cone, attach skirt and framing, and two kick frames

A sample calculation of the 201 Vehicle is included herein, to illustrate methods of calculating weights for these elements.

SAMPLE CALCULATION

UPPER STAGE HUNG TANK AND THRUST STRUCTURE

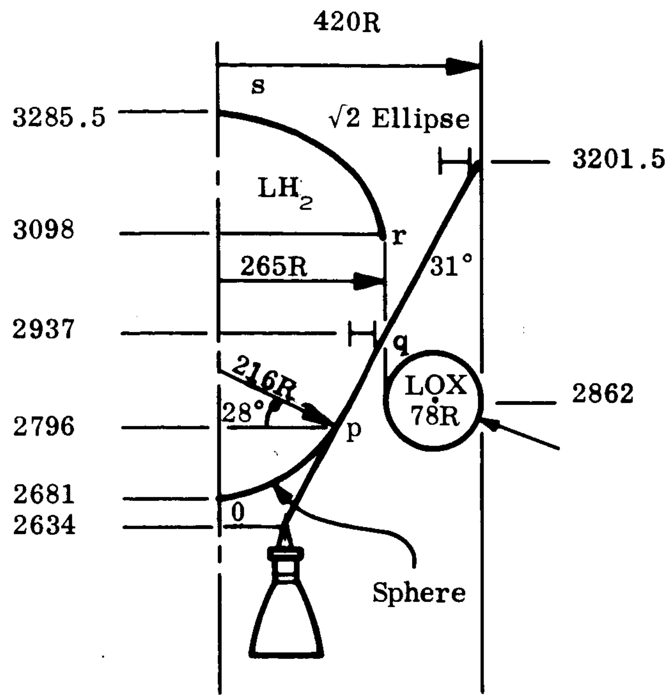

Figure a

Structure Considered

Thrust Cone

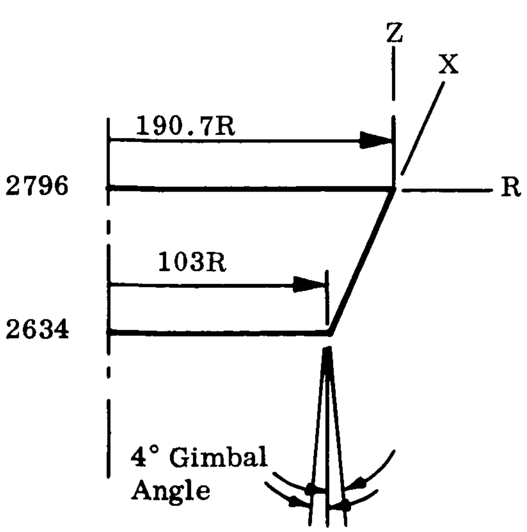

Total Thrust = 2,410,000 lb

Two engine modules

$$N_x^F = \frac{2410000}{2\pi\ R \cos 31°}$$

$$N_R = N_x \sin 31°$$

$$R_2 = \frac{R}{\cos 31°}$$

$$N_x^M = \frac{M}{\pi\ R_2^2}$$

Gimbal Side Thrust for Moment = 2,410,000 sin 4°

$$|M| = \left|(2{,}410{,}000 \sin 4°)(2634 - \text{Station No.})\right|$$

Station No.	R	R_2	$\frac{M}{10^6}$	N_x^F	N_x^M	N_x	$\frac{N_x}{R_2}$
2634	103	120.16	0	3193.7	0	3193.7	26.6
2796	190.7	222.48	27.2	1724.9	175.2	1900.1	8.5
2937	265	309.16	50.9	1241.3	171.9	1413.2	4.5
3201.5	420	489.98	95.4	783.2	128.2	911.3	1.9

Design Point Station 2634

$$N_x = 3193.7$$

$$\frac{N_x}{R_2} = 26.6$$

Use a Z-stringer shell as shown in Figure b.

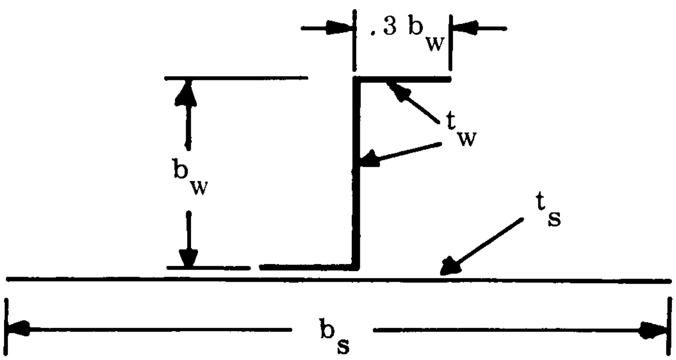

Figure b. Z-Stringer

From Figure 6-22

$$\epsilon_{max} = 0.89$$

For $N_x/R = 26.6$, Figure 6-20 gives

$$\sigma = (0.89)^{3/8}(35{,}500) = 33973$$

$$\bar{t}_P = \frac{N_x}{\sigma} = \frac{3193.7}{33973}$$

$$= 0.094 \text{ in.}$$

$$\bar{t}_T = \frac{4}{3}\bar{t}_P = 0.125 \text{ in.}$$

Cone Weight $= 2\pi R \bar{t}_T \gamma = 6.28 \times 103 \times 0.125 \times 0.101 = 8.2$ lb/in.

Total Cone Weight Between Stations 2634 and 2796 = <u>1543</u> pounds

THRUST RING IN GIMBAL PLANE

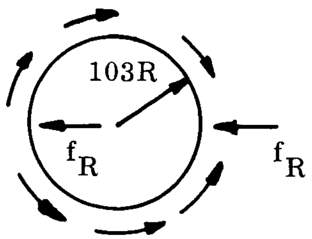

$$f_R = F \sin 4° = 82061 \text{ lb}$$

$$M_{max} = 0.4 \times 82061 \times 103$$

$$= 3,380,913 \text{ in./lb}$$

$$\sigma = \frac{Mc}{I}$$

$$\frac{I}{c} = \frac{M}{f_{att}} = \frac{M}{\frac{F_{Tu}}{1.4}} = 61.47$$

Assume

$$I = 2A^2$$

$$h = 3.46\sqrt{A} = 2c$$

$$\therefore \frac{I}{h} = 30.735 = \frac{2}{3.46} A^{3/2} = 0.578A^{3/2}$$

$$A = \left[\frac{1}{0.578}(30.735)\right]^{2/3} \cong 14.3 \text{ in.}^2$$

$$h = 13.03 \text{ in.}$$

$$I = 403.28 \text{ in.}^4$$

$$\text{Weight} = 6.28 \times 14.2\left(103 - \frac{13.03}{2}\right) \times 0.101 = \underline{869} \text{ lb}$$

BEARING LONGERONS

$$A_{BRg} = \frac{1,405,000}{55,000} = 25.6 \text{ in.}^2$$

Assume taper to 2 in.^{2}

$$W = 2\left(\frac{27.6}{2} \times \frac{162}{0.8572} \times 0.101\right) = \underline{1051.9} \text{ lb}$$

Thrust Structure Summary

Cone	=	1543
Ring	=	869
Longerons	=	1051.9
Total		3463.9

LH_2 TANK

Assume tank is full

Spherical cap between stations 2681 and 2796

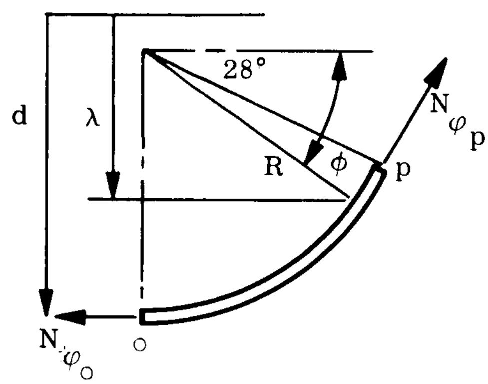

$P_{ullage} = 27 \pm 3$, use 30 psi

In general

$$N_\varphi = \beta\gamma R \left(\frac{d - R}{2} + \frac{R}{3} \, \frac{1 - \sin^3\phi}{\cos^2\phi} \right)$$

$$N_\Theta = \beta\gamma R \left(\frac{d - R}{2} + \frac{R}{3} \, \frac{\sin^3\phi + 3\phi\cos^2\phi - 1}{\cos^2\varphi} \right)$$

At $\varphi = \pi/2$

$$N_\Theta = N_\varphi = \beta\gamma d \frac{R}{2}$$

$$d = 3285.5 - 2681 = 604.5 \text{ in.}$$

$$\beta = 5.55, \; \gamma = 0.00256 \text{ lb in.}^3; \; \beta\gamma = 0.0142$$

At $\varphi = \pi/2$

$$N_\Theta^H = N_\varphi^H = 0.0142 \times 604.5 \times \frac{216}{2} = 927 \text{ lb/in.}$$

Stress due to ullage

$$N_\varphi^P = N_\Theta^P = 30 \times \frac{216}{2} = 3240 \text{ lb/in.}$$

Total stress at 0

$$N_\varphi = N_\Theta = \underline{4167} \text{ lb/in.}$$

Design stresses:

Material	F_{Ty}	F_{Tu}	$F_{Ty}/1.1$	$F_{Tu}/1.4$	Material	$t_o = N_\varphi/F_{Tu}/1.4$
2219-T87	50000	62000	45454	44286	2219-T87	0.09409
QMV5-Be	64500	75000	58636	53571	QMV5-Be	0.07778
6Al-4V—Ti	126000	130000	114545	92857	6Al-4V—Ti	0.04487

At point p $\phi = 28°$

From general equations plus ullage

$N_\phi = 4090$ lb/in

$N_\Theta = 3905$ lb/in

Material	t_p	Material	t_{avg}	γ	$t_{avg}\,\gamma$
2219-T87	0.09235	2219-T87	0.0932	0.102	0.00951
QMV5-Be	0.07634	QMV5-Be	0.0771	0.067	0.00516
6Al-4V—Ti	0.04404	6Al-4V—Ti	0.0444	0.16	0.00710

Surface area $= 2\pi R^2 (1 - \sin 28°) = 155{,}445.13$ in.^{2}

Weight $= \gamma\, t_{avg} \times 155{,}445.13$

Material	Dome Weight
2219-T87	1478
QMV5-Be	802
6Al-4V—Ti	1104

Cylinder calculation (refer to Figure 1, points q and r)

At any point

$$N_\Theta = PR = (\beta\gamma h + p_{ullage})R$$

Method

$$\overline{N}_\theta = \frac{N_\theta^{\,q} + N_\theta^{\,r}}{2}, \quad \overline{t} = \frac{1.4\overline{N}_\theta}{F_{Tu}}$$

$$\text{Weight} = 530\pi \times 161 \times \gamma\overline{t}$$

Material	Weight
2219-T87	5455
QMV5-Be	2908
6Al-4V—Ti	4012

ELLIPTICAL HEAD

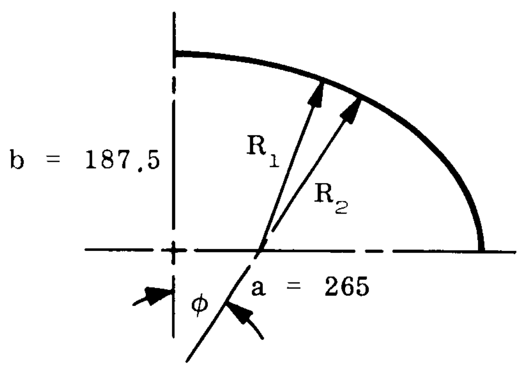

$$\frac{x^2}{a^2} + \frac{y^2}{b^2} = 1, \quad \frac{a}{b} = \sqrt{2}$$

$$R_2 = \frac{a}{\sqrt{\dfrac{1 + \sin^2\phi}{2}}}$$

$$R_1 = \frac{R_2}{1 + \sin^2\phi}$$

$$x = R_2 \sin\varphi, \quad y = \frac{b}{a}\sqrt{a^2 - x^2}$$

$$N_\varphi = PR_2/Z$$

$$N_\Theta = R_1\left(p - \frac{N_\varphi}{R_2}\right)$$

$$p = B\gamma(b - y) + P_{ullage} = \beta\gamma\left[b\left(1 - \frac{1}{a}\sqrt{a^2 - x^2}\right)\right] + P_{ullage}$$

ϕ	N_ϕ	N_θ	N_{design}
0	4872	4872	4872
30	4969	3942	4969
60	4271	2439	4271
90	4195	2097	4195

Material	ϕ	$t = \dfrac{1.4\ N_{des}}{F_{Tu}}$	$\bar{t}$
2219-T87	0	0.11001	
	30	0.11220	
	60	0.09644	
	90	0.09472	0.103
QMV5-Be	0	0.0909	
	30	0.09280	
	60	0.0797	
	90	0.0783	0.0854
6Al-4V—Ti	0	0.0525	
	30	0.0535	
	60	0.0460	
	90	0.0452	0.0493

Head weight tabulation; Weight $= \bar{t}\ \gamma \times$ Surface Area

Material	Weight
2219-T87	4644
QMV5-Be	2521
6Al-4V—Ti	3516

CONICAL FRUSTUM

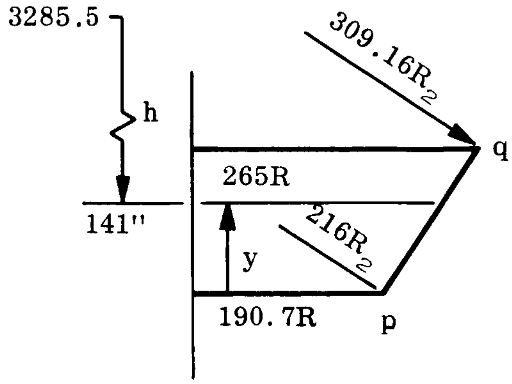

$$N_\Theta = P_{total} R_2$$

$$P_{total} = \gamma \beta h + P_{ullage}$$

Station	y	R_2	P_r	N_Θ
p	0	216	36.95	7981
(p + q)/2	70.5	265.35	35.95	9539
q	141	309.16	34.95	10805

Note: N_x loads in the frustum from thrust were small and therefore ignored in this calculation.

$$\bar{t} = 1.4 \times 9539 / F_{Tu}$$

$$\text{Surface Area} = \pi\,(190.7 + 265)\left(\frac{141}{0.8572}\right) = 235,368 \text{ in.}^2$$

$$\text{Weight} = \gamma \bar{t} \times \text{Surface Area}$$

Material	$\bar{t}$	$\gamma \bar{t}$	Weight
2219-T87	0.215	0.02193	5162
QMV5-Be	0.178	0.01068	2514
6Al-4V—Ti	0.102	0.01632	3841

Summary of LH_2 Tank Weights

	2219-T87	QMV5-Be	6Al-4V—Ti
Lower Dome	1478	802	1104
Conical Frustum	5162	2514	3841
Cylinder	5455	2908	4012
Upper Dome	4644	2521	3516
Total	16739	8745	12473

LOX TANK (TORUS) See Appendix D for Equations

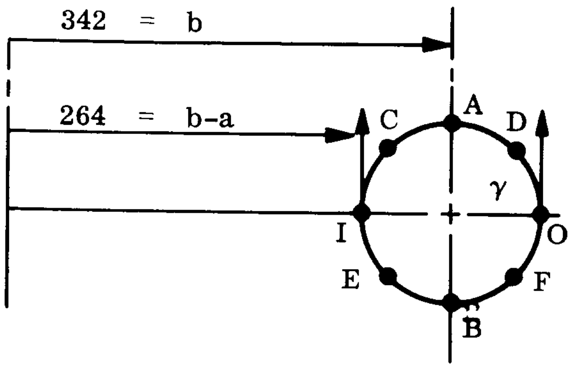

$\gamma = 0.0413 \text{ lb/in.}^3$

$P_{ullage} = 20 \pm 3 \text{ psi}$

Point	N_ϕ	$t = 1.4\ N_\varphi / F_{Tu}$, Al Only
A	2475	0.055
B	3956	0.089
C	1819	0.041
D	1563	0.035
E	3254	0.073
F	2408	0.054
I	4728	0.106
O	3505	0.079

$$\bar{t} = \frac{\Sigma t}{8} = 0.066$$

Material	$\bar{t}$	$\bar{t}\gamma$	Weight = $S\bar{t}\gamma \times 1.25$
2219-T87	0.066	0.00673	8850
QMV5-Be	0.055	0.00368	4840
6Al-4V—Ti	0.031	0.00496	6523

Where

$$S = 4\pi^2 ab = 1{,}052{,}059 \text{ in.}^2$$

Factor of 1.25 is used to account for reinforcements at attachments, attachments, and stiffening ribs on thin-walled tanks.

UPPER SKIRT

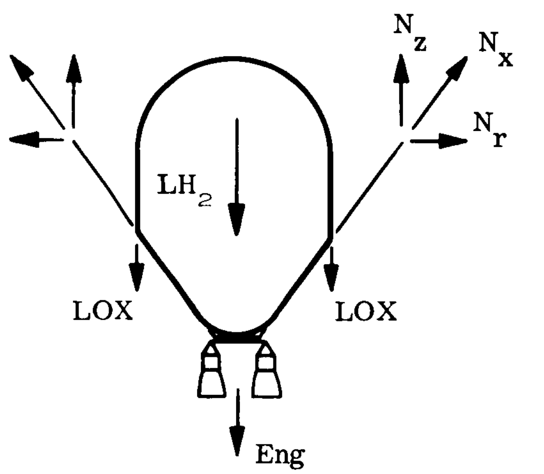

Total Loads @ β = 1

LH_2	=	234,206 lb
LOX	=	799,000
Eng	=	29,964
		1,063,170 lb

$$\beta W = 5{,}900{,}594 \text{ lb}$$

$$N_z = 5{,}900{,}594/(6.28 \times 420) = 2237$$

$$N_x = N_z/0.8572 = 2610$$

$$N_r = N_z/0.6009 = 1344$$

KICK FRAME @ Station 3201.5

$$I = \frac{r^3 N_r}{3E}$$

$$I = 2A^2 \;, \quad h = 3.46\sqrt{A} \;, \quad R = 420 - h/2$$

$$\text{Weight} = 2\pi RA\gamma$$

Material	I	A	Weight
2219-T87	2969	38.5	10104
QMV5-Be	715.49	18.9	3280
6Al-4V—Ti	1943	31.1	12823

SKIRT

Station 3201.5

$$t = 1.4\ N_x/F_{Tu}$$

Material	t
2219-T87	0.0589
QMV5-Be	0.0487
6Al-4V—Ti	0.0281

Station 2937+

$$N_x = 4136\ \text{lb/in.}$$

Material	t
2219-T87	0.0934
QMV5-Be	0.0772
6Al-4V—Ti	0.0445

Material	$\bar{t}$	$\gamma\bar{t}$	Weight
2219-T87	0.07615	0.00777	4983
QMV5-Be	0.06295	0.00422	2706
6Al-4V—Ti	0.03630	0.00581	3725

$$\text{Weight} = \gamma\bar{t} \times \text{Surface Area}$$

FRAME @ STATION 2862

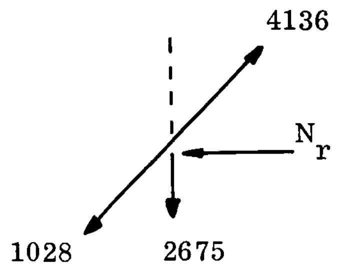

$$\Sigma F_r = 0 \; ; \; N_r = 1600$$

$$I = \frac{N_r \Gamma^3}{3E} \; ; \; I = 2A^2 \; ; \; h = 3.46\sqrt{A}$$

Material	I	A	W
Al	901	21.2	3511
Be	223.1	10.5	1146
Ti	585.65	17.1	4430

Estimate an additional 15 percent for the conical frustum between stations 2796 and 3201.5 since cone needs stiffening frames for constructions and for resisting engine thrust.

	Al	Be	Ti
Tank	5162	2514	3841
Skirt	4983	2706	3725
Σ	10145	5220	7566
0.15Σ	1522	783	1134

← Framing

SUMMARY OF UPPER STAGE 201

Component	Al	Be	Ti
LOX Tank	8850	4840	6523
LH_2 Tank	16739	8745	12473
Thrust Cone	3464	1851	4157
Skirt	4983	2706	3725
Frame 3201.5	10104	3280	12823
Frame 2937	3511	1146	4430
Skirt Framing	1522	783	1134
Total	48173	23351	45265

Engine modules assumed to be 26,500 lbs for all materials.

SECTION 7

EVALUATION OF STRUCTURAL ANALYSIS TECHNIQUES

7.1 INTRODUCTION

Certain special techniques and criteria for the analysis of structures are discussed in this section. The consideration of biaxial stress fields, namely, Hill's theory, is studied for its effect on reducing weight for textured-titanium constructed structures. The effect on weight reduction is also considered by varying the buckling coefficients for axially compressed cylinders.

Structural analysis techniques tend to be limited in use by their mathematical complexities and to some extent the types of materials used in the construction of structural components. Theoretically methods are often configuration oriented. Because of the complexity of the mathematical solution, certain concepts are often not utilized to their optimum advantage because of the stress analysis inability or the unwarranted expense involved in extending the solution to more general configuration-load situation. A special technique discussed here, namely pressure coupling, is such a case in point. This study is technology oriented in that existing solutions of problems are used to design certain components and hopefully reduce the weight over "normal" methods of analysis. Limited development of new approaches of analysis were used where feasible.

The findings of this study are to be considered as pertaining to the type of structures used in the study which are in general buckling controlled in their final design, thus the judgment of the true value of a method must be viewed in this context. For instance, pressure coupling was found to be of minimal value in reducing weight for the large low-pressure tanks used in the class of vehicle considered here. Other investigators have indicated possible savings in high pressure thin-walled pressure vessels and thus the method should be thoroughly investigated in that area. Further it should be pointed out that the variation in buckling coefficients, while attractive, is test-to-failure oriented and the trends of weight reductions shown should be viewed in that light.

Supplementary studies of plastic deformation theory in thin walled pressure vessels were also considered. The details of this supplementary study are presented in Appendix E.

7.2 PRESSURE COUPLING

7.2.1 SUMMARY

The General Electric Company has investigated the possibility of achieving weight savings using the pressure coupling concept in support of the NAS2-3811 contract. In general, the pressures encountered in the basic vehicle tanks were too low to indicate a discernable weight savings in the types of structures considered.

7.2.2 RESULTS

The object of this study was to observe the effects of considering pressure coupling as a possible method of reducing the weight of a pressure vessel. Pressure coupling is the inclusion of the stiffening effect of the membrane forces in the shell when calculating the discontinuity shears and moments at the geometric discontinuities in pressure vessels. Previous work on pressure coupling has been reported in References 27, 28, 29, and 50.

The type of vessel considered in this study was composed of a cylindrical barrel and a hemispherical cap. Ten cases were considered at varying pressure levels. Six cases were vessels that were 80 feet in diameter and subjected to uniform pressure levels of 27, 36, and 50 psi. The four other cases were for more severe loading conditions: two vessels were 520 inches in diameter and two were 260 inches in diameter, both being subjected to 680 psi. The cases were studied in pairs: (1) with the cap-barrel thickness ratio equal to 0.5, and (2) with the cap-barrel thickness ratio equal to unity. The results of this study are summarized in Table 7-1.

It is seen that pressure coupling tends to lower the barrel discontinuity stresses in the neighborhood of the juncture compared to the regular method used for calculating these stress levels. The membrane stress, $X = \infty$ in the table, is used to size the vessel. A comparison shows that, in general, at least one point in the regular case exceeds the membrane level by a very small amount and this never by more than 2.86 percent. It would appear that a weight savings of less than 1 percent could be optimistically realized in the cylindrical barrel for the cases considered. Cap discontinuity stresses also reflect the consideration of pressure coupling.

In order to determine the relative effect of the possible use of the pressure coupling concept on cap weight, cases I through VI were analyzed by nonpressure coupling methods of Reference 52. The results indicated that the merits of a pressure coupling analysis would not realize weight savings of significant magnitudes. A typical cap will be discussed in paragraph 7.2.4.

Cases VII through X are out of range of the types of loadings that occur in the vehicles comprising the basis of this study and were not investigated further. Such vessels are more in the load/size range where pressure coupling is expected to achieve measureable weight savings.

7.2.3 EXPLANATION OF TABLE 7-1

Table 7-1 lists the pertinent results from the study. The cases are listed in ordered pairs where the difference is in the cap-barrel thickness ratio only. Each column is identified as follows:

Case Numbers I, II, III, etc.
Cap-barrel thickness ratio.
Vessel radius, R.
Pressure load, p.
Distance to the point on the hoop stress curve where stress is a maximum, X.
Discontinuity moments, M, and shears, V, for pressure coupling, PC, and nonpressure coupling, Reg.
Maximum barrel hoop stresses.
Cap discontinuity stresses. The cap discontinuity stress reflects the maximum principal stress, either meridional, or circumferential.

7.2.4 TYPICAL CASE

7.2.4.1 Analysis (Case Numbers III and IV, Table 7-1)

The typical vessel considered was a cylindrical shell with hemispherical caps. The barrel length was 780 inches and the shell diameter was 960 inches, total shell length was 1740 inches.

Two cases were considered as follows:

a. Cap and barrel thickness ratio equal 1.
b. Cap and barrel thickness ratio equal 0.5.

The design load considered was for a uniform internal pressure of 36 psi. The material properties used were those for 2219-T87 aluminum alloy and are summarized in Table 7-2.

Table 7-1

Results of Pressure Coupling Analysis

Case No.	$\frac{h_1}{h_2}$	R (in.)	p (psi)	X (in.)	Discontinuity Loads				Barrel Stresses		Cap Discontinuity	
					PC		Reg					
					M	V	M	V	PC	Reg	PC	Reg
I	0.5	480	27	0	-1.1	37.6	-12.2	5.9	41,900	42,300	48,700	49,800
				18.2					43,500			
				24.5						44,900		
				53.4						44,680		
				∞					44,700	44,700	44,700	44,700
II	1.0	480	27	0	0	151.0	0	31.0	33,500	33,500	-33,600	33,600
				18.2					39,900			
				19.9						45,980		
				23.3						45,690		
				∞					44,700	44,700	22,300	22,300
III	0.5	480	36	0	-1.1	57.2	-16.3	7.9	55,900	56,460	65,600	66,471
				15.4					57,600	60,118		
				24.5						59,850		
				44.2						59,600		
				∞					59,600	59,600	59,600	59,600

Table 7-1

Results of Pressure Coupling Analysis (Cont.)

Case No.	$\frac{h_1}{h_2}$	R (in.)	p (psi)	X (in.)	Discontinuity Loads				Barrel Stresses		Cap Discontinuity	
					PC		Reg					
					M	V	M	V	PC	Reg	PC	Reg
IV	1.0	480	36	0	0	233.0	0	41.3	44,700	44,700	-44,700	44,700
				15.4					51,600			
				20						61,305		
				52.1						59,530		
				∞					59,600	59,600	29,800	29,800
V	0.5	480	50	0	-2.8	80.5	-31.2	12.8	56,200	56,700	64,900	66,700
				18.1						60,390		
				21.8					58,300			
				28.8						60,120		
				∞					59,900	59,900	59,900	59,900
VI	1.0	480	50	0	0	324.0	0	67.5	44,900	44,900	-44,900	44,900
				21.8					53,700			
				23.5						61,580		
				27.4						61,190		
				57.7					59,900	59,900	29,900	29,900

Table 7-1
Results of Pressure Coupling Analysis (Cont.)

Case No.	$\frac{h_1}{h_2}$	R (in.)	p (psi)	X (in.)	Discontinuity Loads				Barrel Stresses		Cap Discontinuity	
					PC		Reg					
					M	V	M	V	PC	Reg	PC	Reg
VII	0.5	260	680	0	-283.0	558.0	-711.0	226.0	134,000	135,100	156,000	159,000
				0.133					133,000			
				23.4						143,850		
				37.3						143,230		
				43.4					142,000			
				∞					143,000	143,000	143,000	143,000
VIII	1.0	260	680	0	0	2,330.0	0	1,187.0	107,000	106,940	107,000	106,940
				30.4						146,690		
				35.4						145,800		
				43.8					141,000			
				74.3						142,560		
				∞					143,000	143,000	71,300	71,300
IX	0.5	130	680	0	-41.4	315.0	-143.4	101.5	166,000	167,520	193,000	197,700
				10.5						178,380		
				16.7						177,600		
				46.2					177,000			
				∞					177,000	177,000	177,000	177,000

Table 7-1

Results of Pressure Coupling Analysis (Cont.)

Case No.	$\frac{h_1}{h_2}$	R (in.)	p (psi)	X (in.)	Discontinuity Loads				Barrel Stresses		Cap Discontinuity	
					PC		Reg					
					M	V	M	V	PC	Reg	PC	Reg
X	1.0	130	680	0	0	1,290.0	0	533.0	133,000	132,600	132,400	132,600
				13.6						181,900		
				15.9						180,760		
				35.6						176,600		
				46.2					177,000			
				∞					177,000	177,000	88,400	88,400

Table 7-2

Material Properties—2219-T87 Aluminum

F_{tu}	62,000
F_{ty}	47,000
F_{cy}	49,000
E	1,030,000

The analytical equations used are presented in Appendix D.

Safety factors used were 1.4 on F_{tu} and 1.1 on F_{ty}. Gauge thickness selection was based on an apparent F'_{tu} defined as 1.4/1.1 (47,000) 59,800 psi. The gauge thickness as used in the cap and barrel respectively were $h_1 = h_2 = 0.290$ for case I. The results are summarized in Table 7-3 where X is the point in the barrel of maximum stress, PC implies use of pressure coupling terms, Reg implies ignoring the pressure coupling terms, and $X = \infty$ for membrane stress.

Table 7-3

Result of Analysis of Cylindrical Shell with Hemispherical Caps

h_1/h_2	X_1, in.	Barrel Stresses	
		PC	Reg
0.5	0	55,900	56,460
	15.4	57,600	60,118
	24.5		59,850
	44.2		59,600
	∞	59,600	59,600
1.0	0	44,700	44,700
	15.4	51,600	
	20.0		61,305
	52.1		59,530
	∞	59,600	59,600

The consideration of the pressure coupling terms resulted in the membrane stress being maximum whereas when they were ignored, short segments in each cylinder considered exceeds F'_{tu}. For the structure with $h_1/h_2 = 0.5$, the excess was 0.531 percent and where the ratio $h_1/h_2 = 1$ the excess was 2.516 percent. Since these excesses occur over short shell lengths and are principal stresses, it was concluded that the use of pressure coupling could not reduce the barrel weight by an appreciable amount for this design.

The caps were investigated for stress distributions without pressure coupling to see if the results merited further investigation utilizing the concept.

A summary of the cap discontinuity stresses is given with and without pressure coupling terms in Table 7-4.

Table 7-4

Summary of Cap Discontinuity Stresses

h_1/h_2	PC	Reg
0.5	65,600	66,471
1.0	44,700	44,700

where $h_1/h_2 = 0.5$ the discontinuity stresses exceed the membrane in F'_{tu} sizing stress, however, insignificant differences exist between the use of pressure coupling or ignoring it.

Table 7-5 summarizes the non pressure coupled stresses in the cap through the meridional angle ϕ, defined in Figure 7-1, until the stresses attenuate into practically pure membrane stresses.

Table 7-5 shows that the stresses attenuate to membrane conditions very rapidly. For the case $h_1/h_2 = 0.5$, this takes place in 7.2 degrees and in 13.5 degrees for the case of $h_1/h_2 = 1.0$

Investigation of Table 7-5 shows that the stresses exceed $F'_{tu} = 59,800$ in a band of about 2 degrees from the joint of the cap and barrel where $h_1/h_2 = 0.5$. Therefore, it was concluded that the pressure coupling concept need not be considered further as it would not reduce the weight of the cap an appreciable amount, since the best it could

Table 7-5

Summary of Nonpressure Coupled Stresses

h_1/h_2	ϕ	σ_ϕ Max	σ_θ Max
0.5	90	64,238	66,471
	89.1	61,873	61,690
	88.2	60,611	59,709
	82.8	59,586	59,586
1.0	90	29,793	44,669
	89.1	38,502	36,862
	88.2	35,010	31,151
	82.8	29,804	29,816
	76.5	29,793	29,793

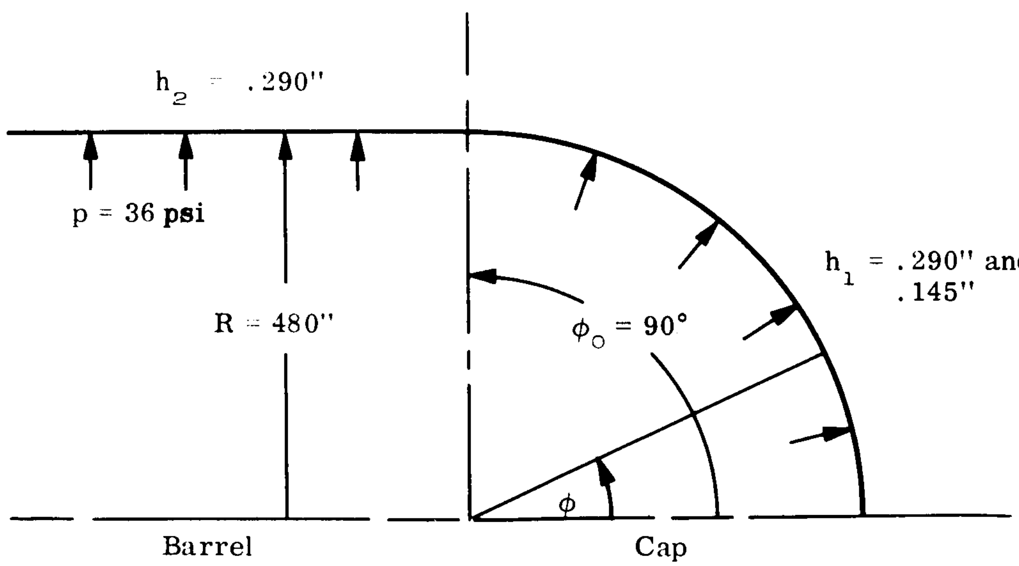

Figure 7-1. Definition of Meridional Angle ϕ

do would be to reduce the large discontinuity stress, which occurs only over 2 short shell segments.

An approximation of the weight savings can be calculated and upper and lower bounds determined. The 2-degree band width of excessive stress comprises 3.49 percent of the cap surface area. Since the maximum discontinuity stress was 66,471 or 11.15 percent greater than the $F'_{tu} = 59,800$ for the case where $h_1/h_2 = 0.5$ the upper bound of the weight savings would be

$$0.0349 \times \frac{66,471 - 59,800}{66,471} \times 100 = 0.35 \text{ percent}$$

Assuming the actual average stress in the 2-degree band is 63,000 psi the lower bound would be

$$0.0349 \times \frac{63,000 - 59,800}{63,000} \times 100 = 0.18 \text{ percent}$$

7.2.4.2 Limitations of Investigation

Limitations of the investigation include the following:

a. The investigation was limited to the use of known solutions given in references 44, 28, 27, and 50. Those solutions were good for uniform internal pressure only and for cylinders and spherical caps.

b. Such vessels of the magnitude used in the analysis are usually limited to caps other than hemispheres and the barrel designs are usually controlled by buckling loads, since the tank walls are ordinarily a part of the vehicle body proper.

7.2.4.3 Conclusions

The following conclusions were determined:

a. Pressure coupling for low-pressure, thin-walled vessels does little to reduce weights in hemispherical caps attached to long cylindrical barrels, since membrane stresses tend to dominate the design. This is not an unexpected result and is referred to by other investigators (References 44, 27, 51, and 50).

b. Shells such as occur in the post-Saturn type of vehicle have not been investigated for other than uniform internal pressures. Available solutions would only be suitable for hung LH_2 tanks where hydrostatic stresses are lowest.

c. Subsequent considerations, such as highly pressurized "short" or "medium" cylinders, where bending dominates are apt to be more conducive to weight savings by using pressure coupling. Most investigations of cylinders have been for long cylinders (References 44, 27, and 51) and for a limited range of caps (Reference 50). Design curves in Reference 50 point out the merits of pressure coupling as occurs in the attenuation region for a family of shells subjected to a range of pressure parameters.

d. Efficient use of the pressure coupling solution is probably material oriented, that is, for brittle or stiff materials where the modulus of resilience is of the same order of magnitude as the modulus of toughness in which case the elastic solution is probably the safest solution. Where the modulus of resilience is small compared to the modulus of toughness, the membrane loads will dominate and pressure coupling can be replaced by a limit analysis utilizing a theory of strength, such as Hill's or von Mises' flow rule to obtain weight reductions.

7.3 CONSIDERATION OF BIAXIAL STRESS FIELDS

7.3.1 INTRODUCTION

Some materials, such as titanium alloys, exhibit strengths in biaxial tension stress fields that are significantly greater than those predicted by the von Mises failure criterion. These materials are strongly dependent upon the inherent thickness anisotropy in a biaxial stress condition. Hill's failure criterion is commonly used for predicting the yielding of such materials. This criterion may be expressed in terms of the principal stresses for biaxial stress fields as

$$N_o^2 = N_1^2 - 2\mu_p N_1 N_2 + N_2^2 \tag{7-1}$$

where:

N_1, N_2	principal stress resultants
μ_p	plastic Poisson's ratio
N_o	equivalent uniaxial stress resultant.

It is clear from Equation 7-1 that if $\mu_p = 0.5$, the von Mises criterion becomes a special case of Hill's theory.

7.3.2 RESULTS

The von Mises theory has been used in this study where biaxial stress fields occur for determining component weights, hence it is the nominal or basis of comparison for deviating results. The part of the weight sensitivity study reported in this section evaluated the effect of varying μ_p from 0.5 to 0.7 for the 201 Vehicle using textured titanium for the construction material.

The maximum principal stress theory was also considered for further comparison. The study is summarized by means of Figure 7-2 where the percent weight savings is plotted as a function of μ_p and construction type.

Reference 41 reports that a value of μ_p slightly greater than 0.7 has been achieved in titanium. Using $\mu_p = 0.7$ the reduction in overall structural weight of the 201 Vehicle is in the range from 1/2 to 2 percent depending on the type of construction used in the vehicle.

7.4 EFFECT OF VARIATIONS IN BUCKLING COEFFICIENTS

7.4.1 GENERAL

This study was performed to examine the effect of buckling coefficients on the resulting weight of an axially loaded cylindrical structure. Buckling coefficients are correction factors usually determined experimentally and are often applied to theoretical equations in order to assure structural integrity. Inadequate data may foster the use of necessarily conservative correction factors. The study reported here demonstrates the sensitivity of the weight of a particular launch vehicle made of families of aluminum constructions to a range of changes to the buckling coefficients used in the design of various structural components.

7.4.2 THEORY

The weight, W, of a cylindrical shell in axial compression can be expressed as a function of the square root of the ratio of the meridional stress, N_x, to the buckling coefficient C. That is to say

$$W = W\left(\sqrt{\frac{N_x}{C}}\right) \tag{7-2}$$

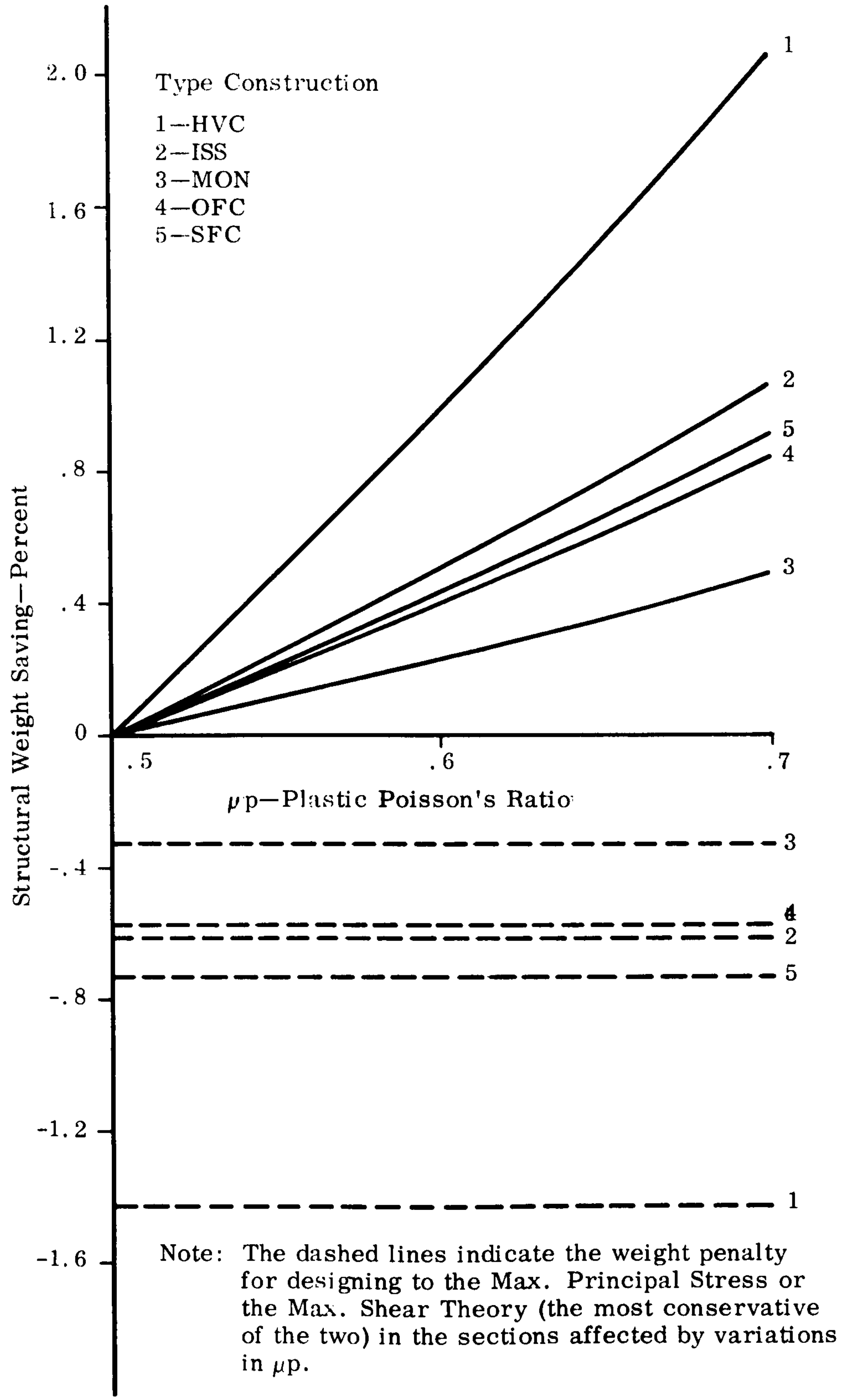

Figure 7-2. The Effect of Variation in μ_p On Structural Weight

A study of Equation 7-2 shows that W can be changed by varying either N_x or C. In this study, changes in W were assumed to be the result of changes in the buckling coefficient C.

7.4.3 RESULTS

A short program was written to calculate the ratios

$$R_1 = N_x/N_{nom} \tag{7-3}$$

and

$$R_2 = N_o/N_{o_{nom}} \tag{7-4}$$

for various sections of the 201 Launch Vehicle.

The ratios calculated by Equations 7-3 and 7-4 were used to study the effect of changes in buckling coefficients on structural weights by the methods explained in Section 4. Figure 7-3 summarizes the complete study graphically for various types of aluminum constructions and the 201 Launch Vehicle.

To give an example of the buckling coefficient values used for orthotropic cylinders, refer to Figure 7-4. The nominal design value used is approximately 0.4; the range of values studied is shown plotted on either side of the nominal design curve.

Figure 7-5 shows a plot of nominal values used for monocoque cylinders. The vehicle considered had a nominal domain of $1000 \leq R/t \leq 8400$ for a nominal range of $0.07 \leq C \leq 0.15$. The band plotted on Figure 7-5 demonstrates the sets of values covered in this study. It is of academic interest to note that recent tests (Reference 57) performed on monocoque cylinders showed 70 to 80 percent of the theoretical value can be achieved by very closely controlled fabrication.

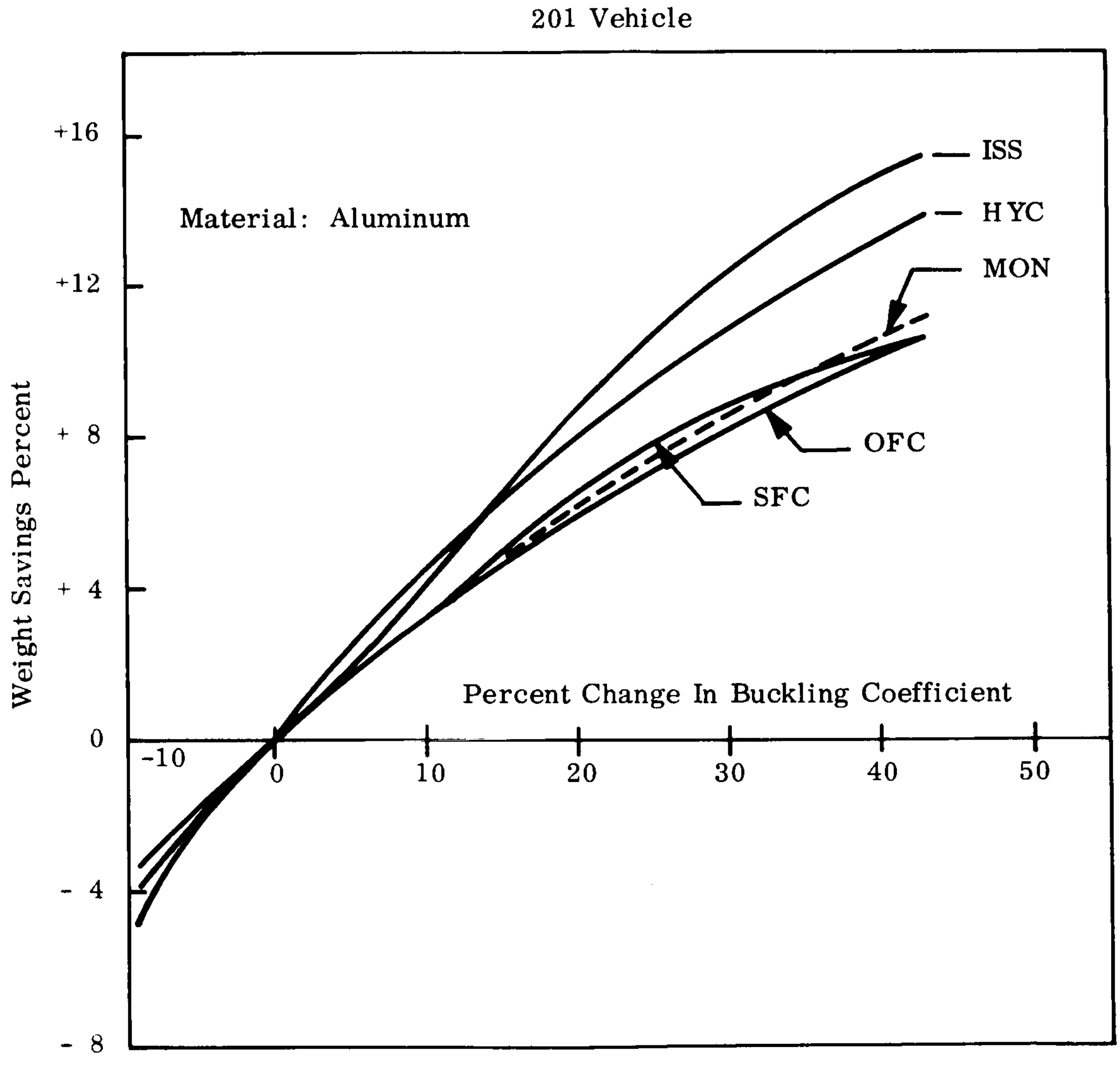

Figure 7-3. Sensitivity of 201 Vehicle Structural Weight to Changes in Buckling Coefficient

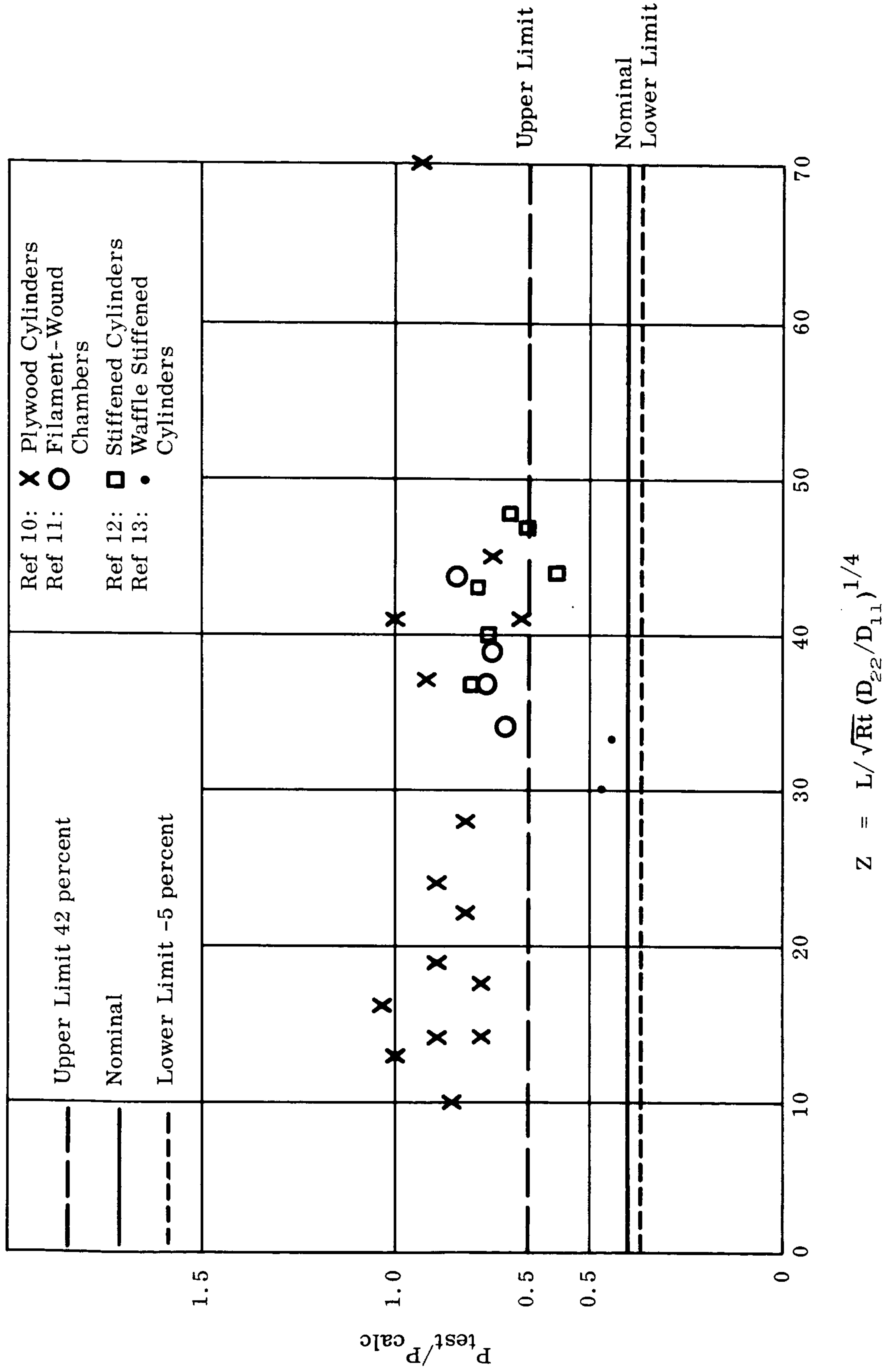

Figure 7-4. Axially Loaded Orthotropic Cylinders

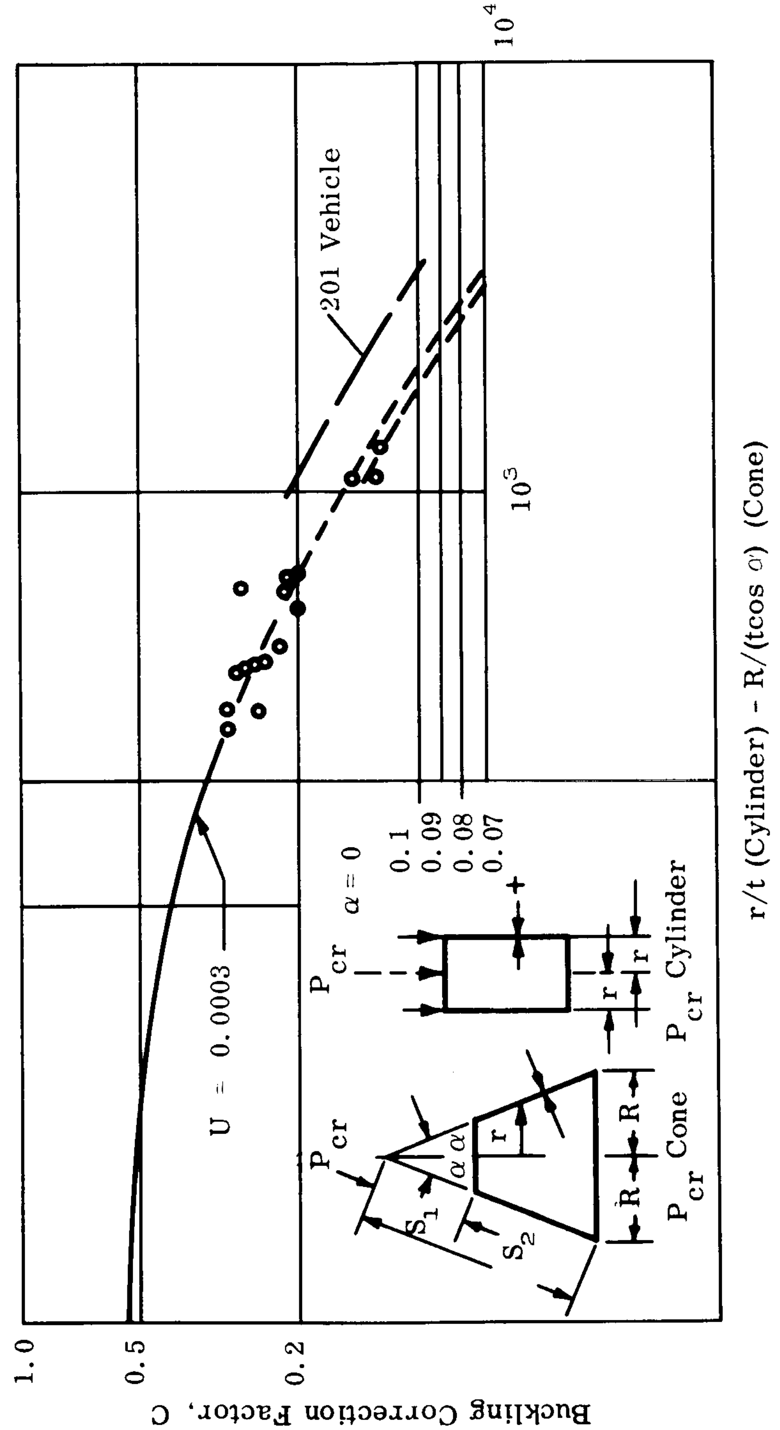

Figure 7-5. Buckling Correction Factor, C, for Cylinders or Cones

SECTION 8

MATERIALS AND FABRICATION PROCESSES

8.1 GENERAL CONSIDERATIONS

The aerospace industry's demanding requirements for specialized materials, fabrication processes, and inspection techniques for aerospace structures are responsible for the accelerated advancements in current technology. Materials, fabrication processes, and inspection techniques, both old and new, are under continuous investigation and development.

It appears that none of the established materials have reached the limit of their potential properties. Therefore, in considering materials for future use, the older established materials cannot be overlooked. Aluminum alloys, for example, are currently being widely used in the aerospace industry and indications are that they will continue to play a large part because of ease of fabrication and low comparative cost. Newer high strength alloys are currently under development for cryogenic service.

Alloys of titanium, magnesium, and beryllium are assuming a more important role in aerospace structures. These materials, it appears, will play a large part in future applications.

Since aluminum alloys are so widely used, they serve as a good basis of comparing their properties and characteristics with those of newer metal materials (see Table 8-1).

Composite materials which only a short time ago appeared to be materials for distant future application, today are a reality. The use of fiber-reinforced composites is receiving increased recognition as a solution for achieving extremely strong lightweight materials. Structurally efficient fibrous composites, such as pressure containers of glass filament reinforced plastics, are already in widespread use in aerospace and other industries. These materials are stronger, pound for pound, than the high-strength steels.

Table 8-1

Comparative Properties of Metal Materials

Material	Density (lbs/in^3)	Ult. Tensile Strength (10^3 psi)	Yield Strength (10^3 psi)	Mod. of Elasticity (10^6 psi)	Strength to Density Ratio (10^6)	Modulus to Density Ratio (10^9)
2014-T6 Aluminum Alloy	0.101	64	56	10.7	0.630	0.106
2024-T4 Aluminum Alloy	0.100	63	42	10.7	0.630	0.107
2219-T87 Aluminum Alloy	0.102	62	50	10.4	0.610	0.102
7075-T6 Aluminum Alloy	0.101	77	64	10.5	0.770	0.105
X2021 Aluminum Alloy	0.100	75	66	10.0	0.750	0.100
X7007 Aluminum Alloy	0.100	77	69	10.0	0.770	0.100
6 Al-4V Titanium Alloy	0.160	130	126	16.0	0.810	0.100
5 Al-2.5 Sn Titanium Alloy	0.160	115	110	16.0	0.740	0.100
HK31A-H24 Magnesium Alloy	0.065	35	25	6.5	0.540	0.100
LA 141A Magnesium-Lithium Alloy	0.049	19	15	6.5	0.388	0.133
LA91 Magnesium-Lithium Alloy	0.0525	22	16.5	6.6	0.419	0.125
LAZ933 Magnesium-Lithium Alloy	0.0564	30	21.5	6.4	0.532	0.114
Y5804, QMV-5 Beryllium	0.067	75	64.5	42.0	1.120	0.627
Beryllium-Alluminum Alloy	0.075	50	40	29.0	0.670	0.387
PH15-7 Mo, RH950 Stainless Steel	0.277	225	210	30.0	0.812	0.108
A1S1 4340 Alloy Steel	0.283	260	242	29.0	0.918	0.102

Of all the potentially useful fiber-reinforced materials, none have the strength of whiskers (single crystal filaments), which in some cases approach the theoretical strength of single crystals. When these fibrous materials can be incorporated effectively into a suitable matrix, a strong, stiff, low density material will result.

The usefulness of the newer materials cannot be limited by the lack of suitable fabrication techniques or additional high cost. Therefore, to meet the demands of space age hardware, fabrication methods also must make advancements. The challenge to inventive engineering, precision craftsmanship, and versatile tooling is continuous. The basic techniques of forming, machining, and joining all are being improved and some new processes are being developed. High-energy-rate forming is receiving considerable interest where large parts, such as domes, are to be formed. Lasers, which are new on the scene and only in their infancy, show tremendous potential for welding and drilling.

Inspection techniques, which permit testing or inspection of materials and parts without impairing their future usefulness, have grown in the past few years. Indications are that nondestructive inspection will continue to grow at an accelerated rate with the projected use of composite materials and newer construction techniques in the aerospace industry. Most of the current inspection methods will continue to find application to aerospace structures with newer techniques, such as thermal, infrared, and ultrasonics, finding increased usefulness.

8.2 ADVANCED MATERIALS

Titanium alloys, with their high strength to density ratios, make them very attractive for weight savings on projects requiring intermediate strength levels. The two main attributes of these metals are high strength-to-density ratio and good corrosion resistance. High cost, difficult fabricability, and limited weldability are the main disadvantages of titanium materials at the present time.

Magnesium alloys are not as strong as other structural materials, but they do have the lowest density; therefore, they should be considered for those applications where weight considerations are of prime importance and strength is of secondary importance. They are characterized by lightness and good formability. Magnesium-lithium alloys are the lightest structural material commercially available.

Beryllium is one of the newer materials that has come into prominence in recent years in the aerospace industry. Theoretically, beryllium is the outstanding structural material with its exceptional modulus (42 by 10^6 psi; Reference 61) and remarkably low density (0.067 lbs/in^3). The disadvantages of beryllium are toxicity of the metal and its limited low-temperature ductility. Beryllium can be machined and handled safely by using recommended procedures. However, need for strigent safety precautions adds to cost of producing and fabricating the metal. The problem of brittleness is under extensive investigation with hopes of a solution or ways to circumvent it.

High-strength steels possess an impressive combination of properties of direct concern to the aerospace industry. Advantages of steels include the availability of matereial, the experience already gained in processing techniques, the wealth of knowledge concerning properties and the low cost when compared with other materials considered for space vehicles. It appears that the potential properties of steels have not been reached and intensive research into methods of improving strength, ductility, and weldability are in progress. Continued improvements in the established materials and new alloys should result in the production of steel components which can be used in service with complete reliability at an applied stress level of 400 by 10^3 psi.

Tables 8-2 through 8-10 show material properties versus temperature for aluminum alloys 2014-T6, 2024-T4, 2219-T87; titanium alloy 6Al-4V; alloy steel AISI4340; magnesium alloy HK31A-H24; stainless steel PH15-7MO, and beryllium Y5804, QM-5. These tables indicate material property changes as the temperature varies from room temperature to -300°F.

Composite materials are fast appearing on the aerospace structural scene because of their potential reduction of structural weights. Most impressive are those displaying high efficiency in carrying compressive loads and characterized by high modulus-to-density ratios.

The use of filamentary composites, such as high modulus glass in epoxy, boron fiber in epoxy, are some currently being developed, and many more composites are receiving considerable attention. Composites are not limited to plastic binders; metallic binders appear attractive for future applications. Steel wire in an aluminum matrix, and beryllium wire in an aluminum matrix are two examples of such composites.

Whiskers are potentially stronger than any other filamentary material because they are single crystals having nearly perfect structure and are receiving considerable evaluation for potential use.

Table 8-2

Material Properties versus Temperature for 2014-T6 Aluminum Clad

Temp (°F)	Percent σ_y at Room Temp	Percent σ_{ult} at Room Temp	σ_y ($x10^3$psi)	σ_{ult} ($x10^3$psi)	σ_o* ($x10^3$psi)	$\sigma_{0.85}$* ($x10^3$psi)	Percent E_c at Room Temp	E_c ($x10^6$psi)	ρ (lbs/ft^3)	μ
Room	100	100	56	64	63	58	100	10.7	174	0.30
0	101.5	102.5	57	65.5	64.5	59	101	10.8	174	0.30
- 50	103	105	58	67	66	60	102	10.9	174	0.30
-100	107	109	60	70	68.6	62	103	11.0	174	0.30
-150	109	111	61	71	70	63.3	103.5	11.1	174	0.30
-200	110	112.5	62	72	71	64	104	11.15	174	0.30
-250	113	123.5	63.5	79	77.9	65.5	105	11.25	174	0.30
-300	116	128	65	82	80.7	67.2	106	11.35	174	0.30

*The properties from -50° to -300°F have been obtained by using the same percent increase as for yield.

NOMENCLATURE

E_c Compressive modulus of elasticity (psi).

E_{sec} Compressive secant modulus (psi).

E_{tan} Compressive tangent modulus (psi).

η Tangent - secant modulus reduction factor.

η_w Tangent modulus reduction factor.

η_i Secant modulus reduction factor.

ρ Density of material (lbs/ft^3).

σ_{yield} Yield stress (psi).

σ_{ult} Ultimate stress (psi).

σ_o Secant yield stress at 0.70 E (psi).

$\sigma_{0.85}$ Secant yield stress at 0.85 E (psi).

μ Poisson's ratio.

Table 8-3

Material Properties versus Temperature for 7075-T6 Aluminum

Temp (°F)	Percent σ_y at Room Temp	Percent σ_{ult} at Room Temp	σ_y ($\times 10^3$ psi)	σ_{ult} ($\times 10^3$ psi)	σ_0 ** ($\times 10^3$ psi)	$\sigma_{0.85}$ * ($\times 10^3$ psi)	Percent E_c at Room Temp	E_c ($\times 10^6$ psi)	ρ (lbs/ft^3)	μ
Room	100	100	64	77	70	63	100	10.5	174.5	0.30
0	107	103.5	68.5	79.5	73.75	67.5	100.75	10.575	174.5	0.30
- 50	114	107	73	82	77.5	72	101.5	10.65	174.5	0.30
-100	117	110	75	85	79.5	73.5	102	10.7	174.5	0.30
-150	120	113	77	87	81.5	75.5	102.5	10.75	174.5	0.30
-200	125	116	80	89	84.5	78.5	103	10.85	174.5	0.30
-250	127	117	81	90	85.5	80	104	10.9	174.5	0.30
-300	130	121	83	93	88	82	106	11	174.5	0.30

* These properties from -50° to -300°F have been obtained by using the same percent increase as for the yield since the room temperature properties are almost identical.

**These properties from -50°F to -300°F have been obtained by using the average percent increase between that used for yield and ultimate.

Table 8-4

Material Properties versus Temperature for 2024-T4 Aluminum

Temp (°F)	Percent σ_y at Room Temp	Percent σ_{ult} at Room Temp	σ_y ($\times 10^3$ psi)	σ_{ult} ($\times 10^3$ psi)	σ_0 * ($\times 10^3$ psi)	$\sigma_{0.85}$ * ($\times 10^3$ psi)	Percent E_c at Room Temp	E_c ($\times 10^6$ psi)	ρ (lbs/ft^3)	μ
Room	100	100	42	63	46	43	100	10.7	172.8	0.3
0	100.5	100	42.25	63	46.25	43.25	102	10.9	172.8	0.3
- 50	101	100	42.5	63	46.5	43.5	104	11.1	172.8	0.3
-100	101	100	42.5	63	46.5	43.5	106	11.3	172.8	0.3
-150	102	101.5	43	64	47	44	107	11.45	172.8	0.3
-200	107	106	45	67	49	46	108	11.60	172.8	0.3
-250	113	108	47.5	68	52	48.5	110	11.8	172.8	0.3
-300	124	111	52	70	57	53.2	112	12.0	172.8	0.3

*These properties from -50° to -300°F have been obtained by using the same percent increases as for yield since the room temperature properties are approximately equal.

Table 8-5

Material Properties versus Temperature for 2219-T87 Aluminum

Temp (°F)	Percent σ_y at Room Temp	Percent σ_{ult} at Room Temp	σ_y ($x10^3$ psi)	σ_{ult} ($x10^3$ psi)	σ_o ($x10^3$ psi)	$\sigma_{o,85}$ ($x10^3$ psi)	Percent E_c at Room Temp	E_c ($x10^6$ psi)	ρ (lbs/ft^3)	μ
Room	100	100	50	62	52	50	100	10.4	172.8	0.30
0	102	102	51	63.25	52.25	51	100.5	10.45	172.8	0.30
- 50	104	104	52	64.5	52.5	52	101	10.5	172.8	0.30
-100	105	106	52.5	65.6	53	52.5	102	10.6	172.8	0.30
-150	107	107	53.5	66.3	55	53.5	103	10.7	172.8	0.30
-200	110	110	55	68.1	57	55	104	10.8	172.8	0.30
-250	113	114	56.5	70.6	59	56.5	106	11.0	172.8	0.30
-300	117	120	58.5	74.4	62	58.5	107	11.1	172.8	0.30

Table 8-6

Material Properties versus Temperature for 6A1-4V Titanium

Temp (°F)	Percent σ_y at Room Temp	Percent σ_{ult} at Room Temp	σ_y ($x10^3$psi)	σ_{ult} ($x10^3$psi)	σ_o* ($x10^3$psi)	$\sigma_{o,85}$* ($x10^3$psi)	Percent E_c at Room Temp	E_c ($x10^6$psi)	ρ (lbs/ft^3)	μ
Room	100	100	126	130	128	124	100	16	276	0.3
0	106	106	133.5	137.5	135.5	128	101	16.15	276	0.3
- 50	112	112	141	145	143.5	132.5	102	16.3	276	0.3
-100	117	118	148	154	151	146	103	16.5	276	0.3
-150	123	123	155	160	157.5	152.5	103.5	16.6	276	0.3
-200	128	128	162	166	164	158.5	104	16.65	276	0.3
-250	135	135	170	175	173	167.5	105	16.8	276	0.3
-300	144	144	182	187	184.5	178.5	107.5	17.2	276	0.3

*The same percent increases that were used for yield and ultimate were used for the secant yield stresses at 70 percent and 85 percent.

Table 8-7

Material Properties versus Temperature for AISI 4340 Alloy Steel

Temp (°F)	Percent σ_y at Room Temp	Percent σ_{ult} at Room Temp	σ_y (x10^3psi)	σ_{ult} (x10^3psi)	σ_0* (x10^3psi)	$\sigma_{0.85}$** (x10^3psi)	Percent E_c at Room Temp	E_c (x10^6psi)	ρ (lbs/ft^3)	μ
Room	100	100	242	260	255	225	100	29	483	0.3
0	100.5	101	243.5	262.5	257.5	222.5	101.7	29.5	483	0.3
- 50	101	102	245	265	260	227	103.5	30	483	0.3
-100	103	104	250	270	266	234	103.5	30	483	0.3
-150	107	106	260	275	270	238	103.5	30	483	0.3
-200	109.5	109.5	265	285	279	246	103.5	30	483	0.3
-250	115	111.5	280	290	284	251	105	30.5	483	0.3
-300	120	115	290	300	293	259	105	30.5	483	0.3

*** The same percent increases that are used for ultimate are used for the secant yield of 70 percent E.**
****The same percent increases that are used for yield are used for the secant yield at 85 percent E.**

Table 8-8

Material Properties versus Temperature for HK 31A-H24 Magnesium

Temp (°F)	Percent σ_y at Room Temp	Percent σ_{ult} at Room Temp	σ_y (x10^3psi)	σ_{ult} (x10^3psi)	σ_0* (x10^3psi)	$\sigma_{0.85}$* (x10^3psi)	Percent E_c at Room Temp	E_c (x10^6psi)	ρ (lbs/ft^3)	μ
Room	100	100	25	35	25	23.5	100	6.5	112	0.30
0	101.5	104	25.4	36.5	25.8	23.85	100	6.5	112	0.30
- 50	103	108	25.8	38	25.8	24.2	100	6.5	112	0.30
-100	106	117	26.5	41	26.5	24.9	101.5	6.6	112	0.30
-150	109	124	27.2	43.7	27.2	25.6	103	6.7	112	0.30
-200	112	131	28	46	28	26.3	104.5	6.8	112	0.30
-250	114	136.5	28.5	47.7	28.5	26.8	106	6.9	112	0.30
-300	116	142	29	50	29	27.2	108	7.0	112	0.30

*These properties from -50° to -300°F have been obtained by using the same percent increase as for the yield since the room temperature properties are approximately equal.

Table 8-9

Material Properties versus Temperature for PH15-7Mo, RH 950 Condition

Temp (°F)	Percent σ_y at Room Temp	Percent σ_{ult} at Room Temp	σ_y ($x10^3$ psi)	σ_{ult} ($x10^3$ psi)	σ_0 *** ($x10^3$ psi)	$\sigma_{0.85}$ ** ($x10^3$ psi)	Percent E_c * at Room Temp	E_c ($x10^6$ psi)	ρ (lbs/ft^3)	μ
Room	100	100	210	225	215	200	100	30	478	0.30
0	101.25	101.75	212.5	229	219	202	101.75	30.5	478	0.30
- 50	102.5	103.5	215.5	233.5	223	205	103.5	31	478	0.30
-100	106	107.5	222	242	232	212	103.5	31	478	0.30
-150	110	110	231	248.5	237	220	103.5	31	478	0.30
-200	114	113	240	255	244	228	103.5	31	478	0.30
-250	114	113	240	255	244	228	103.5	31	478	0.30
-300	114	113	240	255	244	228	103.5	31	478	0.30

* Assume same increases as AISI 4340, Table 8-7.

** The same percent increases that are used for yield are used for the secant yield at 85 percent E.

***The same percent increases that are used for ultimate are used for the secant yield at 70 percent E.

Table 8-10

Material Properties versus Temperature for Y5804, QMV-5 Beryllium*

Temp (°F)	Percent σ_y at Room Temp	Percent σ_{ult} at Room Temp	σ_y ($x10^3$psi)	σ_{ult} ($x10^3$psi)	σ_0 ($x10^3$psi)	$\sigma_{0.85}$ ($x10^3$psi)	Percent E_c at Room Temp	E_c ($x10^6$psi)	ρ (lbs/ft^3)	μ
Room	100	100	64.5	75	54	43.5	100	42	115	
- 50										
-100										
-150										
-200										
-250										
-300										

***Use room temperatures properties of beryllium from -50° to -300°F since applicable data is not available at this time.**

Many problems currently exist, from growing whiskers to conducting tests to prove performance, as well as high cost of whiskers at the present time. However, because of their exceptionally high strength they are attractive candidates as reinforcing agents.

When whiskers are incorporated in a matrix, the filaments are discontinuous. Consequently, the strength of such a composite depends primarily on the ability of the matrix to transmit the load by shear to each of the embedded whiskers. This means that the whiskers must be in intimate contact with and well bonded to the matrix before any appreciable strengthening of the composite can be observed. When stresses are effectively transferred to the reinforcing whiskers, the strength of the whiskers and their volume fraction essentially determine the strength of the composite.

Another area of potential improvement is associated with the use of shaped fibers designed to improve the transverse properties of a uniaxial composite. A process has been developed for the disposition of thin films of boron on a plastic substrate (Reference 37). The important characteristics of these thin films is that they have demonstrated the same high mechanical properties as boron filaments. By cementing together layers of these thin films, a laminated composite can be built up having biaxial properties approaching those of the primarily unidirectional properties of the filamentary composites. At present, the thickness of plastic substrate used limits the volume fraction of boron in the laminated film to 30 percent. This material has a modulus that is slightly lower than those of isotropic boron fiber epoxy composite and will differ little in performance from the latter material. However, Reference 37 projects ahead to 50 percent volume fraction boron; and it is anticipated that the performance of such a composite (yet to be evaluated) would be substantially superior to that for other boron/epoxy composites.

8.3 FABRICATION TECHNIQUES

The ideal materials usually have the characteristics and properties which make them difficult in either forming, machining, or joining. Therefore, some of the old reliable processes of metal forming are being adapted or modified to handle many of the new requirements as well as newer processes being developed to meet the increasing needs of the industry.

High-energy-rate forming methods are being developed and refined and in all probability will play a large role as a future fabrication technique. Most high-energy-rate forming methods are not really new, but the range of unique applications has broadened to increase their importance. Domes 10 feet in diameter are currently being formed by explosive forming, and studies are underway to provide the technology for explosively forming 10- to 50-foot diameter domes. Principal advantages of this process are very low capital investment required to form large parts and the low cost of dies that are required. However, prime limitation at the present time is the lack of understanding for controlling the effects of the many variables in the process.

Lasers, which at the present time are not much more than a laboratory curiosity, show tremendous potential as a future fabrication technique and possibly as an inspection method. The rate of advancement of this technique has been very rapid, but at the present time it is only in its infancy. Lasers have been used for drilling, milling, and welding. Inspection of materials is a possibility by taking minute samples of a material for analysis without imparing the usefulness of the parent material.

The demand, within the industry, for quality welds free from atmospheric impurities has led to the use of inert-gas welding and electron-beam welding methods. Inert-gas welding is conducted in an inert atmosphere to eliminate contaminations which normally cause cracks, porosity, and loss of ductility in a weld. Electron-beam welding is performed in a vacuum and is the cleanest welding method known. The method offers ultrahigh cleanliness and also a minimum of heat-affected area. The heat produced by electron-beam welding is capable of melting any known material. Furnace brazing is not a new process, but in the aerospace industry, it is finding applications to many complex assemblies that are not adaptable to other welding techniques and to the joining of dissimilar metals.

Machining operations, such as electric discharge, electrochemical, chemical milling, and ultrasonic vibration, are growing rapidly in application. The extremely fine detail that can be achieved with these processes, along with speed, relative simplicity, and cost of tooling are making them very attractive to industry.

The best structural materials and fabrication processes would be of limited use without the knowledge of how they could best be utilized in construction of vehicle components. Some of the typical construction techniques currently in use are monocoque, semimonocoque, integral stringer and ring, open faced corrugation, single faced corrugation, and honeycomb sandwich. Honeycomb sandwich construction, because it offers a substantial reduction in structural weight over other techniques, is receiving considerable attention.

8.4 INSPECTION TECHNIQUES

The primary purpose of inspection is to determine the quality of a part or material for the purpose of acceptance or rejection. Many of the current methods of inspection are not new, but have found application to aerospace structures. Inspection techniques, such as visual, pressure and leak, and penetrant, are not new, but will continue to play a large part in determining the adequacy of parts for specific applications. For example, visual inspection is the oldest and simplest method of inspection, but it is very important and sometimes reveals flaws that have not been detected by other methods of inspection. Visual inspection should always supplement other inspection methods.

X-ray and gamma ray radiographic inspection is one of the more widely used non-destructive inspection methods. Ultrasonic, eddy current, and thermal infrared inspections also are widely used. The selection of a particular inspection method is dependent upon the part or the material to be inspected. The choice of an inspection method, the technique applied, and the interpretation of inspection results requires skill and experience on the part of the inspector. Inspection standards are needed by inspectors to aid in evaluating the results of inspections so that acceptance or rejection can be based on standards rather than relying entirely on judgment.

In order to fulfill the needs of the advancing technology in materials and fabrication, inspection methods and techniques also must make advancements and new methods and instrumentation must be developed. The use of nondestructive inspection techniques has grown in the past few years and indications are that they will continue to grow with the use of newer construction techniques in the aerospace industry.

8.5 ADDITIONAL INFORMATION

A summary compilation of additional data and references on materials and fabrication is contained in an informal Technical Note, entitled "Aerospace Structural Materials, Fabrication Processes, and Inspection Techniques" prepared by General Electric Company during this study. A limited number of copies are available upon request through the NASA Mission Analysis Division.

REFERENCES

1. Martin Company Report, "NOVA Vehicle Systems Study—Part I, Volume III Configurations" (U), dated 3 April 1963 (NAS8-5135) (Confidential).

2. Martin Company Report, "NOVA Vehicle Systems Study—Part II, Volume III Configurations" (U), dated September 1963 (NAS8-5135) (Confidential).

3. Martin Company, NOVA TN-35, NOVA Preliminary Design Study, "Propellant Tank Pressurization System Study," dated February 1963 (NAS8-5135) (U).

4. Martin Company, PSTN-III-27, Post Saturn Launch Vehicle Study, "Propellant Tank Pressurization System Study," dated November 1964 (NAS8-11123) (U).

5. J.R. Scoggins and W.W. Vaughn, "Cape Canaveral Wind Shear Data (1 through 80 km) for Use in Vehicle Design and Performance Studies," NASA TND-1274 (U).

6. Air Force Series in Geophysics No. 140, "Proceedings of the National Symposium on Winds for Aerospace Vehicle Design—Volume II," dated March 1962 (U).

7. J. Muraca, "An Empirical Method for Determining the Static Distributed Aerodynamic Loads on Axisymmetric Multistage Launch Vehicles," NASA TND-3283, March 1966 (U).

8. The Boeing Company, "Aerodynamic Pressures and Loads—WS—133B—Minuteman" (U), Boeing Report No. D2-14135 Volume III, 27 April 1963 (Confidential).

9. S.L. Treon, et al., "Effect of Nose Shape and Afterbody Flare on the Transonic Characteristics of a Low Fineness Ratio Body of Revolution" (U), NASA TMX-164, March 1960 (Confidential).

10. MSFC Memorandum, "Saturn V Design Ground Rules," M-P&VE-VA-102-63, dated 20 May 1963 (U).

11. NASA Space Vehicle Design Criteria, "Prelaunch Ground Wind Loads," NASA SP-8008, dated November 1965 (U).

12. "Saturn V Launch Vehicle Design Data" (U), MSFC IN-P&VE-62-2, 17 December 1962 (Confidential).

13. N.E. Munch, "Technical Memorandum on the Influence of Wind Criteria on Saturn V Launch Vehicle Structural Weight," General Electric Company, Apollo Support Department, IE-M-8, dated 27 March 1964 (U).

14. Martin Company PSTN-III-12, "Controls Analysis Post Saturn Vehicle," dated August 1964 (NAS8-11123) (U).

15. Martin Company PSTN- III-29, "Thrust Vector Control Study Post Saturn Vehicle Systems Study" (U), Contract NAS8-11123 (Confidential).

16. Pratt and Whitney Aircraft, "Plug Cluster Nozzle Study" (U), NAS8-11023, dated 8 September 1964 (Confidential).

17. A.R. Graham, "Plug Nozzle Handbook" (U), General Electric Company MTSD, NAS9-3748, dated 14 February 1966 (Confidential).

18. B.W. Rosen, "Elastic Analysis of Fibrous Composites and Non-Homogeneous Laminates," General Electric Company, Space Sciences Laboratory, dated June 1966 (U).

19. Office of Manned Space Flight, Apollo Program Office, "Structural Systems and Program Decisions," Volumes 1 and 2, NASA SP-6008 (U).

20. B.W. Rosen, "Elastic Analysis of Fibrous Composites and Non-Homogeneous Laminates," General Electric Company, Space Sciences Laboratory, Mechanics Section Report No. 66-101, dated June 1966 (U).

21. S. F. Kahn, "Results of a Study to Determine Load Distributions (Normal and Axial) on a Series of Large Scale Booster Configurations," General Electric Company, Re-entry Systems Department, Aerodynamics Technology Component Data Memorandum 66-18, dated 12 September 1966 (U).

22. L. Lackman and J. Penzien, "Buckling of Circular Cones Under Axial Compression," ASME Paper No. 60-APM-17, 18 June 1959 (U).

23. H. Becker, "General Instability of Stiffened Cylinders," NACA TN 4237, July 1958 (U).

24. Z. Hashin and B.W. Rosen, "The Elastic Moduli of Fiber-Reinforced Materials," Journal of Applied Mechanics, Volume 31E, June 1964 (U).

25. N. F. Dow and B.W. Rosen, "Structural Efficiency of Orthotropic Cylindrical Shells Subjected to Axial Compression," AIAA Journal, Volume 4, Number 3, pp 481-485, March 1966 (U).

26. B.W. Rosen and N. F. Dow, "Influence of Constituent Properties Upon the Structural Efficiency of Fibrous Composite Shells," AIAA Journal of Spacecraft and Rockets, September 1966 (U).

27. W. B. Grossman, "Investigation of Maximum Stresses in Long, Pressurized Cylindrical Shells," AIAA Journal, May 1963, p 1129 (U).

28. G. B. Cline, "Effect of Internal Pressure on the Influence Coefficients of Spherical Shells," Journal of Applied Mechanics, March 1963, p 91 (U).

29. B.C.F. Wei, "Structural Analysis of Solid Propellent Rocket Casings," American Rocket Society preprint 1590-61, February 1961 (U).

30. Martin Company NTN-14, "Structural Design Methods for Conceptual Design, Part I, 4 March 1963 (U).

31. R. F. Crawford and A. B. Burns, "Minimum Weight Potentials and Design Information for Stiffened Plates and Shells," 2424-62 American Rocket Society, Launch Vehicles: Structures and Materials Conference, 3-5 April 1962, Ramada Inn, Phoenix, Arizona (U).

32. F.R. Shanley, "Weight-Strength Analysis of Aircraft Structures," Dover Publications, Inc., New York, New York, 1960, p 15 and p 67 (U).

33. E. Sechler and G. Dunn, "Airplane Structural Analysis and Design," Dover Publications, Inc., New York, New York, 1963, pp 168, 169 (U).

34. General Electric Company, Schedule No. ARC-1, "Study of Structural Weight Sensitivities for Large Rocket Systems," 15 August 1966 (U).

35. Friedman, E., "A Tensile Failure Mechanism for Whisker Reinforced Composites," Paper No. 4A, presented at 22nd Annual SPI Reinforced Plastics Division Conference, Washington, D. C., January 1967.

36. Rosen, B. Walter, "Mechanics of Composite Strengthening", Fiber Composite Materials, ASM, Metals Park, Ohio, 1965.

37. Anon, "Advanced Filaments and Composites Program Review," WPAFB, December 6-8, 1965.

38. Anon, "Buckling of Thin-Walled Circular Cylinders", NASA SP-8007, pp 13 and 37, September 1965.

39. "Study of the Relationship of Properties of Composite Materials to Properties of Their Constituents", Quarterly Progress Report #3, NASw-1377, February 15, 1967, to be published.

40. Rosen, B. Walter and L. Shu, "Application of the Methods of Limit Analysis to the Evaluation of the Strength of Fiber-Reinforced Composites", to be published.

41. Anon, George C. Marshall Space Flight Center, Astronautics Structural Manual.

42. Roark, R. J., "Formulas for Stress and Strain", McGraw-Hill Book Company, Inc., New York Fourth Edition, 1965.

43. Williams, C. D., and Harris, E. C., "Structural Design In Metals", The Ronald Press Company, New York, New York, Second Edition, 1957.

44. Hetenyi, M., "Beams On Elastic Foundation". Ann Arbor, The University of Michigan Press, 1961.

45. Seely, F. B. and Smith, J. O., "Advanced Mechanics of Materials". John Wiley and Sons, Inc., New York. Second Edition, 1952.

46. Harris, C. M. and Crede, C. E., "Shock and Vibration Handbook, Vol. I. McGraw-Hill Book Co., Inc., New York, 1961.

47. Flugge, W., "Stress in Shells". Springer-Vertag, 1960.

48. Tong, K. N., "Theory of Mechanical Vibrations". John Wiley and Sons, Inc., New York, 1963.

49. Martin Company PSTN-III-5, "Structures-TIORE-3A Thrust Structure Design and Engine Vibration Analysis", June 1964 Contract NAS8-11125.

50. Nishioka, K., "Effect of Pressure Coupling On Discontinuity Stresses in Shells". MS Thesis, Oregon State University, June 1966.

51. Wilson, P. E. and Speir, E. E., "Nonlinear Pressure Coupling In Cylindrical Shell Analysis", AIAA Journal, February 1964, pp 370-372.

52. Horvey, G. and Clausin, I. M., "Membrane and Bending Analysis of Axisymmetrically Loaded Axisymmetric Shells, J. Applied Mechanics, March 1955, pp 25-30.

53. Hodge, P. G., Jr., "Plastic Analysis of Structures". McGraw-Hill Book Co., New York, 1959.

54. Ramberg, W. and Osgood, W. R., "Description of Stress-Strain Curves by Three Parameters". NACA TN 902, July 1943.

55. Hoffman, O., and Sachs, G., "Introduction to the Theory of Plasticity for Engineers". McGraw-Hill Book Co., New York, 1953.

56. Mendelson, A., and Manson, S. C., "Practical Solution of Plastic Deformation Problems in Elastic—Plastic Range". NACA TN 4088, September 1957.

57. "Thin Booster Walls Yield Payload Hike", Technology Weekly, December 12, p. 35.

58. Micks, W. R., "Minimum Weight of Stiffened Cylindrical Shells in Pure Bending", J. Aero. Sci. Vol. 17, April 1950, pp. 211-216.

59. Morita, W.H., "Parametric Booster Tankage Design Studies", Paper presented at the AIAA Fifth Annual Structures and Materials Conference, Palm Springs, California, April 1964.

60. Gomersall, E. W., Bucy, R. W., and Nishioka, K., "A Survey of Advanced Structural Technologies Applicable to Future Large Launch Vehicles", a paper presented at the SAE Annual Launch Vehicle Symposium—Second Space Technology Conference, NASA/Ames Research Center, May 12, 1967.

61. Battelle Memorial Institute, "The Current Status and 1970 Potential of Selected Defense Materials", DMIC Memorandum 183, October 31, 1963.

APPENDIX A

DESCRIPTION OF THE SSPD COMPUTER PROGRAM

APPENDIX A

DESCRIPTION OF THE SSPD COMPUTER PROGRAM

A1 GENERAL

Extensive utilization of computer programs has been effective in providing optimized structural weights in a short period of time. The overall arrangement of the computational modules was presented in Volume I and is repeated here for clarity (see Figure A-1).

The first step in the analysis is to determine the loads which are imposed on the launch vehicle structure by external forces such as winds, engine thrust loads, and tank pressures. The loads then are analyzed for specified material properties and types of construction to determine the lowest structural weight which is required to prevent all failure modes considered.

The GASP, LASS-1, and SWOP modules are included under the general heading, Structural Systems and Program Decisions (SSPD) computer program. The SSPD computer program, including all equations and typical printouts, is documented in Reference 19. The SSPD computer program is used for the analysis of isotropic materials only, but the load intensities (or stress resultants) derived by the program are used as inputs to the LILAC and SPACE programs to compute optimized structural weights for anisotropic, composite materials. Equations for the LILAC and SPACE computer programs are documented in Reference 20.

The large size of the computer programs mentioned here precludes an exhaustive description in this volume of all the features that are available to the user. Rather, the salient points of each of the computational modules which are pertinent to this study will be presented, and the reader is referred to the parent documents (References 19 and 20) for more detail.

A2 DESCRIPTION OF GASP COMPUTATIONAL MODULE

A2.1 GENERAL DESCRIPTION AND ORGANIZATION

The GASP module is a rigid-body trajectory analysis which operates with three degrees of freedom (X, Z, and θ) as represented in Figure A-2. The vehicle characteristics

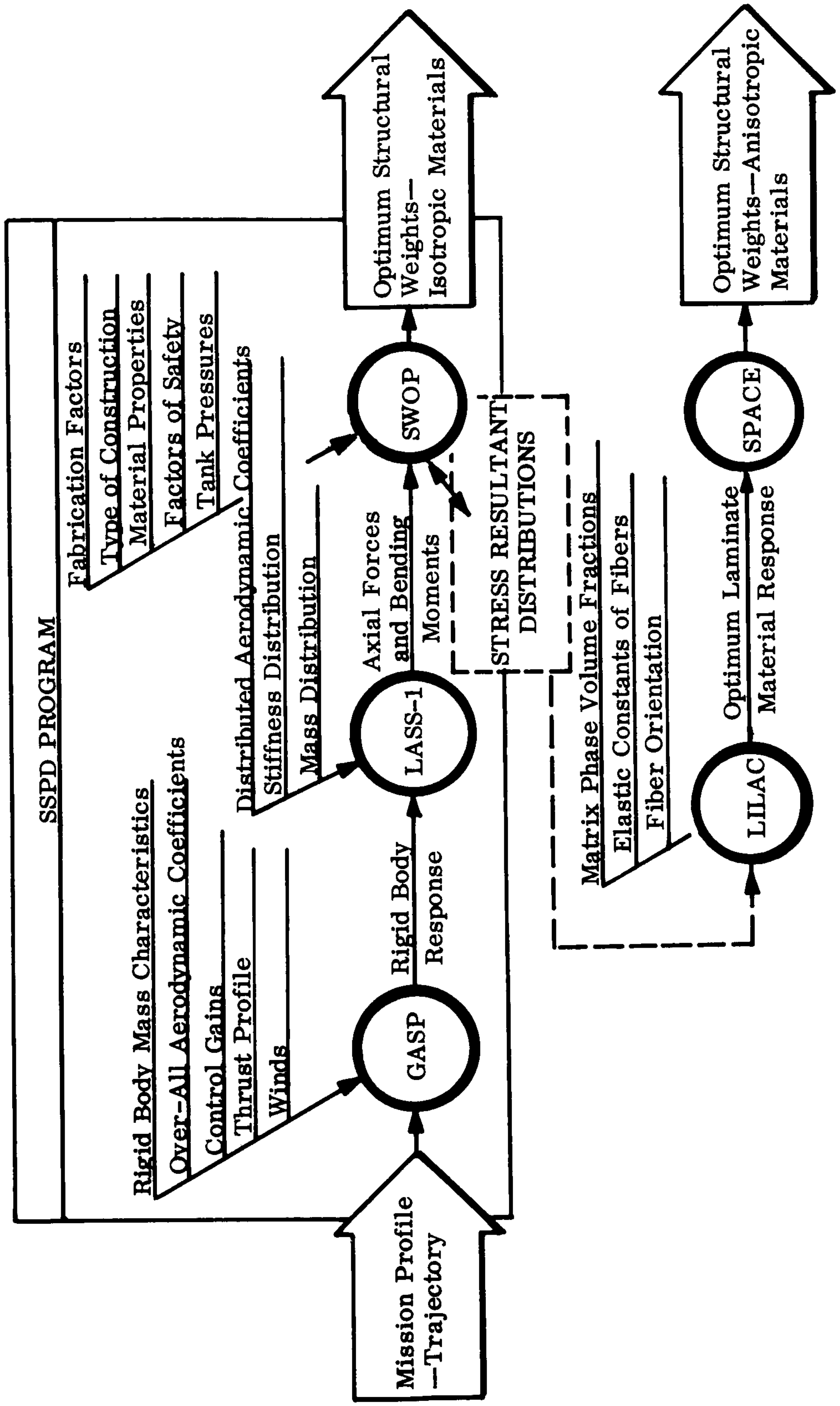

Figure A-1. Structural Weight Optimization Computer Programs

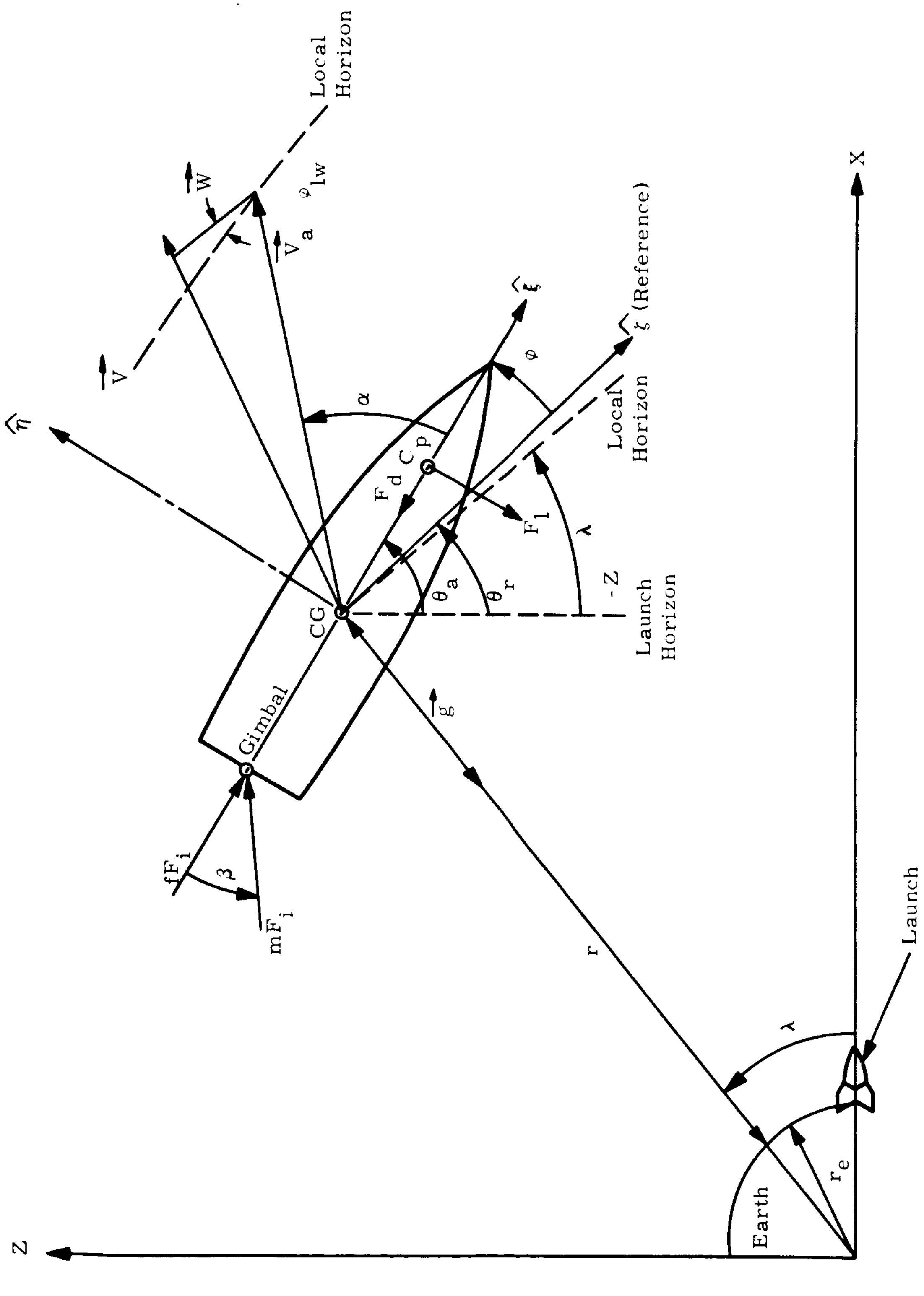

Figure A-2. Reference Coordinates for Wind Stress Launch Simulation Analysis and the environment to which it is exposed are specified as input parameters in tabular form. The analysis, in general, calculates the rigid body response of an artificially stabilized space vehicle as it is flown through a synthetic wind profile. Specific input and output parameters are listed in Table A-1. At any instant, the rigid body model of the vehicle is characterized by its total mass, pitch moment of inertia, total aerodynamic force, center of pressure location, and total thrust. At a given altitude, the environment is described by the local wind velocity and by the properties of the atmosphere according to the 1959 ARDC model. A control scheme is introduced to stabilize the space vehicle utilizing thrust-vector-control (TVC). The equations of motion then are integrated using a Runge-Kutta technique to determine the position, velocity, and accelerations of the space vehicle throughout the flight.

Table A-1

GASP Input and Output Summary

Major Input Parameters
• Overall normal aerodynamic force coefficient versus Mach number.
• Overall axial aerodynamic force coefficient versus Mach number.
• Center of pressure location versus Mach number.
• Rigid body polar inertia versus vehicle weight.
• Center of gravity location versus vehicle weight.
• Control system gains versus flight time.
• Wind profile.
• Total initial weight and nominal weight rate.
• Vacuum thrust of engines.
• ARDC atmosphere model.
• Pitch rate profile.
Major Output Parameters
• Engine gimbal angle versus flight time.
• Mach number versus flight time.
• Lateral acceleration versus flight time.
• Angular acceleration versus flight time.
• Angle of attack versus flight time.
• Dynamic pressure versus flight time.

A2.2 MAJOR EQUATIONS OF GASP MODULE

The equations of motion for the rigid body are given by,

$$\ddot{X} = \frac{(F_{ax} + F_x)}{m} + g_x$$

$$\ddot{Z} = \frac{(F_{az} + F_z)}{m} + g_z$$

$$\dot{\omega}_p = \ddot{\theta}_a = \frac{T_{tot}}{I_p}$$

where:

$\ddot{X}$, $\ddot{Z}$, $\ddot{\theta}_a$	are the components of the acceleration vector.
F_{ax} and F_{az}	are the components of axial drag referred to inertial coordinates.
F_x and F_z	are the components of the thrust referred to inertial coordinates.
g_x and g_z	are the components of the acceleration of gravity referred to inertial coordinates.
T_{tot}	is the total moment about the pitch axis.
I_p	is the polar moment of inertia about the pitch axis.
m	is the mass of the vehicle.

The components of aerodynamic force in the $\hat{\eta} - \hat{\xi}$ coordinate system are given by the expressions

$$\vec{F}_d = -C_D S q \hat{\xi}$$

$$\vec{F}_l = C_{Z_\alpha} S q \alpha \hat{\eta}$$

where:

F_d	is the magnitude of the axial force.
F_l	is the magnitude of the normal force.
C_D	is the axial force coefficient.
S	is the reference area.
C_{Z_α}	is the gradient of the normal force coefficient.
α	is the angle of attack.

q	is the dynamic pressure
$\hat{\xi}$ and $\hat{\eta}$	are unit vectors.

These components of aerodynamic force $\vec{F}_d$ and $\vec{F}_l$ are rotated to the inertial coordinates X and Z by the expressions,

$$F_{ax} = F_d \cdot \xi_x + F_l \frac{\left(\xi_x \cos\alpha - \frac{\dot{X}_a}{|V_a|}\right)}{\sin\alpha}$$

and

$$F_{az} = F_d \cdot \xi_z + F_l \frac{\left(\xi_z \cos\alpha - \frac{\dot{Z}_a}{|V_a|}\right)}{\sin\alpha}$$

where:

$|V_a| = \left(\dot{X}_a^2 + \dot{Z}_a^2\right)^{\frac{1}{2}}$ is the magnitude of the relative wind velocity whose components are $\dot{X}_a$ and $\dot{Z}_a$.

ξ_Z, ξ_X are direction cosines.

The moments acting on the vehicle due to the aerodynamic loads are:

$$T_l \hat{\zeta} = (-F_l)\hat{\eta} \times (CP - CG)\hat{\xi}$$

where:

$\hat{\zeta}, \hat{\eta}, \hat{\xi}$	are orthogonal unit vectors.
CP	is the distance from the engine gimbal point to the center of pressure.
CG	is the distance from the engine gimbal point to the center of gravity.

The other external force acting on the vehicle is the thrust of the engines. The vehicle has f fixed engines and m gimballed engines, each with a thrust of F_i where,

$$F_i = F_{vac} - PAe$$

where:

F_{vac}	is the vacuum thrust of the engine.
P	is the local atmospheric pressure.
A	is the nozzle throat area.
e	is the nozzle expansion ratio.

The axial and normal components of thrust are, respectively,

$$F_{t_\xi}\hat{\xi} = (f F_i + m F_i \cos\beta)\hat{\xi}$$

$$F_{t_\eta}\hat{\eta} = (m F_i \sin\beta)\hat{\eta}$$

where β is the gimbal angle of the movable engines. Referring these components of thrust to the X-Z coordinate system,

$$F_X = F_{t_\xi} \cdot \xi_X + F_{t_\eta} \cdot \eta_X$$

$$F_Z = F_{t_\xi} \cdot \xi_Z + F_{t_\eta} \cdot \eta_Z$$

The moment applied to the vehicle due to the thrust loads is,

$$T_t\hat{\zeta} = F_{t_\eta}\hat{\eta} \times (-CG)\hat{\xi}$$

where T_t is the magnitude of the control moment acting in the $\hat{\zeta}$ direction.

The total moment acting on the vehicle is, therefore,

$$|T_{tot}|\hat{\zeta} = (T_t + T_l)\hat{\zeta}$$

The engine gimbal angle required for control is,

$$\beta = K_\theta \phi + K_r \dot{\phi}$$

where K_θ and K_r are time varying control gains and ϕ and $\dot{\phi}$ are the errors in rate of angular displacement and angular displacement, respectively, given by the expressions,

$$\phi = \theta_a - \theta_r$$

$$\dot{\phi} = \dot{\theta}_a - \dot{\theta}_r$$

where θ_a and $\dot{\theta}_a$ are the actual instantaneous values of pitch and pitch rate and θ_r and $\dot{\theta}_r$ are the desired values for pitch and pitch rate.

The components of gravitational acceleration are given by,

$$g_X = \frac{-GmX}{r^3}$$

$$g_Z = \frac{-GmZ}{r^3}$$

where:

$r = (X^2 + Z^2)^{\frac{1}{2}}$ = radius from the origin to the vehicle.

G is the universal gravitational constant.

m is the instantaneous mass of the vehicle.

The required input variables listed in Table A-1 are entered in tabular form, and linear interpolation is used to find instantaneous values. The forces then are entered into the equations of motion, and a Runge-Kutta integration method is used to evaluate the output parameters throughout the flight.

A3 DESCRIPTION OF LASS-1 COMPUTATIONAL MODULE

A3.1 GENERAL DESCRIPTION AND ORGANIZATION

The LASS-1 module calculates the bending moment distributions and axial force distributions of the vehicles at each of several specific design points throughout the flight. There are, of course, an infinite number of instantaneous time points that could be analyzed throughout the flight of a vehicle, but a relatively small number of points will serve to describe the worst loading conditions. The following five design points were considered.

- Prelaunch—Pressurized
- Prelaunch—Unpressurized
- Maximum $q\alpha$ Product
- Maximum Pressure on Tank Bottom Heads
- Maximum Thrust

The two inflight design points (maximum $q\alpha$ product and maximum thrust) were selected on the basis of the results of the rigid-body analysis. The prelaunch design conditions were also included to insure a complete loads envelope.

At each design point, the distribution of aerodynamic forces and mass along the vehicle axis was established. The amount of tabular input data for the LASS-1 program was, therefore, quite large. Table A-2 lists the major input and output parameters for the LASS-1 module. The aerodynamic coefficient distributions along the vehicle axis were entered as input for several arbitrary Mach numbers which span the region of interest in the analysis. For the analysis at a specific design point, a linear interpolation was performed to find the aerodynamic coefficient distribution for the particular mach number of interest.

The mass distribution was determined in a similar manner. Based on a propellant burn rate and mixture ratio, a relationship between propellant loading and flight time was established. For a specified flight time, expended propellants were extracted from the tops of the proper tanks to obtain the mass distribution to be used in the analysis. The flight times and the Mach numbers associated with the design points were, of course, those calculated in the rigid-body analysis described earlier.

A3.2 MAJOR EQUATIONS OF LASS-1 MODULE

A3.2.1 Prelaunch Analysis

During prelaunch and while on the launch pad, the vehicle was subjected to a ground wind profile. The wind loads caused large bending moments to be applied to the base of the structure (sometimes the critical loading condition) for certain portions of the vehicle structure.

The local dynamic pressure is,

$$q_j = \frac{1}{2}\rho v_j^2$$

where:

q_j	is the dynamic pressure at station j.
v_j	is the ground wind velocity at station j.
ρ	is the density of the atmosphere at the launch pad.

The local lateral wind force is,

$$d_j = C_{z_{Co_j}} q_j S$$

Table A-2

Major Input and Output Summary for LASS-1 Module

Major Input Parameters
• Normal force coefficient distributions for several fixed Mach numbers.
• Ground wind profile.
• Lateral bending stiffness distribution.
• Axial force coefficient distributions for several fixed Mach numbers.
• Dry weight distribution of vehicle.
• Propellant weight distribution with associated burn times.
• Total thrust versus time.
• Several time points which are identified as design points are selected from the GASP outputs with the associated angle of attacks, Mach numbers, dynamic pressures, and engine gimbal angles.
Major Output Parameters
• Bending moment distribution for each design time.
• Axial force distribution for each design time.

where:

d_j	is the lateral aerodynamic force at station j.
$C_{z_{Co_j}}$	is the aerodynamic coefficient at station j.
S	is the reference area of the launch vehicle.

Then the shear distribution, V_j, is found by the operation,

$$V_j = \sum_{j=1}^{j} d_j$$

The moment distribution, M_{w_i}, due to these wind forces is,

$$M_{w_i} = \sum_{j=1}^{i} V_j \Delta X_{j-1}$$

where:

$$\Delta X_{j-1} = X_j - X_{j-1}$$

and X_j is the longitudinal distance from the reference point to station j.

There were also wind loadings resulting from vortex shedding which would be in addition to the moment distribution, M_{w_i}. The lateral loads due to vortex shedding were assumed to be maximum at the tip of the vehicle and to attenuate to zero at the base of the vehicle in a linear fashion. The magnitude of this loading was selected such that the bending moment at the base of the vehicle due to vortex shedding was half the maximum bending moment due to direct wind loads. The vortex shedding bending moment M_{v_i} was, therefore, found from the equation

$$M_{v_j} = \frac{0.25\left(M_{w_{i=H_b}}\right)}{(\ell - H_b)^3} (X_i^3 - 3H_b X_i^2 + 6H_b \ell X_i - 3H_b \ell^2 - 3\ell^2 X_i + 2\ell^3)$$

where:

ℓ is the length of the vehicle

H_b is the station at the base of the vehicle where the bending moment is restrained.

For the axial force analysis, the weight distribution was determined by considering the propellant remaining in the tank as a point mass. This point mass acts at the attachment point of the bottom head of the tank to the outer skin.

The resulting weight distribution was designated by the symbol Λ. The total weight, W, of the vehicle was, therefore,

$$W = \sum_j \Lambda_j$$

The axial force distribution, δ_i, was, therefore, given by the operation,

$$\delta_i = \sum_{j}^{i} \Lambda_j$$

A3.2.2 Inflight Analysis

The weight distribution for the lateral analysis was determined by adding the dry weight distribution and the remaining propellant distribution, station by station. The resulting weight distribution, w_i, is then used to calculate the total weight, W, mass moment of inertia, I_p, and station of the center of gravity, CG, by the following equations,

$$W = \sum_{i} w_i$$

$$I_p = \frac{1}{g} \sum (CG - X_i)^2 w_i$$

$$CG = \frac{\sum_{i} w_i X_i}{W}$$

The lateral aerodynamic force distribution, f_i, is given by the equation,

$$f_i = S C_{z_{\alpha_i}} \alpha q_i$$

where $C_{z_{\alpha_i}}$ is the gradient of the normal aerodynamic force distribution at station i; S is the reference area; α is the angle of attack; and q_i is the local dynamic pressure.

The total normal aerodynamic force, N, is therefore,

$$N = \sum_{i} f_i$$

and the location of the center of pressure is,

$$CP = \frac{\sum_i f_i X_i}{N}$$

The total aerodynamic overturning moment, M_a, is then,

$$M_a = N(CP - CG)$$

The lateral component of the thrust vector is,

$$T_g = T \sin \beta$$

where:

T_g	is the lateral component of thrust.
T	is the magnitude of the thrust.
β	is the engine gimbal angle.

The total control moment, M_c, is given by the expression,

$$M_c = (C_o - CG)\,T_g - \sum_i M_{s_i} + \sum_i (CG - X_i)\,F_{s_i}$$

where

C_o	is the engine gimbal station.
M_{s_i}	is an externally applied couple at station i.
F_{s_i}	is an externally applied lateral force at station i.

The lateral rigid-body acceleration, ϵ, is therefore,

$$\epsilon = \frac{\left(N + T_g - \sum_i F_{s_i}\right)g}{W}$$

and the angular rigid-body acceleration, Ω, is,

$$\Omega = \frac{M_c + M_a}{I_p}$$

The lateral acceleration, a_i, at each station along the axis of the vehicle is therefore,

$$a_i = \epsilon + \Omega (X_i - CG)$$

The resultant inertia forces, r_i, are therefore,

$$r_i = - \frac{1}{g} (a_i w_i)$$

The total force distribution, F_i, for equilibrium is then found by summing all the separate force distributions,

$$F_i = r_i + f_i + (T_g)_{i=C_o} - F_{s_i}$$

The force distribution is integrated to give the shear distribution, V_i,

$$V_i = \sum_j^i F_j$$

and the shear distribution is integrated and added to M_{s_i} to get the total bending moment distribution M_i,

$$M_i = \sum_j^i (V_j \Delta X_j) + M_{s_i}$$

For the axial force analysis, the weight distribution was determined by considering the propellant remaining in a tank as a point mass. This point mass acts at the attachment point of the bottom head of the tank to the outer skin. The resulting weight distribution is designated by the symbol Λ_i.

The external forces acting on the vehicle in the axial direction were the thrust and the drag forces. The axial component of thrust, T_a, is,

$$T_a = T \cos \beta$$

and the drag force distribution, μ_i, is,

$$\mu_i = S C_{d_i} q_i$$

where:

C_{d_i} is the axial drag coefficient at station i.

The total drag force D is therefore,

$$D = \sum_i \mu_i$$

The axial acceleration, ϕ, is therefore,

$$\phi = \frac{(T_a - D) g}{W}$$

and the axial force distribution, δ_i, is

$$\delta_i = - \sum_j^i \left(\mu_j + \frac{\phi}{g} \Lambda_j \right) + (T_a)_{i=C_o}$$

A4 DESCRIPTION OF SWOP COMPUTATIONAL MODULE

A4.1 GENERAL DESCRIPTION AND ORGANIZATION

In the SWOP module, the vehicles are described as a collection of thin shells of revolution. The geometry of the shells can be either conical, cylindrical, elliptical, or spherical. Other important input parameters are the tank propellant loadings, tank pressure profiles, and the bending moment and axial force distributions for each design condition. The latter is read in directly from the tape written by the LASS-1 module. It is also required to specify the factors of safety to be used in the analyses as well as the materials and types of construction.

Presently, the SWOP module has the capability of analyzing any of the eight types of construction which are in Figure A-3. Each type of construction is subject to certain practical constraints which are summarized in Table A-3. For convenience, certain of these constraints are stored within the computer program, but the values of these constraints may be changed if the need arises. Other constraints must be supplied as input for each run. Table A-3 also lists a fabrication factor for each type of construction. The fabrication factor is used to increase the idealized structural weight to account for noncalculable items. These factors have been estimated from experience on various structural designs and may be updated as applicable data becomes available.

Properties of several common materials are also stored within the computer for easy access. Those materials listed below are specified in any computer run by giving the identification number of the material.

1.	Aluminum	7075-T6
2.	Aluminum	2024-T4
3.	Aluminum	2014-T6
4.	Aluminum	2219-T87
5.	Magnesium	HK 31A-H24
6.	Beryllium	Y5804, QMV-5
7.	Stainless Steel	15-7
8.	Steel	AISI 4340 Alloy
9.	Titanium	6AL-4V

Other materials can be used by the program by entering the necessary data as input in tabular form. The parameters which are necessary to define a material completely are illustrated by the typical example of Table A-4. The material properties are tabulated as a function of temperature, and a linear interpolation routine is used to find the properties at the temperature of each particular station of the vehicle. The material properties σ_o and $\sigma_{0.85}$ are used to describe the shape of the stress-strain curve in the Ramberg-Osgood relationship. The definitions of these two variables are understood by examining the typical stress-strain curve of Figure A-4.

The organization of the SWOP module is represented in Figure A-5. An executive control program is used to process input and output as well as controlling the separate elements of the module. In the normal operation of SWOP, the stress element is the first to be used. In stress, all the loads on the vehicle including bending moments, axial forces, and tank pressures are resolved into orthogonal stress resultants in the plane of the shells. All loads are considered to be axisymmetric where the equivalent axial force F_{eq} due to the bending moment is given by,

$$F_{eq} = \frac{2M}{r}$$

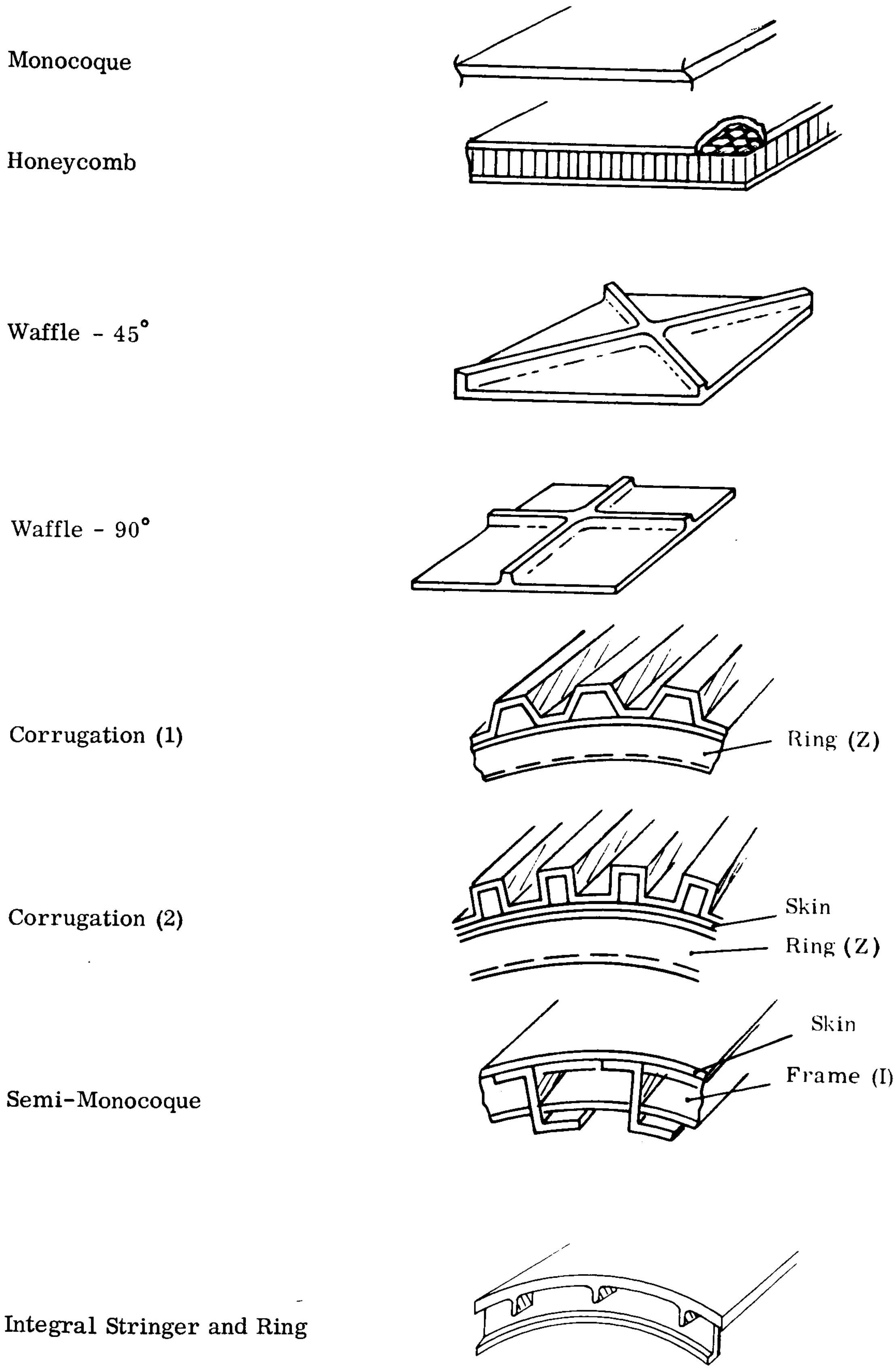

Figure A-3. Types of Construction Considered in SWOP

Table A-3

Material Parameters for Various Types of Construction

Type Construction	Parameter	Limiting Value (inches)						Fabrication Factor
		Aluminum	Magnesium	Steel	Titanium	Fiber-glass	Beryllium	
Monocoque	Skin Thickness - Minimum	.020	.032	.020	.020	.020	.020	1.05
Honeycomb Sandwich	Face Thickness - Minimum	.012	.016	.005	.005	.030	.012	1.25
	Core Thickness - Minimum	.125	.125	.125	1.25	.125	.125	
	- Maximum	←		Input			→	
	Core Density (Modulus) - Minimum	←		Input			→	
	- Maximum	←		Input			→	
	Cell Diameter - Minimum	←		Input			→	
Waffle - 45° and 90°	Rib Spacing - Minimum	≥ Cutting Head Diameter + Rib Thickness						
	Rib Thickness - Minimum	.080	.080	.080	.080	-	.080	1.20
	Skin Thickness - Minimum	.080	.080	.080	.080	-	.080	
	Over-All Thickness - Minimum	←		Input			→	
	- Maximum	←		Input			→	
	Rib Spacing - Maximum	←		15 x Overall Height			→	
Corrugation	Skin Thickness - Minimum	.020	.032	.020	.020	.020	.020	1.20
	Corrugation Thickness - Minimum	.020	.032	.020	.020	.020	.020	
	Depth - Minimum	←		Input			→	
	- Maximum	←		Input			→	
	Ring Thickness - Minimum	.020	.032	.020	.020	.020	.020	
Semi-Monocoque	Skin Thickness - Minimum	.020	.032	.020	.020	.020	.020	1.20
	Ring Spacing - Minimum, Maximum	←		Input			→	
	Stringer Spacing - Minimum, Maximum	←		Input			→	
	Ring/Stringer Height - Minimum	←		Input			→	
	- Maximum	←		Input			→	
	Ring/Stringer Thickness - Minimum	←		Input			→	
Integral Ring and Stringer	Skin Thickness - Minimum	.080	.080	.080	.080	-	.080	1.20
	Ring Thickness - Minimum	.080	.080	.080	.080	-	.080	
	Stringer Thickness - Minimum	.080	.080	.080	.080	-	.080	
	Ring/Stringer Height - Minimum	←		Input			→	
	- Maximum	←		Input			→	
All Construction	Sheet Length - Maximum	←		Input			→	

Table A-4

Material Properties versus Temperatures for 7075-T6 Aluminum

Temp (°F)	Percent σ_y at Room Temp	Percent σ_{ult} at Room Temp	σ_y ($x10^3$psi)	σ_{ult} ($x10^3$psi)	σ_0 ($x10^3$psi)	$\sigma_{0.85}$ ($x10^3$psi)	Percent E_c at Room Temp	E_c ($x10^6$psi)	ρ (lbs/ft^3)	μ
Room	100	100	64	77	70	63	100	10.5	174.5	0.30
0	107	103.5	68.5	79.5	73.75	67.5	100.75	10.575	174.5	0.30
- 50	114	107	73	82	77.5	72	101.5	10.65	174.5	0.30
-100	117	110	75	85	79.5	73.5	102	10.7	174.5	0.30
-150	120	113	77	87	81.5	75.5	102.5	10.75	174.5	0.30
-200	125	116	80	89	84.5	78.5	103	10.85	174.5	0.30
-250	127	117	81	90	85.5	80	104	10.9	174.5	0.30
-300	130	121	83	93	88	82	106	11	174.5	0.30

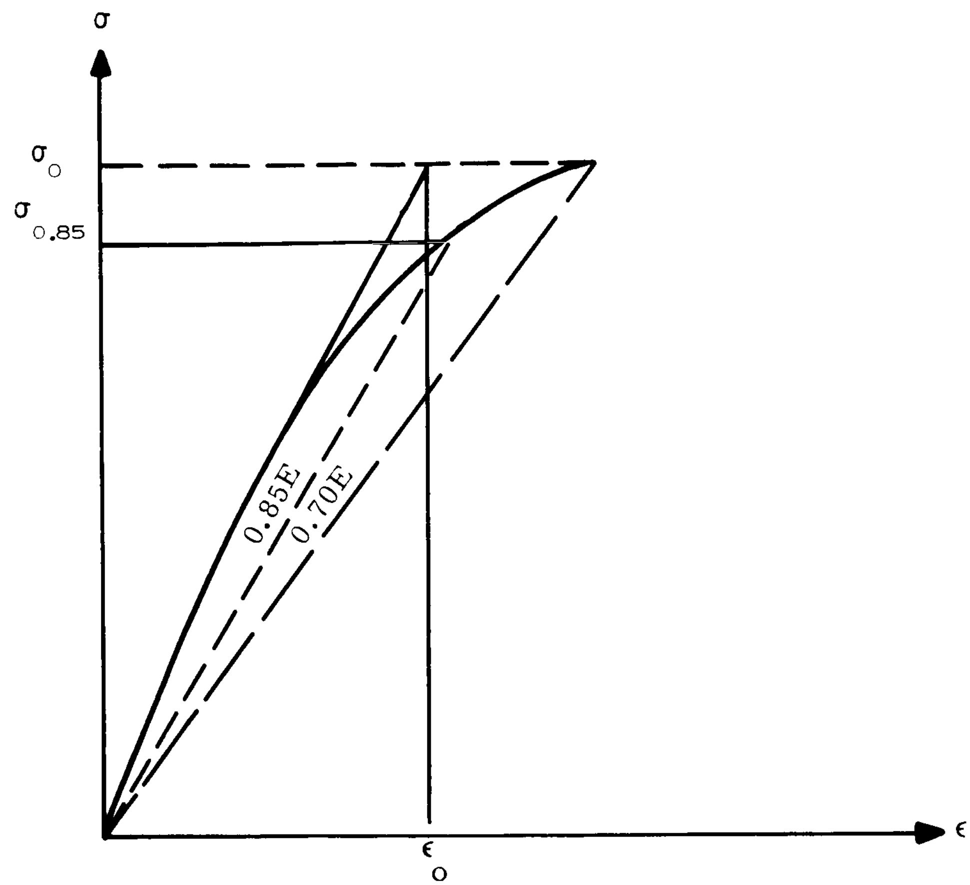

Figure A-4. Material Stress-Strain Curve

where M is the local bending moment and r is the local radius. The analysis of stress calculates the stress resultants at every design point and at every discrete point along the vehicle axis. The output of the stress element, therefore, provides a time history of all the combined loads at each station of the vehicle.

The loads history is then used as input to any of the eight elements of the SWOP module corresponding to different types of wall construction. The material properties are obtained from the stored tables described earlier where a linear interpolation is used to find the appropriate properties at the temperature specified for each discrete station. Subject to the constraints imposed, the dimensions of each type of wall construction are optimized so that the structure can sustain the loads which are imposed on it.

For each type of construction analyzed, the optimum configuration is selected such that it is the lightest structure that will satisfy a strength criterion and one or more stability criteria for the worst loading conditions. Once the dimensions of the wall

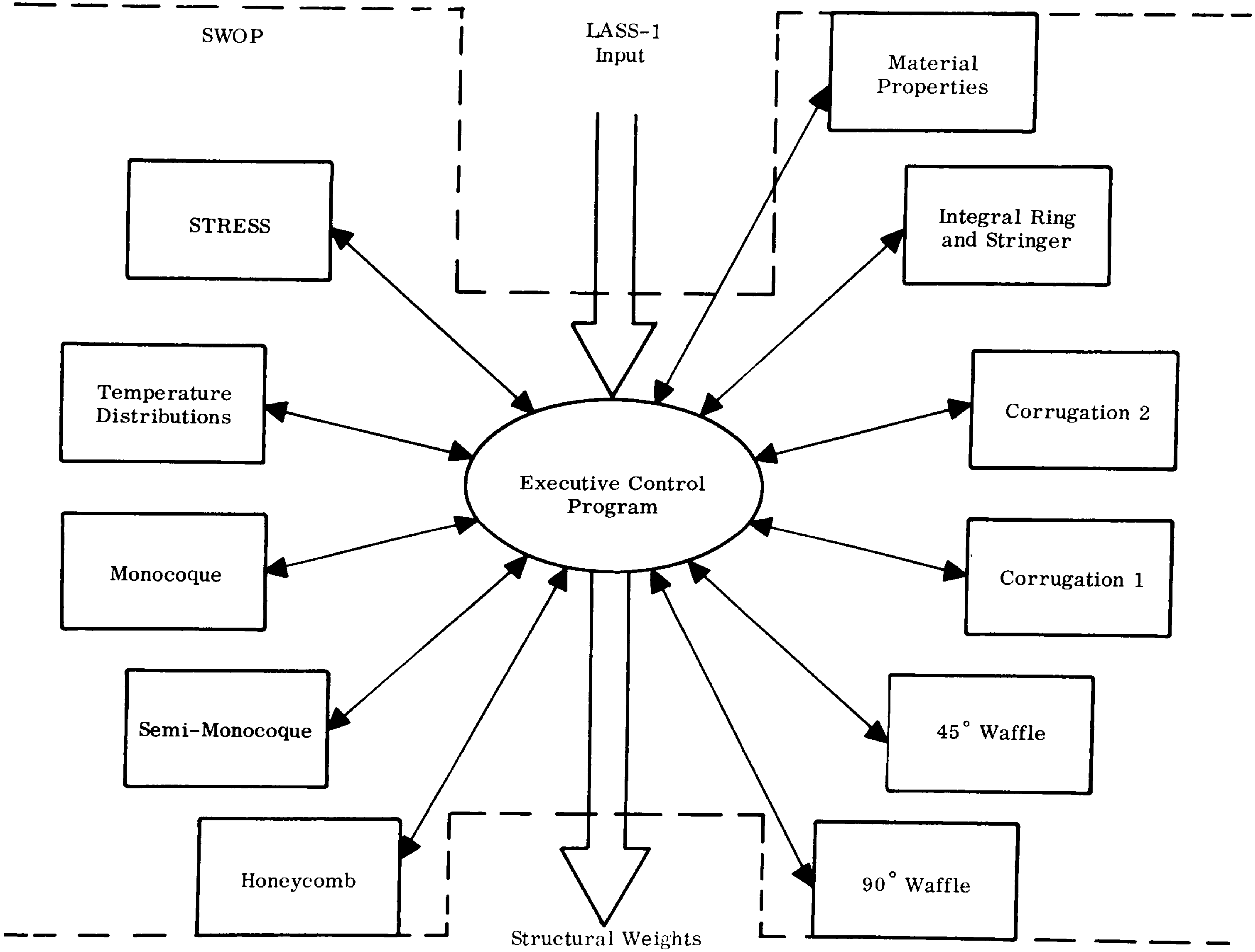

Figure A-5. Organization of SWOP

construction (stringer height, ring spacing, etc.) have been established, the weight of the structure is easily computed.

A4.2 MAJOR EQUATIONS OF SWOP MODULE

A4.2.1 Stress Element Equations

The stress resultants for the meridional and circumferential directions of a general conical section are given by the equations shown in Figure A-6.

$$N_x = -\frac{\beta\gamma}{6r\cos\phi}(2\bar{r}^3 - 3r\,\bar{r}^2 + r^3) + \frac{\beta\gamma d}{2r\sin\phi}(\bar{r}^2 - r^2) + \frac{Pr}{2\sin\phi} + \frac{F}{2\pi r\sin\phi} \pm \frac{M}{\pi r^2\sin\phi}$$

$$N_\theta = \frac{r}{\sin\phi}(\beta\gamma d + P)$$

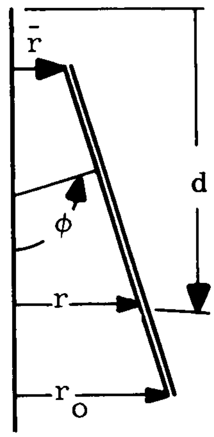

where:

β = Acceleration in g's.
P = Ullage pressure.
F = Axial force.
M = Bending moment.

Figure A-6. Stress Resultant Expressions

These equations are valid for all conical shells. For shell segments above a propellant level, one must set the propellant density, γ, to zero.

It is more difficult to express a general set of equations for an elliptical head since the form of the equations depends upon the orientation. Consider first of all an elliptical head that is a lower dome of a separate bulkhead tank as shown in Figure A-7.

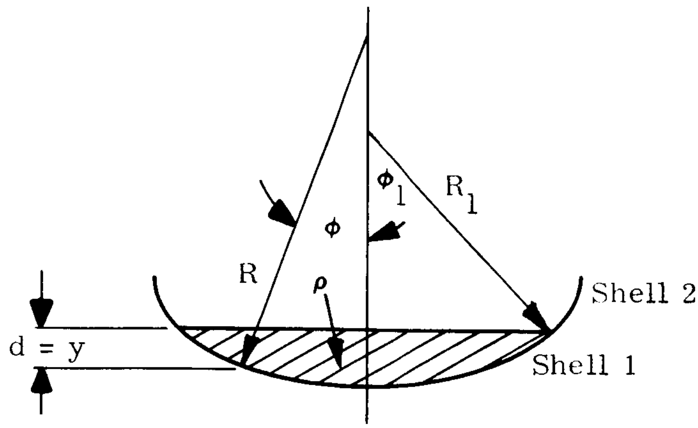

Figure A-7. Elliptical Lower Dome Head of Bulkhead Tank

For the shell below the liquid level, the stress resultants are given by,

$$N_x = \frac{PR}{2} + \frac{\beta\gamma R}{2}\left\{d + \frac{R\sin\phi}{3}\left[\frac{2}{k}\left(1 + \frac{\cot^2\phi}{k^2}\right)^{\frac{3}{2}} - \frac{3}{k^2}\cot\phi - \frac{2}{k^4}\cot^3\phi\right]\right\}$$

$$N_\theta = \frac{PR}{2}\left(2 - \frac{R}{R_s}\right) + \beta\gamma dR$$

$$- \frac{\beta\gamma R^2}{2R_s}\left\{d + \frac{R\sin\phi}{3}\left[\frac{2}{k}\left(1 + \frac{\cot^2\phi}{k^2}\right)^{\frac{3}{2}} - \frac{3}{k^2}\cot\phi - \frac{2}{k^4}\cot^3\phi\right]\right\}$$

For the portion of the shell above the liquid level, the stress resultants become,

$$N_x = \frac{PR}{2} + \frac{W(\phi_1)}{2\pi R\sin^2\phi}$$

$$N_\theta = \frac{PR}{2}\left(2 - \frac{R}{R_s}\right) - \frac{W(\phi_1)}{2\pi R_s\sin^2\phi}$$

where:

$$W(\phi_1) = \frac{\beta\gamma\pi R^3\sin^3\phi_1}{3}\left[\frac{2}{k}\left(1 + \frac{\cot^2\phi_1}{k^2}\right)^{\frac{3}{2}} - \frac{2}{k^2}\cot\phi_1 - \frac{2}{k^4}\cot^3\phi_1\right]$$

The equations for an upper dome are somewhat different. The stress resultants for the shell shown in Figure A-8 are,

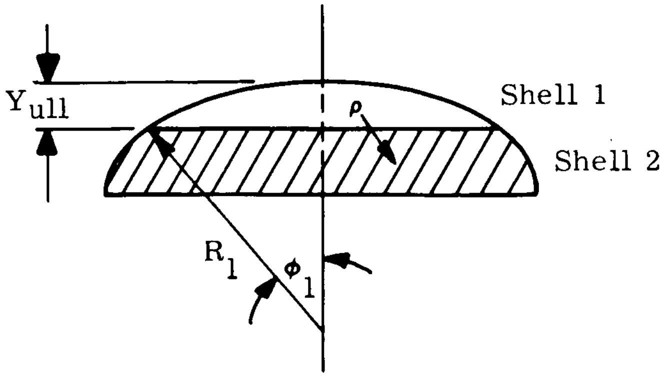

Figure A-8. Elliptical Upper Dome Head of Bulkhead Tank

For the portion of the shell below the liquid level,

$$N_x = \frac{PR}{2} + \frac{V_u}{\sin\phi}$$

$$N_\theta = \frac{PR}{2}\left(2 - \frac{R}{R_s}\right) + \beta\gamma R\left(b - \frac{R}{k^2}\cos\phi - y_{ull}\right) - \frac{R}{R_s}\frac{V_u}{\sin\phi}$$

where:

$$V_u = \frac{\beta\gamma k^2}{R\sin\phi}\left\{\frac{b + y_{ull}}{2}\left[\left(b - \frac{R}{k^2}\cos\phi\right)^2 - y_{ull}^2\right]\right.$$

$$+ \frac{1}{3}\left[y_{ull}^3 - \left(b - \frac{R}{k^2}\cos\phi\right)^3\right]$$

$$\left. + by_{ull}\left[y_{ull} - \left(b - \frac{R}{k^2}\cos\phi\right)\right]\right\}$$

The equations for the stress resultants of the portion of the shell above the liquid level are the same as those given above, with γ set equal to zero.

After the N_x's and N_θ's are calculated, the largest negative value of N_x is selected for each station of the vehicle to be used in the stability analyses to follow. The values of

N_x and N_θ are combined according to the von Mises-Hencky theory to find an equivalent uniaxial stress resultant, N_o, at each station where,

$$N_o = (N_x^2 - N_x N_\theta + N_\theta^2)^{\frac{1}{2}}$$

The maximum value of N_o for each vehicle station is also selected to be used in the strength analyses to follow.

A4.2.2 Buckling of Monocoque Cylinders

The lowest critical buckling load for circular cones under axial compression has been determined in Reference 22 as,

$$P = \frac{2Et^2 \pi \cos^2 \alpha}{3(1 - \mu^2)^{\frac{1}{2}}}$$

It is well known that a considerable discrepancy exists between experimental and theoretical buckling loads of thin shells, particularly when calculations are based upon small deflection theory. In practice, this discrepancy is usually handled by multiplying the classical load by an experimental correction factor, C, using equations of the form,

$$P_{cr} = 2\pi C E t^2 \cos^2 \alpha$$

$$\sigma_{cr} = \frac{CEt \cos \alpha}{r}$$

The buckling correction factor can be approximated by,

$$C = 9 \left(\frac{t \cos \alpha}{R} \right)^{0.6}$$

Substituting the required thickness for buckling into the allowable buckling stress equation,

$$t_{buckling} = \left[\frac{N_x R^{1.6}}{9E (\cos \alpha)^{1.6}} \right]^{0.385}$$

Lackman and Penzien (Reference 22) have presented an experimentally determined curve for the correction coefficient for cones and cylinders as shown in Figure A-9.

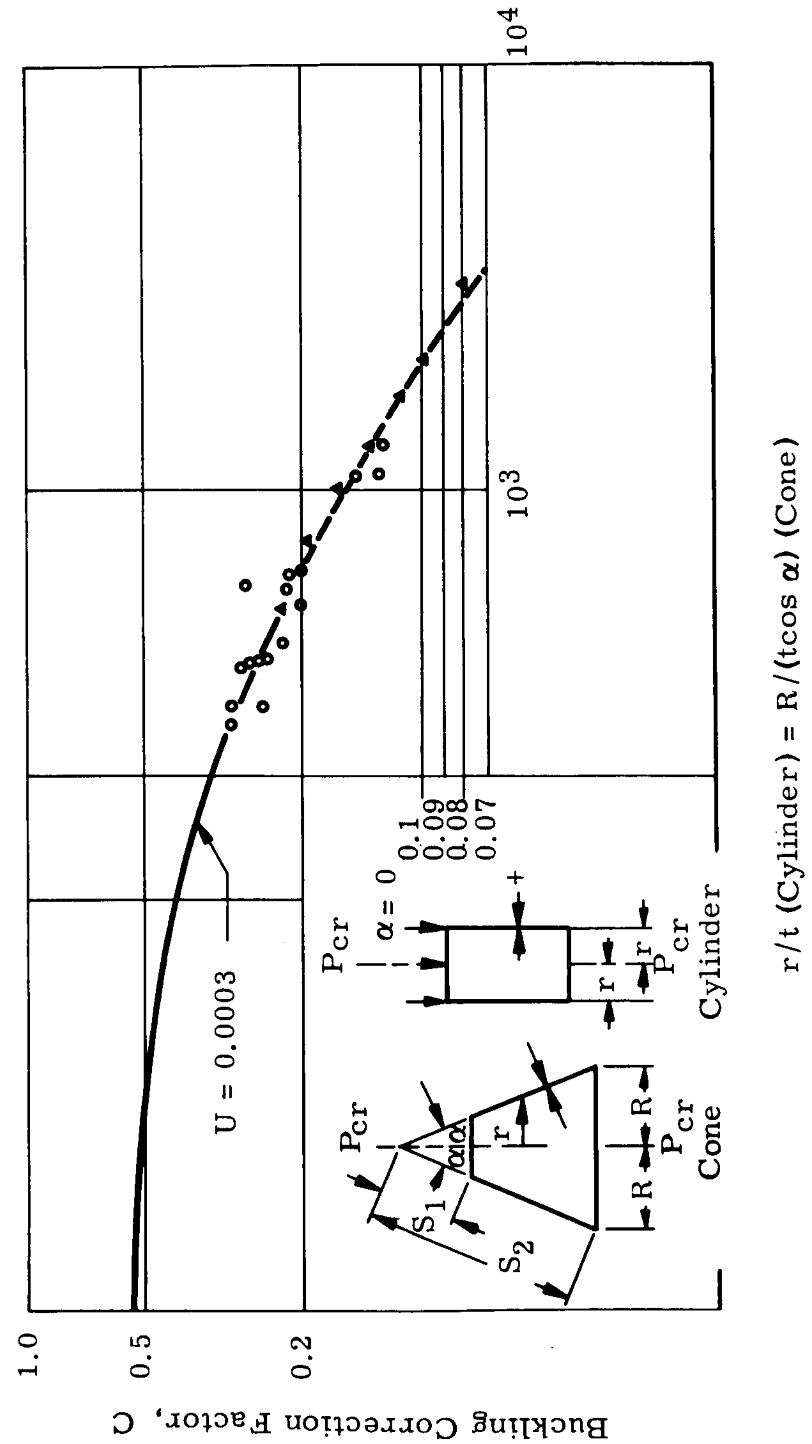

Figure A-9. Buckling Correction Factor, C, for Cylinders or Cones

The equations for P_{cr} and σ_{cr} discussed previously are applicable to cones and reduce to the equations generally used for cylinders when the semivertex angle, α, equals zero.

A4.2.3 Buckling of Orthotropic Cylinders

The buckling criteria for orthotropic shells is slightly different from those for monocoque cylinders.

In the selection of orthotropic buckling criteria, the following requirements have to be fulfilled:

a. Generalized formulae that would be applicable for the various types of orthotropic structures being considered.
b. Selection of a theory that is substantiated with test data.

Based on these requirements, a generalized form of the Becker (Reference 23) equation is used, as follows,

$$P_{cr} = 4\pi\left(\frac{\beta^2 D_{11} + D_{33}}{\frac{\beta^2}{A_{11}} + \frac{1}{2A_{33}}}\right)^{\frac{1}{2}}$$

where:

$$\beta^2 = P_o + \left(P_o^2 + Q_o\right)^{\frac{1}{2}}$$

$$P_o = \frac{A_{33}}{A_{22}}\left(\frac{A_{22}D_{11} - A_{11}D_{22}}{A_{11}D_{22} - 2A_{33}D_{33}}\right)$$

$$Q_o = \frac{A_{11}}{A_{22}}\left(\frac{A_{22}D_{11} - 2A_{33}D_{33}}{A_{11}D_{22} - 2A_{33}D_{33}}\right)$$

and

A_{11} is the extensional stiffness in longitudinal direction (lb/inch).

A_{22} is the extensional stiffness in hoop direction (lb/inch).

A_{33} is the shear stiffness (lb/inch).

D_{11} is the flexural stiffness in longitudinal direction (inch-lb/radian).

D_{22} is the flexural stiffness in hoop direction (inch-lb/radian).

D_{33} is the torsional stiffness (inch-lb/radian).

P_{cr} is the critical buckling load (pounds).

By defining the stiffness parameters, the equation is adaptable for any type of orthotropic cylinder. In fact, by substituting the correct stiffness parameters for an isotropic cylinder, the equation reduces to the classical buckling solution for isotropic cylinders with the exception of Poisson's ratio, which has been assumed equal to zero. However, since we are dealing with the square of a very small number (Poisson's ratio), the difference is very slight.

In order to substantiate the theory, a literature survey was conducted to locate test data for axially loaded orthotropic cylinders. The theoretical buckling loads were calculated based on the generalized Becker equation and compared with the test results. The results of the study are shown on Figure A-10. As can be expected from past experience with the buckling of isotropic cylinders, the data shows considerable scatter. It can be concluded that a correction factor is required for each type of construction considered, as has been the case for isotropic cylinders.

A4.2.4 Major Equations for Optimization of Types of Construction

The description of the equations used in the optimization of structural weight for the eight different types of construction illustrated in Figure A-3 are documented in detail in Reference 19. An attempt to present those equations in condensed form has been unsuccessful, and repetition of the bulk of Reference 19 does not seem warranted in this document. Suffice it to say that all the methods of analysis represent what is considered to be the current state of the art and are in general usage throughout the aerospace industry. Each type of construction is required to satisfy a strength criterion based on the von Mises-Hencky criteria, and a general instability criterion. Where appropriate, local instability requirements must also be satisfied depending upon the type of construction.

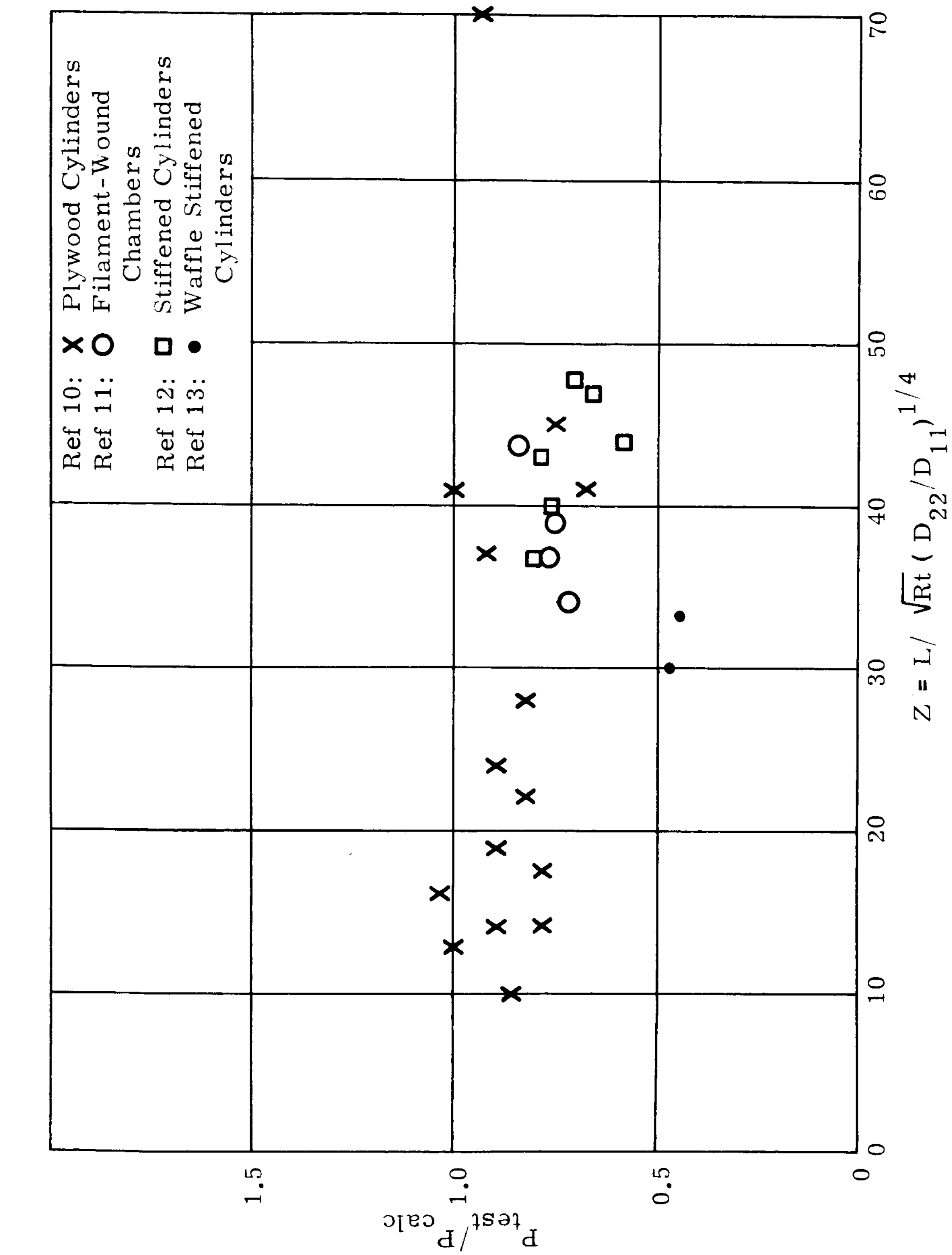

Figure A-10. Axially Loaded Orthotropic Cylinders

APPENDIX B

LILAC AND SPACE COMPUTER PROGRAM

APPENDIX B

LILAC AND SPACE COMPUTER PROGRAM

B1 GENERAL DESCRIPTION AND ORGANIZATION

The SPACE and LILAC modules calculate optimum structural weights of anisotropic materials for the loads envelope generated by the SWOP module. The treatment of fibrous composites for this application is greatly enhanced by the LILAC computer program. This program accepts as input the mechanical and geometrical properties of the constituents of a fibrous laminate. From this, the elastic constants of a single layer (a uniaxial composite) of the laminate are computed by the rigorous methods of Reference 24. These are utilized to compute the effective laminate properties and the stresses in each of the layers with respect to any Cartesian reference frame.

The emphasis in the SPACE program is upon the behavior of structural elements; whereas, the LILAC program is concerned with material response. The stiffness properties of heterogeneous configurations are computed for any type of composite or isotropic materials. These are then used in an appropriate anisotropic stability analysis (e.g., Reference 25) which along with the strength criteria is used to define the optimum structural configurations.

The method outlined on the following pages for the analysis of composite materials was developed at General Electric's Space Sciences Laboratory. The derivation of the equations presented can be found in greater detail in References 20, 24, 25, and 26. The properties of a lamina are derived in Reference 24. In Reference 20 the properties of a laminate assembly are developed. The efficiency study of a composite cylinder is presented in greater detail in References 25 and 26.

For the tank heads, a pressure vessel netting analysis was used. Since the loads are such that the principal stresses are in tension, the fibers will be assumed to be aligned in these two directions, zero degrees and ninety degrees to the vertical.

B2 MAJOR EQUATIONS AND METHOD OF ANALYSIS

The stress-strain law for a particular lamina can be written as,

$$\sigma_i = C_{ij}\,\epsilon_j; \qquad i, j = 1, 2, 3$$

where repeated indices indicate summation. For the orthotropic lamina of a filament wound material, these properties can be written as,

$$C_{11} = \frac{E_1}{1 - \nu_{21}\,\nu_{12}}$$

$$C_{22} = \frac{E_2}{1 - \nu_{21}\,\nu_{12}}$$

$$C_{12} = C_{21} = \frac{\nu_{21}\,E_2}{1 - \nu_{12}\,\nu_{21}}$$

$$C_{33} = 2G_{12}$$

where:

E_1 = Young's modulus in fiber direction.

E_2 = Young's modulus normal to fiber direction.

G_{12} = Shear modulus in fiber plane.

ν_{12} = Ratio of strain in the fiber direction to strain normal to fiber direction for a stress applied normal to the fiber direction.

The values for these constants can be bounded through the use of the minimum potential and complementary energy theorems. For a random array consisting of various sized concentric circles of binder and fiber with a constant volume ratio ν_f/ν_b of fiber to binder and completely filling the space, these bounds coincide for all but E_2 for which the upper bound is used.

These constants can be expressed in terms of the laminate axes by using the following coordinate transformation,

$$\sigma_i = T_{ij}\,\overline{\sigma}_j$$

$$\epsilon_i = T_{ij}\,\overline{\epsilon}_j$$

where:

$$T_{ij} = \begin{bmatrix} \cos^2\theta & \sin^2\theta & 2\sin\theta\cos\theta \\ \sin^2\theta & \cos^2\theta & -2\sin\theta\cos\theta \\ -\sin\theta\cos\theta & \sin\theta\cos\theta & \cos^2\theta - \sin^2\theta \end{bmatrix}$$

and where the bar indicates quantities referenced to the laminate axes. Thus,

$$\overline{C}_{ij} = L_{im} C_{mn} T_{nj}$$

where:

$$L_{im} = (T_{im})^{-1}$$

For a laminate consisting of a large number n of symmetric laminae, the bending and extensional stresses are uncoupled. Neglecting transverse shear, the strains in all layers will be the same. Thus, the average stress $\overline{\tau}_i$ will be,

$$\overline{\tau}_i = \sum_{k=1}^{n} C_{ij}^{k} \overline{\epsilon}_j \tau_k$$

or:

$$\tau_i = \overline{A}_{ij} \overline{\epsilon}_j$$

where τ_i is the fraction of total thickness in the k_{th} layer and,

$$\overline{A}_{ij} = \sum_{k>1}^{n} \overline{C}_{ij}^{k} \tau_k$$

This stress-strain law for the laminate can also be written as,

$$\overline{\epsilon}_j = \overline{B}_{ij} \overline{\tau}_i$$

The elastic constants of the laminate can be defined as,

$$E_L = \frac{1}{\overline{B}_{11}}$$

$$E_T = \frac{1}{\overline{B}_{22}}$$

$$G_{LT} = \frac{1}{\overline{B}_{33}}$$

$$\nu_{TL} = -\frac{\overline{B}_{12}}{\overline{B}_{11}}$$

$$\nu_{LT} = \frac{\overline{B}_{12}}{\overline{B}_{22}}$$

The stress components within the kth layer and referenced to axes making an angle β with respect to the longitudinal and transverse axes are given by,

$$\sigma_i^k = \tau_{ij} (\overline{C}_{jl}^k \overline{\epsilon}_l)$$

where τ_{ij} is now defined in terms of the angle β instead of θ.

The structural efficiency analysis used involves the determination of generalized weights of structural shell required to carry given axial loading intensities. The appropriate parameters for this generalization have been found to be weight per unit surface area divided by shell radius (W/R), as a function of axial load per unit length of circumference divided by shell radius (N_x/R). Evaluations of the minimum-weight configuration in each case required the application of the appropriate shell failure criteria, which were taken here as either elastic buckling or compressive yielding or fracture. The elastic buckling criterion is based on the small-deflection orthotropic shell stability results of Reference 25, wherein it is shown that the buckling mode is governed by a parameter, Φ, where $\Phi = \gamma^{1/2}$ or 1, whichever is smaller, and the shear stiffness ratio γ is given by

$$\gamma = \frac{2G_{LT}\left[1 + (\nu_{LT}\,\nu_{TL})^{\frac{1}{2}}\right]}{(E_L E_T)^{\frac{1}{2}}}$$

where G_{LT} is the shear modulus in plane of shell, E_L and E_T are the longitudinal (axial) and transverse (circumferential) stretching moduli of shell, and ν_{LT} and ν_{TL} are the Poisson's ratios. If $\gamma > 1$, the buckling mode is symmetric (bellows-type deformation) and the buckling stress σ_{cr} is given by

$$\sigma_{cr} = \frac{k\left(\frac{t}{R}\right)\overline{E}}{\sqrt{3}}$$

where

$$\overline{E} = \left[\frac{E_L E_T}{(1 - \nu_{LT}\,\nu_{TL})}\right]^{\frac{1}{2}}$$

and $\overline{E}$ is the effective stiffness, t is the shell thickness, R is the shell radius, and k is the empirical factor to account for initial imperfections in shell, i.e., $k \leq 1$. (Herein k is taken from Reference 38). If $\gamma < 1$, the buckling mode is asymmetric (checker-board type deformations) and

$$\sigma_{cr} = \left(\frac{k^{\frac{1}{2}}}{3}\right)\left(\frac{t}{R}\right)\left\{\frac{2G_{LT}(E_L E_T)^{\frac{1}{2}}}{\left[1 - (\nu_{LT}\,\nu_{TL})^{\frac{1}{2}}\right]}\right\}^{\frac{1}{2}}$$

The structural efficiency equation employing this expression for elastic buckling is

$$\frac{W}{R} = \frac{\rho_s\left(\frac{N_x}{R}\right)^{\frac{1}{2}}}{\left[\left(\frac{k^{\frac{1}{2}}}{3}\right) E\,\Phi\right]^{\frac{1}{2}}}$$

where, as before, Φ is $\gamma^{1/2}$ or 1, whichever is the smaller, and N_x is the axial load divided by shell circumference.

The above procedure is applicable only to simple monocoque shells, but illustrates the methods used throughout this study. Details of the application of these methods to sandwich shells are presented in Reference 25. Use of these methods requires the definition of a maximum allowable average stress for a given laminate. The procedure utilized herein is that of Reference 39 described below.

When a laminate is subjected to a known set of stress resultants, the average stresses in any lamina can be computed by the LILAC program. With a strength criterion defined for a single lamina, it is possible to construct an approximation to the laminate stress-strain curve. The strength criterion utilized for the individual lamina is a maximum stress criterion based on extensional strengths in the longitudinal and transverse directions and/or in-plane shear stress with respect to the principal elastic axes. These strengths are based on: experimental data for the longitudinal tensile stress; on the methods of Reference 36 for the longitudinal compressive strength; and on those of Reference 40 for in-plane shear and transverse direct stress. Whenever a stress component in the fiber direction equal to the assumed strength for that layer is attained, immediate laminate failure is postulated. When the transverse direction stress or in-plane shear stress reaches the maximum allowable value, it is postulated that that stress component remains constant and that the transverse Young's (E_2) and in-plane shear (G_{12}) moduli drop to zero. This procedure yields a piecewise linear stress-strain curve leading finally to a horizontal slope or ultimate stress condition.

The present approach is therefore to evaluate the initial maximum lamina stress condition and define that load as the laminate material yield stress. Then a "netting" analysis is performed to determine the lowest load which yields a lamina failure in the fiber direction. The average stress at this load is defined as the laminate material ultimate stress. This simplified procedure bypasses the need for analytic determination of the entire stress-strain curve. Rather, the initial departure from elastic behavior is evaluated and the maximum stress is conservatively estimated. Hence, the procedure is suitable for parametric studies such as the present one.

For shell designs, the yield and ultimate stresses for a given laminate are determined as above. This design criterion can be represented by an interaction curve. Example curves for the three materials being considered are shown in Figure B-1. These curves are constructed by selecting a skin thickness which will resist 1.1 times an arbitrary load (a combination of axial and transverse loads) at yield and 1.4 times this load at ultimate. The load components divided by this required thickness are then plotted as shown. To use this chart, a line is constructed with a slope equal to the

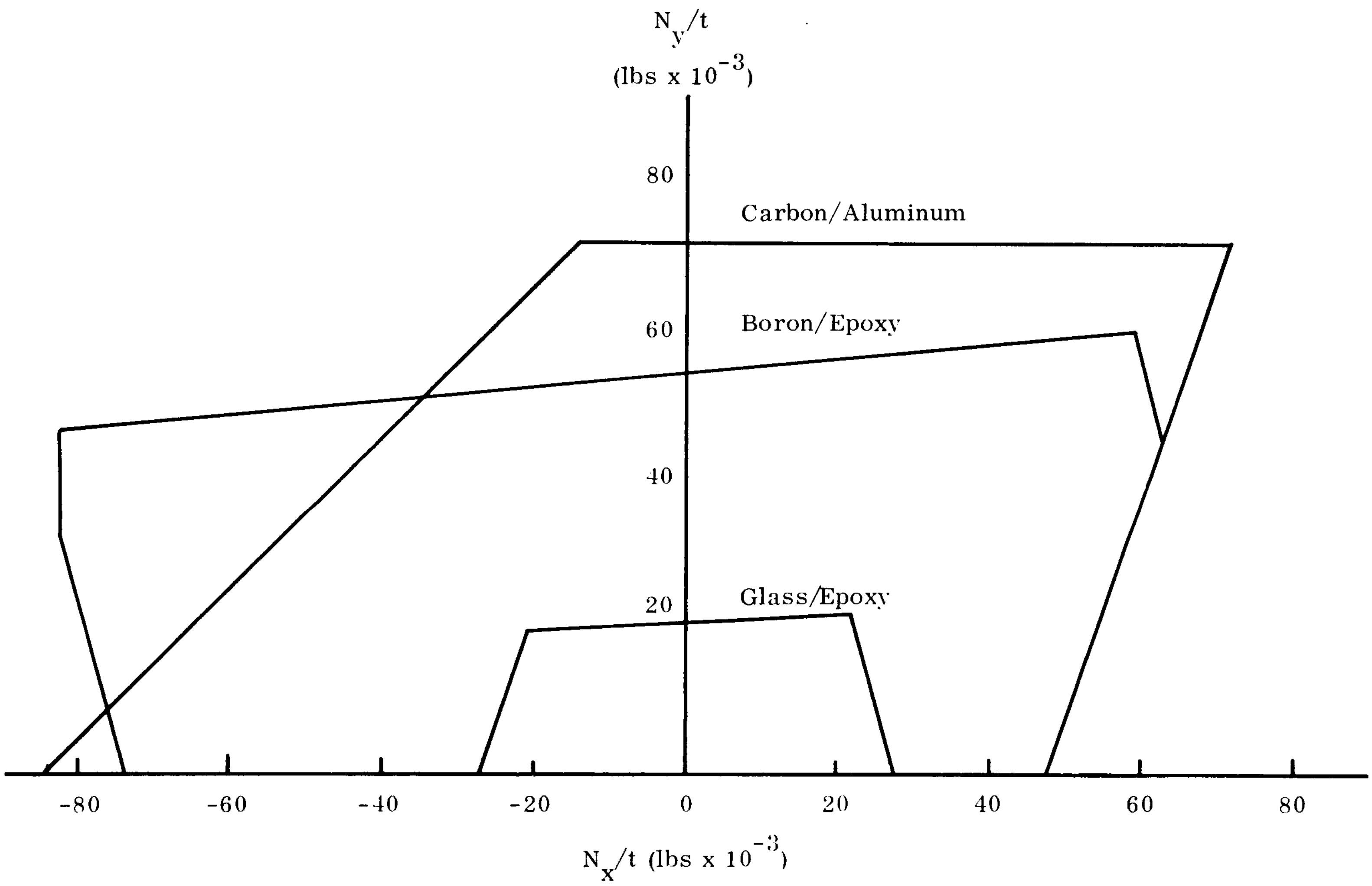

Figure B-1. Interaction Curves, Isotropic Winding ratio of the given load components. The required thickness can then be computed from either N_x/t or N_y/t corresponding to the intersection of this line and the interaction curve.

The monocoque shell is sized so that it will have at least this required thickness and will not buckle elastically at 1.4 times the axial component of the limit load.

For a sandwich shell the face sheet thickness associated with an elastic stability design for 1.4 × limit load and with an optimized core thickness is determined. If this is less than one-half the required monocoque thickness for the strength criteria (yield or ultimate) then the latter is used and the core thickness is that required for stability at 1.4 times limit load. In this latter computation elastic stiffnesses have been used for simplicity. In actuality when ultimate stress governs the face sheet thickness, a reduced modulus would be appropriate. Neglect of this reduces the buckling margin to an unassessed value between ten and forty percent.

APPENDIX C

WEIGHT/LOAD MATRICES

APPENDIX C
WEIGHT/LOAD MATRICES

The Weight/Loads Matrices were developed as a convenient tool to evaluate the structural weights for the many variations of vehicle parameters considered in this study. They were used in conjunction with the Loads Summary Charts as explained in Section 4.

It was observed in examining the matrices that some of the types of construction were sensitive to variations in N_x, but were insensitive to variations in N_o over the range of loads considered. This was especially true for the very inefficient types of construction such as monocoque. The weight of the most efficient type of construction, honeycomb sandwich, on the other hand was sensitive to changes in both N_x and N_o.

The reason for these differences became apparent when the mechanics of the various failure modes were considered. The greater the magnitude of N_x, the more likely was the occurrence of an instability failure. Buckling failures were prevented by increasing the bending stiffness of the walls. The bending stiffness was improved either by an increase of the elastic modulus, or the use of a more efficient type of construction. For a given material, the bending stiffness of a monocoque wall was increased only by making the walls thicker. Since the elastic modulus of most materials is low enough, the thickness required to prevent a buckling failure was more than sufficient to withstand any strength failures.

The bending stiffness of a honeycomb sandwich, on the other hand, was improved by increasing the distance between the face sheets, (i.e., increasing the depth of the core). Hence as N_x increased the core depth increased, however since a low density core material is used, the total weight was changed only by the slight increase in core weight. As N_o increases, however, the structural weight was much more sensitive. This was due to the increase in thickness of the much higher density face sheets which were directly proportional to changes in strength loading, N_o.

The same reasoning can be applied to the other types of construction which fall between these two extremes. It was observed that when materials with a much higher modulus-to-density ratio (such as beryllium) were used, the gap that existed between the weights of monocoque and honeycomb sandwich was reduced. This was true because the inherent stiffness of the beryllium allows one to approach the ideal state of having a monocoque buckling thickness which is no greater than the thickness required to withstand the strength loads.

Weight/Load Matrices - 101 Vehicle

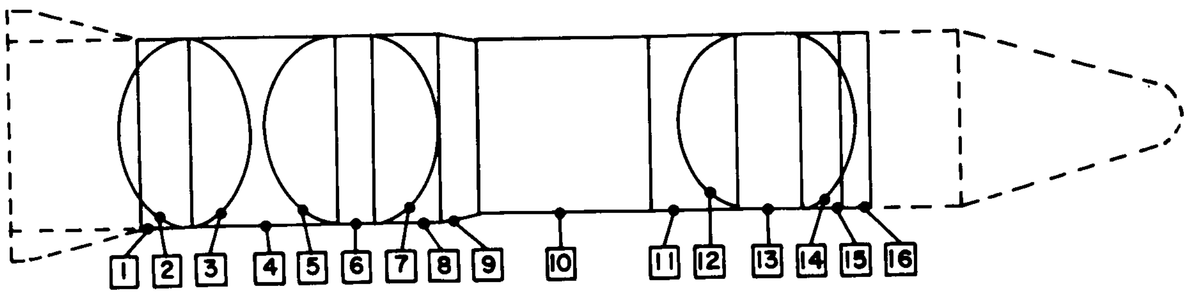

101 Vehicle Configuration
Section Number 1
Thrust Takeout (643" - 856")

Material: Titanium
N_x Nominal: -12,005 lbs/in.
N_o Nominal: 12,005 lbs/in.

$\frac{N_x}{N_x}$ Nom ↓ $\frac{N_o}{N_o}$ Nom →		.7	.8	.9	1.0	1.1
.7	HYC	13,333				
	ISS	42,064				
	MON	93,307				
	OFC	43,388				
	SFC	34,625				
.8	HYC		14,909			
	ISS		45,952			
	MON		98,230			
	OFC		46,384			
	SFC		37,266			
.9	HYC			16,473		
	ISS			50,422		
	MON			102,786		
	OFC			49,197		
	SFC			39,432		
1.0	HYC				18,042	
	ISS				55,241	
	MON				107,041	
	OFC				51,859	
	SFC				41,592	
1.1	HYC					19,595
	ISS					60,151
	MON					111,042
	OFC					54,390
	SFC					43,562

101 Vehicle Configuration
Section Number 2
RP-1 Tank Bottom Head

Material: Titanium
N_x Nominal: ----
N_o Nominal: 5,607 lbs/in.

$\frac{N_x}{N_x}$ Nom ↓ $\frac{N_o}{N_o}$ Nom →		.7	.8	.9	1.0	1.1
.7	HYC					
	ISS					
	MON					
	OFC					
	SFC					
.8	HYC					
	ISS					
	MON					
	OFC					
	SFC					
.9	HYC					
	ISS					
	MON					
	OFC					
	SFC					
1.0	HYC	7,035	8,026	9,016	10,007	10,997
	ISS					
	MON	5,824	6,656	7,489	8,321	9,153
	OFC					
	SFC					
1.1	HYC					
	ISS					
	MON					
	OFC					
	SFC					

101 Vehicle Configuration
Section Number 3
RP-1 Tank Top Head

Material: Titanium
N_x Nominal: ----
N_o Nominal: 4,462 lbs/in.

$\frac{N_x}{N_x}$ Nom ↓ $\frac{N_o}{N_o}$ Nom →		.7	.8	.9	1.0	1.1
.7	HYC					
	ISS					
	MON					
	OFC					
	SFC					
.8	HYC					
	ISS					
	MON					
	OFC					
	SFC					
.9	HYC					
	ISS					
	MON					
	OFC					
	SFC					
1.0	HYC	5,221	5,964	6,686	7,418	8,150
	ISS					
	MON	4,306	4,921	5,536	6,151	6,766
	OFC					
	SFC					
1.1	HYC					
	ISS					
	MON					
	OFC					
	SFC					

101 Vehicle Configuration
Section Number 4
Intertank (856" - 1477")

Material: Titanium
N_x Nominal: -11,407 lbs/in.
N_o Nominal: 11,407 lbs/in.

$\frac{N_x}{N_x}$ Nom ↓ $\frac{N_o}{N_o}$ Nom →		.7	.8	.9	1.0	1.1
.7	HYC	37,306				
	ISS	121,496				
	MON	266,961				
	OFC	149,328				
	SFC	96,082				
.8	HYC		41,684			
	ISS		132,730			
	MON		281,044			
	OFC		159,638			
	SFC		105,831			
.9	HYC			46,046		
	ISS			144,515		
	MON			294,082		
	OFC			169,322		
	SFC			112,166		
1.0	HYC				50,369	
	ISS				157,011	
	MON				306,257	
	OFC				178,461	
	SFC				118,310	
1.1	HYC					54,713
	ISS					172,859
	MON					317,703
	OFC					187,193
	SFC					124,161

101 Vehicle Configuration
Section Number 5
LOX Tank Bottom Head

Material: Titanium
N_x Nominal: ----
N_o Nominal: 8,288 lbs/in.

$\frac{N_x}{N_x}$ Nom ↓ $\frac{N_o}{N_o}$ Nom →		.7	.8	.9	1.0	1.1
.7	HYC					
	ISS					
	MON					
	OFC					
	SFC					
.8	HYC					
	ISS					
	MON					
	OFC					
	SFC					
.9	HYC					
	ISS					
	MON					
	OFC					
	SFC					
1.0	HYC	7,868	8,977	10,085	11,194	12,302
	ISS					
	MON	6,518	7,449	8,380	9,311	10,243
	OFC					
	SFC					
1.1	HYC					
	ISS					
	MON					
	OFC					
	SFC					

101 Vehicle Configuration
Section Number 6
LOX Tank Cylinder (1477" - 1627")

Material: Titanium
N_x Nominal: -6,467 lbs/in.
N_o Nominal: 11,809 lbs/in.

$\frac{N_x}{N_x}$ Nom ↓ $\frac{N_o}{N_o}$ Nom →		.7	.8	.9	1.0	1.1
.7	HYC	6,714	7,187	7,711	8,269	8,853
	ISS	20,880	20,880	20,880	20,880	20,880
	MON	50,730	50,730	50,730	50,730	50,730
	OFC					
	SFC					
.8	HYC	6,975	7,416	7,915	8,460	9,020
	ISS	22,638	22,638	22,638	22,638	22,638
	MON	53,406	53,406	53,406	53,406	53,406
	OFC					
	SFC					
.9	HYC	7,237	7,645	8,118	8,637	9,188
	ISS	24,328	24,328	24,328	24,328	24,328
	MON	55,884	55,884	55,884	55,884	55,884
	OFC					
	SFC					
1.0	HYC	7,539	7,875	8,322	8,821	9,356
	ISS	25,959	25,959	25,959	25,959	25,959
	MON	58,197	58,197	58,197	58,197	58,197
	OFC					
	SFC					
1.1	HYC	7,879	8,114	8,527	9,005	9,523
	ISS	27,203	27,203	27,203	27,203	27,203
	MON	60,373	60,373	60,373	60,373	60,373
	OFC					
	SFC					

Weight/Load Matrices - 101 Vehicle

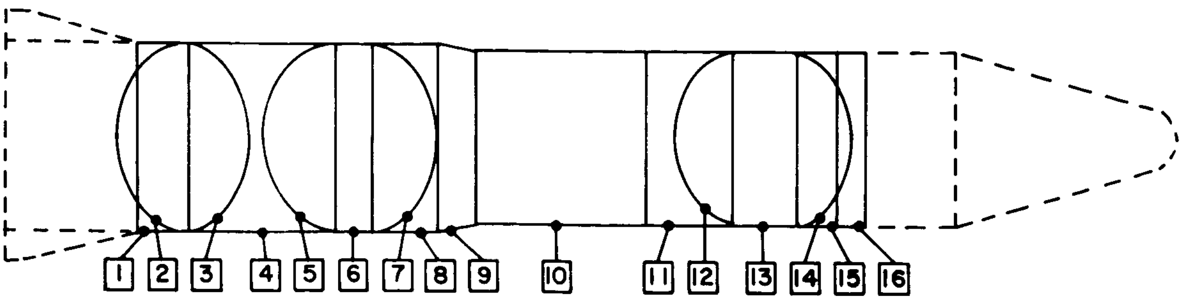

101 Vehicle Configuration
Section Number 7
LOX Tank Top Head

Material: Titanium
N_x Nominal: ----
N_o Nominal: 4,695 lbs/in.

$\frac{N_x}{N_x \text{ Nom}}$ ↓	$\frac{N_o}{N_o \text{ Nom}}$ →	.7	.8	.9	1.0	1.1
.7	HYC					
	ISS					
	MON					
	OFC					
	SFC					
.8	HYC					
	ISS					
	MON					
	OFC					
	SFC					
.9	HYC					
	ISS					
	MON					
	OFC					
	SFC					
1.0	HYC	4,658	5,309	5,960	6,611	7,262
	ISS					
	MON	3,828	4,375	4,921	5,468	6,015
	OFC					
	SFC					
1.1	HYC					
	ISS					
	MON					
	OFC					
	SFC					

101 Vehicle Configuration
Section Number 8
Stage 1 Forward Skirt (1627" - 1905")

Material: Titanium
N_x Nominal: -9,277 lbs/in.
N_o Nominal: 9,277 lbs/in.

$\frac{N_x}{N_x \text{ Nom}}$ ↓	$\frac{N_o}{N_o \text{ Nom}}$ →	.7	.8	.9	1.0	1.1
.7	HYC	14,084				
	ISS	47,551				
	MON	110,252				
	OFC	43,388				
	SFC	37,374				
.8	HYC		15,689			
	ISS		50,379			
	MON		116,068			
	OFC		46,384			
	SFC		39,687			
.9	HYC			17,285		
	ISS			54,921		
	MON			121,453		
	OFC			49,197		
	SFC			45,496		
1.0	HYC				18,874	
	ISS				58,504	
	MON				126,481	
	OFC				51,859	
	SFC				48,004	
1.1	HYC					20,456
	ISS					63,022
	MON					131,208
	OFC					54,390
	SFC					50,009

101 Vehicle Configuration
Section Number 9
Interstage (1905" - 2075")

Material: Titanium
N_x Nominal: -9,818 lbs/in.
N_o Nominal: 9,818 lbs/in.

$\frac{N_x}{N_x \text{ Nom}}$ ↓	$\frac{N_o}{N_o \text{ Nom}}$ →	.7	.8	.9	1.0	1.1
.7	HYC	8,843				
	ISS	29,919				
	MON	68,038				
	OFC	21,685				
	SFC	23,092				
.8	HYC		9,857			
	ISS		32,111			
	MON		71,628			
	OFC		23,182			
	SFC		24,873			
.9	HYC			10,857		
	ISS			34,926		
	MON			74,950		
	OFC			24,589		
	SFC			28,125		
1.0	HYC				11,861	
	ISS				37,246	
	MON				78,053	
	OFC				25,919	
	SFC				29,512	
1.1	HYC					12,860
	ISS					40,095
	MON					80,970
	OFC					27,184
	SFC					30,969

101 Vehicle Configuration
Section Number 10
Stage 2 Lower Skirt (2075" - 2795")

Material: Titanium
N_x Nominal: -9,651 lbs/in.
N_o Nominal: 9,651 lbs/ in.

$\frac{N_x}{N_x \text{ Nom}}$ ↓	$\frac{N_o}{N_o \text{ Nom}}$ →	.7	.8	.9	1.0	1.1
.7	HYC	33,925				
	ISS	107,757				
	MON	251,627				
	OFC	105,964				
	SFC	86,607				
.8	HYC		37,867			
	ISS		118,702			
	MON		264,901			
	OFC		113,281			
	SFC		99,257			
.9	HYC			41,788		
	ISS			127,332		
	MON			277,190		
	OFC			120,152		
	SFC			105,386		
1.0	HYC				45,693	
	ISS				138,051	
	MON				288,665	
	OFC				126,652	
	SFC				111,196	
1.1	HYC					49,570
	ISS					149,613
	MON					299,454
	OFC					132,833
	SFC					115,567

101 Vehicle Configuration
Section Number 11
Intertank (2795" - 3162.6")

Material: Titanium
N_x Nominal: -4,484 lbs/in.
N_o Nominal: 4,484 lbs/in.

$\frac{N_x}{N_x \text{ Nom}}$ ↓	$\frac{N_o}{N_o \text{ Nom}}$ →	.7	.8	.9	1.0	1.1
.7	HYC	9,649				
	ISS	37,365				
	MON	95,567				
	OFC	32,999				
	SFC	30,171				
.8	HYC		10,610			
	ISS		39,274			
	MON		100,608			
	OFC		35,278			
	SFC		32,290			
.9	HYC			11,572		
	ISS			42,089		
	MON			105,276		
	OFC			37,418		
	SFC			34,239		
1.0	HYC				12,525	
	ISS				43,917	
	MON				109,634	
	OFC				39,442	
	SFC				36,125	
1.1	HYC					13,482
	ISS					46,446
	MON					113,732
	OFC					41,367
	SFC					37,858

101 Vehicle Configuration
Section Number 12
LH_2 Tank Bottom Head

Material: Titanium
N_x Nominal: ----
N_o Nominal: 9,144 lbs/ in

$\frac{N_x}{N_x \text{ Nom}}$ ↓	$\frac{N_o}{N_o \text{ Nom}}$ →	.7	.8	.9	1.0	1.1
.7	HYC					
	ISS					
	MON					
	OFC					
	SFC					
.8	HYC					
	ISS					
	MON					
	OFC					
	SFC					
.9	HYC					
	ISS					
	MON					
	OFC					
	SFC					
1.0	HYC	6,685	7,628	8,571	9,514	10,457
	ISS					
	MON	5,544	6,336	7,128	7,921	8,713
	OFC					
	SFC					
1.1	HYC					
	ISS					
	MON					
	OFC					
	SFC					

Weight/Load Matrices - 101 Vehicle

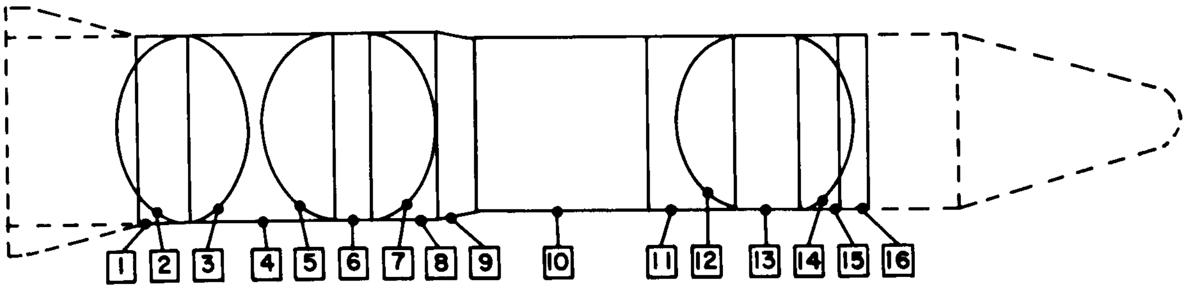

101 Vehicle Configuration
Section Number 13
LH_2 Tank Cylinder (3162.6" - 3439.4")

Material: Titanium
N_x Nominal: - 684 lbs/in.
N_o Nominal: 12,839 lbs/in.

$N_x/\overline{N_x}$ Nom ↓	$N_o/\overline{N_o}$ Nom →	.7	.8	.9	1.0	1.1
.7	HYC	8,694	9,846	11,006	12,185	13,362
	ISS	15,226	15,226	15,226	15,226	15,226
	MON	33,873	33,873	33,873	33,873	33,873
	OFC					
	SFC					
.8	HYC	8,742	9,888	11,044	12,214	13,385
	ISS	15,257	15,257	15,257	15,257	15,257
	MON	35,660	35,660	35,660	35,660	35,660
	OFC					
	SFC					
.9	HYC	8,791	9,931	11,082	12,242	13,408
	ISS	15,288	15,288	15,288	15,288	15,288
	MON	37,314	37,314	37,314	37,314	37,314
	OFC					
	SFC					
1.0	HYC	8,840	9,973	11,120	12,276	13,439
	ISS	15,319	15,319	15,319	15,319	15,319
	MON	38,859	38,859	38,859	38,859	38,859
	OFC					
	SFC					
1.1	HYC	8,888	10,016	11,158	12,311	13,471
	ISS	15,349	15,349	15,349	15,349	15,349
	MON	40,311	40,311	40,311	40,311	40,311
	OFC					
	SFC					

101 Vehicle Configuration
Section Number 14
LH_2 Tank Top Head

Material: Titanium
N_x Nominal: ----
N_o Nominal: 7,388 lbs/in.

$N_x/\overline{N_x}$ Nom ↓	$N_o/\overline{N_o}$ Nom →	.7	.8	.9	1.0	1.1
.7	HYC					
	ISS					
	MON					
	OFC					
	SFC					
.8	HYC					
	ISS					
	MON					
	OFC					
	SFC					
.9	HYC					
	ISS					
	MON					
	OFC					
	SFC					
1.0	HYC	5,738	6,546	7,534	8,161	8,969
	ISS					
	MON	4,749	5,427	6,106	6,784	7,463
	OFC					
	SFC					
1.1	HYC					
	ISS					
	MON					
	OFC					
	SFC					

101 Vehicle Configuration
Section Number 15
Stage 2 Forward Skirt (3439.4" - 3610")

Material: Titanium
N_x Nominal: -2,762 lbs/in.
N_o Nominal: 2,762 lbs/in.

$N_x/\overline{N_x}$ Nom ↓	$N_o/\overline{N_o}$ Nom →	.7	.8	.9	1.0	1.1
.7	HYC	3,247				
	ISS	12,911				
	MON	36,797				
	OFC	10,764				
	SFC	11,017				
.8	HYC		3,535			
	ISS		13,867			
	MON		38,738			
	OFC		11,507			
	SFC		11,767			
.9	HYC			3,817		
	ISS			15,242		
	MON			40,535		
	OFC			12,205		
	SFC			12,464		
1.0	HYC				4,098	
	ISS				15,651	
	MON				42,213	
	OFC				12,865	
	SFC				13,150	
1.1	HYC					4,376
	ISS					16,729
	MON					43,791
	OFC					13,493
	SFC					13,804

101 Vehicle Configuration
Section Number 16
Instrument Unit (3610" - 3730")

Material: Titanium
N_x Nominal: -2,418 lbs/in.
N_o Nominal: 2,418 lbs/in.

$N_x/\overline{N_x}$ Nom ↓	$N_o/\overline{N_o}$ Nom →	.7	.8	.9	1.0	1.1
.7	HYC	2,113				
	ISS	8,422				
	MON	24,813				
	OFC	14,606				
	SFC	7,244				
.8	HYC		2,290			
	ISS		9,302			
	MON		35,912			
	OFC		15,614			
	SFC		7,763			
.9	HYC			2,465		
	ISS			9,890		
	MON			27,114		
	OFC			16,561		
	SFC			8,232		
1.0	HYC				2,640	
	ISS				10,444	
	MON				28,236	
	OFC				17,457	
	SFC				8,629	
1.1	HYC					2,813
	ISS					11,057
	MON					29,291
	OFC					18,309
	SFC					9,056

Weight/Load Matrices - 101 Vehicle

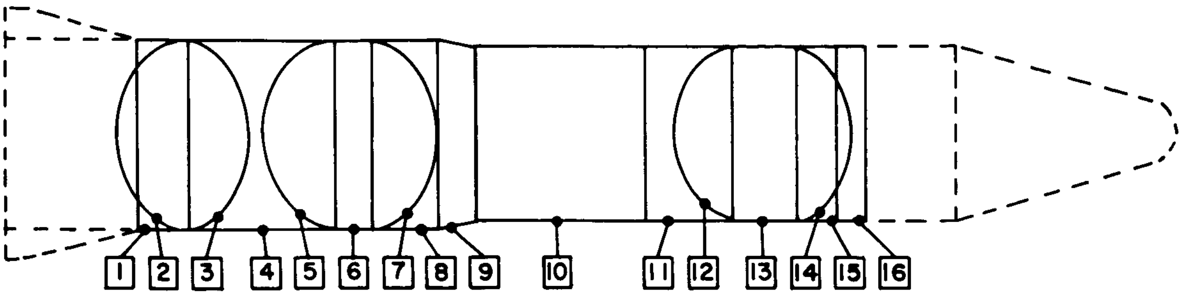

101 Vehicle Configuration
Section Number 1
Thrust Takeout (856.0" - 643.0")

Material: Beryllium
N_x Nominal: -12,005 lbs/in.
N_o Nominal: 12,005 lbs/in.

N_x ↓ $\overline{N_x}$ Nom	N_o → $\overline{N_o}$ Nom	.7	.8	.9	1.0	1.1
.7	HYC	8,828				
	ISS	11,259				
	MON	26,313				
	OFC	46,519				
	SFC	9,604				
.8	HYC		9,925			
	ISS		11,321			
	MON		28,227			
	OFC		49,731			
	SFC		9,594			
.9	HYC			11,038		
	ISS			11,589		
	MON			29,537		
	OFC			52,748		
	SFC			9,648		
1.0	HYC				12,169	
	ISS				12,322	
	MON				30,759	
	OFC				55,601	
	SFC				10,067	
1.1	HYC					13,271
	ISS					13,036
	MON					31,909
	OFC					58,314
	SFC					10,501

101 Vehicle Configuration
Section Number 2
RP-1 Tank Bottom Head

Material: Beryllium
N_x Nominal: ----
N_o Nominal: 5,607 lbs/in.

N_x ↓ $\overline{N_x}$ Nom	N_o → $\overline{N_o}$ Nom	.7	.8	.9	1.0	1.1
.7	HYC					
	ISS					
	MON					
	OFC					
	SFC					
.8	HYC					
	ISS					
	MON					
	OFC					
	SFC					
.9	HYC					
	ISS					
	MON					
	OFC					
	SFC					
1.0	HYC	5,109	5,824	6,540	7,255	7,971
	ISS					
	MON	4,207	4,807	5,408	6,009	6,610
	OFC					
	SFC					
1.1	HYC					
	ISS					
	MON					
	OFC					
	SFC					

101 Vehicle Configuration
Section Number 3
RP-1 Tank Top Head

Material: Beryllium
N_x Nominal: ----
N_o Nominal: 4,462 lbs/in.

N_x ↓ $\overline{N_x}$ Nom	N_o → $\overline{N_o}$ Nom	.7	.8	.9	1.0	1.1
.7	HYC					
	ISS					
	MON					
	OFC					
	SFC					
.8	HYC					
	ISS					
	MON					
	OFC					
	SFC					
.9	HYC					
	ISS					
	MON					
	OFC					
	SFC					
1.0	HYC	3,798	4,326	4,855	5,384	5,913
	ISS					
	MON	3,110	3,554	3,998	4,442	4,887
	OFC					
	SFC					
1.1	HYC					
	ISS					
	MON					
	OFC					
	SFC					

101 Vehicle Configuration
Section Number 4
Intertank (856.0" - 1477.0")

Material: Beryllium
N_x Nominal: -11,407 lbs/in.
N_o Nominal: 11,407 lbs/in.

N_x ↓ $\overline{N_x}$ Nom	N_o → $\overline{N_o}$ Nom	.7	.8	.9	1.0	1.1
.7	HYC	24,625				
	ISS	30,290				
	MON	76,714				
	OFC	174,483				
	SFC	26,523				
.8	HYC		27,645			
	ISS		31,778			
	MON		80,761			
	OFC		186,531			
	SFC		26,663			
.9	HYC			30,700		
	ISS			33,469		
	MON			84,507		
	OFC			197,846		
	SFC			27,059		
1.0	HYC				33,798	
	ISS				35,629	
	MON				88,005	
	OFC				208,548	
	SFC				28,519	
1.1	HYC					36,947
	ISS					37,717
	MON					91,295
	OFC					218,727
	SFC					29,932

101 Vehicle Configuration
Section Number 5
LOX Tank Bottom Head

Material: Beryllium
N_x Nominal: ----
N_o Nominal: 8,288 lbs/in.

N_x ↓ $\overline{N_x}$ Nom	N_o → $\overline{N_o}$ Nom	.7	.8	.9	1.0	1.1
.7	HYC					
	ISS					
	MON					
	OFC					
	SFC					
.8	HYC					
	ISS					
	MON					
	OFC					
	SFC					
.9	HYC					
	ISS					
	MON					
	OFC					
	SFC					
1.0	HYC	8,066	9,203	10,340	11,477	12,614
	ISS					
	MON	6,685	7,639	8,594	9,549	10,504
	OFC					
	SFC					
1.1	HYC					
	ISS					
	MON					
	OFC					
	SFC					

101 Vehicle Configuration
Section Number 6
LOX Tank Cylinder (1477.0" - 1627.8")

Material: Beryllium
N_x Nominal: -6,467 lbs/in.
N_o Nominal: 11,809 lbs/in.

N_x ↓ $\overline{N_x}$ Nom	N_o → $\overline{N_o}$ Nom	.7	.8	.9	1.0	1.1
.7	HYC	4,936	5,571	6,223	6,883	7,547
	ISS	8,791	8,791	8,791	8,791	8,791
	MON	14,877	14,877	14,877	14,877	14,877
	OFC					
	SFC					
.8	HYC	5,013	5,622	6,260	6,912	7,571
	ISS	8,840	8,840	8,840	8,840	8,840
	MON	15,662	15,662	15,662	15,662	15,662
	OFC					
	SFC					
.9	HYC	5,123	5,691	6,308	6,948	7,601
	ISS	8,888	8,888	8,888	8,888	8,888
	MON	16,389	16,389	16,389	16,389	16,389
	OFC					
	SFC					
1.0	HYC	5,279	5,786	6,372	6,995	7,638
	ISS	8,937	8,937	8,937	8,937	8,937
	MON	17,067	17,067	17,067	17,067	17,067
	OFC					
	SFC					
1.1	HYC	5,498	5,915	6,457	7,055	7,683
	ISS	8,985	8,985	8,985	8,985	8,985
	MON	17,705	17,705	17,705	17,705	17,706
	OFC					
	SFC					

Weight/Load Matrices - 101 Vehicle

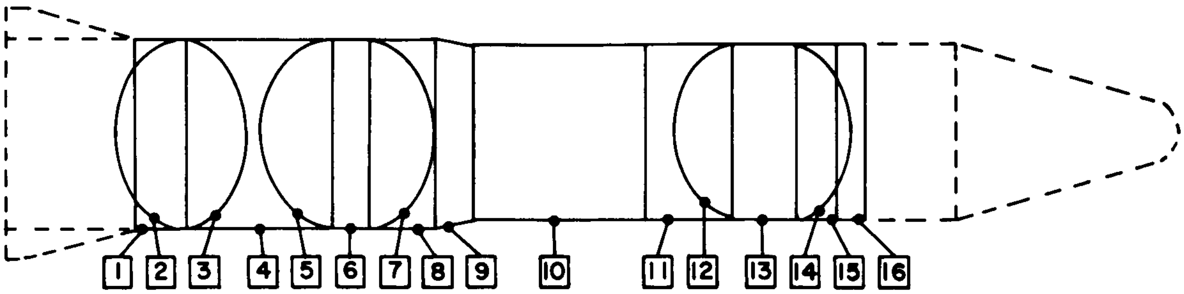

101 Vehicle Configuration
Section Number 7
LOX Tank Top Head

Material: Beryllium
N_x Nominal: ----
N_o Nominal: 4,659 lbs/in.

$\frac{N_x}{\bar{N}_x}$ Nom ↓ $\frac{N_o}{\bar{N}_o}$ Nom →		.7	.8	.9	1.0	1.1
.7	HYC					
	ISS					
	MON					
	OFC					
	SFC					
.8	HYC					
	ISS					
	MON					
	OFC					
	SFC					
.9	HYC					
	ISS					
	MON					
	OFC					
	SFC					
1.0	HYC	4,303	4,904	5,504	6,104	6,705
	ISS					
	MON	3,530	4,034	4,539	5,043	5,547
	OFC					
	SFC					
1.1	HYC					
	ISS					
	MON					
	OFC					
	SFC					

101 Vehicle Configuration
Section Number 8
Stage 1 Forward Skirt

Material: Beryllium
N_x Nominal: -9,277 lbs/in.
N_o Nominal: 9,277 lbs/in.

$\frac{N_x}{\bar{N}_x}$ Nom ↓ $\frac{N_o}{\bar{N}_o}$ Nom →		.7	.8	.9	1.0	1.1
.7	HYC	9,244				
	ISS	11,840				
	MON	31,682				
	OFC	43,061				
	SFC	9,675				
.8	HYC		10,323			
	ISS		12,666			
	MON		33,353			
	OFC		46,035			
	SFC		10,302			
.9	HYC			11,409		
	ISS			12,944		
	MON			34,900		
	OFC			48,827		
	SFC			10,938		
1.0	HYC				12,504	
	ISS				14,196	
	MON				36,345	
	OFC				51,468	
	SFC				11,519	
1.1	HYC					13,609
	ISS					14,618
	MON					37,704
	OFC					53,980
	SFC					12,091

101 Vehicle Configuration
Section Number 9
Interstage (1905" - 2075")

Material: Beryllium
N_x Nominal: -9,818 lbs/in.
N_o Nominal: 9,818 lbs/in.

$\frac{N_x}{\bar{N}_x}$ Nom ↓ $\frac{N_o}{\bar{N}_o}$ Nom →		.7	.8	.9	1.0	1.1
.7	HYC	5,807				
	ISS	7,432				
	MON	19,551				
	OFC	19,401				
	SFC	6,097				
.8	HYC		6,491			
	ISS		7,452			
	MON		20,583			
	OFC		20,741			
	SFC		6,388			
.9	HYC			7,181		
	ISS			8,230		
	MON			21,538		
	OFC			21,999		
	SFC			6,783		
1.0	HYC				7,877	
	ISS				8,754	
	MON				22,429	
	OFC				23,189	
	SFC				7,156	
1.1	HYC					8,581
	ISS					9,281
	MON					23,268
	OFC					24,321
	SFC					7,488

101 Vehicle Configuration
Section Number 10
Stage 2 Lower Skirt (2075" - 2795")

Material: Beryllium
N_x Nominal: -9,651 lbs/in.
N_o Nominal: 9,651 lbs/in.

$\frac{N_x}{\bar{N}_x}$ Nom ↓ $\frac{N_o}{\bar{N}_o}$ Nom →		.7	.8	.9	1.0	1.1
.7	HYC	22,338				
	ISS	29,639				
	MON	72,307				
	OFC	10,677				
	SFC	23,900				
.8	HYC		25,025			
	ISS		29,726			
	MON		76,122			
	OFC		114,136			
	SFC		23,904			
.9	HYC			27,737		
	ISS			31,891		
	MON			79,653		
	OFC			121,060		
	SFC			25,292		
1.0	HYC				30,480	
	ISS				32,058	
	MON				82,950	
	OFC				127,606	
	SFC				26,683	
1.1	HYC					33,259
	ISS					33,886
	MON					86,051
	OFC					133,837
	SFC					28,008

101 Vehicle Configuration
Section Number 11
Intertank (2795" - 3162.6")

Material: Beryllium
N_x Nominal: -4,484 lbs/in.
N_o Nominal: 4,484 lbs/in.

$\frac{N_x}{\bar{N}_x}$ Nom ↓ $\frac{N_o}{\bar{N}_o}$ Nom →		.7	.8	.9	1.0	1.1
.7	HYC	6,134				
	ISS	8,211				
	MON	27,462				
	OFC	30,653				
	SFC	7,730				
.8	HYC		6,865			
	ISS		8,699			
	MON		28,911			
	OFC		32,770			
	SFC		8,268			
.9	HYC			7,647		
	ISS			9,774		
	MON			30,252		
	OFC			34,758		
	SFC			8,757		
1.0	HYC				8,249	
	ISS				10,793	
	MON				31,504	
	OFC				36,638	
	SFC				9,282	
1.1	HYC					8,860
	ISS					11,621
	MON					32,682
	OFC					38,426
	SFC					9,739

101 Vehicle Configuration
Section Number 12
LH_2 Tank Bottom Head

Material: Beryllium
N_x Nominal: ----
N_o Nominal: 9,144 lbs/in.

$\frac{N_x}{\bar{N}_x}$ Nom ↓ $\frac{N_o}{\bar{N}_o}$ Nom →		.7	.8	.9	1.0	1.1
.7	HYC					
	ISS					
	MON					
	OFC					
	SFC					
.8	HYC					
	ISS					
	MON					
	OFC					
	SFC					
.9	HYC					
	ISS					
	MON					
	OFC					
	SFC					
1.0	HYC	6,942	7,921	8,901	9,881	10,860
	ISS					
	MON	5,760	6,583	7,406	8,229	9,051
	OFC					
	SFC					
1.1	HYC					
	ISS					
	MON					
	OFC					
	SFC					

Weight/Load Matrices - 101 Vehicle

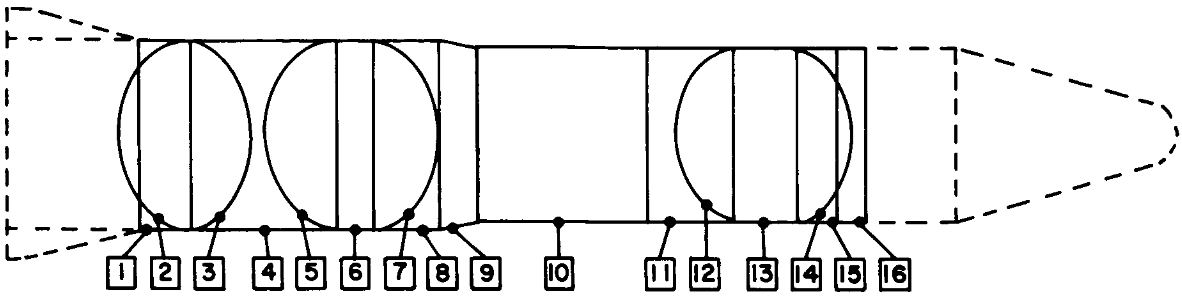

101 Vehicle Configuration
Section Number 13
LH_2 Tank Cylinder (3162.6" - 3439.4")

Material: Beryllium
N_x Nominal: - 684 lbs/in.
N_o Nominal: 12,839 lbs/in.

$\frac{N_x}{N_x \text{ Nom}}$ ↓ $\frac{N_o}{N_o \text{ Nom}}$ →		.7	.8	.9	1.0	1.1
.7	HYC	8,791	10,038	11,286	12,533	13,780
	ISS	15,259	15,259	15,259	15,259	15,259
	MON	10,008	10,008	10,008	10,477	11,525
	OFC					
	SFC					
.8	HYC	8,791	10,038	11,286	12,533	13,780
	ISS	15,259	15,259	15,259	15,259	15,259
	MON	10,536	10,536	10,536	10,582	11,526
	OFC					
	SFC					
.9	HYC	8,791	10,038	11,286	12,533	13,780
	ISS	15,259	15,259	15,259	15,259	15,259
	MON	11,025	11,025	11,025	11,025	11,525
	OFC					
	SFC					
1.0	HYC	8,791	10,038	11,286	12,533	13,780
	ISS	15,259	15,259	15,259	15,259	15,259
	MON	11,482	11,482	11,482	11,482	11,603
	OFC					
	SFC					
1.1	HYC	8,791	10,038	11,286	12,533	13,780
	ISS	15,259	15,259	15,259	15,259	15,259
	MON	11,911	11,911	11,911	11,911	11,911
	OFC					
	SFC					

101 Vehicle Configuration
Section Number 14
LH_2 Tank Top Head

Material: Beryllium
N_x Nominal: ----
N_o Nominal: 7,399 lbs/in.

$\frac{N_x}{N_x \text{ Nom}}$ ↓ $\frac{N_o}{N_o \text{ Nom}}$ →		.7	.8	.9	1.0	1.1
.7	HYC					
	ISS					
	MON					
	OFC					
	SFC					
.8	HYC					
	ISS					
	MON					
	OFC					
	SFC					
.9	HYC					
	ISS					
	MON					
	OFC					
	SFC					
1.0	HYC	5,655	6,451	7,247	8,043	8,838
	ISS					
	MON	4,679	5,348	6,016	6,685	7,353
	OFC					
	SFC					
1.1	HYC					
	ISS					
	MON					
	OFC					
	SFC					

101 Vehicle Configuration
Section Number 15
Stage 2 Forward Skirt (3439.4" - 3610")

Material: Beryllium
N_x Nominal: -2,762 lbs/in.
N_o Nominal: 2,762 lbs/in.

$\frac{N_x}{N_x \text{ Nom}}$ ↓ $\frac{N_o}{N_o \text{ Nom}}$ →		.7	.8	.9	1.0	1.1
.7	HYC	1,913				
	ISS	3,505				
	MON	10,574				
	OFC	9,430				
	SFC	2,816				
.8	HYC		2,129			
	ISS		3,528			
	MON		11,132			
	OFC		10,081			
	SFC		3,012			
.9	HYC			2,348		
	ISS			3,623		
	MON			11,648		
	OFC			10,693		
	SFC			3,191		
1.0	HYC				2,562	
	ISS				3,715	
	MON				12,130	
	OFC				11,271	
	SFC				3,365	
1.1	HYC					2,758
	ISS					3,804
	MON					12,584
	OFC					11,821
	SFC					3,530

101 Vehicle Configuration
Section Number 16
Instrument Unit (3610" - 3730")

Material: Beryllium
N_x Nominal: -2,418 lbs/in.
N_o Nominal: 2,418 lbs/in.

$\frac{N_x}{N_x \text{ Nom}}$ ↓ $\frac{N_o}{N_o \text{ Nom}}$ →		.7	.8	.9	1.0	1.1
.7	HYC	1,213				
	ISS	2,343				
	MON	7,073				
	OFC	19,242				
	SFC	1,856				
.8	HYC		1,348			
	ISS		2,397			
	MON		7,446			
	OFC		20,571			
	SFC		1,985			
.9	HYC			1,482		
	ISS			2,457		
	MON			7,791		
	OFC			21,819		
	SFC			2,107		
1.0	HYC				1,614	
	ISS				2,515	
	MON				8,114	
	OFC				22,999	
	SFC				2,212	
1.1	HYC					1,748
	ISS					2,572
	MON					8,417
	OFC					24,121
	SFC					2,321

Weight/Load Matrices - 101 Vehicle

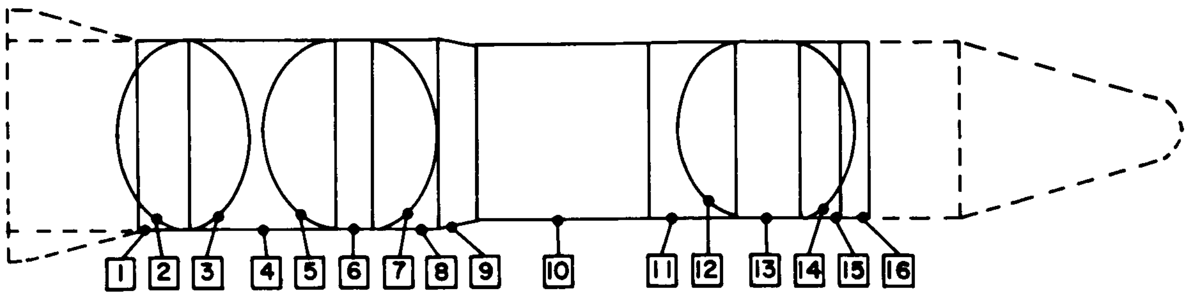

101 Vehicle Configuration
Section Number 1
Thrust Takeout (643.0" - 856.0")

Material: Aluminum 2219 - T87
N_x Nominal: -12,005 lbs/in.
N_o Nominal: 12,005 lbs/in.

$N_x/\overline{N}_x$ Nom ↓	$N_o/\overline{N}_o$ Nom →	.7	.8	.9	1.0	1.1
.7	HYC	17,464				
	ISS	37,999				
	MON	68,957				
	OFC	34,463				
	SFC	26,983				
.8	HYC		19,751			
	ISS		41,013			
	MON		72,595			
	OFC		36,843			
	SFC		28,869			
.9	HYC			22,026		
	ISS			44,201		
	MON			75,962		
	OFC			39,078		
	SFC			32,737		
1.0	HYC				24,311	
	ISS				47,291	
	MON				77,042	
	OFC				41,192	
	SFC				34,946	
1.1	HYC					25,945
	ISS					49,982
	MON					79,921
	OFC					43,201
	SFC					44,515

101 Vehicle Configuration
Section Number 2
RP-1 Tank Bottom Head

Material: Aluminum, 2219 - T87
N_x Nominal: ----
N_o Nominal: 5,607 lbs/in.

$N_x/\overline{N}_x$ Nom ↓	$N_o/\overline{N}_o$ Nom →	.7	.8	.9	1.0	1.1
.7	HYC					
	ISS					
	MON					
	OFC					
	SFC					
.8	HYC					
	ISS					
	MON					
	OFC					
	SFC					
.9	HYC					
	ISS					
	MON					
	OFC					
	SFC					
1.0	HYC	9,204	10,504	11,804	13,105	14,405
	ISS					
	MON	7,646	8,738	9,831	10,923	12,015
	OFC					
	SFC					
1.1	HYC					
	ISS					
	MON					
	OFC					
	SFC					

101 Vehicle Configuration
Section Number 3
RP-1 Tank Top Head

Material: Aluminum, 2219 - T87
N_x Nominal: ----
N_o Nominal: 4,462 lbs/in.

$N_x/\overline{N}_x$ Nom ↓	$N_o/\overline{N}_o$ Nom →	.7	.8	.9	1.0	1.1
.7	HYC					
	ISS					
	MON					
	OFC					
	SFC					
.8	HYC					
	ISS					
	MON					
	OFC					
	SFC					
.9	HYC					
	ISS					
	MON					
	OFC					
	SFC					
1.0	HYC	6,825	7,786	8,747	9,708	10,670
	ISS					
	MON	5,652	6,460	7,267	8,075	8,882
	OFC					
	SFC					
1.1	HYC					
	ISS					
	MON					
	OFC					
	SFC					

101 Vehicle Configuration
Section Number 4
Intertank (856.0" - 1477.0")

Material: Aluminum, 2219 - T87
N_x Nominal: -11,407 lbs/in.
N_o Nominal: 11,407 lbs/in.

$N_x/\overline{N}_x$ Nom ↓	$N_o/\overline{N}_o$ Nom →	.7	.8	.9	1.0	1.1
.7	HYC	48,639				
	ISS	106,690				
	MON	197,293				
	OFC	118,924				
	SFC	76,906				
.8	HYC		54,999			
	ISS		116,195			
	MON		207,701			
	OFC		127,135			
	SFC		82,290			
.9	HYC			61,366		
	ISS			125,700		
	MON			217,336		
	OFC			134,847		
	SFC			91,752		
1.0	HYC				67,584	
	ISS				135,205	
	MON				226,333	
	OFC				142,142	
	SFC				99,653	
1.1	HYC					73,951
	ISS					144,710
	MON					234,793
	OFC					149,079
	SFC					112,985

101 Vehicle Configuration
Section Number 5
LOX Tank Bottom Head

Material: Aluminum, 2219 - T87
N_x Nominal: ----
N_o Nominal: 8,288 lbs/in.

$N_x/\overline{N}_x$ Nom ↓	$N_o/\overline{N}_o$ Nom →	.7	.8	.9	1.0	1.1
.7	HYC					
	ISS					
	MON					
	OFC					
	SFC					
.8	HYC					
	ISS					
	MON					
	OFC					
	SFC					
.9	HYC					
	ISS					
	MON					
	OFC					
	SFC					
1.0	HYC	12,267	14,027	15,766	17,506	19,246
	ISS					
	MON	10,230	11,691	13,153	14,614	16,075
	OFC					
	SFC					
1.1	HYC					
	ISS					
	MON					
	OFC					
	SFC					

101 Vehicle Configuration
Section Number 6
LOX Tank Cylinder (1477.0" - 1627.0")

Material: Aluminum, 2219 - T87
N_x Nominal: -8,467 lbs/in.
N_o Nominal: 11,809 lbs/in.

$N_x/\overline{N}_x$ Nom ↓	$N_o/\overline{N}_o$ Nom →	.7	.8	.9	1.0	1.1
.7	HYC	8,009	9,038	10,079	11,128	12,183
	ISS	16,757	16,757	16,757	16,757	16,757
	MON	37,536	37,536	37,536	37,536	37,536
	OFC					
	SFC					
.8	HYC	8,090	9,095	10,129	11,173	12,225
	ISS	18,097	18,097	18,097	18,097	18,097
	MON	39,517	39,517	39,517	39,517	39,517
	OFC					
	SFC					
.9	HYC	8,271	9,164	10,181	11,219	12,267
	ISS	19,648	19,648	19,648	19,648	19,267
	MON	41,350	41,350	41,350	41,350	41,350
	OFC					
	SFC					
1.0	HYC	8,843	9,293	10,242	11,267	12,309
	ISS	20,971	20,971	20,971	20,971	20,971
	MON	43,062	43,062	43,062	43,062	43,062
	OFC					
	SFC					
1.1	HYC	9,533	9,652	10,341	11,321	12,353
	ISS	22,539	22,539	22,539	22,539	22,539
	MON	44,671	44,671	44,671	44,671	44,671
	OFC					
	SFC					

Weight/Load Matrices - 101 Vehicle

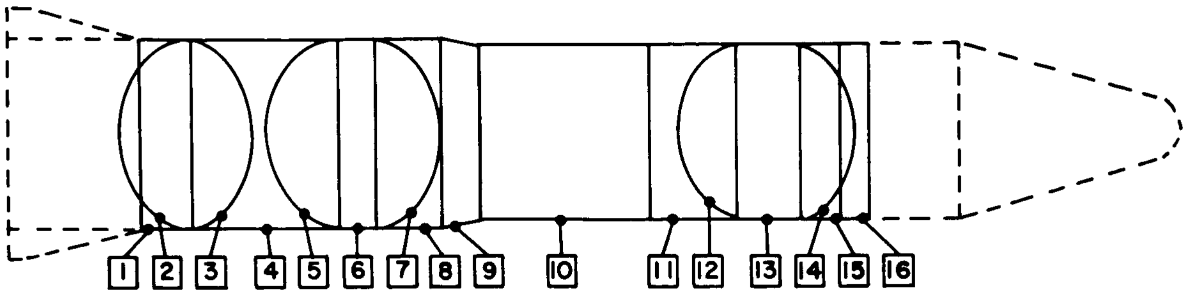

101 Vehicle Configuration
Section Number 7
LOX Tank Top Head

Material: Aluminum, 2219 - T87
N_x Nominal: ----
N_o Nominal: 4,659 lbs/in.

N_x ↓ $\frac{N_x}{N_x \text{ Nom}}$	N_o → $\frac{N_o}{N_o \text{ Nom}}$	.7	.8	.9	1.0	1.1
.7	HYC					
	ISS					
	MON					
	OFC					
	SFC					
.8	HYC					
	ISS					
	MON					
	OFC					
	SFC					
.9	HYC					
	ISS					
	MON					
	OFC					
	SFC					
1.0	HYC	7,055	8,049	9,042	10,036	11,029
	ISS					
	MON	5,842	6,676	7,511	8,345	9,180
	OFC					
	SFC					
1.1	HYC					
	ISS					
	MON					
	OFC					
	SFC					

101 Vehicle Configuration
Section Number 8
Stage 1 Forward Skirt (1627.0" - 1905.0")

Material: Aluminum, 2219 - T87
N_x Nominal: -9,277 lbs/in.
N_o Nominal: 9,277 lbs/in.

N_x ↓ $\frac{N_x}{N_x \text{ Nom}}$	N_o → $\frac{N_o}{N_o \text{ Nom}}$	.7	.8	.9	1.0	1.1
.7	HYC	17,960				
	ISS	38,512				
	MON	81,480				
	OFC	34,388				
	SFC	31,006				
.8	HYC		20,312			
	ISS		43,159			
	MON		85,778			
	OFC		36,762			
	SFC		33,061			
.9	HYC			22,621		
	ISS			47,733		
	MON			89,757		
	OFC			38,992		
	SFC			35,089		
1.0	HYC				24,929	
	ISS				52,357	
	MON				93,473	
	OFC				41,101	
	SFC				37,010	
1.1	HYC					27,217
	ISS					55,615
	MON					96,967
	OFC					43,107
	SFC					39,862

101 Vehicle Configuration
Section Number 9
Interstage (1905.0" - 2075.0")

Material: Aluminum, 2219 - T87
N_x Nominal: -9,818 lbs/in.
N_o Nominal: 9,818 lbs/in.

N_x ↓ $\frac{N_x}{N_x \text{ Nom}}$	N_o → $\frac{N_o}{N_o \text{ Nom}}$	.7	.8	.9	1.0	1.1
.7	HYC	11,315				
	ISS	24,768				
	MON	50,282				
	OFC	17,141				
	SFC	19,182				
.8	HYC		12,793			
	ISS		27,844			
	MON		52,935			
	OFC		18,324			
	SFC		20,523			
.9	HYC			14,255		
	ISS			30,641		
	MON			55,391		
	OFC			19,436		
	SFC			21,784		
1.0	HYC				15,708	
	ISS				33,583	
	MON				57,684	
	OFC				20,487	
	SFC				22,978	
1.1	HYC					17,168
	ISS					35,716
	MON					59,840
	OFC					21,487
	SFC					26,074

101 Vehicle Configuration
Section Number 10
Stage 2 Lower Skirt (2075.0" - 2795.0")

Material: Aluminum, 2219 - T87
N_x Nominal: -9,651 lbs/in.
N_o Nominal: 9,651 lbs/in.

N_x ↓ $\frac{N_x}{N_x \text{ Nom}}$	N_o → $\frac{N_o}{N_o \text{ Nom}}$	.7	.8	.9	1.0	1.1
.7	HYC	43,864				
	ISS	92,517				
	MON	185,960				
	OFC	84,019				
	SFC	71,584				
.8	HYC		49,606			
	ISS		103,193			
	MON		195,770			
	OFC		89,820			
	SFC		76,579			
.9	HYC			55,290		
	ISS			113,641		
	MON			204,852		
	OFC			95,268		
	SFC			81,277		
1.0	HYC				60,983	
	ISS				121,428	
	MON				213,332	
	OFC				100,421	
	SFC				92,673	
1.1	HYC					66,624
	ISS					128,991
	MON					221,306
	OFC					105,323
	SFC					97,257

101 Vehicle Configuration
Section Number 11
Intertank (2795.0" - 3162.6")

Material: Aluminum 2219 - T87
N_x Nominal: -4,484 lbs/in.
N_o Nominal: 4,484 lbs/in.

N_x ↓ $\frac{N_x}{N_x \text{ Nom}}$	N_o → $\frac{N_o}{N_o \text{ Nom}}$	.7	.8	.9	1.0	1.1
.7	HYC	11,256				
	ISS	28,719				
	MON	70,627				
	OFC	26,108				
	SFC	23,487				
.8	HYC		12,652			
	ISS		31,077			
	MON		74,353			
	OFC		27,911			
	SFC		25,009			
.9	HYC			14,045		
	ISS			32,956		
	MON			77,802		
	OFC			29,604		
	SFC			26,536		
1.0	HYC				15,432	
	ISS				35,527	
	MON				81,023	
	OFC				31,205	
	SFC				27,955	
1.1	HYC					16,812
	ISS					37,954
	MON					84,051
	OFC					32,729
	SFC					30,883

101 Vehicle Configuration
Section Number 12
LH_2 Tank Bottom Head

Material: Aluminum, 2219 - T87
N_x Nominal: ----
N_o Nominal: 9,144 lbs/in.

N_x ↓ $\frac{N_x}{N_x \text{ Nom}}$	N_o → $\frac{N_o}{N_o \text{ Nom}}$	.7	.8	.9	1.0	1.1
.7	HYC					
	ISS					
	MON					
	OFC					
	SFC					
.8	HYC					
	ISS					
	MON					
	OFC					
	SFC					
.9	HYC					
	ISS					
	MON					
	OFC					
	SFC					
1.0	HYC	10,471	11,955	13,439	14,923	16,406
	ISS					
	MON	8,725	9,971	11,218	12,464	13,710
	OFC					
	SFC					
1.1	HYC					
	ISS					
	MON					
	OFC					
	SFC					

Weight/Load Matrices - 101 Vehicle

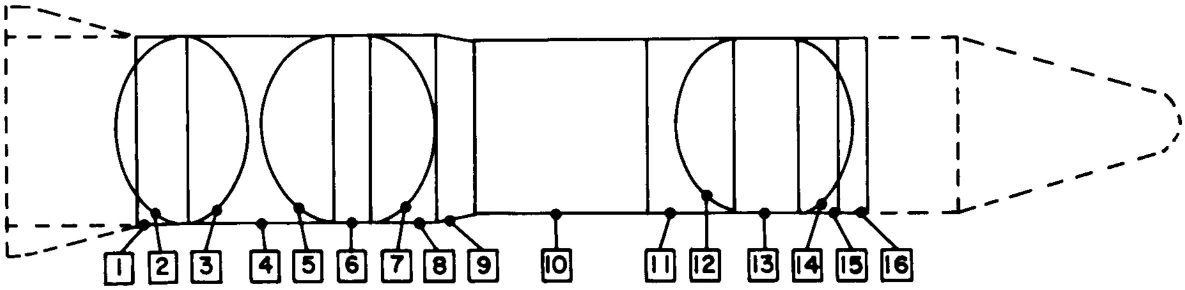

101 Vehicle Configuration
Section Number 13
LH_2 Tank Cylinder (3162.6" - 3439.4")

Material: Aluminum, 2219 - T87
N_x Nominal: - 684 lbs/in.
N_o Nominal: 12,839 lbs/in.

$\frac{N_x}{\bar{N}_x}$ Nom ↓	$\frac{N_o}{\bar{N}_o}$ Nom →	.7	.8	.9	1.0	1.1
.7	HYC	13,302	15,188	17,077	18,967	20,856
	ISS	23,886	23,886	23,886	23,886	23,886
	MON	25,102	25,102	25,102	25,102	25,102
	OFC					
	SFC					
.8	HYC	13,306	15,190	17,079	18,969	20,858
	ISS	24,128	24,128	24,128	24,128	24,128
	MON	26,427	26,427	26,427	26,427	26,427
	OFC					
	SFC					
.9	HYC	13,310	15,192	17,081	18,970	20,859
	ISS	24,371	24,371	24,371	24,371	24,371
	MON	27,652	27,652	27,652	27.652	27,652
	OFC					
	SFC					
1.0	HYC	13,313	15,193	17,082	18,972	20,816
	ISS	24,613	24,613	24,613	24,613	24,613
	MON	28,797	28,797	28.797	28,797	28,797
	OFC					
	SFC					
1.1	HYC	13,316	15,195	17,084	18,973	20,862
	ISS	24,856	24,856	24,856	24,856	24,856
	MON	29,874	29,874	29,874	29,874	29,874
	OFC					
	SFC					

101 Vehicle Configuration
Section Number 14
LH_2 Tank Top Head

Material: Aluminum 2219 - T87
N_x Nominal: ----
N_o Nominal: 7,399 lbs/in.

$\frac{N_x}{\bar{N}_x}$ Nom ↓	$\frac{N_o}{\bar{N}_o}$ Nom →	.7	.8	.9	1.0	1.1
.7	HYC					
	ISS					
	MON					
	OFC					
	SFC					
.8	HYC					
	ISS					
	MON					
	OFC					
	SFC					
.9	HYC					
	ISS					
	MON					
	OFC					
	SFC					
1.0	HYC	8,883	10,139	11,396	12,653	13,910
	ISS					
	MON	7,390	8,446	9,502	10,557	11,613
	OFC					
	SFC					
1.1	HYC					
	ISS					
	MON					
	OFC					
	SFC					

101 Vehicle Configuration
Section Number 15
Stage 2 Forward Skirt (3439.4" - 3610.0")

Material: Aluminum, 2210 - T87
N_x Nominal: -2,762 lbs/in.
N_o Nominal: 2,762 lbs/ in.

$\frac{N_x}{\bar{N}_x}$ Nom ↓	$\frac{N_o}{\bar{N}_o}$ Nom →	.7	.8	.9	1.0	1.1
.7	HYC	3,449				
	ISS	10,386				
	MON	27,194				
	OFC	8,504				
	SFC	8,550				
8	HYC		3,855			
	ISS		11,071			
	MON		28,629			
	OFC		9,091			
	SFC		9,127			
.9	HYC			4,262		
	ISS			11,771		
	MON			29,957		
	OFC			9,642		
	SFC			9,690		
1.0	HYC				4,666	
	ISS				12,523	
	MON				31,197	
	OFC				10,164	
	SFC				10,191	
1.1	HYC					5,072
	ISS					13,248
	MON					32,363
	OFC					10,660
	SFC					10,697

101 Vehicle Configuration
Section Number 16
Instrument Unit (3610.0" - 3730.0")

Material: Aluminum, 2219 - T87
N_x Nominal: -2,418 lbs/in.
N_o Nominal: 2,418 lbs/in.

$\frac{N_x}{\bar{N}_x}$ Nom ↓	$\frac{N_o}{\bar{N}_o}$ Nom →	.7	.8	.9	1.0	1.1
.7	HYC	2,177				
	ISS	6,835				
	MON	18,190				
	OFC	11,679				
	SFC	5,609				
.8	HYC		2,432			
	ISS		7,519			
	MON		19,150			
	OFC		12,486			
	SFC		6,002			
.9	HYC			2,685		
	ISS			8,192		
	MON			20,038		
	OFC			13,243		
	SFC			6,372		
1.0	HYC				2,934	
	ISS				8,736	
	MON				20,867	
	OFC				13,959	
	SFC				6,722	
1.1	HYC					3,184
	ISS					9,263
	MON					21,647
	OFC					14,641
	SFC					7,056

Weight/Load Matrices - 201 Vehicle

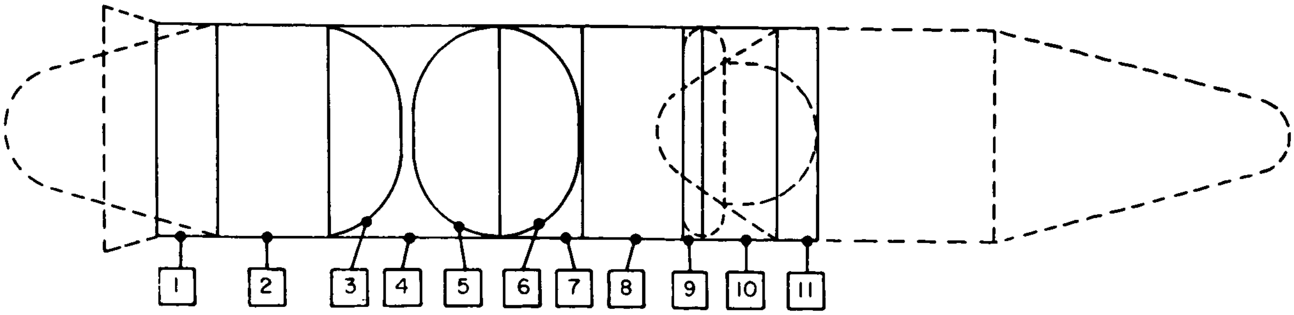

201 Vehicle Configuration
Section Number 1
Thrust Takeout (710" - 960")

Material: Aluminum, 2219-T87
N_x Nominal: -10,163 lb/in.
N_o Nominal: 10,163 lb/in.

$\frac{N_x}{N_x \text{ Nom}}$ ↓ $\frac{N_o}{N_o \text{ Nom}}$ →		.7	.8	.9	1.0	1.1
.7	HYC	17,842				
	ISS	39,517				
	MON	79,861				
	OFC	35,005				
	SFC	30,427				
.8	HYC		20,164			
	ISS		43,665			
	MON		84,074			
	OFC		37,421			
	SFC		32,553			
.9	HYC			22,462		
	ISS			48,896		
	MON			87,975		
	OFC			39,692		
	SFC			34,552		
1.0	HYC				24,754	
	ISS				53,698	
	MON				91,616	
	OFC				41,962	
	SFC				36,448	
1.1	HYC					27,038
	ISS					57,125
	MON					95,041
	OFC					43,881
	SFC					41,362

201 Vehicle Configuration
Section Number 2
LH_2 Tank Cylinder (960" - 1380")

Material: Aluminum, 2219 - T87
N_x Nominal: - 6,457 lbs/in.
N_o Nominal: 14,356 lbs/in.

$\frac{N_x}{N_x \text{ Nom}}$ ↓ $\frac{N_o}{N_o \text{ Nom}}$ →		.7	.8	.9	1.0	1.1
.7	HYC	28,520	32,290	36,090	39,911	43,747
	ISS	59,754	59,754	59,754	59,754	59,754
	MON	116,596	116,596	116,596	116,596	116,596
	OFC					
	SFC					
.8	HYC	28,690	32,440	36,226	40,035	43,860
	ISS	60,867	60,867	60,867	60,867	60,867
	MON	122,747	122,747	122,747	122,747	122,747
	OFC					
	SFC					
.9	HYC	28,869	32,591	36,360	40,157	43,974
	ISS	61,984	61,984	61,984	61,984	61,984
	MON	128,442	128,442	128,442	128,442	128,442
	OFC					
	SFC					
1.0	HYC	29,120	32,746	36,496	40,281	44,088
	ISS	63,411	63,411	63,411	63,411	63,411
	MON	133,759	133,759	133,759	133,759	133,759
	OFC					
	SFC					
1.1	HYC	29,841	32,932	36,634	40,404	44,201
	ISS	67,484	67,484	67,484	67,484	67,484
	MON	138,758	138,758	133,758	138,758	138,758
	OFC					
	SFC					

201 Vehicle Configuration
Section Number 3
LH_2 Tank Top Head

Material: Aluminum, 2219 - T87
N_x Nominal: ----
N_o Nominal: 8,137 lbs/in.

$\frac{N_x}{N_x \text{ Nom}}$ ↓ $\frac{N_o}{N_o \text{ Nom}}$ →		.7	.8	.9	1.0	1.1
.7	HYC					
	ISS					
	MON					
	OFC					
	SFC					
.8	HYC					
	ISS					
	MON					
	OFC					
	SFC					
.9	HYC					
	ISS					
	MON					
	OFC					
	SFC					
1.0	HYC	13,394	15,291	17,188	19,085	20,982
	ISS					
	MON	11,154	12,748	14,341	15,935	17,528
	OFC					
	SFC					
1.1	HYC					
	ISS					
	MON					
	OFC					
	SFC					

201 Vehicle Configuration
Section Number 4
Intertank (1380" - 2073")

Material: Aluminum, 2219 - T87
N_x Nominal: -10,334 lbs/in.
N_o Nominal: 10,334 lbs/in.

$\frac{N_x}{N_x \text{ Nom}}$ ↓ $\frac{N_o}{N_o \text{ Nom}}$ →		.7	.8	.9	1.0	1.1
.7	HYC	53,173				
	ISS	115,361				
	MON	235,813				
	OFC	126,048				
	SFC	90,154				
.8	HYC		60,097			
	ISS		127,605			
	MON		248,253			
	OFC		134,751			
	SFC		96,316			
.9	HYC			66,958		
	ISS			145,892		
	MON			259,770		
	OFC			142,925		
	SFC			102,235		
1.0	HYC				73,784	
	ISS				156,026	
	MON				270,524	
	OFC				150,657	
	SFC				107,841	
1.1	HYC					80,633
	ISS					165,879
	MON					280,635
	OFC					158,010
	SFC					122,378

201 Vehicle Configuration
Section Number 5
LOX Tank Bottom Head

Material: Aluminum, 2219 - T87
N_x Nominal: ----
N_o Nominal: 9,386 lbs/in.

$\frac{N_x}{N_x \text{ Nom}}$ ↓ $\frac{N_o}{N_o \text{ Nom}}$ →		.7	.8	.9	1.0	1.1
.7	HYC					
	ISS					
	MON					
	OFC					
	SFC					
.8	HYC					
	ISS					
	MON					
	OFC					
	SFC					
.9	HYC					
	ISS					
	MON					
	OFC					
	SFC					
1.0	HYC	16,227	18,527	20,827	23,127	25,427
	ISS					
	MON	13,523	15,455	17,387	19,318	21,250
	OFC					
	SFC					
1.1	HYC					
	ISS					
	MON					
	OFC					
	SFC					

201 Vehicle Configuration
Section Number 6
LOX Tank Top Head

Material: Aluminum, 2219 - T87
N_x Nominal: ----
N_o Nominal: 4,308 lbs/in.

$\frac{N_x}{N_x \text{ Nom}}$ ↓ $\frac{N_o}{N_o \text{ Nom}}$ →		.7	.8	.9	1.0	1.1
.7	HYC					
	ISS					
	MON					
	OFC					
	SFC					
.8	HYC					
	ISS					
	MON					
	OFC					
	SFC					
.9	HYC					
	ISS					
	MON					
	OFC					
	SFC					
1.0	HYC	7,403	8,445	9,486	10,527	11,568
	ISS					
	MON	6,122	6,997	7,871	8,746	9,620
	OFC					
	SFC					
1.1	HYC					
	ISS					
	MON					
	OFC					
	SFC					

Weight/Load Matrices - 201 Vehicle

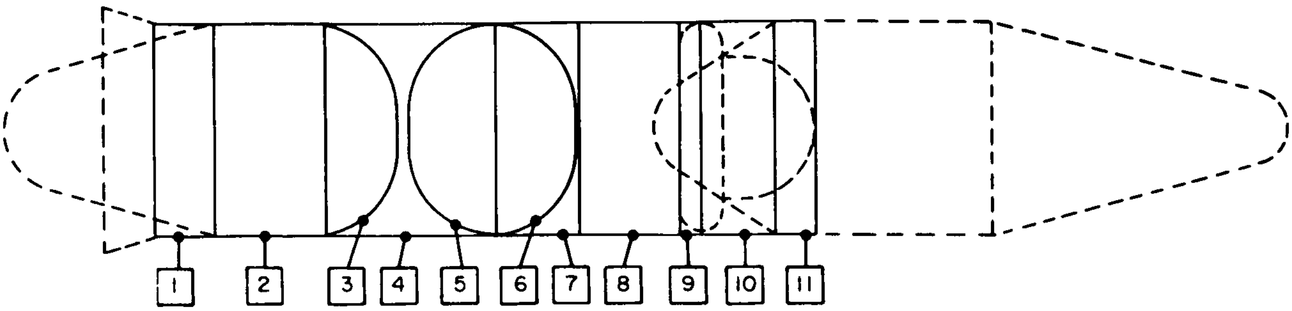

201 Vehicle Configuration
Section Number 7
Stage 1 Forward Skirt (2073" - 2370")

Material: Aluminum, 2219 - T87
N_x Nominal: -6,617 lbs/in.
N_o Nominal: 6,617 lbs/in.

$N_x/\bar{N}_x$ Nom ↓	$N_o/\bar{N}_o$ Nom →	.7	.8	.9	1.0	1.1
.7	HYC	15.208				
	ISS	36.603				
	MON	85.003				
	OFC	34,454				
	SFC	28,746				
.8	HYC		17.126			
	ISS		40.435			
	MON		89.487			
	OFC		36.833			
	SFC		30.820			
.9	HYC			19.046		
	ISS			43.946		
	MON			93.639		
	OFC			39,067		
	SFC			34.964		
1.0	HYC				20.950	
	ISS				46,882	
	MON				97,515	
	OFC				41,181	
	SFC				36,879	
1.1	HYC					22,862
	ISS					48,875
	MON					101,160
	OFC					43.190
	SFC					38.704

201 Vehicle Configuration
Section Number 8
Interstage (2370.0" - 2797.0")

Material: Aluminum, 2219 - T87
N_x Nominal: -6,279 lbs/in.
N_o Nominal: 6,279 lbs/in.

$N_x/\bar{N}_x$ Nom ↓	$N_o/\bar{N}_o$ Nom →	.7	.8	.9	1.0	1.1
.7	HYC	20.860				
	ISS	52.056				
	MON	119.838				
	OFC	76,260				
	SFC	40.443				
.8	HYC		23.516			
	ISS		56,275			
	MON		126,159			
	OFC		81.526			
	SFC		43.042			
.9	HYC			26.137		
	ISS			60,746		
	MON			132,012		
	OFC			86,471		
	SFC			48,215		
1.0	HYC				28.746	
	ISS				65.266	
	MON				137.480	
	OFC				91.149	
	SFC				51.700	
1.1	HYC					31.336
	ISS					69.557
	MON					142.615
	OFC					95,597
	SFC					54,258

201 Vehicle Configuration
Section Number 9
Stage 2 Lower Skirt (2797" - 2862")

Material: Aluminum, 2219 - T87
N_x Nominal: -6041 lbs/in.
N_o Nominal: 6041 lbs/in.

$N_x/\bar{N}_x$ Nom ↓	$N_o/\bar{N}_o$ Nom →	.7	.8	.9	1.0	1.1
.7	HYC	2.064				
	ISS	8.283				
	MON	17.983				
	OFC	2.619				
	SFC	6.034				
.8	HYC		2.356			
	ISS		8.981			
	MON		18.931			
	OFC		2,800			
	SFC		6.419			
.9	HYC			2.649		
	ISS			9.691		
	MON			19,810		
	OFC			2,970		
	SFC			6,852		
1.0	HYC				2,941	
	ISS				10,389	
	MON				20,630	
	OFC				3,131	
	SFC				7.733	
1.1	HYC					3.234
	ISS					11.042
	MON					21.401
	OFC					3,283
	SFC					8,116

201 Vehicle Configuration
Section Number 10
Intertank (2862" - 3201.5")

Material: Aluminum, 2219 - T87
N_x Nominal: -3,867 lbs/in.
N_o Nominal: 3,867 lbs/in.

$N_x/\bar{N}_x$ Nom ↓	$N_o/\bar{N}_o$ Nom →	.7	.8	.9	1.0	1.1
.7	HYC	10.860				
	ISS	31.434				
	MON	78.852				
	OFC	44,767				
	SFC	25,218				
.8	HYC		12.188			
	ISS		34.045			
	MON		83.012			
	OFC		47.858			
	SFC		26.988			
.9	HYC			13.502		
	ISS			36.549		
	MON			86,862		
	OFC			50,761		
	SFC			28.653		
1.0	HYC				14.795	
	ISS				38,963	
	MON				90,458	
	OFC				53,507	
	SFC				30.138	
1.1	HYC					16,069
	ISS					41,048
	MON					93,839
	OFC					56,118
	SFC					31,559

201 Vehicle Configuration
Section Number 11
IU and Forward Skirt (3201.5" - 3321.5")

Material: Aluminum, 2219 - T87
N_x Nominal: -3,069 lbs/in.
N_o Nominal: 3,069 lbs/in.

$N_x/\bar{N}_x$ Nom ↓	$N_o/\bar{N}_o$ Nom →	.7	.8	.9	1.0	1.1
.7	HYC	3.176				
	ISS	10.120				
	MON	25.577				
	OFC	25,684				
	SFC	7,987				
.8	HYC		3,552			
	ISS		11,312			
	MON		26.927			
	OFC		27.457			
	SFC		8.548			
.9	HYC			3.925		
	ISS			12.172		
	MON			28.176		
	OFC			29,123		
	SFC			9,077		
1.0	HYC				4.292	
	ISS				13,004	
	MON				29.343	
	OFC				30.698	
	SFC				9.481	
1.1	HYC					4,662
	ISS					13,830
	MON					30.439
	OFC					32,197
	SFC					9,949

Weight/Load Matrices - 201 Vehicle

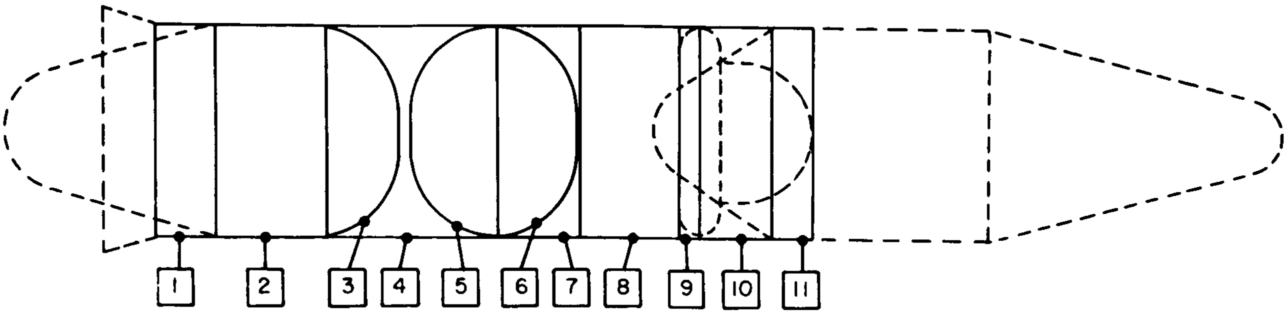

201 Vehicle Configuration
Section Number 1
Thrust Takeout (710" - 960")

Material: Beryllium
N_x Nominal: -10.163 lbs/in
N_o Nominal: 10.163 lbs/in

$N_x/N_{x\,Nom}$ ↓	$N_o/N_{o\,Nom}$ →	.7	.8	.9	1.0	1.1
.7	HYC	9.156				
	ISS	11.747				
	MON	31.053				
	OFC	46.459				
	SFC	9.603				
.8	HYC		10,231			
	ISS		11,873			
	MON		32,690			
	OFC		49,667			
	SFC		10,134			
.9	HYC			11,312		
	ISS			13,114		
	MON			34,208		
	OFC			52,680		
	SFC			10,761		
1.0	HYC				12,404	
	ISS				13,953	
	MON				35,623	
	OFC				55,529	
	SFC				11,317	
1.1	HYC					13,505
	ISS					14,765
	MON					36,955
	OFC					58,239
	SFC					11,878

201 Vehicle Configuration
Section Number 2
LH_2 Tank Cylinder (960" - 1380")

Material: Beryllium
N_x Nominal: - 6.457 lbs/in
N_o Nominal: 14.356 lbs/in

$N_x/N_{x\,Nom}$ ↓	$N_o/N_{o\,Nom}$ →	.7	.8	.9	1.0	1.1
.7	HYC	17.705	20.081	22.487	24.908	27.338
	ISS	32.527	32.527	32.527	32.527	32.527
	MON	46.416	46.416	46.416	46.416	46.416
	OFC					
	SFC					
.8	HYC	17.855	20.188	22.570	24.978	27.400
	ISS	33,131	33,131	33,131	33,131	33,131
	MON	48,865	48,865	48,865	48,865	48,865
	OFC					
	SFC					
.9	HYC	18,059	20,325	22,673	25,061	27,470
	ISS	33,733	33,733	33,733	33,733	33,733
	MON	51,132	51,132	51,132	51,132	51,132
	OFC					
	SFC					
1.0	HYC	18.338	20.505	22.801	25.161	27.553
	ISS	34.337	34.337	34.337	34.337	34.337
	MON	53.249	53.249	53.249	53.249	53.249
	OFC					
	SFC					
1.1	HYC	18.716	20.741	22.965	25.284	27.652
	ISS	34.939	34.939	34.939	34.939	34.939
	MON	55.239	55.239	55.239	55.239	55.239
	OFC					
	SFC					

201 Vehicle Configuration
Section Number 3
LH_2 Tank Top Head

Material: Beryllium
N_x Nominal: —
N_o Nominal: 8137 lbs/in

$N_x/N_{x\,Nom}$ ↓	$N_o/N_{o\,Nom}$ →	.7	.8	.9	1.0	1.1
.7	HYC					
	ISS					
	MON					
	OFC					
	SFC					
.8	HYC					
	ISS					
	MON					
	OFC					
	SFC					
.9	HYC					
	ISS					
	MON					
	OFC					
	SFC					
1.0	HYC	8.434	9.622	10.811	11.999	13.188
	ISS					
	MON	6,988	7,986	8,984	9,982	10.981
	OFC					
	SFC					
1.1	HYC					
	ISS					
	MON					
	OFC					
	SFC					

201 Vehicle Configuration
Section Number 4
Intertank (1380" - 2073")

Material: Beryllium
N_x Nominal: -10.334 lbs/in
N_o Nominal: 10.334 lbs/in

$N_x/N_{x\,Nom}$ ↓	$N_o/N_{o\,Nom}$ →	.7	.8	.9	1.0	1.1
.7	HYC	27.251				
	ISS	34.416				
	MON	91.691				
	OFC	176,287				
	SFC	28,666				
.8	HYC		30,463			
	ISS		35,141			
	MON		96,529			
	OFC		188,459			
	SFC		29,985			
.9	HYC			33,699		
	ISS			38,812		
	MON			101,007		
	OFC			199,890		
	SFC			31,812		
1.0	HYC				36.965	
	ISS				40.825	
	MON				105.188	
	OFC				210,703	
	SFC				33.565	
1.1	HYC					40.264
	ISS					43.178
	MON					109.119
	OFC					220.987
	SFC					35.235

201 Vehicle Configuration
Section Number 5
LOX Tank Bottom Head

Material: Beryllium
N_x Nominal: —
N_o Nominal: 9386 lbs/in

$N_x/N_{x\,Nom}$ ↓	$N_o/N_{o\,Nom}$ →	.7	.8	.9	1.0	1.1
.7	HYC					
	ISS					
	MON					
	OFC					
	SFC					
.8	HYC					
	ISS					
	MON					
	OFC					
	SFC					
.9	HYC					
	ISS					
	MON					
	OFC					
	SFC					
1.0	HYC	10.648	12.151	13.653	15.157	16.660
	ISS					
	MON	8.836	10.099	11.361	12.623	13.886
	OFC					
	SFC					
1.1	HYC					
	ISS					
	MON					
	OFC					
	SFC					

201 Vehicle Configuration
Section Number 6
LOX Tank Top Head

Material: Beryllium
N_x Nominal: —
N_o Nominal: 4308 lbs/in

$N_x/N_{x\,Nom}$ ↓	$N_o/N_{o\,Nom}$ →	.7	.8	.9	1.0	1.1
.7	HYC					
	ISS					
	MON					
	OFC					
	SFC					
.8	HYC					
	ISS					
	MON					
	OFC					
	SFC					
.9	HYC					
	ISS					
	MON					
	OFC					
	SFC					
1.0	HYC	4.519	5.149	5.778	6.407	7.036
	ISS					
	MON	3,699	4,228	4,756	5,284	5,813
	OFC					
	SFC					
1.1	HYC					
	ISS					
	MON					
	OFC					
	SFC					

Weight/Load Matrices - 201 Vehicle

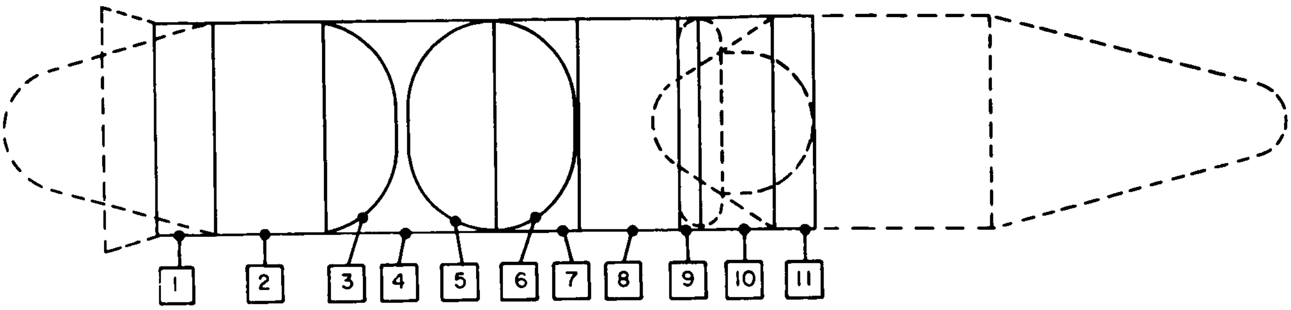

201 Vehicle Configuration
Section Number 7
Stage 1 Forward Skirt (2073" - 2370")

Material: Beryllium
N_x Nominal: -6617 lbs/in
N_o Nominal: 6617 lbs/in

N_x/N_x Nom ↓	N_o/N_o Nom →	.7	.8	.9	1.0	1.1
.7	HYC	8,252				
	ISS	10,548				
	MON	33,052				
	OFC	43,190				
	SFC	9,549				
.8	HYC		9,119			
	ISS		11,838			
	MON		34,796			
	OFC		46,172			
	SFC		10,266			
.9	HYC			9,988		
	ISS			12,666		
	MON			36,401		
	OFC			48,973		
	SFC			10,900		
1.0	HYC				10,863	
	ISS				13,706	
	MON				37,917	
	OFC				51,622	
	SFC				11,483	
1.1	HYC					11,741
	ISS					14,318
	MON					39,334
	OFC					54,142
	SFC					12,036

201 Vehicle Configuration
Section Number 8
Interstage (2370.0" - 2797.0")

Material: Beryllium
N_x Nominal: -6279 lbs/in
N_o Nominal: 6279 lbs/in

N_x/N_x Nom ↓	N_o/N_o Nom →	.7	.8	.9	1.0	1.1
.7	HYC	11,258				
	ISS	14,535				
	MON	46,597				
	OFC	119,344				
	SFC	13,389				
.8	HYC		12,596			
	ISS		16,756			
	MON		49,055			
	OFC		127,584			
	SFC		14,359			
.9	HYC			13,769		
	ISS			17,930		
	MON			51,330		
	OFC			135,324		
	SFC			15,245		
1.0	HYC				14,956	
	ISS				19,363	
	MON				53,455	
	OFC				142,644	
	SFC				16,068	
1.1	HYC					16,148
	ISS					19,600
	MON					55,453
	OFC					149,606
	SFC					16,865

201 Vehicle Configuration
Section Number 9
Stage 2 Lower Skirt (2797" - 2862")

Material: Beryllium
N_x Nominal: -6041 lbs/in
N_o Nominal: 6041 lbs/in

N_x/N_x Nom ↓	N_o/N_o Nom →	.7	.8	.9	1.0	1.1
.7	HYC	1,143				
	ISS	2,217				
	MON	6,992				
	OFC	867				
	SFC	2,009				
.8	HYC		1,304			
	ISS		2,453			
	MON		7,361			
	OFC		927			
	SFC		2,129			
.9	HYC			1,465		
	ISS			2,753		
	MON			7,703		
	OFC			984		
	SFC			2,283		
1.0	HYC				1,626	
	ISS				2,931	
	MON				8,021	
	OFC				1,037	
	SFC				2,409	
1.1	HYC					1,766
	ISS					3,102
	MON					8,321
	OFC					1,087
	SFC					2,512

201 Vehicle Configuration
Section Number 10
Intertank (2862" - 3201.5")

Material: Beryllium
N_x Nominal: -3867 lbs/in
N_o Nominal: 3867 lbs/in

N_x/N_x Nom ↓	N_o/N_o Nom →	.7	.8	.9	1.0	1.1
.7	HYC	6,073				
	ISS	8,769				
	MON	30,660				
	OFC	69,008				
	SFC	8,341				
.8	HYC		6,753			
	ISS		9,059			
	MON		32,278			
	OFC		73,772			
	SFC		8,914			
.9	HYC			7,441		
	ISS			9,815		
	MON			33,775		
	OFC			78,247		
	SFC			9,465		
1.0	HYC				8,123	
	ISS				10,630	
	MON				35,173	
	OFC				82,480	
	SFC				9,948	
1.1	HYC					8,847
	ISS					11,582
	MON					36,488
	OFC					86,506
	SFC					10,470

201 Vehicle Configuration
Section Number 11
IU and Forward Skirt (3301.5" - 3321.4")

Material: Beryllium
N_x Nominal: -3069 lbs/in
N_o Nominal: 3069 lbs/in

N_x/N_x Nom ↓	N_o/N_o Nom →	.7	.8	.9	1.0	1.1
.7	HYC	1,763				
	ISS	2,922				
	MON	9,945				
	OFC	46,057				
	SFC	2,628				
.8	HYC		1,961			
	ISS		3,014			
	MON		10,470			
	OFC		49,237			
	SFC		2,810			
.9	HYC			2,159		
	ISS			3,103		
	MON			10,956		
	OFC			52,224		
	SFC			2,981		
1.0	HYC				2,354	
	ISS				3,313	
	MON				11,409	
	OFC				55,049	
	SFC				3,144	
1.1	HYC					2,538
	ISS					3,500
	MON					11,836
	OFC					57,736
	SFC					3,298

Weight/Load Matrices - 201 Vehicle

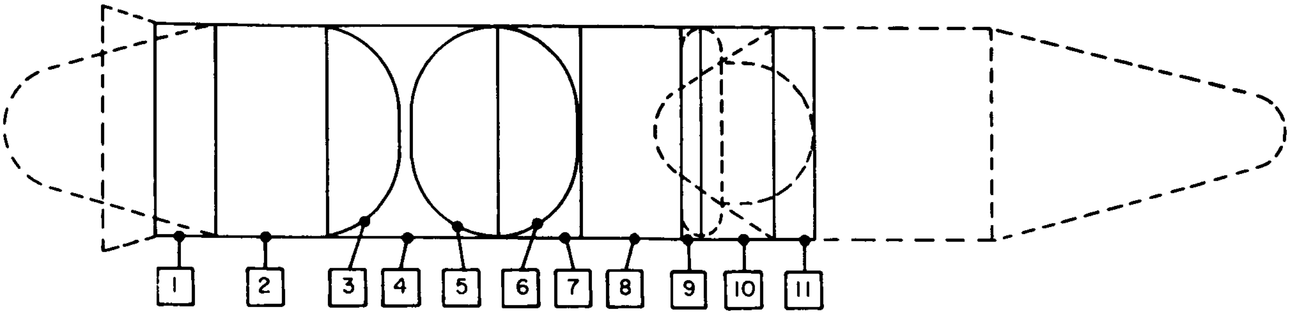

201 Vehicle Configuration
Section Number 1
Thrust Takeout (710" - 960")

Material: Titanium
N_x Nominal: -10,163 lbs/in
N_o Nominal: 10,163 lbs/in

N_x ↓ $\frac{N_x}{N_x \text{ Nom}}$	N_o → $\frac{N_o}{N_o \text{ Nom}}$	.7	.8	.9	1.0	1.1
.7	HYC	13,953				
	ISS	48,327				
	MON	108,062				
	OFC	44,093				
	SFC	36,620				
.8	HYC		15,549			
	ISS		51,265			
	MON		113,763			
	OFC		47,136			
	SFC		39,278			
.9	HYC			17,136		
	ISS			55,731		
	MON			119,040		
	OFC			49,996		
	SFC			44,617		
1.0	HYC				18,715	
	ISS				59,444	
	MON				123,967	
	OFC				52,700	
	SFC				46,810	
1.1	HYC					20,288
	ISS					63,938
	MON					128,602
	OFC					55,272
	SFC					49,121

201 Vehicle Configuration
Section Number 2
LH_2 Tank Cylinder (960" - 1380")

Material: Titanium
N_x Nominal: - 6,457 lbs/in
N_o Nominal: 14,356 lbs/in

N_x ↓ $\frac{N_x}{N_x \text{ Nom}}$	N_o → $\frac{N_o}{N_o \text{ Nom}}$	.7	.8	.9	1.0	1.1
.7	HYC	22,625	24,511	26,534	28,654	30,843
	ISS	63,394	63,394	63,394	63,394	63,394
	MON	157,720	157,720	157,720	157,720	157,720
	OFC					
	SFC					
.8	HYC	23,350	25,142	27,101	29,205	31,310
	ISS	68,678	68,678	68,678	68,678	68,678
	MON	166,040	166,040	166,040	166,040	166,040
	OFC					
	SFC					
.9	HYC	24,075	25,783	27,668	29,678	31,778
	ISS	73,747	73,747	73,747	73,747	73,747
	MON	173,743	173,743	173,743	173,743	173,743
	OFC					
	SFC					
1.0	HYC	24,802	26,420	28,235	30,189	32,244
	ISS	78,635	78,635	78,635	78,635	78,635
	MON	180,936	180,936	180,936	180,936	180,936
	OFC					
	SFC					
1.1	HYC	25,543	27,056	28,803	30,702	32,711
	ISS	83,372	83,372	83,372	83,372	83,372
	MON	187,696	187,696	187,696	187,696	187,696
	OFC					
	SFC					

201 Vehicle Configuration
Section Number 3
LH_2 Tank Top Head

Material: Titanium
N_x Nominal: —
N_o Nominal: 8,137 lbs/in

N_x ↓ $\frac{N_x}{N_x \text{ Nom}}$	N_o → $\frac{N_o}{N_o \text{ Nom}}$	.7	.8	.9	1.0	1.1
.7	HYC					
	ISS					
	MON					
	OFC					
	SFC					
.8	HYC					
	ISS					
	MON					
	OFC					
	SFC					
.9	HYC					
	ISS					
	MON					
	OFC					
	SFC					
1.0	HYC	8,672	9,894	11,116	12,339	13,561
	ISS					
	MON	7,187	8,214	9,241	10,268	11,294
	OFC					
	SFC					
1.1	HYC					
	ISS					
	MON					
	OFC					
	SFC					

201 Vehicle Configuration
Section Number 4
Intertank (1380" - 2073")

Material: Titanium
N_x Nominal: -10,334 lbs/in
N_o Nominal: 10,334 lbs/in

N_x ↓ $\frac{N_x}{N_x \text{ Nom}}$	N_o → $\frac{N_o}{N_o \text{ Nom}}$	.7	.8	.9	1.0	1.1
.7	HYC	41,479				
	ISS	138,573				
	MON	319,064				
	OFC	158,518				
	SFC	107,988				
.8	HYC		46,237			
	ISS		149,451			
	MON		335,917			
	OFC		169,462			
	SFC		116,618			
.9	HYC			50,970		
	ISS			162,661		
	MON			351,500		
	OFC			179,742		
	SFC			131,491		
1.0	HYC				55,682	
	ISS				173,406	
	MON				366,051	
	OFC				189,465	
	SFC				138,693	
1.1	HYC					60,375
	ISS					186,632
	MON					379,733
	OFC					198,712
	SFC					145,337

201 Vehicle Configuration
Section Number 5
LOX Tank Bottom Head

Material: Titanium
N_x Nominal: —
N_o Nominal: 9,386 lbs/in.

N_x ↓ $\frac{N_x}{N_x \text{ Nom}}$	N_o → $\frac{N_o}{N_o \text{ Nom}}$	.7	.8	.9	1.0	1.1
.7	HYC					
	ISS					
	MON					
	OFC					
	SFC					
.8	HYC					
	ISS					
	MON					
	OFC					
	SFC					
.9	HYC	10,386	11,852	13,317	14,782	16,248
	ISS					
	MON	8,616	9,847	11,078	12,309	13,540
	OFC					
	SFC					
1.0	HYC					
	ISS					
	MON					
	OFC					
	SFC					
1.1	HYC					
	ISS					
	MON					
	OFC					
	SFC					

201 Vehicle Configuration
Section Number 6
LOX Tank Top Head

Material: Titanium
N_x Nominal: —
N_o Nominal: 4,308 lbs/in

N_x ↓ $\frac{N_x}{N_x \text{ Nom}}$	N_o → $\frac{N_o}{N_o \text{ Nom}}$	.7	.8	.9	1.0	1.1
.7	HYC					
	ISS					
	MON					
	OFC					
	SFC					
.8	HYC					
	ISS					
	MON					
	OFC					
	SFC					
.9	HYC					
	ISS					
	MON					
	OFC					
	SFC					
1.0	HYC	4,891	5,573	6,225	6,937	7,620
	ISS					
	MON	4,011	4,584	5,157	5,731	6,304
	OFC					
	SFC					
1.1	HYC					
	ISS					
	MON					
	OFC					
	SFC					

Weight/Load Matrices - 201 Vehicle

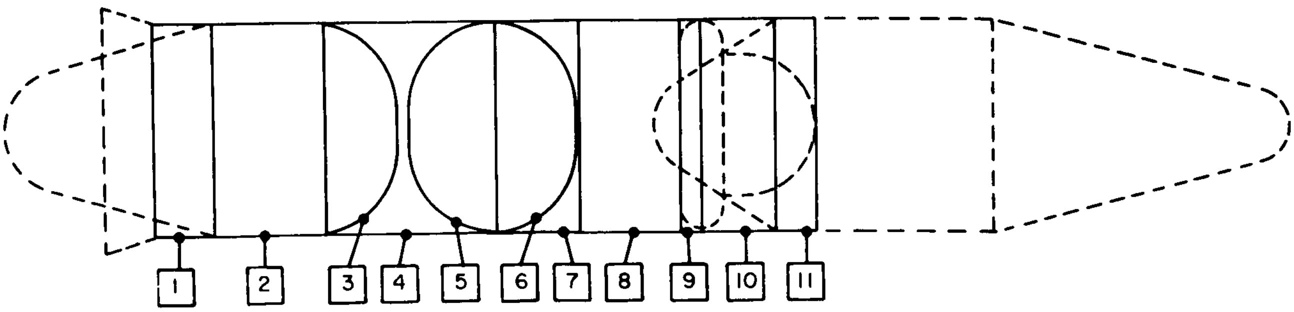

201 Vehicle Configuration
Section Number 7
Stage 1 Forward Skirt (2073" - 2370")

Material: Titanium
N_x Nominal: -6617 lbs/in
N_o Nominal: 6617 lbs/in

N_x / N_x Nom ↓ N_o / N_o Nom →		.7	.8	.9	1.0	1.1
.7	HYC	12,555				
	ISS	46,859				
	MON	115,020				
	OFC	43,470				
	SFC	37,221				
.8	HYC		13,883			
	ISS		49,305			
	MON		121,087			
	OFC		46,472			
	SFC		39,830			
.9	HYC			15,205		
	ISS			52,880		
	MON			126,705		
	OFC			49,291		
	SFC			42,285		
1.0	HYC				16,521	
	ISS				56,323	
	MON				131,950	
	OFC				51,957	
	SFC				44,470	
1.1	HYC					17,831
	ISS					59,215
	MON					136,882
	OFC					54,493
	SFC					46,405

201 Vehicle Configuration
Section Number 8
Interstage (2370.0" - 2797.0")

Material: Titanium
N_x Nominal: -6279 lbs/in
N_o Nominal: 6279 lbs/in

N_x / N_x Nom ↓ N_o / N_o Nom →		.7	.8	.9	1.0	1.1
.7	HYC	17,380				
	ISS	65,301				
	MON	162,155				
	OFC	95,546				
	SFC	52,215				
.8	HYC		19,196			
	ISS		70,737			
	MON		170,709			
	OFC		102,143			
	SFC		55,878			
.9	HYC			21,006		
	ISS			75,952		
	MON			178,628		
	OFC			108,339		
	SFC			59,326		
1.0	HYC				22,804	
	ISS				80,982	
	MON				186,023	
	OFC				114,200	
	SFC				62,593	
1.1	HYC					24,594
	ISS					85,854
	MON					192,976
	OFC					119,774
	SFC					64,994

201 Vehicle Configuration
Section Number 9
Stage 2 Lower Skirt

Material: Titanium
N_x Nominal: -6041 lbs/in
N_o Nominal: 6041 lbs/in

N_x / N_x Nom ↓ N_o / N_o Nom →		.7	.8	.9	1.0	1.1
.7	HYC	1,576				
	ISS	10,298				
	MON	24,333				
	OFC	3,373				
	SFC	7,822				
.8	HYC		1,799			
	ISS		10,520			
	MON		25,616			
	OFC		3,606			
	SFC		8,372			
.9	HYC			2,022		
	ISS			10,743		
	MON			26,805		
	OFC			3,824		
	SFC			8,802		
1.0	HYC				2,244	
	ISS				10,965	
	MON				27,914	
	OFC				4,031	
	SFC				9,283	
1.1	HYC					2,467
	ISS					11,187
	MON					28,958
	OFC					4,228
	SFC					9,741

201 Vehicle Configuration
Section Number 10
Intertank (2862" - 3201.5")

Material: Titanium
N_x Nominal: -3867 lbs/in
N_o Nominal: 3867 lbs/in

N_x / N_x Nom ↓ N_o / N_o Nom →		.7	.8	.9	1.0	1.1
.7	HYC	9,856				
	ISS	38,121				
	MON	106,696				
	OFC	56,118				
	SFC	32,557				
.8	HYC		10,771			
	ISS		41,991			
	MON		112,325			
	OFC		59,993			
	SFC		34,788			
.9	HYC			11,679		
	ISS			45,041		
	MON			117,535		
	OFC			63,632		
	SFC			36,885		
1.0	HYC				12,563	
	ISS				48,047	
	MON				122,401	
	OFC				67,074	
	SFC				38,793	
1.1	HYC					13,461
	ISS					50,845
	MON					126,976
	OFC					70,346
	SFC					40,715

201 Vehicle Configuration
Section Number 11
IU and Forward Skirt (3201.5" - 3321.5")

Material: Titanium
N_x Nominal: -3069 lbs/in
N_o Nominal: 3069 lbs/in

N_x / N_x Nom ↓ N_o / N_o Nom →		.7	.8	.9	1.0	1.1
.7	HYC	3,024				
	ISS	12,656				
	MON	34,610				
	OFC	32,014				
	SFC	10,251				
.8	HYC		3,285			
	ISS		13,715			
	MON		36,436			
	OFC		34,224			
	SFC		10,969			
.9	HYC			3,544		
	ISS			14,483		
	MON			38,126		
	OFC			36,300		
	SFC			11,645		
1.0	HYC				3,800	
	ISS				15,445	
	MON				39,704	
	OFC				38,264	
	SFC				12,285	
1.1	HYC					4,055
	ISS					16,376
	MON					41,188
	OFC					40,132
	SFC					12,895

Weight/Load Matrices - 202 Vehicle

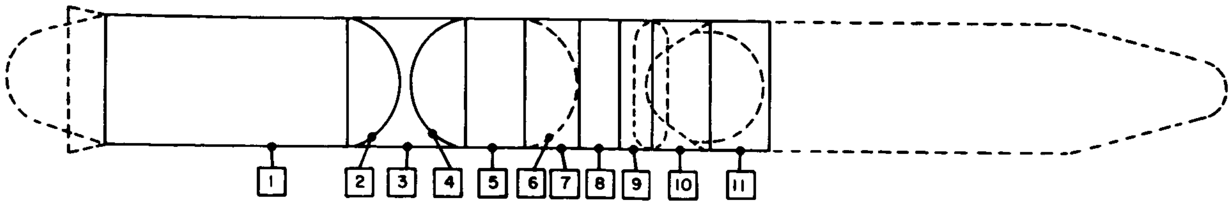

202 Vehicle Configuration
Section Number 1
LH_2 Tank Cylinder (609.7" - 1910.2")

Material: Aluminum 2219 - T87
N_x Nominal: -9529 lbs/in.
N_o Nominal: 15,666 lbs/in.

$N_x/N_{x\,Nom}$ ↓ $N_o/N_{o\,Nom}$ →		.7	.8	.9	1.0	1.1
.7	HYC	75,973	86,041	96,110	106,179	116,247
	ISS	143,000	143,000	143,000	143,000	143,000
	MON	283,682	283,682	283,682	283,682	283,682
	OFC					
	SFC	175,665	175,665	175,665	175,665	175,665
.8	HYC	77,493	86,402	96,458	106,513	116,568
	ISS	156,181	156,181	156,181	156,181	156,181
	MON	298,647	298,647	298,647	298,647	298,647
	OFC					
	SFC	175,814	175,814	175,814	175,814	175,814
.9	HYC	83,493	90,162	96,831	106,888	116,907
	ISS	168,200	168,200	168,200	168,200	168,200
	MON	312,502	312,502	312,502	312,502	312,502
	OFC					
	SFC	175,962	175,962	175,962	175,962	175,962
1.0	HYC	88,547	95,707	101,727	107,282	117,245
	ISS	181,402	181,402	181,402	181,402	181,402
	MON	325,438	325,438	325,438	325,438	325,438
	OFC					
	SFC	176,111	176,111	176,111	176,111	176,111
1.1	HYC	95,777	101,251	106,726	112,200	117,674
	ISS	194,500	194,500	194,500	194,500	194,500
	MON	337,601	337,601	337,601	337,601	337,601
	OFC					
	SFC	176,260	176,260	176,260	176,260	176,260

202 Vehicle Configuration
Section Number 2
LH_2 Tank Top Head

Material: Aluminum 2219 - T87
N_x Nominal: -
N_o Nominal: 8139 lbs/in.

$N_x/N_{x\,Nom}$ ↓ $N_o/N_{o\,Nom}$ →		.7	.8	.9	1.0	1.1
.7	HYC					
	ISS					
	MON					
	OFC					
	SFC					
.8	HYC					
	ISS					
	MON					
	OFC					
	SFC					
.9	HYC					
	ISS					
	MON					
	OFC					
	SFC					
1.0	HYC	8,270	9,441	10,612	11,783	12,955
	ISS					
	MON	6,887	7,871	8,854	9,838	10,822
	OFC					
	SFC					
1.1	HYC					
	ISS					
	MON					
	OFC					
	SFC					

202 Vehicle Configuration
Section Number 3
Intertank 1 (1910.2" - 2462.4")

Material: Aluminum 2219 - T87
N_x Nominal: -13,577 lbs/in.
N_o Nominal: 13,577 lbs/in.

$N_x/N_{x\,Nom}$ ↓ $N_o/N_{o\,Nom}$ →		.7	.8	.9	1.0	1.1
.7	HYC	41,967				
	ISS	80,200				
	MON	141,324				
	OFC					
	SFC	61,851				
.8	HYC		47,575			
	ISS		86,650			
	MON		148,780			
	OFC					
	SFC		82,668			
.9	HYC			53,163		
	ISS			93,200		
	MON			155,682		
	OFC					
	SFC			87,846		
1.0	HYC				58,937	
	ISS				99,728	
	MON				162,127	
	OFC					
	SFC				90,996	
1.1	HYC					64,892
	ISS					106,200
	MON					168,186
	OFC					
	SFC					98,561

202 Vehicle Configuration
Section Number 4
LOX Tank Bottom Head

Material: Aluminum 2219 - T87
N_x Nominal: -
N_o Nominal: 9091 lbs/in.

$N_x/N_{x\,Nom}$ ↓ $N_o/N_{o\,Nom}$ →		.7	.8	.9	1.0	1.1
.7	HYC					
	ISS					
	MON					
	OFC					
	SFC					
.8	HYC					
	ISS					
	MON					
	OFC					
	SFC					
.9	HYC					
	ISS					
	MON					
	OFC					
	SFC					
1.0	HYC	9,738	11,117	12,497	13,877	15,257
	ISS					
	MON	8,113	9,272	10,431	11,590	12,749
	OFC					
	SFC					
1.1	HYC					
	ISS					
	MON					
	OFC					
	SFC					

202 Vehicle Configuration
Section Number 5
LOX Tank Cylinder (2462.4" - 2827.8")

Material: Aluminum 2219 - T87
N_x Nominal: -6875 lbs/in.
N_o Nominal: 12,865 lbs/in.

$N_x/N_{x\,Nom}$ ↓ $N_o/N_{o\,Nom}$ →		.7	.8	.9	1.0	1.1
.7	HYC	17,210	18,551	19,892	21,232	22,573
	ISS	32,935	32,935	32,935	32,935	32,935
	MON	70,180	70,180	70,180	70,180	70,180
	OFC	38,920	38,920	38,920	38,920	38,920
	SFC					
.8	HYC	18,222	19,563	20,904	22,245	23,586
	ISS	35,822	35,822	35,822	35,822	35,822
	MON	73,882	73,882	73,882	73,882	73,882
	OFC	38,967	38,967	38,967	38,967	38,967
	SFC					
.9	HYC	19,236	20,576	21,917	23,257	24,598
	ISS	37,477	37,477	37,477	37,477	37,477
	MON	77,309	77,309	77,309	77,309	77,309
	OFC					
	SFC	39,014	39,014	39,014	39,014	39,014
1.0	HYC	20,247	21,588	22,929	24,270	26,623
	ISS	40,449	40,449	40,449	40,449	40,449
	MON	80,510	80,510	80,510	80,510	80,510
	OFC					
	SFC	39,061	39,061	39,061	39,061	39,061
1.1	HYC	21,260	22,601	23,942	25,282	26,623
	ISS	43,730	43,730	43,730	43,730	43,730
	MON	83,519	83,519	83,519	83,519	83,519
	OFC					
	SFC	39,108	39,108	39,108	39,108	39,108

202 Vehicle Configuration
Section Number 6
LOX Tank Top Head

Material: Aluminum 2219 - T87
N_x Nominal: -
N_o Nominal: 4307 lbs/in.

$N_x/N_{x\,Nom}$ ↓ $N_o/N_{o\,Nom}$ →		.7	.8	.9	1.0	1.1
.7	HYC					
	ISS					
	MON					
	OFC					
	SFC					
.8	HYC					
	ISS					
	MON					
	OFC					
	SFC					
.9	HYC					
	ISS					
	MON					
	OFC					
	SFC					
1.0	HYC	4,569	5,212	5,855	6,497	7,140
	ISS					
	MON	3,779	4,318	4,858	5,398	5,938
	OFC					
	SFC					
1.1	HYC					
	ISS					
	MON					
	OFC					
	SFC					

Weight/Load Matrices - 202 Vehicle

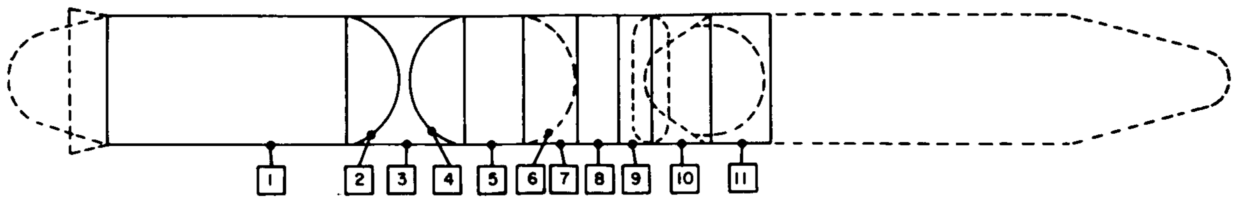

202 Vehicle Configuration
Section Number 7
Stage 1 Forward Skirt (2828.8" - 3061.1")

Material: Aluminum 2219 - T87
N_x Nominal: -8069 lbs/in.
N_o Nominal: 8069 lbs/in.

$N_x / \bar{N}_x$ Nom ↓	$N_o / \bar{N}_o$ Nom →	.7	.8	.9	1.0	1.1
.7	HYC	10,968				
	ISS	24,304				
	MON	48,854				
	OFC					
	SFC	18,673				
.8	HYC		12,397			
	ISS		26,071			
	MON		51,431			
	OFC					
	SFC		19,981			
.9	HYC			13,820		
	ISS			29,842		
	MON			53,817		
	OFC					
	SFC			21,211		
1.0	HYC				15,231	
	ISS				31,677	
	MON				56,045	
	OFC					
	SFC				22,288	
1.1	HYC					16,641
	ISS					33,654
	MON					58,139
	OFC					
	SFC					25,287

202 Vehicle Configuration
Section Number 8
Interstage (3061.1" - 3250")

Material: Aluminum 2219 - T87
N_x Nominal: -7897 lbs/in.
N_o Nominal: 7897 lbs/in.

$N_x / \bar{N}_x$ Nom ↓	$N_o / \bar{N}_o$ Nom →	.7	.8	.9	1.0	1.1
.7	HYC	8,712				
	ISS	19,300				
	MON	39,235				
	OFC					
	SFC	15,005				
.8	HYC		9,846			
	ISS		20,900			
	MON		41,305			
	OFC					
	SFC		16,059			
.9	HYC			10,974		
	ISS			22,500		
	MON			43,221		
	OFC					
	SFC			17,555		
1.0	HYC				12,093	
	ISS				24,126	
	MON				45,010	
	OFC					
	SFC				17,903	
1.1	HYC					13,203
	ISS					25,700
	MON					46,692
	OFC					
	SFC					20,207

202 Vehicle Configuration
Section Number 9
Stage 2 Aft Skirt (3250" - 3447.6")

Material: Aluminum 2219 - T87
N_x Nominal: -7669 lbs/in.
N_o Nominal: 7669 lbs/in.

$N_x / \bar{N}_x$ Nom ↓	$N_o / \bar{N}_o$ Nom →	.7	.8	.9	1.0	1.1
.7	HYC	8,871				
	ISS	18,945				
	MON	40,575				
	OFC					
	SFC	15,450				
.8	HYC		10,020			
	ISS		21,364			
	MON		42,716			
	OFC					
	SFC		16,534			
.9	HYC			11,166		
	ISS			23,592		
	MON			44,698		
	OFC					
	SFC			17,555		
1.0	HYC				12,308	
	ISS				25,863	
	MON				46,548	
	OFC					
	SFC				18,436	
1.1	HYC					13,437
	ISS					26,009
	MON					48,288
	OFC					
	SFC					19,349

202 Vehicle Configuration
Section Number 10
Intertank 2 (3447.6" - 3811.8")

Material: Aluminum 2219 - T87
N_x Nominal: -5920 lbs/in.
N_o Nominal: 5920 lbs/in.

$N_x / \bar{N}_x$ Nom ↓	$N_o / \bar{N}_o$ Nom →	.7	.8	.9	1.0	1.1
.7	HYC	12,958				
	ISS	31,343				
	MON	67,603				
	OFC					
	SFC	23,766				
.8	HYC		14,619			
	ISS		33,562			
	MON		71,169			
	OFC					
	SFC		26,285			
.9	HYC			16,276		
	ISS			34,913		
	MON			74,471		
	OFC					
	SFC			28,365		
1.0	HYC				17,920	
	ISS				36,971	
	MON				77,554	
	OFC					
	SFC				29,926	
1.1	HYC					19,548
	ISS					40,108
	MON					80,452
	OFC					
	SFC					31,329

202 Vehicle Configuration
Section Number 11
Stage 2 Forward Skirt (3811.8" - 4088.1")

Material: Aluminum 2219 - T87
N_x Nominal: -4835 lbs/in.
N_o Nominal: 4835 lbs/in.

$N_x / \bar{N}_x$ Nom ↓	$N_o / \bar{N}_o$ Nom →	.7	.8	.9	1.0	1.1
.7	HYC	8,199				
	ISS	19,649				
	MON	47,493				
	OFC					
	SFC	16,056				
.8	HYC		9,229			
	ISS		22,688			
	MON		49,999			
	OFC					
	SFC		17,107			
.9	HYC			10,259		
	ISS			24,488		
	MON			52,318		
	OFC					
	SFC			18,627		
1.0	HYC				11,279	
	ISS				25,561	
	MON				54,484	
	OFC					
	SFC				20,503	
1.1	HYC					12,299
	ISS					26,489
	MON					56,520
	OFC					
	SFC					21,520

Weight/Load Matrices - 202 Vehicle

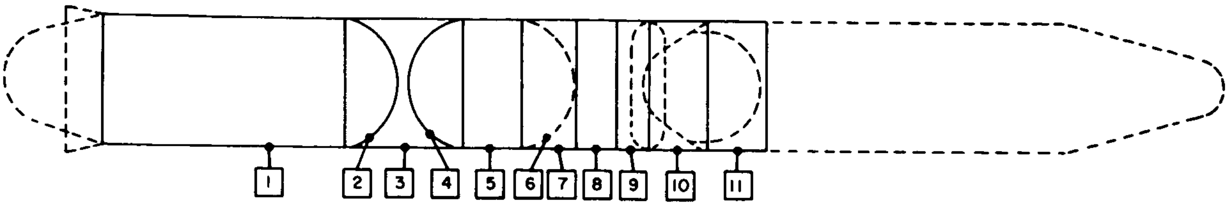

202 Vehicle Configuration
Section Number 1
LH_2 Tank Cylinder (609.7" - 1910.2")

Material: Beryllium
N_x Nominal: -9529 lbs/in.
N_o Nominal: 15,666 lbs/in.

$\frac{N_x}{N_x\ Nom}$ ↓	$\frac{N_o}{N_o\ Nom}$ →	.7	.8	.9	1.0	1.1
.7	HYC	47,937	54,141	60,425	66,709	72,994
	ISS	84,863	84,863	84,863	84,863	84,863
	MON	112,906	112,906	112,906	112,906	112,906
	OFC					
	SFC	110,271	110,271	110,271	110,271	110,271
.8	HYC	48,894	54,609	60,924	67,132	73,339
	ISS	88,599	88,599	88,599	88,599	88,599
	MON	118,862	118,862	118,862	118,862	118,862
	OFC					
	SFC	110,324	110,324	110,324	110,324	110,324
.9	HYC	50,445	55,934	61,421	67,690	73,907
	ISS	92,335	92,335	92,335	92,335	92,335
	MON	124,376	124,376	124,376	124,376	124,376
	OFC					
	SFC	110,377	110,377	110,377	110,377	110,377
1.0	HYC	53,235	58,356	63,478	68,246	74,474
	ISS	96,071	96,071	96,071	96,071	96,071
	MON	129,525	129,525	129,525	129,525	129,525
	OFC					
	SFC	110,430	110,430	110,430	110,430	110,430
1.1	HYC	56,023	60,778	65,533	70,288	75,043
	ISS	99,087	99,087	99,087	99,087	99,087
	MON	134,366	134,366	134,366	134,366	134,366
	OFC					
	SFC	110,483	110,483	110,483	110,483	110,483

202 Vehicle Configuration
Section Number 2
LH_2 Tank Top Head

Material: Beryllium
N_x Nominal: -
N_o Nominal: 8139 lbs/in.

$\frac{N_x}{N_x\ Nom}$ ↓	$\frac{N_o}{N_o\ Nom}$ →	.7	.8	.9	1.0	1.1
.7	HYC					
	ISS					
	MON					
	OFC					
	SFC					
.8	HYC					
	ISS					
	MON					
	OFC					
	SFC					
.9	HYC					
	ISS					
	MON					
	OFC					
	SFC					
1.0	HYC	5,207	5,941	6,675	7,408	8,142
	ISS					
	MON	4,314	4,931	5,547	6,163	6,780
	OFC					
	SFC					
1.1	HYC					
	ISS					
	MON					
	OFC					
	SFC					

202 Vehicle Configuration
Section Number 3
Intertank 1 (1910.2" - 2462.4")

Material: Beryllium
N_x Nominal: -13,577 lbs/in.
N_o Nominal: 13,577 lbs/in.

$\frac{N_x}{N_x\ Nom}$ ↓	$\frac{N_o}{N_o\ Nom}$ →	.7	.8	.9	1.0	1.1
.7	HYC	20,951				
	ISS	28,491				
	MON	54,951				
	OFC					
	SFC	23,337				
.8	HYC		23,722			
	ISS		29,047			
	MON		57,850			
	OFC					
	SFC		24,417			
.9	HYC			26,652		
	ISS			29,603		
	MON			60,534		
	OFC					
	SFC			24,497		
1.0	HYC				29,590	
	ISS				30,159	
	MON				63,040	
	OFC					
	SFC				24,577	
1.1	HYC					32,523
	ISS					30,716
	MON					65,396
	OFC					
	SFC					24,657

202 Vehicle Configuration
Section Number 4
LOX Tank Bottom Head

Material: Beryllium
N_x Nominal: -
N_o Nominal: 9091 lbs/in.

$\frac{N_x}{N_x\ Nom}$ ↓	$\frac{N_o}{N_o\ Nom}$ →	.7	.8	.9	1.0	1.1
.7	HYC					
	ISS					
	MON					
	OFC					
	SFC					
.8	HYC					
	ISS					
	MON					
	OFC					
	SFC					
.9	HYC					
	ISS					
	MON					
	OFC					
	SFC					
1.0	HYC	6,391	7,292	8,194	9,095	9,997
	ISS					
	MON	5,301	6,059	6,816	7,573	8,331
	OFC					
	SFC					
1.1	HYC					
	ISS					
	MON					
	OFC					
	SFC					

202 Vehicle Configuration
Section Number 5
LOX Tank Cylinder (2462.4" - 2827.8")

Material: Beryllium
N_x Nominal: -6875 lbs/in.
N_o Nominal: 12,865 lbs/in.

$\frac{N_x}{N_x\ Nom}$ ↓	$\frac{N_o}{N_o\ Nom}$ →	.7	.8	.9	1.0	1.1
.7	HYC	10,942	11,956	12,969	13,983	14,996
	ISS	20,121	20,121	20,121	20,121	20,121
	MON	27,892	27,892	27,892	27,892	27,892
	OFC					
	SFC	23,584	23,584	23,584	23,584	23,584
.8	HYC	11,463	12,467	13,490	14,504	15,517
	ISS	20,245	20,245	20,245	20,245	20,245
	MON	29,364	29,364	29,364	29,364	29,364
	OFC					
	SFC	23,603	23,603	23,603	23,603	23,603
.9	HYC	11,984	12,998	13,994	15,025	16,038
	ISS	20,369	20,369	20,369	20,369	20,369
	MON	30,726	30,726	30,726	30,726	30,726
	OFC					
	SFC	23,622	23,622	23,622	23,622	23,622
1.0	HYC	12,505	13,519	14,532	15,528	16,559
	ISS	20,493	20,493	20,493	20,493	20,493
	MON	31,998	31,998	31,998	31,998	31,998
	OFC					
	SFC	23,641	23,641	23,641	23,641	23,641
1.1	HYC	13,026	14,040	15,053	16,067	17,080
	ISS	20,617	20,617	20,617	20,617	20,617
	MON	33,194	33,194	33,194	33,194	33,194
	OFC					
	SFC	23,660	23,660	23,660	23,660	23,660

202 Vehicle Configuration
Section Number 6
LOX Tank Top Head

Material: Beryllium
N_x Nominal: -
N_o Nominal: 4307 lbs/in.

$\frac{N_x}{N_x\ Nom}$ ↓	$\frac{N_o}{N_o\ Nom}$ →	.7	.8	.9	1.0	1.1
.7	HYC					
	ISS					
	MON					
	OFC					
	SFC					
.8	HYC					
	ISS					
	MON					
	OFC					
	SFC					
.9	HYC					
	ISS					
	MON					
	OFC					
	SFC					
1.0	HYC	2,789	3,178	3,566	3,954	4,343
	ISS					
	MON	2,283	2,609	2,936	3,262	3,588
	OFC					
	SFC					
1.1	HYC					
	ISS					
	MON					
	OFC					
	SFC					

Weight/Load Matrices - 202 Vehicle

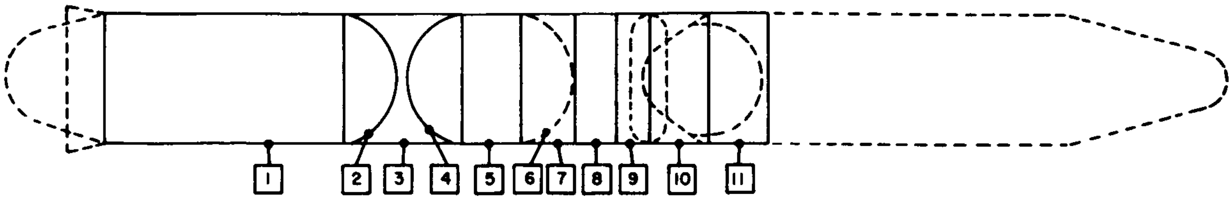

202 Vehicle Configuration
Section Number 7
Stage 1 Forward Skirt (2827.8" - 3061.1")

Material: Beryllium
N_x Nominal: -8069 lbs/in.
N_o Nominal: 8069 lbs/in.

$\frac{N_x}{\bar{N}_x}$ Nom ↓ $\frac{N_o}{\bar{N}_o}$ Nom →		.7	.8	.9	1.0	1.1
.7	HYC	5,628				
	ISS	6,973				
	MON	18,996				
	OFC					
	SFC	5,918				
.8	HYC		6,290			
	ISS		7,296			
	MON		19,996			
	OFC					
	SFC		6,204			
.9	HYC			6,957		
	ISS			8,059		
	MON			20,928		
	OFC					
	SFC			6,588		
1.0	HYC				7,630	
	ISS				8,576	
	MON				21,792	
	OFC					
	SFC				6,951	
1.1	HYC					8,310
	ISS					9,076
	MON					22,606
	OFC					
	SFC					7,296

202 Vehicle Configuration
Section Number 8
Interstage (3061.1" - 3250")

Material: Beryllium
N_x Nominal: -7897 lbs/in.
N_o Nominal: 7897 lbs/in.

$\frac{N_x}{\bar{N}_x}$ Nom ↓ $\frac{N_o}{\bar{N}_o}$ Nom →		.7	.8	.9	1.0	1.1
.7	HYC	4,478				
	ISS	5,562				
	MON	15,256				
	OFC					
	SFC	4,690				
.8	HYC		5,003			
	ISS		5,893			
	MON		16,061			
	OFC					
	SFC		4,979			
.9	HYC			5,531		
	ISS			6,411		
	MON			16,806		
	OFC					
	SFC			5,276		
1.0	HYC				6,063	
	ISS				6,932	
	MON				17,501	
	OFC					
	SFC				5,566	
1.1	HYC					6,601
	ISS					7,338
	MON					18,155
	OFC					
	SFC					5,829

202 Vehicle Configuration
Section Number 9
Stage 2 Aft Skirt (3250" - 3447.6")

Material: Beryllium
N_x Nominal: -7669 lbs/in.
N_o Nominal: 7669 lbs/in.

$\frac{N_x}{\bar{N}_x}$ Nom ↓ $\frac{N_o}{\bar{N}_o}$ Nom →		.7	.8	.9	1.0	1.1
.7	HYC	4,573				
	ISS	5,629				
	MON	15,777				
	OFC					
	SFC	4,790				
.8	HYC		5,105			
	ISS		6,160			
	MON		16,609			
	OFC					
	SFC		5,126			
.9	HYC			5,640		
	ISS			6,442		
	MON			17,380		
	OFC					
	SFC			5,443		
1.0	HYC				6,179	
	ISS				7,065	
	MON				18,099	
	OFC					
	SFC				5,743	
1.1	HYC					6,724
	ISS					7,476
	MON					18,776
	OFC					
	SFC					6,002

202 Vehicle Configuration
Section Number 10
Intertank 2 (3447.6" - 3811.8")

Material: Beryllium
N_x Nominal: -5920 lbs/in.
N_o Nominal: 5920 lbs/in.

$\frac{N_x}{\bar{N}_x}$ Nom ↓ $\frac{N_o}{\bar{N}_o}$ Nom →		.7	.8	.9	1.0	1.1
.7	HYC	6,964				
	ISS	8,968				
	MON	25,256				
	OFC					
	SFC	7,734				
.8	HYC		7,701			
	ISS		9,760			
	MON		27,673			
	OFC					
	SFC		8,289			
.9	HYC			8,468		
	ISS			10,456		
	MON			28,957		
	OFC					
	SFC			8,801		
1.0	HYC				9,241	
	ISS				10,993	
	MON				30,155	
	OFC					
	SFC				9,269	
1.1	HYC					10,020
	ISS					11,728
	MON					31,282
	OFC					
	SFC					9,720

202 Vehicle Configuration
Section Number 11
Stage 2 Forward Skirt (3811.8" - 4088.1")

Material: Beryllium
N_x Nominal: -4836 lbs/in.
N_o Nominal: 4836 lbs/in.

$\frac{N_x}{\bar{N}_x}$ Nom ↓ $\frac{N_o}{\bar{N}_o}$ Nom →		.7	.8	.9	1.0	1.1
.7	HYC	4,430				
	ISS	5,634				
	MON	18,487				
	OFC					
	SFC	5,301				
.8	HYC		4,980			
	ISS		6,408			
	MON		19,441			
	OFC					
	SFC		5,666			
.9	HYC			5,434		
	ISS			7,075		
	MON			20,343		
	OFC					
	SFC			6,042		
1.0	HYC				5,890	
	ISS				7,521	
	MON				21,185	
	OFC					
	SFC				6,388	
1.1	HYC					6,358
	ISS					7,906
	MON					21,977
	OFC					
	SFC					6,676

Weight/Load Matrices - 203 Vehicle

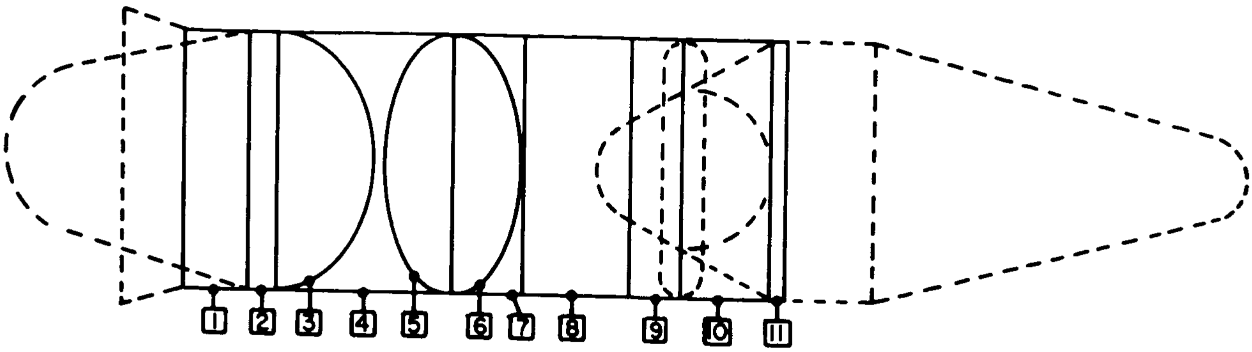

203 Vehicle Configuration
Section Number 1
Thrust Takeout (710" - 960")

Material: Aluminum 2219 - T87
N_x Nominal: -9058 lbs/in.
N_o Nominal: 9058 lbs/in.

N_x ↓ $\frac{N_x}{N_x\ Nom}$	N_o → $\frac{N_o}{N_o\ Nom}$	.7	.8	.9	1.0	1.1
.7	HYC	19,681				
	ISS	46,661				
	MON	100,307				
	OFC					
	SFC	34,696				
.8	HYC		22,209			
	ISS		51,116			
	MON		105,599			
	OFC					
	SFC		39,708			
.9	HYC			24,714		
	ISS			55,706		
	MON			110,497		
	OFC					
	SFC			42,065		
1.0	HYC				27,208	
	ISS				60,423	
	MON				115,072	
	OFC					
	SFC				44,457	
1.1	HYC					29,703
	ISS					66,850
	MON					119,373
	OFC					
	SFC					46,656

203 Vehicle Configuration
Section Number 2
LH_2 Tank Cylinder (960" - 1058.8")

Material: Aluminum 2219 - T87
N_x Nominal: -5248 lbs/in.
N_o Nominal: 13,913 lbs/in.

N_x ↓ $\frac{N_x}{N_x\ Nom}$	N_o → $\frac{N_o}{N_o\ Nom}$	.7	.8	.9	1.0	1.1
.7	HYC	7,376	8,363	9,350	10,336	11,323
	ISS	16,559	16,559	16,559	16,559	16,559
	MON	31,367	31,367	31,367	31,367	31,367
	OFC					
	SFC	19,223	19,223	19,223	19,223	19,223
.8	HYC	7,418	8,391	9,385	10,368	11,351
	ISS	16,715	16,715	16,715	16,715	16,715
	MON	33,022	33,022	33,022	33,022	33,022
	OFC					
	SFC	19,313	19,313	19,313	19,313	19,313
.9	HYC	7,461	8,440	9,405	10,399	11,379
	ISS	16,872	16,872	16,872	16,872	16,872
	MON	34,554	34,554	34,554	34,554	34,554
	OFC					
	SFC	19,405	19,405	19,405	19,405	19,405
1.0	HYC	7,504	8,480	9,456	10,420	11,407
	ISS	17,170	17,170	17,170	17,170	17,170
	MON	35,984	35,984	35,984	35,984	35,984
	OFC					
	SFC	19,496	19,496	19,496	19,496	19,496
1.1	HYC	7,552	8,523	9,494	10,464	11,435
	ISS	17,185	17,185	17,185	17,185	17,185
	MON	37,329	37,329	37,329	37,329	37,329
	OFC					
	SFC	19,587	19,587	19,587	19,587	19,587

203 Vehicle Configuration
Section Number 3
LH_2 Tank Top Head

Material: Aluminum 2219 - T87
N_x Nominal: -
N_o Nominal: 8138 lbs/in.

N_x ↓ $\frac{N_x}{N_x\ Nom}$	N_o → $\frac{N_o}{N_o\ Nom}$	.7	.8	.9	1.0	1.1
.7	HYC					
	ISS					
	MON					
	OFC					
	SFC					
.8	HYC					
	ISS					
	MON					
	OFC					
	SFC					
.9	HYC					
	ISS					
	MON					
	OFC					
	SFC					
1.0	HYC	17,495	19,973	22,451	24,929	27,407
	ISS					
	MON	14,570	16,651	18,732	20,814	22,895
	OFC					
	SFC					
1.1	HYC					
	ISS					
	MON					
	OFC					
	SFC					

203 Vehicle Configuration
Section Number 4
Intertank (1058.8" - 1685.7")

Material: Aluminum 2219 - T87
N_x Nominal: -8823 lbs/in.
N_o Nominal: 8823 lbs/in.

N_x ↓ $\frac{N_x}{N_x\ Nom}$	N_o → $\frac{N_o}{N_o\ Nom}$	.7	.8	.9	1.0	1.1
.7	HYC	48,219				
	ISS	117,620				
	MON	249,052				
	OFC					
	SFC	86,145				
.8	HYC		54,425			
	ISS		128,684			
	MON		262,190			
	OFC					
	SFC		98,464			
.9	HYC			60,551		
	ISS			139,595		
	MON			274,353		
	OFC					
	SFC			104,522		
1.0	HYC				66,655	
	ISS				151,807	
	MON				285,711	
	OFC					
	SFC				110,261	
1.1	HYC					72,759
	ISS					168,750
	MON					296,389
	OFC					
	SFC					115,728

203 Vehicle Configuration
Section Number 5
LOX Tank Bottom Head

Material: Aluminum 2219 - T87
N_x Nominal: -
N_o Nominal: 24,209 lbs/in.

N_x ↓ $\frac{N_x}{N_x\ Nom}$	N_o → $\frac{N_o}{N_o\ Nom}$	.7	.8	.9	1.0	1.1
.7	HYC					
	ISS					
	MON					
	OFC					
	SFC					
.8	HYC					
	ISS					
	MON					
	OFC					
	SFC					
.9	HYC					
	ISS					
	MON					
	OFC					
	SFC					
1.0	HYC	39,927	45,612	51,297	56,982	62,667
	ISS					
	MON	33,429	38,204	42,980	47,755	52,531
	OFC					
	SFC					
1.1	HYC					
	ISS					
	MON					
	OFC					
	SFC					

203 Vehicle Configuration
Section Number 6
LOX Tank Top Head

Material: Aluminum 2219 - T87
N_x Nominal: -
N_o Nominal: 4266 lbs/in.

N_x ↓ $\frac{N_x}{N_x\ Nom}$	N_o → $\frac{N_o}{N_o\ Nom}$	.7	.8	.9	1.0	1.1
.7	HYC					
	ISS					
	MON					
	OFC					
	SFC					
.8	HYC					
	ISS					
	MON					
	OFC					
	SFC					
.9	HYC					
	ISS					
	MON					
	OFC					
	SFC					
1.0	HYC	9,483	10,815	12,148	13,481	14,814
	ISS					
	MON	7,836	8,956	10,075	11,195	12,314
	OFC					
	SFC					
1.1	HYC					
	ISS					
	MON					
	OFC					
	SFC					

Weight/Load Matrices - 203 Vehicle

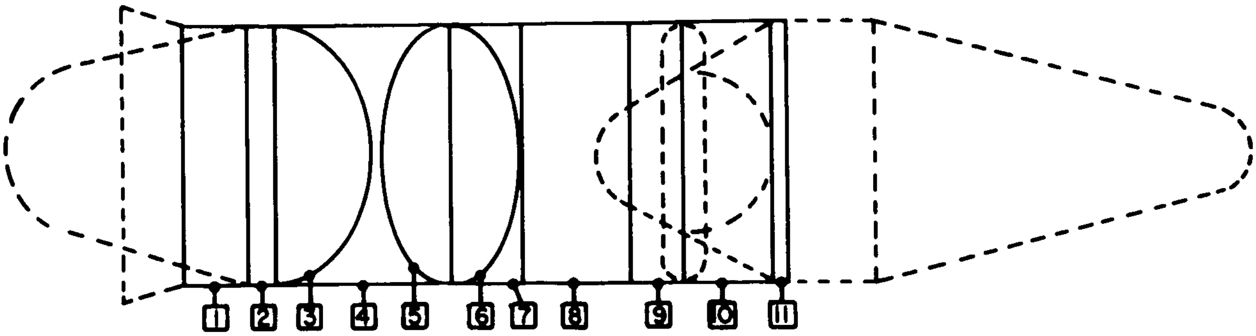

203 Vehicle Configuration
Section Number 7
Stage 1 Forward Skirt (1685.7" - 1937.2")

Material: Aluminum 2219 - T87
N_x Nominal: -5648 lbs/in.
N_o Nominal: 5648 lbs/in.

$\frac{N_x}{N_x \text{ Nom}}$ ↓	$\frac{N_o}{N_o \text{ Nom}}$ →	.7	.8	.9	1.0	1.1
.7	HYC	13,031				
	ISS	36,497				
	MON	84,115				
	OFC					
	SFC	27,757				
.8	HYC		14,648			
	ISS		39,150			
	MON		88,553			
	OFC					
	SFC		29,523			
.9	HYC			16,254		
	ISS			41,800		
	MON			92,661		
	OFC					
	SFC			31,252		
1.0	HYC				17,844	
	ISS				44,531	
	MON				96,497	
	OFC					
	SFC				32,799	
1.1	HYC					19,434
	ISS					47,306
	MON					100,103
	OFC					
	SFC					34,568

203 Vehicle Configuration
Section Number 8
Interstage (1937.2" - 2465")

Material: Aluminum 2219 - T87
N_x Nominal:
N_o Nominal:

$\frac{N_x}{N_x \text{ Nom}}$ ↓	$\frac{N_o}{N_o \text{ Nom}}$ →	.7	.8	.9	1.0	1.1
.7	HYC	25,676				
	ISS	72,899				
	MON	172,252				
	OFC					
	SFC	56,428				
.8	HYC		29,079			
	ISS		79,117			
	MON		181,337			
	OFC					
	SFC		60,397			
.9	HYC			32,246		
	ISS			85,097		
	MON			189,751		
	OFC					
	SFC			63,640		
1.0	HYC				35,402	
	ISS				91,099	
	MON				197,607	
	OFC					
	SFC				66,785	
1.1	HYC					38,541
	ISS					96,172
	MON					204,992
	OFC					
	SFC					70,163

203 Vehicle Configuration
Section Number 9
Stage 2 Aft Skirt (2465" - 2548")

Material: Aluminum 2219 - T87
N_x Nominal: -5106 lbs/in.
N_o Nominal: 5106 lbs/in.

$\frac{N_x}{N_x \text{ Nom}}$ ↓	$\frac{N_o}{N_o \text{ Nom}}$ →	.7	.8	.9	1.0	1.1
.7	HYC	2,550				
	ISS	11,348				
	MON	26,707				
	OFC					
	SFC	8,706				
.8	HYC		2,910			
	ISS		12,322			
	MON		28,116			
	OFC					
	SFC		9,318			
.9	HYC			3,271		
	ISS			13,258		
	MON			29,420		
	OFC					
	SFC			9,894		
1.0	HYC				3,632	
	ISS				14,164	
	MON				30,638	
	OFC					
	SFC				10,295	
1.1	HYC					3,993
	ISS					14,886
	MON					31,784
	OFC					
	SFC					10,797

203 Vehicle Configuration
Section Number 10
Intertank 2 (2548" - 2852.7")

Material: Aluminum 2219 - T87
N_x Nominal: -2848 lbs/in.
N_o Nominal: 2848 lbs/in.

$\frac{N_x}{N_x \text{ Nom}}$ ↓	$\frac{N_o}{N_o \text{ Nom}}$ →	.7	.8	.9	1.0	1.1
.7	HYC	9,076				
	ISS	29,745				
	MON	80,319				
	OFC					
	SFC	24,442				
.8	HYC		10,123			
	ISS		32,917			
	MON		84,556			
	OFC					
	SFC		26,116			
.9	HYC			11,160		
	ISS			34,550		
	MON			88,478		
	OFC					
	SFC			27,728		
1.0	HYC				12,168	
	ISS				37,658	
	MON				92,141	
	OFC					
	SFC				29,254	
1.1	HYC					13,214
	ISS					39,916
	MON					95,585
	OFC					
	SFC					30,636

203 Vehicle Configuration
Section Number 11
Stage 2 Forward Skirt (2852.7" - 2888.7")

Material: Aluminum 2219 - T87
N_x Nominal: -2327 lbs/in.
N_o Nominal: 2327 lbs/in.

$\frac{N_x}{N_x \text{ Nom}}$ ↓	$\frac{N_o}{N_o \text{ Nom}}$ →	.7	.8	.9	1.0	1.1
.7	HYC	378				
	ISS	2,464				
	MON	6,349				
	OFC					
	SFC	1,892				
.8	HYC		431			
	ISS		2,678			
	MON		6,684			
	OFC					
	SFC		2,026			
.9	HYC			464		
	ISS			2,834		
	MON			6,984		
	OFC					
	SFC			2,106		
1.0	HYC				537	
	ISS				3,030	
	MON				7,284	
	OFC					
	SFC				2,222	
1.1	HYC					590
	ISS					3,230
	MON					7,556
	OFC					
	SFC					2,330

Weight/Load Matrices - 203 Vehicle

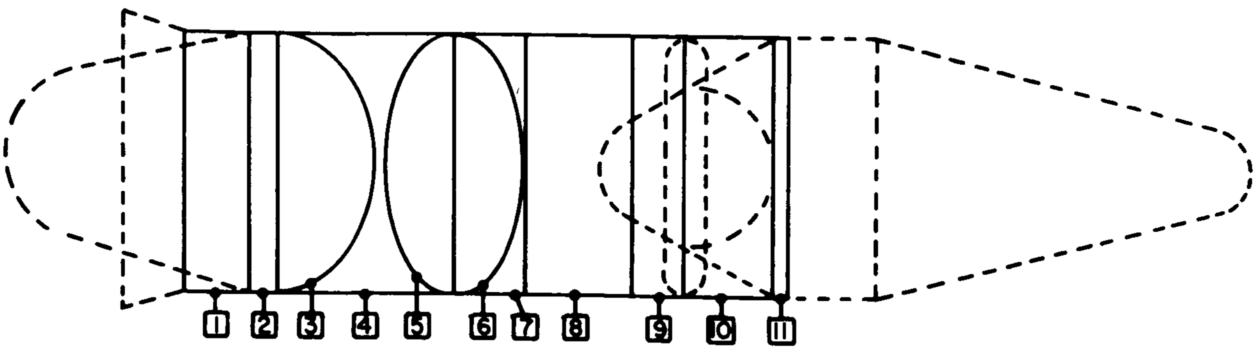

203 Vehicle Configuration
Section Number 1
Thrust Takeout (710" - 960")

Material: Beryllium
N_x Nominal: -9058 lbs/in.
N_o Nominal: 9058 lbs/in.

N_x ↓ / N_x Nom	N_o → / N_o Nom	.7	.8	.9	1.0	1.1
.7	HYC	10,383				
	ISS	13,533				
	MON	39,002				
	OFC					
	SFC	11,548				
.8	HYC		11,529			
	ISS		14,622			
	MON		41,060			
	OFC					
	SFC		12,359			
.9	HYC			12,679		
	ISS			15,411		
	MON			42,965		
	OFC					
	SFC			13,122		
1.0	HYC				13,836	
	ISS				16,395	
	MON				44,744	
	OFC					
	SFC				13,844	
1.1	HYC					14,999
	ISS					17,345
	MON					46,417
	OFC					
	SFC					14,534

203 Vehicle Configuration
Section Number 2
LH_2 Tank Cylinder (960" - 1058.8")

Material: Beryllium
N_x Nominal: -5248 lbs/in.
N_o Nominal: 13.913 lbs/in.

N_x ↓ / N_x Nom	N_o → / N_o Nom	.7	.8	.9	1.0	1.1
.7	HYC	4,590	5,221	5,852	6,482	7,113
	ISS	8,126	8,126	8,126	8,126	8,126
	MON	12,494	12,494	12,494	12,494	12,494
	OFC					
	SFC	12,127	12,127	12,127	12,127	12,127
.8	HYC	4,614	5,235	5,870	6,498	7,127
	ISS	8,353	8,353	8,353	8,353	8,353
	MON	13,153	13,153	13,153	13,153	13,153
	OFC					
	SFC	12,168	12,168	12,168	12,168	12,168
.9	HYC	4,644	5,262	5,880	6,510	7,141
	ISS	8,580	8,580	8,580	8,580	8,580
	MON	13,763	13,763	13,763	13,763	13,763
	OFC					
	SFC	12,209	12,209	12,209	12,209	12,209
1.0	HYC	4,687	5,304	5,920	6,525	7,154
	ISS	8,807	8,807	8,807	8,807	8,807
	MON	14,333	14,333	14,333	14,333	14,333
	OFC					
	SFC	12,249	12,249	12,249	12,249	12,249
1.1	HYC	4,730	5,340	5,950	6,560	7,170
	ISS	9,034	9,034	9,034	9,034	9,034
	MON	14,868	14,868	14,868	14,868	14,868
	OFC					
	SFC	12,290	12,290	12,290	12,290	12,290

203 Vehicle Configuration
Section Number 3
LH_2 Tank Top Head

Material: Beryllium
N_x Nominal: -
N_o Nominal: 8138 lbs/in.

N_x ↓ / N_x Nom	N_o → / N_o Nom	.7	.8	.9	1.0	1.1
.7	HYC					
	ISS					
	MON					
	OFC					
	SFC					
.8	HYC					
	ISS					
	MON					
	OFC					
	SFC					
.9	HYC					
	ISS					
	MON					
	OFC					
	SFC					
1.0	HYC	11,017	12,569	14,121	15,673	17,226
	ISS					
	MON	9,127	10,431	11,735	13,039	14,343
	OFC					
	SFC					
1.1	HYC					
	ISS					
	MON					
	OFC					
	SFC					

203 Vehicle Configuration
Section Number 4
Intertank 1 (1058.8" - 1685.7")

Material: Beryllium
N_x Nominal: -8823 lbs/in.
N_o Nominal: 8823 lbs/in.

N_x ↓ / N_x Nom	N_o → / N_o Nom	.7	.8	.9	1.0	1.1
.7	HYC	25,534				
	ISS	33,867				
	MON	96,839				
	OFC					
	SFC	28,652				
.8	HYC		28,333			
	ISS		36,618			
	MON		101,948			
	OFC					
	SFC		30,643			
.9	HYC			31,144		
	ISS			38,610		
	MON			106,677		
	OFC					
	SFC			32,537		
1.0	HYC				33,969	
	ISS				41,097	
	MON				111,093	
	OFC					
	SFC				34,153	
1.1	HYC					36,809
	ISS					43,500
	MON					115,245
	OFC					
	SFC					35,847

203 Vehicle Configuration
Section Number 5
LOX Tank Bottom Head

Material: Beryllium
N_x Nominal: -
N_o Nominal: 24,209 lbs/in.

N_x ↓ / N_x Nom	N_o → / N_o Nom	.7	.8	.9	1.0	1.1
.7	HYC					
	ISS					
	MON					
	OFC					
	SFC					
.8	HYC					
	ISS					
	MON					
	OFC					
	SFC					
.9	HYC					
	ISS					
	MON					
	OFC					
	SFC					
1.0	HYC	26,135	29,850	33,565	37,280	40,995
	ISS					
	MON	21,844	24,964	28,085	31,205	34,326
	OFC					
	SFC					
1.1	HYC					
	ISS					
	MON					
	OFC					
	SFC					

203 Vehicle Configuration
Section Number 6
LOX Tank Top Head

Material: Beryllium
N_x Nominal: -
N_o Nominal: 4266 lbs/in.

N_x ↓ / N_x Nom	N_o → / N_o Nom	.7	.8	.9	1.0	1.1
.7	HYC					
	ISS					
	MON					
	OFC					
	SFC					
.8	HYC					
	ISS					
	MON					
	OFC					
	SFC					
.9	HYC					
	ISS					
	MON					
	OFC					
	SFC					
1.0	HYC	5,891	6,711	7,531	8,350	9,170
	ISS					
	MON	4,820	5,508	6,197	6,885	7,574
	OFC					
	SFC					
1.1	HYC					
	ISS					
	MON					
	OFC					
	SFC					

Weight/Load Matrices - 203 Vehicle

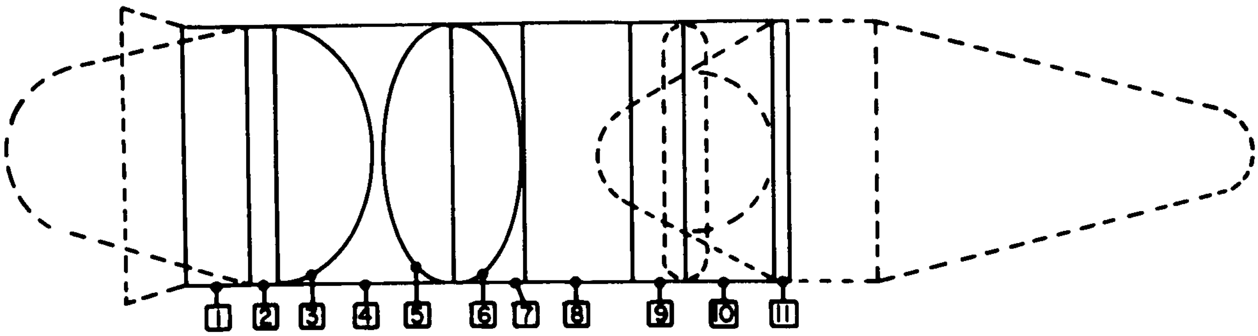

203 Vehicle Configuration
Section Number 7
Stage 1 Forward Skirt (1685.7" - 1937.2")

Material: Beryllium
N_x Nominal: -5648 lbs/in.
N_o Nominal: 5648 lbs/in.

N_x ↓ $\frac{N_x}{N_x\ Nom}$	N_o → $\frac{N_o}{N_o\ Nom}$	.7	.8	.9	1.0	1.1
.7	HYC	7,088				
	ISS	9,437				
	MON	32,707				
	OFC					
	SFC	9,142				
.8	HYC		7,906			
	ISS		10,617			
	MON		34,432			
	OFC					
	SFC		9,773			
.9	HYC			8,745		
	ISS			11,344		
	MON			36,029		
	OFC					
	SFC			10,339		
1.0	HYC				9,554	
	ISS				12,604	
	MON				37,521	
	OFC					
	SFC				10,900	
1.1	HYC					10,286
	ISS					13,621
	MON					38,923
	OFC					
	SFC					11,510

203 Vehicle Configuration
Section Number 8
Interstage (1937.2" - 2465")

Material: Beryllium
N_x Nominal: -5312 lbs/in.
N_o Nominal: 5312 lbs/in.

N_x ↓ $\frac{N_x}{N_x\ Nom}$	N_o → $\frac{N_o}{N_o\ Nom}$	.7	.8	.9	1.0	1.1
.7	HYC	14,211				
	ISS	19,185				
	MON	66,977				
	OFC					
	SFC	18,564				
.8	HYC		15,791			
	ISS		21,236			
	MON		70,510			
	OFC					
	SFC		19,852			
.9	HYC			17,441		
	ISS			23,062		
	MON			73,781		
	OFC					
	SFC			21,124		
1.0	HYC				19,158	
	ISS				24,754	
	MON				76,836	
	OFC					
	SFC				22,136	
1.1	HYC					20,652
	ISS					27,081
	MON					79,707
	OFC					
	SFC					23,346

203 Vehicle Configuration
Section Number 9
Stage 2 Aft Skirt (2465" - 2548")

Material: Beryllium
N_x Nominal: -5106 lbs/in.
N_o Nominal: 5106 lbs/in.

N_x ↓ $\frac{N_x}{N_x\ Nom}$	N_o → $\frac{N_o}{N_o\ Nom}$	.7	.8	.9	1.0	1.1
.7	HYC	1,413				
	ISS	2,946				
	MON	10,385				
	OFC					
	SFC	2,865				
.8	HYC		1,612			
	ISS		3,176			
	MON		10,932			
	OFC					
	SFC		3,063			
.9	HYC			1,810		
	ISS			3,542		
	MON			11,440		
	OFC					
	SFC			3,276		
1.0	HYC				2,009	
	ISS				3,759	
	MON				11,913	
	OFC					
	SFC				3,432	
1.1	HYC					2,207
	ISS					4,076
	MON					12,358
	OFC					
	SFC					3,582

203 Vehicle Configuration
Section Number 10
Intertank 2 (2548" - 2852.7")

Material: Beryllium
N_x Nominal: -2848 lbs/in.
N_o Nominal: 2848 lbs/in.

N_x ↓ $\frac{N_x}{N_x\ Nom}$	N_o → $\frac{N_o}{N_o\ Nom}$	.7	.8	.9	1.0	1.1
.7	HYC	5,119				
	ISS	8,599				
	MON	31,230				
	OFC					
	SFC	8,068				
.8	HYC		5,708			
	ISS		8,937			
	MON		32,888			
	OFC					
	SFC		8,607			
.9	HYC			6,248		
	ISS			9,362		
	MON			34,403		
	OFC					
	SFC			9,136		
1.0	HYC				6,811	
	ISS				9,963	
	MON				35,827	
	OFC					
	SFC				9,623	
1.1	HYC					7,377
	ISS					10,519
	MON					37,166
	OFC					
	SFC					10,098

203 Vehicle Configuration
Section Number 11
Stage 2 Forward Skirt (2852.7" - 2888.7")

Material: Beryllium
N_x Nominal: -2328 lbs/in.
N_o Nominal: 2328 lbs/in.

N_x ↓ $\frac{N_x}{N_x\ Nom}$	N_o → $\frac{N_o}{N_o\ Nom}$	.7	.8	.9	1.0	1.1
.7	HYC	211				
	ISS	726				
	MON	2,469				
	OFC					
	SFC	620				
.8	HYC		241			
	ISS		749			
	MON		2,599			
	OFC					
	SFC		664			
.9	HYC			270		
	ISS			770		
	MON			2,720		
	OFC					
	SFC			704		
1.0	HYC				299	
	ISS				787	
	MON				2,832	
	OFC					
	SFC				740	
1.1	HYC					328
	ISS					835
	MON					2,936
	OFC					
	SFC					777

Weight/Load Matrices - 301 Vehicle

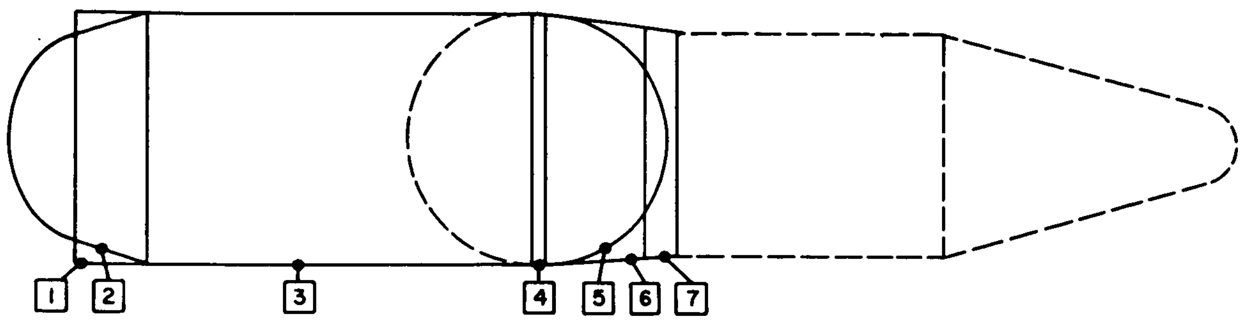

301 Vehicle Configuration
Section Number 1
Thrust Takeout (500" - 770")

Material: Aluminum 2219 - T87
N_x Nominal: -12,831 lbs/in.
N_o Nominal: 12,831 lbs/in.

$\frac{N_x}{N_x}$ Nom ↓	$\frac{N_o}{N_o}$ Nom →	.7	.8	.9	1.0	1.1
.7	HYC	29,170				
	ISS	65,628				
	MON	123,886				
	OFC	109,395				
	SFC	47,846				
.8	HYC		32,979			
	ISS		70,000			
	MON		130,422			
	OFC		116,948			
	SFC		51,199			
.9	HYC			36,758		
	ISS			74,372		
	MON			136,472		
	OFC			124,042		
	SFC			54,353		
1.0	HYC				40,701	
	ISS				78,745	
	MON				142,122	
	OFC				130,752	
	SFC				62,011	
1.1	HYC					44,649
	ISS					83,117
	MON					147,434
	OFC					137,133
	SFC					64,187

301 Vehicle Configuration
Section Number 2
LH_2 Tank Bottom Head

Material: Aluminum 2219 - T87
N_x Nominal: -
N_o Nominal: 7753 lbs/in.

$\frac{N_x}{N_x}$ Nom ↓	$\frac{N_o}{N_o}$ Nom →	.7	.8	.9	1.0	1.1
.7	HYC					
	ISS					
	MON					
	OFC					
	SFC					
.8	HYC					
	ISS					
	MON					
	OFC					
	SFC					
.9	HYC					
	ISS					
	MON					
	OFC					
	SFC					
1.0	HYC	18,758	21,411	24,065	26,718	29,371
	ISS					
	MON	15,601	17,830	20,058	22,287	24,516
	OFC					
	SFC					
1.1	HYC					
	ISS					
	MON					
	OFC					
	SFC					

301 Vehicle Configuration
Section Number 3
LH_2 Tank Cylinder (770" - 2280")

Material: Aluminum 2219 - T87
N_x Nominal: -8806 lbs/in.
N_o Nominal: 15,473 lbs/in.

$\frac{N_x}{N_x}$ Nom ↓	$\frac{N_o}{N_o}$ Nom →	.7	.8	.9	1.0	1.1
.7	HYC	124,663	140,403	156,455	172,648	188,938
	ISS	263,856	263,856	263,856	263,856	263,856
	MON	585,257	585,257	585,257	585,257	585,257
	OFC					
	SFC					
.8	HYC	127,801	141,474	156,603	173,418	189,645
	ISS	281,659	281,659	281,659	281,659	281,659
	MON	616,132	616,132	616,132	616,132	616,132
	OFC					
	SFC					
.9	HYC	134,494	143,910	158,286	174,201	190,355
	ISS	294,161	294,161	294,161	294,161	294,161
	MON	644,714	644,714	644,714	644,714	644,714
	OFC					
	SFC					
1.0	HYC	143,856	151,139	160,276	175,098	175,098
	ISS	316,615	316,615	316,615	316,615	316,615
	MON	671,404	671,404	671,404	671,404	671,404
	OFC					
	SFC					
1.1	HYC	154,820	158,855	167,919	176,784	191,912
	ISS	345,887	345,887	345,887	345,887	345,887
	MON	696,498	696,498	696,498	696,498	696,498
	OFC					
	SFC					

301 Vehicle Configuration
Section Number 4
LOX Tank Cylinder (2280" - 2328")

Material: Aluminum 2219 - T87
N_x Nominal: -1857 lbs/in.
N_o Nominal: 11,065 lbs/in.

$\frac{N_x}{N_x}$ Nom ↓	$\frac{N_o}{N_o}$ Nom →	.7	.8	.9	1.0	1.1
.7	HYC	2,679	3,059	3,440	3,821	4,201
	ISS	4,020	4,020	4,020	4,020	4,020
	MON	10,211	10,211	10,211	10,211	10,211
	OFC					
	SFC					
.8	HYC	2,679	3,059	3,440	3,821	4,201
	ISS	4,411	4,411	4,411	4,411	4,411
	MON	10,749	10,749	10,749	10,749	10,749
	OFC					
	SFC					
.9	HYC	2,679	3,059	3,440	3,821	4,201
	ISS	4,798	4,798	4,798	4,798	4,798
	MON	11,248	11,248	11,248	11,248	11,248
	OFC					
	SFC					
1.0	HYC	2,679	3,059	3,440	3,821	4,201
	ISS	5,189	5,189	5,189	5,189	5,189
	MON	11,713	11,713	11,713	11,713	11,713
	OFC					
	SFC					
1.1	HYC	2,679	3,059	3,440	3,821	4,201
	ISS	5,588	5,588	5,588	5,588	5,588
	MON	12,151	12,151	12,151	12,151	12,151
	OFC					
	SFC					

Weight/Load Matrices - 301 Vehicle

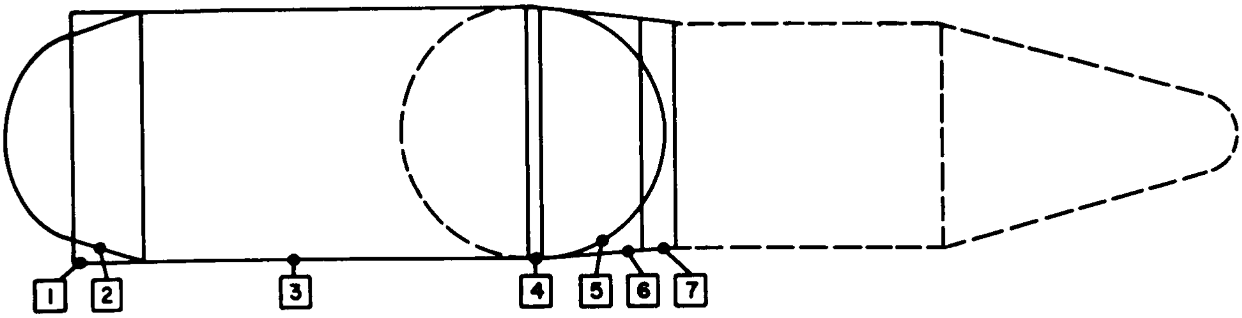

301 Vehicle Configuration
Section Number 5
LOX Tank Top Head

Material: Aluminum 2219 - T87
N_x Nominal: -
N_o Nominal: 4,828 lbs/in.

$N_x / \overline{N_x}$ Nom ↓	$N_o / \overline{N_o}$ Nom →	.7	.8	.9	1.0	1.1
.7	HYC					
	ISS					
	MON					
	OFC					
	SFC					
.8	HYC					
	ISS					
	MON					
	OFC					
	SFC					
.9	HYC					
	ISS					
	MON					
	OFC					
	SFC					
1.0	HYC	12,280	13,985	15,710	17,435	19,159
	ISS					
	MON	10,142	11,591	13,040	14,489	15,938
	OFC					
	SFC					
1.1	HYC					
	ISS					
	MON					
	OFC					
	SFC					

301 Vehicle Configuration
Section Number 6
Forward Skirt (2328" - 2724")

Material: Aluminum 2219 - T87
N_x Nominal: -3880 lbs/in.
N_o Nominal: 3880 lbs/in.

$N_x / \overline{N_x}$ Nom ↓	$N_o / \overline{N_o}$ Nom →	.7	.8	.9	1.0	1.1
.7	HYC	14,268				
	ISS	43,552				
	MON	110,288				
	OFC	46,863				
	SFC	34,750				
.8	HYC		15,974			
	ISS		46,684			
	MON		116,106			
	OFC		50,098			
	SFC		37,130			
.9	HYC			17,669		
	ISS			49,516		
	MON			121,493		
	OFC			53,137		
	SFC			39,418		
1.0	HYC				19,355	
	ISS				52,748	
	MON				126,522	
	OFC				56,012	
	SFC				41,586	
1.1	HYC					21,024
	ISS					55,877
	MON					131,251
	OFC					58,746
	SFC					43,851

301 Vehicle Configuration
Section Number 7
Instrument Unit (2724" - 2844")

Material: Aluminum 2219-T87
N_x Nominal: -3752 lbs/in.
N_o Nominal: 3752 lbs/in.

$N_x / \overline{N_x}$ Nom ↓	$N_o / \overline{N_o}$ Nom →	.7	.8	.9	1.0	1.1
.7	HYC	3,869				
	ISS	12,376				
	MON	34,986				
	OFC	29,716				
	SFC	9,240				
.8	HYC		4,335			
	ISS		12,796			
	MON		30,515			
	OFC		31,768			
	SFC		9,790			
.9	HYC			4,796		
	ISS			13,222		
	MON			31,931		
	OFC			33,695		
	SFC			10,391		
1.0	HYC				5,258	
	ISS				13,647	
	MON				33,252	
	OFC				35,512	
	SFC				10,959	
1.1	HYC					6,718
	ISS					14,072
	MON					34,495
	OFC					37,251
	SFC					11,501

Weight/Load Matrices - 301 Vehicle

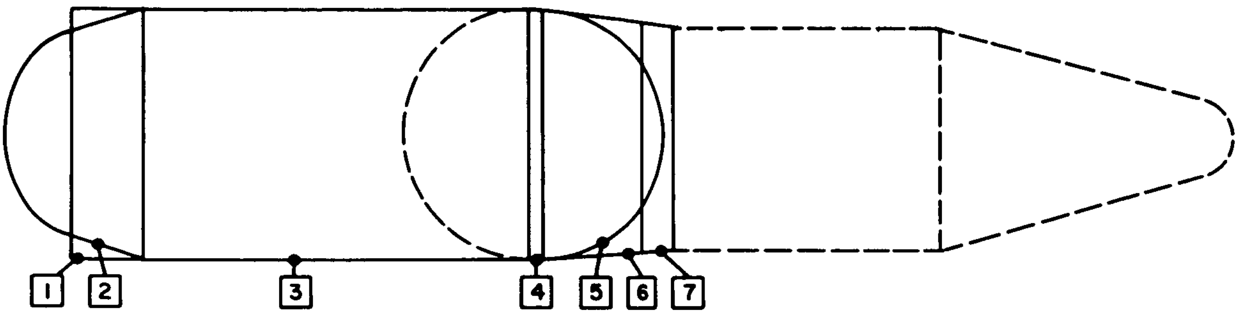

301 Vehicle Configuration
Section Number 1
Thrust Takeout (500" - 770")

Material: Titanium
N_x Nominal: -12,831 lbs/in.
N_o Nominal: 12,831 lbs/in.

$\frac{N_x}{N_x \text{ Nom}}$ ↓	$\frac{N_o}{N_o \text{ Nom}}$ →	.7	.8	.9	1.0	1.1
.7	HYC	22,570				
	ISS	77,411				
	MON	167,633				
	OFC	136,683				
	SFC	57,201				
.8	HYC		25,190			
	ISS		84,790			
	MON		176,477			
	OFC		146,119			
	SFC		65,938			
.9	HYC			27,796		
	ISS			91,255		
	MON			184,664		
	OFC			154,983		
	SFC			69,780		
1.0	HYC				30,391	
	ISS				98,624	
	MON				192,308	
	OFC				163,366	
	SFC				73,604	
1.1	HYC					32,976
	ISS					106,328
	MON					199,496
	OFC					171,340
	SFC					77,247

301 Vehicle Configuration
Section Number 2
LH_2 Tank Bottom Head

Material: Titanium
N_x Nominal: -
N_o Nominal: 7753 lbs/in.

$\frac{N_x}{N_x \text{ Nom}}$ ↓	$\frac{N_o}{N_o \text{ Nom}}$ →	.7	.8	.9	1.0	1.1
.7	HYC					
	ISS					
	MON					
	OFC					
	SFC					
.8	HYC					
	ISS					
	MON					
	OFC					
	SFC					
.9	HYC					
	ISS					
	MON					
	OFC					
	SFC					
1.0	HYC	11,988	13,674	15,360	17,046	18,732
	ISS					
	MON	9,914	11,330	12,747	14,163	15,579
	OFC					
	SFC					
1.1	HYC					
	ISS					
	MON					
	OFC					
	SFC					

301 Vehicle Configuration
Section Number 3
LH_2 Tank Cylinder (770" - 2280")

Material: Titanium
N_x Nominal: -8806 lbs/in.
N_o Nominal: 15,473 lbs/in.

$\frac{N_x}{N_x \text{ Nom}}$ ↓	$\frac{N_o}{N_o \text{ Nom}}$ →	.7	.8	.9	1.0	1.1
.7	HYC	107,339	113,950	121,457	129,592	138,183
	ISS	312,625	312,625	312,625	312,625	312,625
	MON	791,434	791,434	791,434	791,434	791,434
	OFC					
	SFC					
.8	HYC	112,107	118,065	125,123	132,899	141,196
	ISS	337,977	337,977	337,977	337,977	337,977
	MON	833,185	833,185	833,185	833,185	833,185
	OFC					
	SFC					
.9	HYC	117,502	122,227	128,789	136,205	144,210
	ISS	362,231	362,231	362,231	362,231	362,231
	MON	871,837	871,837	871,837	871,837	871,837
	OFC					
	SFC					
1.0	HYC	121,069	127,291	132,489	139,515	147,224
	ISS	393,132	393,132	393,132	393,132	393,132
	MON	907,929	907,929	907,929	907,929	907,929
	OFC					
	SFC					
1.1	HYC	126,893	130,417	136,651	142,846	150,240
	ISS	418,064	418,064	418,064	418,064	418,064
	MON	941,864	941,864	941,864	941,864	941,864
	OFC					
	SFC					

301 Vehicle Configuration
Section Number 4
LOX Tank Cylinder (2280" - 2328")

Material: Titanium
N_x Nominal: -1857 lbs/in.
N_o Nominal: 11,065 lbs/in.

$\frac{N_x}{N_x \text{ Nom}}$ ↓	$\frac{N_o}{N_o \text{ Nom}}$ →	.7	.8	.9	1.0	1.1
.7	HYC	1,730	1,973	2,215	2,458	2,700
	ISS	4,061	4,061	4,061	4,061	4,061
	MON	13,793	13,793	13,793	13,793	13,793
	OFC					
	SFC					
.8	HYC	1,730	1,973	2,215	2,458	2,700
	ISS	4,311	4,311	4,311	4,311	4,311
	MON	14,521	14,521	14,521	14,521	14,521
	OFC					
	SFC					
.9	HYC	1,730	1,973	2,215	2,458	2,700
	ISS	4,560	4,560	4,560	4,560	4,560
	MON	15,194	15,194	15,194	15,194	15,194
	OFC					
	SFC					
1.0	HYC	1,730	1,973	2,215	2,458	2,700
	ISS	4,810	4,810	4,810	4,810	4,810
	MON	15,823	15,823	15,823	15,823	15,823
	OFC					
	SFC					
1.1	HYC	1,730	1,973	2,215	2,458	2,700
	ISS	5,072	5,072	5,072	5,072	5,072
	MON	16,415	16,415	16,415	16,415	16,415
	OFC					
	SFC					

Weight/Load Matrices - 301 Vehicle

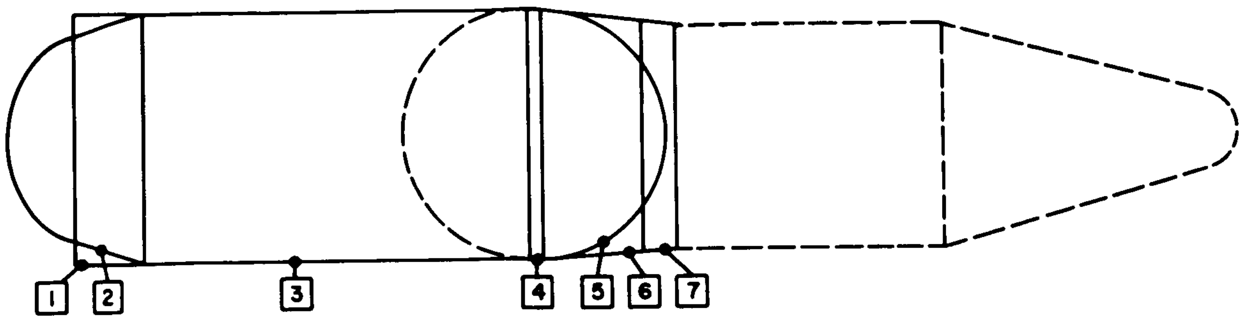

301 Vehicle Configuration
Section Number 5
LOX Tank Top Head

Material: Titanium
N_x Nominal: -
N_o Nominal: 4828 lbs/in.

$\frac{N_x}{N_x \text{ Nom}}$ ↓	$\frac{N_o}{N_o \text{ Nom}}$ →	.7	.8	.9	1.0	1.1
.7	HYC					
	ISS					
	MON					
	OFC					
	SFC					
.8	HYC					
	ISS					
	MON					
	OFC					
	SFC					
.9	HYC					
	ISS					
	MON					
	OFC					
	SFC					
1.0	HYC	8,031	9,141	10,260	11,380	12,499
	ISS					
	MON	6,582	7,522	8,463	9,403	10,343
	OFC					
	SFC					
1.1	HYC					
	ISS					
	MON					
	OFC					
	SFC					

301 Vehicle Configuration
Section Number 6
Forward Skirt (2328" - 2724")

Material: Titanium
N_x Nominal: -3880 lbs/in.
N_o Nominal: 3880 lbs/in.

$\frac{N_x}{N_x \text{ Nom}}$ ↓	$\frac{N_o}{N_o \text{ Nom}}$ →	.7	.8	.9	1.0	1.1
.7	HYC	13,319				
	ISS	53,204				
	MON	149,233				
	OFC	58,945				
	SFC	44,839				
.8	HYC		14,492			
	ISS		56,603			
	MON		157,106			
	OFC		63,015			
	SFC		47,932			
.9	HYC			15,665		
	ISS			60,676		
	MON			164,394		
	OFC			66,837		
	SFC			50,893		
1.0	HYC				16,830	
	ISS				64,595	
	MON				171,200	
	OFC				70,452	
	SFC				53,633	
1.1	HYC					17,988
	ISS					70,449
	MON					177,599
	OFC					73,891
	SFC					56,104

301 Vehicle Configuration
Section Number 7
Instrument Unit (2724" - 2844")

Material: Titanium
N_x Nominal: -3752 lbs/in.
N_o Nominal: 3752 lbs/in.

$\frac{N_x}{N_x \text{ Nom}}$ ↓	$\frac{N_o}{N_o \text{ Nom}}$ →	.7	.8	.9	1.0	1.1
.7	HYC	3,559				
	ISS	14,980				
	MON	39,221				
	OFC	37,035				
	SFC	11,855				
.8	HYC		3,881			
	ISS		15,979			
	MON		41,291			
	OFC		39,592			
	SFC		12,687			
.9	HYC			4,201		
	ISS			17,181		
	MON			43,206		
	OFC			41,994		
	SFC			13,470		
1.0	HYC				4,519	
	ISS				18,875	
	MON				44,995	
	OFC				44,365	
	SFC				14,212	
1.1	HYC					4,835
	ISS					20,030
	MON					46,676
	OFC					46,426
	SFC					14,919

Weight/Load Matrices - 301 Vehicle

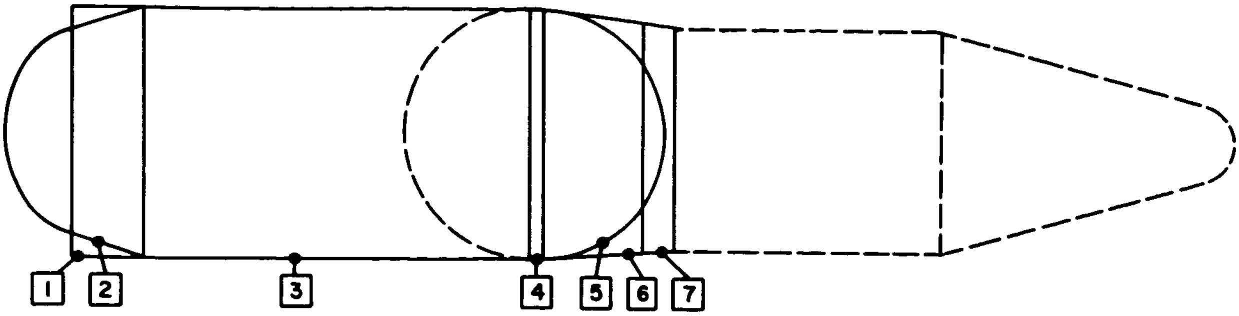

301 Vehicle Configuration
Section Number 1
Thrust Takeout (500" - 770")

Material: Beryllium
N_x Nominal: -12,831 lbs/in.
N_o Nominal: 12,831 lbs/in.

$\frac{N_x}{N_x}$ Nom ↓	$\frac{N_o}{N_o}$ Nom →	.7	.8	.9	1.0	1.1
.7	HYC	14,844				
	ISS	19,396				
	MON	48,171				
	OFC	184,593				
	SFC	15,824				
.8	HYC		16,626			
	ISS		20,554			
	MON		50,712			
	OFC		197,338			
	SFC		15,872			
.9	HYC			18,565		
	ISS			21,713		
	MON			53,064		
	OFC			209,309		
	SFC			16,851		
1.0	HYC				20,647	
	ISS				22,871	
	MON				55,262	
	OFC				220,631	
	SFC				17,779	
1.1	HYC					22,585
	ISS					24,030
	MON					57,327
	OFC					231,399
	SFC					18,625

301 Vehicle Configuration
Section Number 2
LH_2 Tank Bottom Head

Material: Beryllium
N_x Nominal: -
N_o Nominal: 7753 lbs/in.

$\frac{N_x}{N_x}$ Nom ↓	$\frac{N_o}{N_o}$ Nom →	.7	.8	.9	1.0	1.1
.7	HYC					
	ISS					
	MON					
	OFC					
	SFC					
.8	HYC					
	ISS					
	MON					
	OFC					
	SFC					
.9	HYC					
	ISS					
	MON					
	OFC					
	SFC					
1.0	HYC	12,447	14,199	15,950	17,702	19,453
	ISS					
	MON	10,299	11,771	13,242	14,714	16,185
	OFC					
	SFC					
1.1	HYC					
	ISS					
	MON					
	OFC					
	SFC					

301 Vehicle Configuration
Section Number 3
LH_2 Tank Cylinder (770" - 2280")

Material: Beryllium
N_x Nominal: -8806 lbs/in.
N_o Nominal: 15,473 lbs/in.

$\frac{N_x}{N_x}$ Nom ↓	$\frac{N_o}{N_o}$ Nom →	.7	.8	.9	1.0	1.1
.7	HYC	80,243	90,191	100,544	111,093	121,750
	ISS	138,484	138,484	138,484	138,484	138,484
	MON	233,033	233,033	233,033	233,033	233,033
	OFC					
	SFC					
.8	HYC	82,042	91,328	101,340	111,699	122,242
	ISS	138,702	138,702	138,702	138,702	138,702
	MON	245,326	245,326	245,326	245,326	245,326
	OFC					
	SFC					
.9	HYC	84,709	92,949	102,431	112,497	122,865
	ISS	138,921	138,921	138,921	138,921	138,921
	MON	256,708	256,708	256,708	256,708	256,708
	OFC					
	SFC					
1.0	HYC	88,601	95,240	103,928	113,558	123,669
	ISS	139,139	139,139	139,139	139,139	139,139
	MON	267,335	267,335	267,335	267,335	267,335
	OFC					
	SFC					
1.1	HYC	94,175	98,443	105,967	114,968	124,712
	ISS	139,357	139,357	139,357	139,357	139,357
	MON	277,327	277,327	277,327	277,327	277,327
	OFC					
	SFC					

301 Vehicle Configuration
Section Number 4
LOX Tank Cylinder (2280" - 2328")

Material: Beryllium
N_x Nominal: -1857 lbs/in.
N_o Nominal: 11,065 lbs/in.

$\frac{N_x}{N_x}$ Nom ↓	$\frac{N_o}{N_o}$ Nom →	.7	.8	.9	1.0	1.1
.7	HYC	1,755	2,004	2,253	2,501	2,750
	ISS	3,429	3,429	3,429	3,429	3,429
	MON	4,068	4,068	4,068	4,068	4,068
	OFC					
	SFC					
.8	HYC	1,755	2,004	2,253	2,501	2,750
	ISS	3,429	3,429	3,429	3,429	3,429
	MON	4,283	4,283	4,283	4,283	4,283
	OFC					
	SFC					
.9	HYC	1,755	2,004	2,253	2,501	2,750
	ISS	3,429	3,429	3,429	3,429	3,429
	MON	4,481	4,481	4,481	4,481	4,481
	OFC					
	SFC					
1.0	HYC	1,755	2,004	2,253	2,501	2,750
	ISS	3,429	3,429	3,429	3,429	3,429
	MON	4,667	4,667	4,667	4,667	4,667
	OFC					
	SFC					
1.1	HYC	1,755	2,004	2,253	2,501	2,750
	ISS	3,429	3,429	3,429	3,429	3,429
	MON	4,841	4,841	4,841	4,841	4,841
	OFC					
	SFC					

Weight/Load Matrices - 301 Vehicle

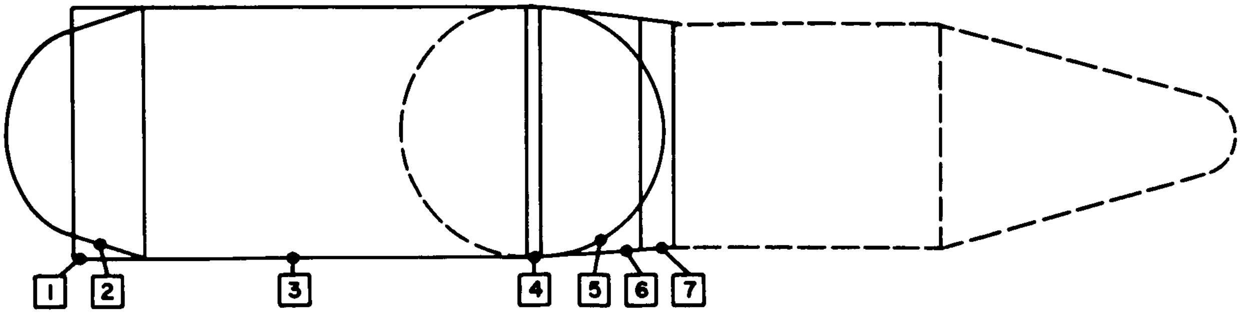

301 Vehicle Configuration
Section Number 5
LOX Tank Top Head

Material: Beryllium
N_x Nominal: -
N_o Nominal: 4828 lbs/in.

$\frac{N_x}{\bar{N}_x}$ Nom ↓	$\frac{N_o}{\bar{N}_o}$ Nom →	.7	.8	.9	1.0	1.1
.7	HYC					
	ISS					
	MON					
	OFC					
	SFC					
.8	HYC					
	ISS					
	MON					
	OFC					
	SFC					
.9	HYC					
	ISS					
	MON					
	OFC					
	SFC					
1.0	HYC	7,688	8,759	9,832	10,903	11,975
	ISS					
	MON	6,302	7,202	8,103	9,003	9,903
	OFC					
	SFC					
1.1	HYC					
	ISS					
	MON					
	OFC					
	SFC					

301 Vehicle Configuration
Section Number 6
Forward Skirt (2328" - 2724")

Material: Beryllium
N_x Nominal: -3880 lbs/in.
N_o Nominal: 3880 lbs/in.

$\frac{N_x}{\bar{N}_x}$ Nom ↓	$\frac{N_o}{\bar{N}_o}$ Nom →	.7	.8	.9	1.0	1.1
.7	HYC	7,877				
	ISS	12,069				
	MON	42,884				
	OFC	65,172				
	SFC	11,483				
.8	HYC		8,791			
	ISS		12,554			
	MON		45,146			
	OFC		69,671			
	SFC		12,282			
.9	HYC			9,692		
	ISS			13,241		
	MON			47,240		
	OFC			73,898		
	SFC			13,022		
1.0	HYC				10,570	
	ISS				14,049	
	MON				49,196	
	OFC				77,695	
	SFC				13,718	
1.1	HYC					11,401
	ISS					15,284
	MON					51,036
	OFC					81,697
	SFC					14,384

301 Vehicle Configuration
Section Number 7
Instrument Unit (2724" - 2844")

Material: Beryllium
N_x Nominal: -3752 lbs/in.
N_o Nominal: 3752 lbs/in.

$\frac{N_x}{\bar{N}_x}$ Nom ↓	$\frac{N_o}{\bar{N}_o}$ Nom →	.7	.8	.9	1.0	1.1
.7	HYC	2,133				
	ISS	3,156				
	MON	11,271				
	OFC	53,470				
	SFC	3,035				
.8	HYC		2,379			
	ISS		3,426			
	MON		11,865			
	OFC		57,162			
	SFC		3,246			
.9	HYC			2,624		
	ISS			3,667		
	MON			12,416		
	OFC			60,629		
	SFC			3,444		
1.0	HYC				2,815	
	ISS				3,898	
	MON				12,930	
	OFC				63,909	
	SFC				3,631	
1.1	HYC					2,876
	ISS					4,276
	MON					13,413
	OFC					67,028
	SFC					3,810

APPENDIX D

PRESSURE COUPLING EQUATIONS

APPENDIX D

PRESSURE COUPLING EQUATIONS

D1 NOMENCLATURE

The equations used here are taken from References 27 and 28.

h_1	Cap thickness, in.
h_2	Barrel thickness, in.
E	Young's modulus of elasticity, lb/in.^{2}
R	Radius, in.
P	Pressure, lb/in.^{2}
M	Moment, in.-lb/in.
V	Shear, lb/in.
σ	Stress, lb/in.
ν	Poisson's ratio, = 0.3.
X	Distance from cap barrel juncture to a point in the barrel, in.

Subscripts

Θ	Hoop
ϕ, χ	Meridional

D2 PARAMETERS

HEMISPHERICAL CAP

$$K_1 = E h_1 / R^2$$

$$\lambda_1 = \sqrt[4]{\frac{3(1-\nu^2)}{R^2 h_1^2}}$$

$$C = E h_1$$

$$\eta_1 = \sqrt[4]{12(1-\nu^2)\left(\frac{R}{h_1}\right)^2}$$

$$\rho = \frac{PR}{4C}\eta_1^2$$

$$C_{11} = \frac{\sqrt{1+\rho}}{1 + 2\rho}\left(\frac{2\lambda_1}{K_1}\right)$$

$$C_{12} = \frac{\sqrt{1+\rho}}{1 + 2\rho}\left(\frac{2\lambda_1^{\;2}}{K_1}\right)$$

$$C_{22} = -\frac{4}{1 + 2\rho}\left(\frac{\lambda_1^{\;3}}{K_1}\right)$$

$$C_{21} = -C_{12}$$

CYLINDRICAL BARREL

$$N = \frac{PR}{2}$$

$$K_2 = \frac{E\,h_2}{R^2}$$

$$\lambda_2 = \sqrt[4]{\frac{3(1 - \nu^2)}{R^2\,h_2^{\;2}}}$$

$$Z = K_2/\lambda_2^{\;2}$$

$$\Delta = \frac{N}{Z}$$

D3 DISCONTINUITY LOADS CALCULATIONS (See Figure D-1)

$$M = \frac{\dfrac{PR^2}{E}\left[\left(1 - \dfrac{\nu}{2}\right)\dfrac{1}{h_2} - (1 - \nu)\,\dfrac{1}{2h_1}\right]}{\left\{\left[C_{11} + \dfrac{2\sqrt{1+\Delta}}{\lambda_2(Z + 2N)}\right]\left[\dfrac{\left(\dfrac{4\lambda_2\sqrt{1+\Delta}}{Z + 2N} - C_{22}\right)}{\left(C_{21} + \dfrac{2}{Z + 2N}\right)}\right] + \left(C_{12} - \dfrac{2}{Z + 2N}\right)\right\}}$$

$$V = M\left[\frac{\left(\frac{4\lambda_2\sqrt{1+\Delta}}{Z+2N} - C_{22}\right)}{\left(C_{21} + \frac{2}{Z+2N}\right)}\right]$$

D4 STRESS CALCULATIONS

D4.1 HEMISPHERICAL CAP DISCONTINUITY STRESS CALCULATIONS

Membrane

$$\sigma = \frac{PR}{2h_1}$$

Total Meridional Stress

$$\sigma_{\phi_1} = \sigma - \frac{V}{h_1} + \frac{6M}{h_1^2}$$

$$\sigma_{\phi_2} = \sigma - \frac{V}{h_2} - \frac{6M}{h_1^2}$$

Total Hoop Stress

$$\sigma_{\Theta_1} = 2\sigma - \frac{2\lambda_1 R}{h_1} V + \frac{2\lambda_1^2}{h_1} RM + \frac{\nu 6M}{h_1^2}$$

$$\sigma_{\Theta_2} = 2\sigma - \frac{2\lambda_1 R}{h_1} V + \frac{2\lambda_1^2}{h_1} RM - \frac{\nu 6M}{h_1^2}$$

D4.2 CYLINDRICAL BARREL STRESS CALCULATIONS

Parameters

$$\alpha = \lambda_2\sqrt{1+\Delta}$$

$$F_1 = -V\lambda_2^2\left(\Delta\lambda_2^2 + \frac{3\nu}{Rh_2}\right) + \alpha M\lambda_2^2\left[-\lambda_2^2 + \frac{3\nu}{Rh_2}(1 - 2\Delta)\right]$$

$$F_2 = -V\lambda_2^2\left(\Delta\lambda_2^2 - \frac{3\nu}{Rh_2}\right) + \alpha M\lambda_2^2\left[-\lambda_2^2 - \frac{3\nu}{Rh_2}(1 - 2\Delta)\right]$$

$$G = \frac{V + 4\alpha M\Delta}{\alpha V - 2M\lambda_2^2 (1 - 2\Delta)^2}$$

$$H = \frac{V + \alpha M(2\Delta - 1)}{1 + 2\Delta}$$

$$J_1 = -\alpha V\lambda_2^2 + M\left[\lambda_2^2 + \frac{3\nu}{Rh_2}(1 + 2\Delta)\lambda_2^2\right]$$

$$J_2 = -\alpha V\lambda_2^2 + M\left[\lambda_2^2 - \frac{3\nu}{Rh_2}(1 + 2\Delta)\lambda_2^2\right]$$

For $N < Z$

$$\beta = \lambda_2\sqrt{1 - \Delta}$$

Meridional stress, σ_X, points where $d\sigma_X/dX = 0$

$$X = \frac{1}{\beta}\arctan \beta G$$

$$\sigma_{X_1} = \frac{6}{h_2^2 e^{\alpha X}}\left(M\cos\beta X - \frac{H}{\beta}\sin\beta X\right) + \frac{N}{h_2}$$

$$\sigma_{X_2} = \frac{-6}{h_2^2 e^{\alpha X}}\left(M\cos\beta X - \frac{H}{\beta}\sin\beta X\right) + \frac{N}{h_2}$$

Hoop stress, σ_Θ, points where $d\sigma_\Theta/dX = 0$

$$X_1 = \frac{1}{\beta}\arctan\left(\frac{F_1 - \alpha J_1}{\frac{\alpha}{\beta}F_1 + \beta J_1}\right)$$

$$X_2 = \frac{1}{\beta}\arctan\left(\frac{F_2 - \alpha J_2}{\frac{\alpha}{\beta}F_2 + \beta J_2}\right)$$

$$\sigma_{\Theta_1} = \frac{R}{h_2}\left\{p + \left(\frac{1}{e^{\alpha X_1}}\right)\left[\frac{1}{\lambda_2^2\left(\Delta + \frac{1}{2}\right)}\right]\left(J_1 \cos\beta X_1 + \frac{F_1}{\beta}\sin\beta X_1\right)\right\}$$

$$\sigma_{\Theta_2} = \frac{R}{h_2}\left\{p + \left(\frac{1}{e^{\alpha X_2}}\right)\left[\frac{1}{\lambda_2^2\left(\Delta + \frac{1}{2}\right)}\right]\left(J_2 \cos\beta X_2 + \frac{F_2}{\beta}\sin\beta X_2\right)\right\}$$

For N > Z

$$\overline{\beta} = \lambda_2 \sqrt{\Delta - 1}$$

Meridional stress, σ_X, point where $d\sigma_X/dX = 0$

$$X = \frac{1}{\overline{\beta}} \text{ arc } \tanh \overline{\beta} G,$$

where

$$X = \frac{1}{2\overline{\beta}} \ln\left(\frac{1 + \overline{\beta} G}{1 - \overline{\beta} G}\right) \qquad 0 < (\overline{\beta} G)^2 < 1$$

If $(\overline{\beta} G)^2 \geq 1$ maximum stress is the discontinuity stress <u>or</u> the membrane stress.

$$\sigma_{X_1} = \frac{6}{e^{\alpha X} h_2^2}\left(M \cosh \overline{\beta} X - \frac{H}{\overline{\beta}} \sinh \overline{\beta} X\right) + \frac{N}{h_2}$$

$$\sigma_{X_2} = \frac{-6}{e^{\alpha X} h_2^2}\left(M \cosh \overline{\beta} X - \frac{H}{\overline{\beta}} \sinh \overline{\beta} X\right) + \frac{N}{h_2}$$

Hoop stress, σ_Θ, points where $d\sigma_\Theta/dX = 0$

$$X_1 = \frac{1}{\overline{\beta}} \text{ arc } \tanh \left(\frac{F_1 - \alpha J_1}{\frac{\alpha}{\beta} F_1 - \overline{\beta} J_1}\right)$$

$$X_2 = \frac{1}{\overline{\beta}} \text{ arc } \tanh \left(\frac{F_2 - \alpha J_2}{\frac{\alpha}{\beta} F_2 - \overline{\beta} J_2}\right)$$

$$\sigma_{\Theta_1} = \frac{R}{h_2}\left\{p + \left(\frac{1}{e^{\alpha X_1}}\right)\left[\frac{1}{\lambda_2^2\left(\Delta + \frac{1}{2}\right)}\right]\left(J_1 \cosh \bar{\beta} X_1 + \frac{F_1}{\beta} \sinh \bar{\beta} X_1\right)\right\}$$

$$\sigma_{\Theta_2} = \frac{R}{h_2}\left\{p + \left(\frac{1}{e^{\alpha X_2}}\right)\left[\frac{1}{\lambda_2^2\left(\Delta + \frac{1}{2}\right)}\right]\left(J_2 \cosh \bar{\beta} X_2 + \frac{F_2}{\beta} \sinh \bar{\beta} X_2\right)\right\}$$

N-Neglected

Parameters, and other terms

$$A = e^{-\lambda_2 X} (\cos \lambda_2 X + \sin \lambda_2 X)$$

$$B = e^{-\lambda_2 X} (\sin \lambda_2 X)$$

$$C = e^{-\lambda_2 X} (\cos \lambda_2 X - \sin \lambda_2 X)$$

$$D = e^{-\lambda_2 X} (\cos \lambda_2 X)$$

$$W = \frac{V}{2M\lambda}$$

$$S_{1,2} = \pm \frac{3\nu}{\sqrt{3(1 - \nu^2)}}$$

Discontinuity loads are the same as for pressure coupling except N, Δ, and ρ are set to zero.

Meridional stress points where $d\sigma_X/dX$

$$X = \text{arc tan} \frac{W}{W - 1}$$

$$\sigma_{X_{1,2}} = \pm \frac{6}{h_2^2}\left[M(A) - \frac{V}{\lambda_2}(B)\right] + \frac{PR}{2h_2}$$

Hoop stress points where $d\sigma_{\Theta}/dX = 0$

$$X_{1,2} = \frac{1}{\lambda} \arctan \left[\frac{W(1 - S_{1,2}) - 1}{S_{1,2} - W(1 + S_{1,2})} \right]$$

Stresses

$$\sigma_{\Theta_{1,2}} = \frac{PR}{h_2} - \frac{2V\lambda_2 D}{h_2} + \frac{2M\lambda_2^{2} RC}{h_2} \pm \frac{6\nu}{h_2^{2}} \left(MA - \frac{VB}{\lambda_2} \right)$$

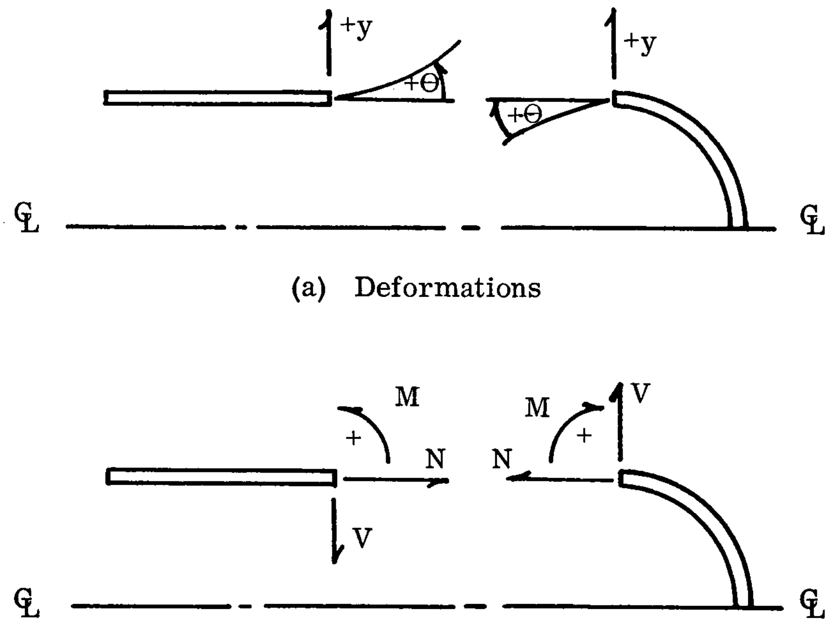

(a) Deformations

(b) Discontinuity Loads

Figure D-1. Sign Convention

APPENDIX E

THIN-WALLED PRESSURE VESSEL FACTOR OF SAFETY EXAMINED BY A PLASTIC DEFORMATION THEORY

APPENDIX E

THIN-WALLED PRESSURE VESSEL FACTOR OF SAFETY EXAMINED BY A PLASTIC DEFORMATION THEORY

E1 FACTOR OF SAFETY EXAMINED BY A PLASTIC DEFORMATION THEORY

E1.1 INTRODUCTION

A certain gap in technique currently exists when lightweight design is required to carry maximum load. In order to attempt to solve this dilemma, current engineering usage generally focuses attention on two theories of elastic breakdown, the von Mises-Hencky theory, and the Tresca-St. Venant theory. It is the purpose of this note to draw attention to the results of a short study which compared the resulting ultimate strengths of cylindrical tubes and spherical shells designed of three aluminum alloys by the two theories mentioned and by the maximum energy theory (Beltrami-Haigh). It was found that the resulting cylindrical structures were conservative when designed by the Tresca and the Beltrami theories, and were unconservative when designed by the von Mises theory. The spheres were unconservative by both the Tresca and von Mises theories, but conservative by the Beltrami theory.

E1.2 METHODOLOGY

Given the following definitions:

F_{TU} = ultimate tensile stress.

F_{TY} = yield stress.

$\sigma_1, \sigma_2, \sigma_3$ = principal stresses, $\sigma_1 \geq \sigma_2 \geq \sigma_3$.

P = limit load.

R_o, h_o = original or unstrained dimensions.

R, h = strained dimensions.

ν = Poisson's ratio.

σ_o = yield stress and Ramberg-Osgood parameter.

For the plane stress state, the three theories of strength used are stated as follows:

von Mises $\quad \sigma_e = \sqrt{\sigma_1^2 + \sigma_2^2 - \sigma_1 \sigma_2}$

Tresca $\sigma_e = \sigma_1 - \sigma_3$

Beltrami $\sigma_e = \sqrt{\sigma_1^2 + \sigma_2^2 - 2\nu\sigma_1\sigma_2}$

where σ_e is the so-called effective stress.

The above equations result in the subsequent design formulas:

CYLINDER:

von Mises $$h_o = 1.4 \frac{PR_o}{F_{TU}} \frac{\sqrt{3}}{2} \tag{E-1}$$

Tresca $$h_o = 1.4 \frac{PR_o}{F_{TU}} \tag{E-2}$$

Beltrami $$h_o = 1.4 \frac{PR_o}{F_{TU}} \frac{\sqrt{3.66}}{2}, \quad \nu = 1/3 \tag{E-3}$$

SPHERE:

von Mises and Tresca $$h_o = 1.4 \frac{PR_o}{2F_{TU}} \tag{E-4}$$

Beltrami $$h_o = 1.4 \frac{PR_o}{\sqrt{3}\ F_{TU}}, \quad \nu = 1/3 \tag{E-5}$$

In Equations E-1 through E-5, 1.4 is the desired factory of safety.

The ultimate load was determined by means of a relatively simple concept which used the Ramberg-Osgood three-parameter method to define the stress-strain curve, and the von Mises flow rule to determine inelastic action in the biaxial state of stress. Complete derivations are given in paragraph E3 for the structures mentioned above and for a uniaxially loaded bar.

E1.3 RESULTS

Figure E-1 graphically demonstrates the relative differences between the three theories used. It is noted that the cylinder where $\sigma_1/\sigma_2 = 2$ provides the greatest discrepancy

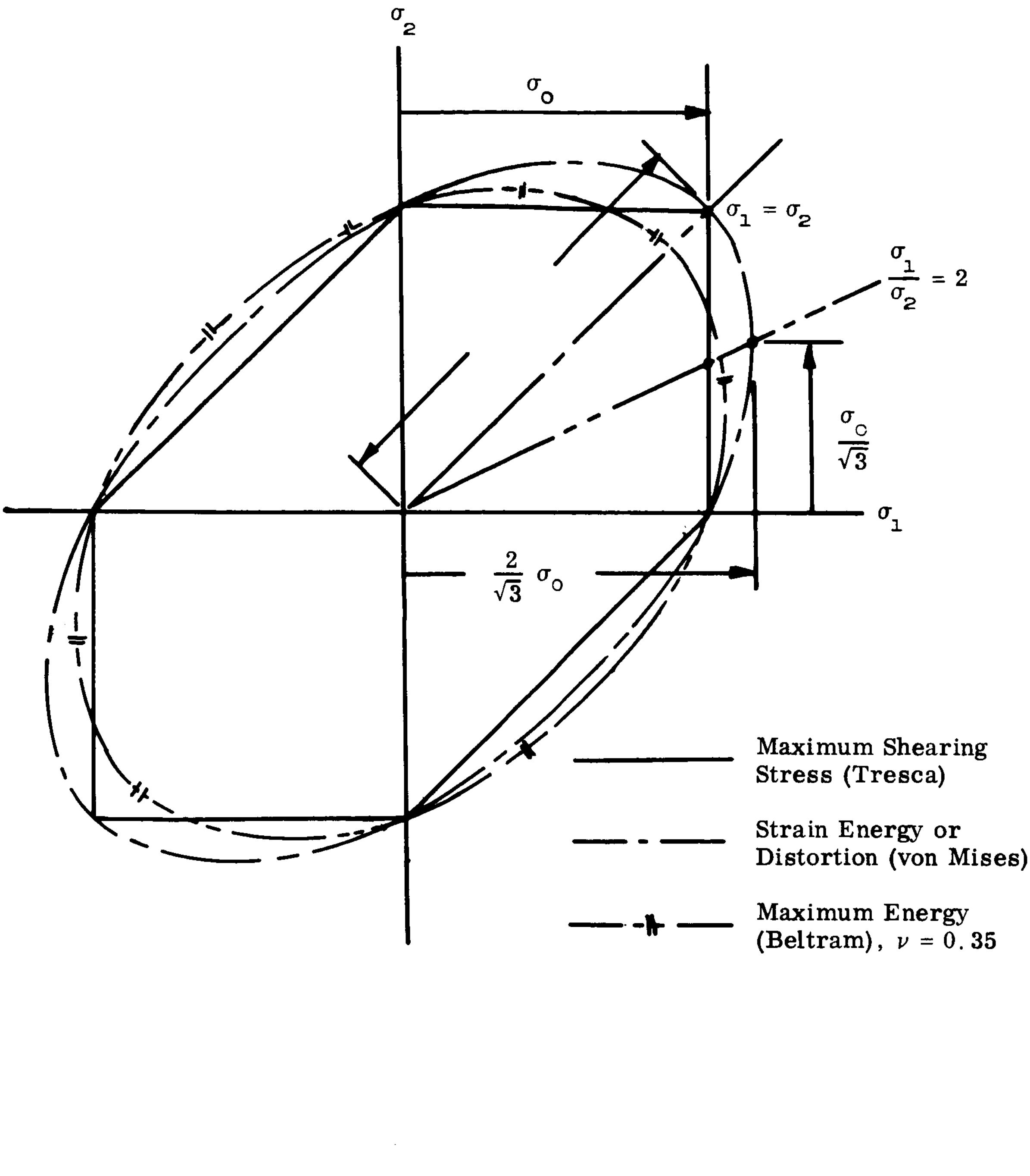

Figure E-1. Graphical Representation of the Yield Condition for Plane Stress ($\sigma_3 = 0$)

between Tresca and von Mises theories, whereas the sphere with $\sigma_1 = \sigma_2$ shows them to be in agreement. The Beltrami theory is sensitive to Poisson's ratio and converges to the von Mises theory when $\nu = 0.5$.

E1.3.1 Cylinder

The cylinder was investigated using three aluminum alloys with the properties given in Tables E-1 and E-2. The materials shown had F_{TU} values nearly equal, but F_{TY} values vary by large amounts. The actual results of the study are given in Tables E-3, E-4, and E-5 and by means of Figure E-2. Figure E-2 indicates by the dashed line that the von Mises theory may converge to the desired 1.4 if the material has the ratio $F_{TU}/F_{TY} = 1$, that is, if it has a flat-topped type of stress-strain curve. This is only true for a rigid plastic material which is defined in Figure E-4. A simple example of a cylinder made of deformable material demonstrates that a strict convergence to 1.4 is not possible with either of Equations E-1 or E-2. For a cylinder stress is of the form

$$PR/h \tag{E-6}$$

Under the loaded condition $R > R_o$ and $h < h_o$, where R_o and h_o are the original undeformed dimensions.

Therefore

$$P\frac{R_o}{h_o} < P\frac{R}{h}$$

Hence

$$P\frac{R_o}{h_o} = KP\frac{R}{h}, \quad K < 1 \tag{E-7}$$

and the resulting $P_{max} < 1.4\,P$, where $P_{max} = 1.4\,P$ is the desired result.

Figure E-2 demonstrates that the cylinder designed by the Tresca theory is always conservative, whereas the Beltrami theory is sensitive to Poisson's ratio and is conservative $\nu = 1/3$.

Table E-1

Ramberg-Osgood Data

Material	σ_o	$\sigma_{0.85}$	$E \times 10^{-6}$
2014-T6	60,100	58,000	10.7
2024-T4	47,330	46,000	10.7
2219-T87	53,200	50,000	10.4

Table E-2

Material F_{TU} and F_{TY} Data

Material	F_{TU}	F_{TY}	F_{TU}/F_{TY}
2014-T6	64,000	56,000	1.14
2024-T4	63,000	42,000	1.46
2219-T87	62,000	50,000	1.24

Table E-3

Cylinder Ultimate Load Data
(von Mises)

Material	h_o	P_{ULT}	$P_{ULT}/200$
2014-T6	0.1676	272.5	1.36
2024-T4	0.1705	263.6	1.32
2219-T87	0.1732	268.5	1.34

Table E-4

Cylinder Ultimate Load Data
(Maximum Shear Stress Theory)

Material	h_o	P_{ULT}	$P_{ULT}/200$
2014-T6	0.1937	315.0	1.58
2024-T4	0.1968	304.2	1.52
2219-T87	0.2	310.0	1.55

Table E-5

Cylinder Ultimate Load Data
(Maximum Energy Theory, $\nu = 1/3$)

Material	h_o	P_{ULT}	$P_{ULT}/200$
2014-T6	0.1851	300.9	1.5
2024-T4	0.1883	291.1	1.46
2219-T87	0.1913	296.6	1.48

E1.3.2 Sphere

A sphere of the same radius and load was designed by Equations E-4 and E-5. The results for the three alloys are given in Tables E-6 and E-7 and shown graphically by Figure E-3. Figure E-3 indicates that the Tresca and von Mises theories converge to 1.4. This is only true for a rigid plastic material. The same argument holds for the sphere as for the cylinder when a deformable material is used; hence the 1.4 safety factor cannot be achieved by Equation E-4.

Table E-6

Sphere Ultimate Load Data
(von Mises and Tresca Theories)

Material	h_o	P_{ULT}	$P_{ULT}/200$
2014-T6	0.09685	274.7	1.37
2024-T4	0.0984	267.8	1.34
2219-T87	0.100	271.5	1.36

Table E-7

Sphere Ultimate Load Data
(Maximum Energy Theory, $\nu = 1/3$)

Material	h_o	P_{ULT}	$P_{ULT}/200$
2014-T6	0.1116	316.6	1.58
2024-T4	0.1135	308.9	1.54
2219-T87	0.1153	313.1	1.56

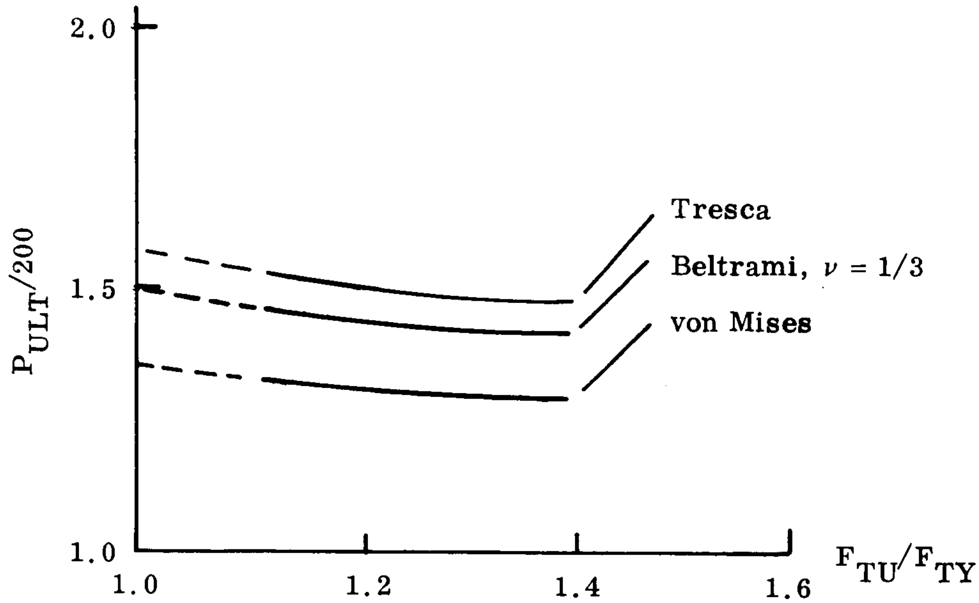

Figure E-2. Actual Factor of Safety versus the F_{TU}/F_{TY} Ratio for Cylindrical Shells

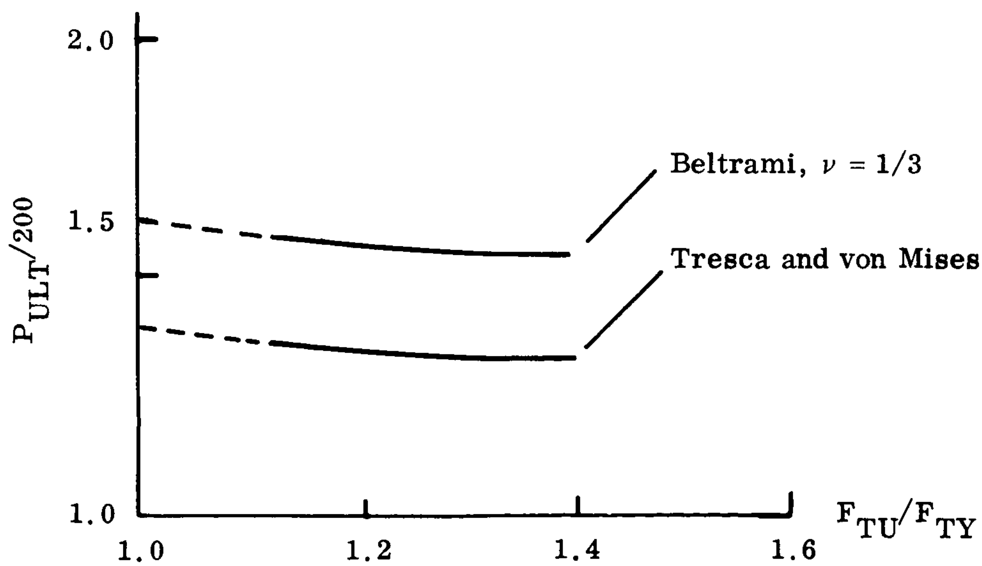

Figure E-3. Actual Factor of Safety versus the F_{TU}/F_{TY} Ratio for Spherical Shells

E1.4 CONCLUSIONS

The results found indicate that the von Mises theory will always result in a nonconservative structure when loaded in biaxial tension, i.e., the true factor of safety will not be obtained when using standard design formulae derived from the equilibrium condition only. It is also seen that the Tresca theory, while generally assumed to be conservative, can in reality result in a nonconservative design in the biaxial stress state where $\sigma_1 \simeq \sigma_2$. The results do not imply that the von Mises theory of elastic breakdown is an incorrect theory, but more the victim of the form of the design equations used. Hence, using a modified theory of strength of the form of the maximum energy theory is required in order to satisfy the factor of safety requirement and still use the standard design equations. It appears that no simple form of equation of theory of strength will always result in the exact factor of safety. This area may be fruitful for investigation in subsequent studies using more extensive data and developed for more complex structures.

E2 METHODS OF PLASTIC ANALYSIS

E2.1 MATERIAL STRESS-STRAIN CURVES

Different types of analyses can be considered for determining the ultimate or collapse loads of pressure vessels. For demonstration purposes of the stress-strain curves used in the various theories of plasticity refer to Figure E-4 (Reference 53).

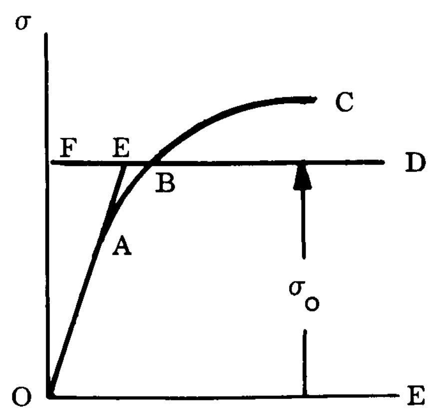

Figure E-4. Stress-Strain Curves for Various Theories of Plasticity

In Figure E-4:

a. Curve OFED is for a rigid plastic material.
b. Curve OAEBD is for an ideal plastic material.
c. Curve OABD is for a perfectly plastic material.
d. Curve OABC is the nominal stress-strain curve for the real material. "Nominal" implies that stress is equal for the load divided by the original cross-sectional area in the simple tension test.

The type of analysis considered here is for the "real" material curve OABC as defined by the Ramberg-Osgood three-parameter method (Reference 54). Other methods are discussed in References 53, 55, and 56.

E2.2 DEFORMATION AND INCREMENTAL THEORIES

In formulating a plastic-flow problem, one must decide whether to use deformation theory or incremental theory. This section briefly discusses each theory.

a. DEFORMATION THEORY establishes a relation between the stress states and the total strains. It presumes that the path of loading does not influence the strains. Such an assumption cannot in general be correct; however Reference 61 argues that the restrictions on the application of deformation theory are not as severe as formerly thought. Deformation theory has the advantage of reduction in computation and if judgment is used, the regions of inapplicability can in many cases be avoided.
b. INCREMENTAL THEORY relates the increment of strain to the increment of stress in a given stress state. This means that one must consider the complete loading history and add up the increments of strain at each point to obtain the final strain. It is evident that considerable computation may be required to arrive at a near-correct solution of the problem.

E3 TENSILE INSTABILITY

E3.1 INTRODUCTION

In order to predict the failure of a structural component by numerical methods, the stresses have to be calculated in regions of plastic flow. It is the purpose of this note to present a simplified stress-strain relation which can furnish sufficiently accurate results when restricted to uniaxial and biaxial states of stress. The method uses the Ramberg-Osgood three-parameter method to define the complete stress-strain curve of the material (the method is easily converted to use of actual material stress-strain data). The deformation theory of plasticity is used. The von Mises yield criterion is used to determine elastic breakdown, and the related flow rule determines the amount of plastic flow in each direction in terms of the final stress components. The geometry at each stress state is determined by means of the logarithmic strain (also called the "natural" strain) relation. The theory that is presented here differs little from that of Reference 55 except for the introduction of the von Mises deformation theory as presented in Reference 56 and the use of the Ramberg-Osgood method of Reference 54 for determining the material uniaxial stress-strain curve.

E3.2 SYMBOLS

$\sigma_1, \sigma_2, \sigma_3$ = the principal stresses.

σ_e = the effective stress.

$\epsilon_1, \epsilon_2, \epsilon_3$ = the principal strains.

ϵ_e = the effective strain.

$\overline{\epsilon}$ = the natural strain.

ϵ = nominal strain.

ϵ_P = plastic stress.

E3.3 SIMPLIFIED STRESS-STRAIN RELATION

E3.3.1 Stress-Strain Relations for von Mises Deformation Theory (Reference 56)

The deformation theory of plasticity makes the following assumptions:

a. The directions of the principal strains coincide with the direction of the principal stresses.

b. The ratios of the principal shear strains are equal to the ratios of the principal shear stresses,

$$\frac{\epsilon_{3P} - \epsilon_{1P}}{\sigma_3 - \sigma_1} = \frac{\epsilon_{3P} - \epsilon_{2P}}{\sigma_3 - \sigma_2} = \frac{\epsilon_{1P} - \epsilon_{2P}}{\sigma_1 - \sigma_2} .$$

c. The volume remains constant in the plastic range,

$$\epsilon_{1P} + \epsilon_{2P} + \epsilon_{3P} = 0 .$$

d. A universal relation exists between the effective stress σ_e and the effective plastic strain ϵ_{eP}, where

$$\sigma_e = \frac{1}{\sqrt{2}} \sqrt{(\sigma_1 - \sigma_2)^2 + (\sigma_1 - \sigma_3)^2 + (\sigma_2 - \sigma_3)^2}$$

$$\epsilon_{eP} = \frac{\sqrt{2}}{3} \sqrt{(\epsilon_{1P} - \epsilon_{2P})^2 + (\epsilon_{1P} - \epsilon_{3P})^2 + (\epsilon_{2P} - \epsilon_{3P})^2}$$

One should note that σ_e and ϵ_{eP} are so defined that they become the stress and strain in the direction of the applied load for a uniaxial stress condition.

E3.3.2 Stress-Strain Relation (References 55 and 56)

The method derived here relates the so-called effective stress σ_e expressed as a function of the maximum principal stress, called the "decisive stress," to the logarithmic value of the effective plastic strain expressed as a function of the largest absolute value of the natural strain (plastic) $|\bar{\epsilon}_{max}|$, called the "decisive strain." The natural or logarithmic strain is related to the conventional strain by the expression

$$\bar{\epsilon} = \ln(1 + \epsilon) . \tag{E-8}$$

In these notes the following expressions for logarithms will be used,

$$\begin{aligned} \ln(\cdot) &= \log_e(\cdot) , \\ \log(\cdot) &= \log_{10}(\cdot) . \end{aligned} \tag{E-9}$$

Since σ_e and ϵ_e are to be expressed as functions of σ_1 and the absolute value of the largest principal plastic strain, one can restrict the theory to using these principal stresses and strains. Further, only the biaxial and uniaxial tension states are to be considered. For a biaxial tension stress state, it is assumed that $\sigma_3 = 0$. The decisive strain $|\bar{\epsilon}_{max}|$ is either $\bar{\epsilon}_1$ or $-\bar{\epsilon}_3$, depending upon the sign of the intermediate principal strain $\bar{\epsilon}_2$. Volume constancy is assumed for the plastic state, thus

$$\bar{\epsilon}_1 + \bar{\epsilon}_2 + \bar{\epsilon}_3 = 0 \tag{E-10}$$

In Equation E-10, subscript P is dropped and will no longer be used. Equation E-10 is satisfied if $\bar{\epsilon}_1 > 0$ and $\bar{\epsilon}_3 < 0$ if one ignores the trivial case where $\bar{\epsilon}_i = 0$, i = 1, 2, 3.

From Equation E-10

$$\bar{\epsilon}_1 = -\bar{\epsilon}_2 - \bar{\epsilon}_3 \tag{E-11}$$

since $\bar{\epsilon}_3 < 0$ always, Equation E-11 may be expressed in the form

$$|\bar{\epsilon}_1| = -\bar{\epsilon}_2 + |\bar{\epsilon}_3| \; . \tag{E-12}$$

Equation E-12 gives rise to three cases as follows:

a. If $\bar{\epsilon}_2 < 0$ then $|\bar{\epsilon}_1| > |\bar{\epsilon}_3|$ and $\bar{\epsilon}_1$ is the decisive strain.

b. If $\bar{\epsilon}_2 > 0$ then $|\bar{\epsilon}_1| < |\bar{\epsilon}_3|$ and $-\bar{\epsilon}_3$ is the decisive strain.

c. When $\bar{\epsilon}_2 = 0$ then $|\bar{\epsilon}_1| = |\bar{\epsilon}_3|$ and the common value $\bar{\epsilon}_1 = -\bar{\epsilon}_3$ is the decisive strain.

E3.4 NECKING OF A TENSILE SPECIMEN (Reference 55)

Instability is considered to occur in a simple tension member when localized necking commences.

In a state of uniaxial tension $\sigma_2 = \sigma_3 = 0$ thus

$$\bar{\epsilon}_2 = \bar{\epsilon}_3 = -\frac{\bar{\epsilon}_1}{2} < 0 \tag{E-13}$$

and $\bar{\epsilon}_1$ is the decisive strain parameter. Tensile instability will be postulated to occur when

$$\frac{dP}{d\bar{\epsilon}_1} = 0 \tag{E-14}$$

$$P = \sigma_1 A \tag{E-15}$$

where A represents the instantaneous area of the bar.

When Equation E-15 is differentiated with respect to $\bar{\epsilon}_1$ the result is:

$$\frac{dP}{d\bar{\epsilon}_1} = \sigma_1 \frac{dA}{d\bar{\epsilon}_1} + A \frac{d\sigma_1}{d\bar{\epsilon}_1} \tag{E-16}$$

If A_o is the unstrained cross-sectional area, then

$$A = A_o(1 + \epsilon_2)(1 + \epsilon_3) \tag{E-17}$$

or

$$A = A_o e^{\bar{\epsilon}_2 + \bar{\epsilon}_3} = A_o e^{-\bar{\epsilon}_1} \qquad \text{(E-18)}$$

Thus

$$\frac{dA}{d\bar{\epsilon}_1} = -A_o e^{-\bar{\epsilon}_1} = -A \qquad \text{(E-19)}$$

Substitute Equation E-19 into Equation E-16 and solve the result by means of Equation E-14 to arrive at Equation E-20

$$\frac{d\sigma_1}{d\bar{\epsilon}_1} = \sigma_1 \qquad \text{(E-20)}$$

The next assumption is that the simple tension curve for the material can be expressed by the Ramberg-Osgood relation (Reference 54)

$$\epsilon_1 = \frac{\sigma_1}{E} + K\left(\frac{\sigma_1}{E}\right)^n$$

where

$$n = 1 + \frac{0.3853}{\log\left(\frac{\sigma_o}{\sigma_{0.85}}\right)} \qquad \text{(E-21)}$$

and

$$K = \left(\frac{1}{0.85} - 1\right)\left(\frac{\sigma_{0.85}}{E}\right)^{1-n}$$

In Equation E-21 $\sigma_{0.85}$ is the secant yield strength where the line

$$\sigma = 0.85\,E\,\epsilon$$

strikes the nominal stress-strain curve, and σ_o is the point on the curve at 0.7 E.

Equation E-20 can now be evaluated numerically since

$$\bar{\epsilon}_1 = \ln(1 + \epsilon_1) = \ln\left[1 + \frac{\sigma_1}{E} + K\left(\frac{\sigma_1}{E}\right)^n\right]$$

and

$$e^{\bar{\epsilon}_1} = 1 + \frac{\sigma_1}{E} + K\left(\frac{\sigma_1}{E}\right)^n \tag{E-22}$$

Differentiating Equation E-22 with respect to $\bar{\epsilon}_1$ gives the relationship

$$\frac{d\sigma_1}{d\bar{\epsilon}_1} = \frac{E\,e^{\bar{\epsilon}_1}}{1 + nK\left(\frac{\sigma}{E}\right)^{n-1}} \tag{E-23}$$

Thus the point where instability occurs or Equation E-24 is found by using Equations E-20 and E-23

$$\sigma_{1_{CRIT}} = \frac{E\,e^{\bar{\epsilon}_{1_{CRIT}}}}{1 + nK\left(\frac{\sigma_{1_{CRIT}}}{E}\right)^{n-1}} \tag{E-24}$$

where the subscript CRIT denotes critical or the stress where $P = P_{max}$.

E3.5 INSTABILITY OF A THIN SPHERE SUBJECTED TO A UNIFORM INTERNAL PRESSURE

For a sphere

$$\sigma_1 = \sigma_2 = \sigma_\theta = \frac{PR}{2h} \tag{E-25}$$

assume

$$\sigma_r \approx 0 = \sigma_3 \tag{E-26}$$

The natural strain is given by

$$\bar{\epsilon}_\theta = \bar{\epsilon}_1 = \ln\left(\frac{R}{R_o}\right) = \bar{\epsilon}_2 \tag{E-27}$$

and

$$\bar{\epsilon}_r = \bar{\epsilon}_3 = \ln\left(\frac{h}{h_o}\right)$$

where R_o and h_o are the unstrained radius and shell thickness respectively, and R and h are the instantaneous radius and shell thickness respectively.

Since volume constancy is assumed (Equation E-10)

$$\bar{\epsilon}_3 = -2\bar{\epsilon}_\theta = \bar{\epsilon}_r \tag{E-28}$$

and the decisive strain is

$$|\bar{\epsilon}|_{max} = |\bar{\epsilon}_3| \tag{E-29}$$

From Equation E-27

$$R = R_o e^{\bar{\epsilon}_\theta},$$

$$h = h_o e^{\bar{\epsilon}_r} \tag{E-30}$$

When Equation E-30 is substituted into Equation E-25 it is found that

$$\sigma_\theta = \frac{P}{2} \frac{R_o}{h_o} e^{\bar{\epsilon}_\theta - \bar{\epsilon}_r}$$

and from Equation E-28

$$\sigma_\theta = \frac{P}{2} \frac{R_o}{h_o} e^{-3/2\,\bar{\epsilon}_r} \tag{E-31}$$

Solving Equation E-31 for P gives ($\bar{\epsilon}_r = \bar{\epsilon}_3$, $\sigma_\theta = \sigma_1$)

$$P = \frac{2h_o}{R_o} \sigma_1 e^{3/2\,\bar{\epsilon}_3} = \frac{2h_o}{R_o} \sigma_1 e^{-3\bar{\epsilon}_1} \tag{E-32}$$

It is postulated that instability occurs when P expressed as a function of $\bar{\epsilon}_3$ reaches a maximum, or

$$\frac{dP}{d|\bar{\epsilon}_3|} = 0 \tag{E-33}$$

Equation E-32 gives the relation

$$\frac{dP}{d(-\bar{\epsilon}_3)} = -\frac{3h_o}{R_o} \sigma_1 e^{3/2\,\bar{\epsilon}_3} + \frac{2h_o}{R_o} e^{3/2\,\bar{\epsilon}_3} \frac{d\sigma_1}{d(-\bar{\epsilon}_3)}$$

Equation E-33 shows that instability occurs when

$$\frac{d\sigma_1}{d(-\bar{\epsilon}_3)} = \frac{3}{2}\sigma_1 = \frac{3}{2}\sigma_\theta \qquad \text{(E-34)}$$

For a sphere the effective stress is given by the relation

$$\sigma_e = \frac{1}{\sqrt{2}}\sqrt{2\sigma_\theta^{\,2}} = \sigma_\theta \qquad \text{(E-35)}$$

The effective strain is assumed to be

$$\epsilon_e = \frac{\sqrt{2}}{3}\sqrt{9\epsilon_\theta^{\,2} + 9\epsilon_\theta^{\,2}} = 2\epsilon_\theta \qquad \text{(E-36)}$$

From Equation E-28 it is shown that

$$\bar{\epsilon}_3 = -\bar{\epsilon}_e \qquad \text{(E-37)}$$

Using Equations E-21 and E-35*

$$\bar{\epsilon}_e = \ln\left[1 + \frac{\sigma_\theta}{E} + K\left(\frac{\sigma_\theta}{E}\right)^n\right] \qquad \text{(E-38)}$$

But

$$\bar{\epsilon}_3 = -\bar{\epsilon}_e\,,$$

thus

$$e^{-\bar{\epsilon}_3} = 1 + \frac{\sigma_\theta}{E} + K\left(\frac{\sigma_\theta}{E}\right)^n \qquad \text{(E-39)}$$

Differentiating Equation E-39 with respect to $-\bar{\epsilon}_3$ to satisfy Equation E-34 gives the relation

$$\frac{d\sigma_1}{d(-\bar{\epsilon}_3)} = \frac{E\,e^{-\bar{\epsilon}_3}}{1 + nK\left(\frac{\sigma_1}{E}\right)^{n-1}} \qquad \text{(E-40)}$$

*If it is assumed that $\nu = 1/2$, this substitution is valid; however, it introduces very little error for the usual value of 0.3 and greatly simplifies the calculations.

Thus, by means of Equations E-34 and E-40, the point can be found where

$$\sigma_{1_{CRIT}} = \frac{\frac{2}{3} E \, e^{-\bar{\epsilon}_{3_{CRIT}}}}{1 + nK\left(\frac{\sigma_{1_{CRIT}}}{E}\right)^{n-1}}$$

at which point

$$P_{max} = \frac{2h_o}{R_o} \sigma_{1_{CRIT}} \, e^{3/2 \, \bar{\epsilon}_{3_{CRIT}}}$$

and the factor of safety becomes $\frac{P_{max}}{P_{limit}}$.

E3.6 INSTABILITY OF THIN-WALLED TUBES SUBJECTED TO A UNIFORM INTERNAL PRESSURE

Assume that end effects can be ignored, then for a thin-walled cylinder

$$\sigma_\theta = \frac{PR}{h} = \sigma_1 \tag{E-41}$$

$$\sigma_Z = \frac{PR}{2h} = \sigma_2 \tag{E-42}$$

$$\sigma_r \approx 0 = \sigma_3 \tag{E-43}$$

From Equation E-41 and E-42

$$\sigma_1 = 2\sigma_2$$

or

$$\sigma_Z = \frac{1}{2}\sigma_\theta \tag{E-44}$$

Thus

$$\sigma_e = \frac{1}{\sqrt{2}} \sqrt{(\sigma_1 - \sigma_2)^2 + \sigma_1^2 + \sigma_2^2}$$

$$= \frac{1}{\sqrt{2}} \sqrt{\frac{\sigma_1^2}{4} + \sigma_1^2 + \frac{\sigma_1^2}{4}}$$

$$\sigma_e = \frac{\sigma_1}{\sqrt{2}} \sqrt{\frac{1+4+1}{4}} = \frac{\sigma_1}{\sqrt{2}} \sqrt{\frac{3}{2}}$$

$$= \frac{\sqrt{3}}{2} \sigma_1 \qquad \text{(E-45)}$$

Using the Ramberg-Osgood relation, the effective strain for the material is found by

$$\epsilon_e = \frac{\sigma_e}{E} + K\left(\frac{\sigma_e}{E}\right)^n$$

Substituting Equation E-45 gives the relation*

$$\epsilon_e = \frac{\sqrt{3}}{2} \frac{\sigma_\theta}{E} + K\left(\frac{\sqrt{3}\,\sigma_\theta}{2E}\right)^n \qquad \text{(E-46)}$$

In the plastic range

$$\epsilon_3 = -\epsilon_1 - \epsilon_2 \qquad \text{(E-47)}$$

When $\sigma_3 = 0$, the resulting equations take on the form of plain stress. Hence, in the plastic range

$$\epsilon_1 = \frac{\epsilon_e}{\sigma_e}\left(\sigma_1 - \frac{1}{2}\sigma_2\right) \qquad \text{(E-48)}$$

$$\epsilon_2 = \frac{\epsilon_e}{\sigma_e}\left(\sigma_2 - \frac{1}{2}\sigma_1\right) \qquad \text{(E-49)}$$

From Equation E-47 it is clear from Equation E-49 that

$$\epsilon_2 = 0 \qquad \text{(E-50)}$$

and that

$$\epsilon_1 = \frac{\epsilon_e}{\sigma_e}\left(\frac{3}{4}\sigma_1\right) \qquad \text{(E-51)}$$

*If it is assumed that $\nu = 1/2$, this substitution is valid; however, it introduces very little error for the usual value of 0.3 and greatly simplifies the calculations.

Substitute Equation E-47 into Equation E-51 for σ_e and

$$\epsilon_1 = \frac{\epsilon_e}{\frac{\sqrt{3}}{2}\sigma_1}\left(\frac{3}{4}\sigma_1\right) = \frac{\sqrt{3}}{2}\epsilon_e \qquad \text{(E-52)}$$

From Equations E-47 and E-50

$$\epsilon_3 = \frac{-\sqrt{3}}{2}\epsilon_e \qquad \text{(E-53)}$$

The natural strains are also defined by

$$\bar{\epsilon}_1 = \ln\left(\frac{R}{R_o}\right)$$

$$\text{(E-54)}$$

$$\bar{\epsilon}_3 = \ln\left(\frac{h}{h_o}\right)$$

from which it is deduced that

$$R = R_o\, e^{\bar{\epsilon}_1}, \qquad h = h_o\, e^{\bar{\epsilon}_3} \qquad \text{(E-55)}$$

Substituting Equation E-55 into Equation E-41 the stress becomes

$$\sigma_1 = P\,\frac{R_o}{h_o}\, e^{\bar{\epsilon}_1 - \bar{\epsilon}_3}$$

From Equation E-47 $\bar{\epsilon}_3 = -\bar{\epsilon}_1$, since $\bar{\epsilon}_2 = 0$, and

$$\sigma_1 = P\,\frac{R_o}{h_o}\, e^{2\bar{\epsilon}_1} \qquad \text{(E-56)}$$

Here $\bar{\epsilon}_1$ is the decisive strain. Solving for $\bar{\epsilon}_1$, gives

$$\bar{\epsilon}_1 = \ln(1 + \epsilon_1) = \ln\left(1 + \frac{\sqrt{3}}{2}\epsilon_e\right) \qquad \text{(E-57)}$$

Substituting Equation E-46 into Equation E-57 for ϵ_e gives

$$\bar{\epsilon} = \ln\left\{1 + \frac{\sqrt{3}}{2}\left[\frac{\sqrt{3}}{2}\,\frac{\sigma_\theta}{E} + K\left(\frac{\sqrt{3}}{2}\,\frac{\sigma_\theta}{E}\right)^n\right]\right\} \qquad \text{(E-58)}$$

From Equation E-56

$$P = \sigma_1 \frac{h_o}{R_o} e^{-2\bar{\epsilon}_1} \tag{E-59}$$

It is postulated that at P_{max} instability occurs.

Differentiate Equation E-59 with respect to $\bar{\epsilon}_1$,

$$\frac{dP}{d\bar{\epsilon}_1} = -2\sigma_1 \frac{h_o}{R_o} e^{-2\bar{\epsilon}_1} + \frac{h_o}{R_o} e^{-2\bar{\epsilon}_1} \frac{d\sigma_1}{d\bar{\epsilon}_1}$$

For P_{max},

$$\frac{dP}{d\bar{\epsilon}_1} = 0 ,$$

and

$$\frac{d\sigma_1}{d\bar{\epsilon}_1} = 2\sigma_1 \tag{E-60}$$

From Equation E-58

$$e^{\bar{\epsilon}_1} = 1 + \frac{\sqrt{3}}{2}\left[\frac{\sqrt{3}}{2}\frac{\sigma_\theta}{E} + K\left(\frac{\sqrt{3}}{2}\frac{\sigma_\theta}{E}\right)^n\right] \tag{E-61}$$

Differentiating Equation E-61 with respect to $\bar{\epsilon}_1$ gives the relation

$$\frac{d\sigma_1}{d\bar{\epsilon}_1} = \frac{\frac{4}{3} E\, e^{\bar{\epsilon}_1}}{1 + nK\left(\frac{\sqrt{3}}{2}\frac{\sigma_\theta}{E}\right)^{n-1}} \tag{E-62}$$

The proper relationship for P_{max} is obtained by combining Equations E-60 and E-62 for $\sigma_{1_{CRIT}} = \sigma_{\theta_{CRIT}}$, the stress causing tensile instability, viz.

$$\sigma_{\theta_{CRIT}} = \frac{\frac{2}{3} E\, e^{\bar{\epsilon}_{1_{CRIT}}}}{1 + nK\left(\frac{\sqrt{3}}{2}\frac{\sigma_{\theta_{CRIT}}}{E}\right)^{n-1}} \tag{E-63}$$

at which point

$$P_{max} = \sigma_{\theta_{CRIT}} \frac{h_o}{R_o} e^{-2\bar{\epsilon}_{1_{CRIT}}} \quad \text{(E-64)}$$

the ultimate load factor of safety becomes $\frac{P_{max}}{P_{limit}}$.

DISTRIBUTION LIST FOR FINAL REPORT

Contract NAS 2-3811

STUDY OF STRUCTURAL WEIGHT SENSITIVITIES
FOR LARGE ROCKET SYSTEMS

NASA Headquarters
Washington, D.C. 20546

R/Dr. Mac C. Adams
R/A. J. Eggers, Jr.
RTP/R. J. Wisniewski
RP/A. O. Tischler and W. Wilcox
RR/H. H. Kurzweg and S. Deutsch
RV-2/M. G. Rosche, D. A. Gilstad and H. S. Wolko
RV/F. Demerritte
RAL/H. H. Brown
PT/W. A. Fleming
SX/J. E. Naugle
SV/J. E. McGolrick and V. K. Johnson
MTY/R. W. Gillespie
MTV/A. D. Schnyer
MA-2/G. L. Roth and T. Keegan
TA/C. R. Morrison

NASA Ames Research Center
Moffett Field, California 94035

Library, Mail Stop 202-3—Atten: H. Julian Allen, Director and C. A. Syvertson, Assistant Director for Astronautics
A. L. Erickson, H. A. Cole, Jr., and R. E. Reed, Jr., Mail Stop 242-1
C. A. Hermach, Mail Stop 240-1
J. F. Pogue, Contracting Officer, Mail Stop 241-1
Patent Council, Mail Stop 200-11a (2 copies)
Technical Information Division, Mail Stop 241-12 (1 plus reproducable)

NASA Mission Analysis Division, OART
Moffett Field, California 94035

Leonard Roberts, Director, D. H. Dennis, and R. C. Savin, Mail Stop 202-5
H. M. Drake and T. J. Gregory, Mail Stop 202-7
F. G. Casal, Mail Stop 202-8
H. Hornby, Mail Stop 202-6
K. Nishioka, Mail Stop 202-6
C. D. Havill, Mail Stop 202-6
E. W. Gomersall, Technical Manager, Mail Stop 202-6 (6 copies)

NASA Electronics Research Center
575 Technology Square
Cambridge, Massachusetts 02139

Library—Atten: James C. Elms, Director

NASA Flight Research Center
Post Office Box 273
Edwards, California 93523

Library—Atten: Paul F. Bikle, Director

NASA Goddard Space Flight Center
Greenbelt, Maryland 20771

Library—Atten: Dr. John F. Clark, Director

Jet Propulsion Laboratory
4800 Oak Grove Drive
Pasadena, California 91103

Library—Atten: Dr. William H. Pickering, Director
H. Burlage, Jr.

NASA Kennedy Space Center
Kennedy Space Center, Florida 32899

Library—Atten: Dr. Kurt H. Debus, Director, and Georg Von Tiesenhausen

NASA Langley Research Center
Langley Station
Hampton, Virginia 23365

Library—Atten: Dr. F. L. Thompson, Director
R.R. Heldenfels, R.A. Anderson, E.E. Mathauser, and H. Schaffer; Mail Stop 188
D.J. Martin and I.E. Garrick, Mail Stop 242
C.H. McLellan and E.B. Pritchard, Mail Stop 131

NASA Lewis Research Center
21000 Brookpark Road
Cleveland, Ohio 44135

Library--Atten: Dr. A. Silverstein, Director, and B.T. Lundin
J.W. Weeton and R.A. Signorelli, Mail Stop 49-1
H.M. Henneberry and W.G. Anderson, Mail Stop 112A

NASA Manned Spacecraft Center
Houston, Texas 77058

Library—Atten: Dr. Robert R. Gilruth, Director, and W. Gillespie (3 copies)

NASA Marshall Space Flight Center
Huntsville, Alabama 35812

Library—Atten: Dr. W. von Braun, Director
G.A. Kroll, J.F. Blumrich, A.J. Verble, Jr., and E.E. Engler;
Code R-P&VE-S
J.E. Kingsbury; Code R-P&VE-M
H.F. Wuenscher; Code R-ME-DIR
J.P. Orr and E.L. Brown; Code R-ME-M
F.L. Williams and D.W. Fellenz; Code R-AS
J. von Puttkamer; Code R-AERO-T

NASA Daytona Beach Operation
P.O. Box 2500
Daytona Beach, Florida 32015

A.S. Lyman, Code MA-2D

Department of the Air Force
Headquarters, USAF, DCS/D
Washington, D.C. 20545

Atten: Technical Library

Army Rocket & Guided Missile Agency
U.S. Army Ordnance Missile Command
Redstone Arsenal
Huntsville, Alabama

Atten: Technical Library

Department of the Navy
Special Projects Office
3010 Munitions Building
19th and Constitution Avenue, N.W.
Washington, D.C. 20360

Atten: Technical Library

Chemical Propulsion Information Agency
Applied Physics Laboratory
8621 Georgia Avenue
Silver Spring, Maryland 20910

Atten: Technical Library

Institute for Defense Analyses
1666 Connecticut Avenue, N.W.
Washington, D.C.

Atten: Technical Library

Aeroject General Corporation
Sacramento, California

Atten: Technical Library

Pratt & Whitney Aircraft
Division of United Aircraft Corporation
Wast Palm Beach, Florida

Atten: Technical Library

TRW Systems
TRW, Inc.
One Space Park
Redondo Beach, California

Atten: Technical Library

Chrysler Corporation
P.O. Box 29200
New Orleans, Louisiana

Atten: Technical Library

Battelle Memorial Institute
Columbus, Ohio

Technical Library—Atten: B.L. Fletcher

The Boeing Company
P.O. Box 3868
Seattle, Washington 98124

Technical Library—Atten: M.T. Braun, P.E. Grafton, and P. Helms

The Boeing Company
Huntsville, Alabama

Technical Library—Atten: J.G. Brunk and J.A. Mayhall

North American Aviation, Inc.; S&ID
12214 S. Lakewood Boulevard
Downey, California

Technical Library—Atten: L.A. Harris, J.A. Boddy and H.S. Oder

McDonnell-Douglas Aircraft Company
Huntington Beach, California

Technical Library—Atten: P. Bono and D.S. Garcia

Lockheed Missiles & Space Company
P.O. Box 24
Mountain View, California

Technical Library—Atten: L.A. Riedinger

General Dynamics/Convair Division
P.O. Box 1128
San Diego, California 92112

Technical Library—Atten: D.J. Peery

Rocketdyne
Division of North American Aviation
6633 Canoga Avenue
Canoga Park, California 91304

Technical Library—Atten: J.F. Kelly, B.O. Wagner, and M. Bensky

8/14/67

Progress Is Our Most Important Product

GENERAL ELECTRIC

TECHNICAL PUBLICATIONS

DB67E033